Fritz Laboratory Reports | Civil and Environmental Engineering

1972

Dynamic analysis of highway bridges using the inite element method, May 1972

William S. Peterson

Celal N. Kostem

LEHIGH UNIVERSITY
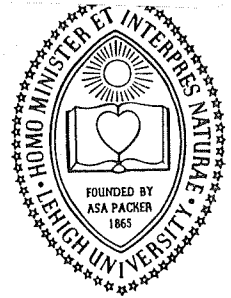
OFFICE

OF

RESEARCH

DYNAMIC ANALYSIS OF HIGHWAY BRIDGES

USING THE FINITE ELEMENT METHOD

BY

WILLIAM S. PETERSON

CELAL N. KOSTEM

FRITZ ENGINEERING LABORATORY REPORT No. 400.7

DYNAMIC ANALYSIS OF HIGHWAY BRIDGES

USING THE FINITE ELEMENT METHOD

by

William S. Peterson

Celal N. Kostem

Fritz Engineering Laboratory
Department of Civil Engineering
Lehigh University
Bethlehem, Pennsylvania

May, 1972

ABSTRACT

An analytical procedure for the determination of the vehicle-induced dynamic response of highway bridges is presented. The equations of motion are established using the Finite Element Method and then numerically integrated with a Runge-Kutta scheme. The analytical results are given in the form of deflection and moment time histories. Comparisons are provided between the analytical solution and the available experimental data.

1. INTRODUCTION

A bridge superstructure will respond to a moving load in a vibratory manner. The induced dynamic behavior produces a response spectrum indicating stresses and deformations which may be greater or less than that of the static load case for a given configuration (Ref. 14).

The oscillatory nature of the dynamic response will induce higher stress ranges and correspondingly reduce the fatigue life of the structure.

A dynamic analysis will reveal if a particular bridge design is "psychologically" unsatisfactory. If the motion of the bridge can be felt by the motorist or the pedestrian, then an adverse public reaction may result.

In earlier studies the entire bridge superstructure, which is composed of several girders and a slab, has been idealized as a single beam for the analytical determination of the dynamic response. The model consisting of one single beam is assigned mass and stiffness properties which are assumed to reflect the actual superstructure. This report presents a pilot study on the vehicle induced dynamic behavior of bridge superstructures using the finite element method.

Advantages of the finite element method over the single beam method are the following:

1. A more realistic model is obtained which treats the entire cross section as a plate with several stiffeners.

2. The dynamic behavior of the superstructure can be obtained in both logitudinal and lateral directions.

3. The individual beam behavior can be investigated.

4. The slab response is obtained.

5. The interaction between the various beams and the slab may be studied.

6. Dynamic load distribution factors can be predicted.

Computer generated moment and deflection time histories are presented. Contour plots of moment and deflection at specific times are also included to illustrate the response characteristics of the entire superstructure. A comparison is then made between the field test data from a full-scale inservice bridge and the reported analytical approach.

2. EQUATIONS OF MOTION

The time dependent displacement of a structure can be defined as a product of a displacement function dependent on the position (x,y) and a time function,

$$w(x,y,t) = w(x,y) \ R(t) \tag{1}$$

The displacement function, $w(x,y)$, can be represented by the series

$$w(x,y) = \sum_{i=1}^{N} A_i f_i(x,y) \tag{2}$$

where A_i are constants to be determined. Proceeding with an energy approach, expressions for the kinetic energy, stain energy of bending, potential energy of the transverse loads, and the energy dissipation due to viscous damping can be obtained (Ref. 1). Application of the Lagrangian approach to the Lagrangian-Energy function leads to the equations of motion:

$$[M] \{v\ddot{R}\} + [\bar{M}] \{v\dot{R}\} + [K] \{vR\} = \{F(x,y,t)\} \tag{3}$$

where $[M]$ = total structural mass matrix

        $[\bar{M}]$ = total damping matrix

        $[K]$ = assembled stiffness matrix

        R = time function

        $\{v\}$ = nodal point displacement vector

        $\{F(x,y,t)\}$ = nodal point force vector

3. STRUCTURAL AND VEHICULAR IDEALIZATION

3.1 Bridge Idealization

For the development of the reported approach an existing bridge, Lehighton Bridge[*], is utilized. A detailed description of the Lehighton Bridge is given in Fritz Engineering Laboratory Report No. 349.4 (Ref. 14). The superstructure consists of three 71 ft. 6 in. length simply supported spans with 90° skew. The reinforced concrete bridge slab has a minimum nominal thickness of 7-1/2 in. and is supported by six 24/45 prestressed concrete I-beams with center-to-center spacing of 6 ft. 9 in. Elevation, cross section, and slab details are shown in Figs. 1 through 3, respectively. In the reported study, interest is focused on the vehicle induced dynamic response of the center span of the bridge.

Bridge surface irregularities tend to incrase the dynamic effect of the moving load. In previous analytical studies the entire bridge span was modeled as a single beam (Refs. 4,5,15), where various sine and parabolic bridge surface variations have been assumed. Experimental studies have been conducted including the effects of the approach profiles, bridge surface, and local disturbances (Refs. 3,4,14). In the present analysis the road surface is assumed to be free of irregularities.

---

[*] Located near Lehighton, Pennsylvania, carries L.R. 164-8 over Pohopoco Creek.

Damping to some degree is present in the bridge systems. Experiments carried out on prestressed concrete bridges indicated that damping is negligible (Refs. 4,8). In this study the damping matrix is assumed to be a null matrix.

In accordance with the Finite Element Method, the bridge superstructure was discretized utilizing a mesh consisting of 20 slab elements and 24 beam elements connected at the node points as shown in Fig. 4. Each prestressed concrete I-beam was divided longitudinally into 4 beam elements. A slab element occupied the entire lateral distance between each set of I-beams and extended one-fourth of the length of the bridge in the longitudinal direction. The structural idealization has 30 node points with 3 unknown displacements (vertical displacement and rotations about x and y axes) per node, making a total of 90 degrees of freedom.

The bridge slab was modeled using a Quadrilateral Element, known as Q-19, assembled from four linear Curvature Compatible Triangular elements, known as LCCT. Detailed description of the derivation of the plate finite elements can be found in Ref. 2. In this study the emphasis is placed on the application of this element to dynamic problems. Only a brief outline of major concepts is presented. The LCCT Element with 12 degrees of freedom, designated as LCCT-12, is composed of three subelements, as shown in Fig. 5a. The subelement displacement field is described by the 10 term cubic polynomial

$$w(x,y) = A_1 + A_2 x + A_3 y + A_4 x^2 + A_5 xy + A_6 y^2$$

$$+ A_7 x^3 + A_8 x^2 y + A_9 xy^2 + A_{10} y^3 \tag{4}$$

Reduction of the LCCT-12 element with 12 degrees of freedom to an LCCT-11 element with 11 degrees of freedom may be accomplished by assuming the slope at the midpoint of the external edge to be an average of the two slopes at the adjacent node points. Four LCCT-11 triangular elements are then assembled to form a quadrilateral, as shown in Fig. 5b, having 12 external degrees of freedom and 7 internal degrees of freedom.

It has been reported that little is to be gained by using the consistent mass model over the lumped mass model (Ref. 2). The lumped mass model is used and forms a diagonal matrix where the contributions to each node point by the bridge slab, beams, parapet section, curb section, and truck are considered (see Appendix).

The Finite Element program that was used considers only symmetrically stiffened plates. Obviously the beam-slab system of the bridge does not fall into this category. To overcome this handicap a modified beam stiffness was used which was approximated as the moment of inertia of the composite section about its gravity axis.

3.2 Vehicle Idealization

The vehicle may be idealized as a system of springs,

dash-pots and masses as shown in Fig. 6a (Refs. 4,5,12,13,15).
Experimental values for the tire-spring, suspension-spring, and
damping characteristics for certain vehicular systems have been
reported (Ref. 4).

A constant force model was adopted, whereby the force
exerted by each tire was assumed to remain constant for the en-
tire run time. Each wheel group was idealized as a concentrated
load, and is linearly distributed to the nearest node points.
The front, drive, and rear axle groups applied a total constant
force of 10.2 kips, 32.2 kips, and 32.67 kips respectively with
wheel spacing as shown in Fig. 6b. This model simulates the
AASHO HS 20-44 design vehicle.

4. NUMERICAL INTEGRATION

The Fourth Order Runge-Kutta numerical integration scheme with Runge Coefficients is used to integrate the equations of motion (Eq. 3) and obtain displacements of node points for particular time values (Ref. 7). Pilot studies carried out on small dynamic models using Runge-Kutta and Newmark's β-parameter (Ref. 9) integration techniques have shown that the Runge-Kutta approach is more efficient; consequently this approach is used throughout the investigation. The Runge-Kutta scheme is applicable to initial value problems and in the present application initial displacement and velocity fields are prescribed.

Equation 3 may be written as

$$[M] \{v\ddot{R}\} + [K] \{vR\} = \{F(t)\} \tag{5}$$

in which the damping contribution has been neglected. Rearrangement of Equation 5 yields

$$\{\ddot{w}\} = [M]^{-1} \{ \{F(t)\} - [K] \{w\} \} \tag{6}$$

$\{w\}$ is the nodal point displacement vector equal to $\{vR\}$ and $\{\ddot{w}\}$ indicates the nodal accelerations.

An advantage of using the lumped mass model is that the inverse of $[M]$ is a diagonal matrix where

$$
\begin{bmatrix}
M_{11} & 0 & . & . & 0 \\
0 & M_{22} & . & . & 0 \\
. & . & . & . & 0 \\
. & . & . & . & 0 \\
0 & 0 & 0 & 0 & M_{NN}
\end{bmatrix}^{-1}
=
\begin{bmatrix}
1/M_{11} & 0 & . & . & 0 \\
0 & 1/M_{22} & . & . & 0 \\
. & . & . & . & 0 \\
. & . & . & . & 0 \\
0 & 0 & 0 & 0 & 1/M_{NN}
\end{bmatrix}
\tag{7}
$$

Equation 6 in expanded form may be expressed as

$$
\ddot{w}_1 = 1/M_{11} \left[F_1 - k_{11} w_1 - k_{12} w_2 \ldots - k_{1N} w_N \right]
$$

$$
\ddot{w}_2 = 1/M_{22} \left[F_2 - k_{21} w_1 - k_{22} w_2 \ldots - k_{2N} w_N \right]
$$

$$
\ddot{w}_N = 1/M_{NN} \left[F_N - k_{N1} w_1 - k_{N2} w_2 \ldots - k_{NN} w_N \right]
\tag{8}
$$

The determination of the dynamic response of the bridge superstructure, which is mathematically modeled by Equation 8, entails the following computational steps:

1. Assemble the stiffness matrix, [K], utilizing the finite element technique.

2. Define a time interval, H, such that the numerical stability and accuracy requirements are met.

3. Define an initial displacement and velocity field for time t.

4. Compute vector $\{k_1\}$ where

$$\{k_1\} = \frac{H^2}{2} [M]^{-1} \left\{ \{F\} - [K] \{w\} \right\} \tag{9}$$

$[M]^{-1}$ and $\{F\}$ are evaluated at time t and $\{w\}$ is the displacement vector for time t.

5. Compute vectors $\{k_2\}$ and $\{k_3\}$ where $\{k_3\}$ equals $\{k_2\}$ and

$$\{k_2\} = \frac{H^2}{2} [M]^{-1} \left\{ \{F\} - [K] \left\{ \{w\} + \frac{H}{2} \{\dot{w}\} + \frac{1}{4} \{k_1\} \right\} \right\} \tag{10}$$

$[M]^{-1}$ and $\{F\}$ are evaluated at time $t + \frac{H}{2}$.

6. Compute vector $\{k_4\}$ where

$$\{k_4\} = \frac{H^2}{2} [M]^{-1} \left\{ \{F\} - [K] \left\{ \{w\} + H \{\dot{w}\} + \{k_3\} \right\} \right\} \tag{11}$$

$[M]^{-1}$ and F are evaluated at time $t + H$.

7. Compute the new displacement vector for time $t + H$ where

$$\{w(t+H)\} = \{w(t)\} + H \{\dot{w}(t)\} + \frac{1}{3} \left\{ \{k_1\} + \{k_2\} + \{k_3\} \right\} \tag{12}$$

8. Compute the new velocity vector where

$$\{\dot{w}(t+H)\} = \{\dot{w}(t)\} + \frac{1}{3H} \left\{ \{k_1\} + 2\{k_2\} + 2\{k_3\} + \{k_4\} \right\} \tag{13}$$

9. Go to step 4 and repeat procedure to obtain the displacement and velocity vectors for succeeding time intervals.

Initial trial runs were made to determine the maximum time step size that could be used without causing numerical instability in the integration scheme. A one milisecond time step size was used after observing that a smaller step size of .5 miliseconds did not result in any appreciable change in the results.

Computer time required to solve the problem depends on the vehicular speed. Analysis of the superstructure with the vehicle traversing at 50 mph required 866 central processing seconds and 1,055 peripheral processing seconds for 1,500 Runge-Kutta integration cycles. Generation and printing of the nodal point forces, the displacements, the element internal moments and the nodal moments averaged over the plate element are included in the computer time. Above figures were obtained at the CDC-6400 installation at Lehigh University Computing Center. It is recognized that different computing systems will have different time requirements.

4.1 Damped Vibration

Damping can easily be incorporated into the solution scheme. The equations for $\{k_1\}$, $\{k_2\}$, $\{k_3\}$ and $\{k_4\}$ can be modified according to the following relations

$$\{k_1\} = \frac{H^2}{2} [M]^{-1}\{ \{F\} - [K] \{w\} - [\bar{M}] \{\dot{w}\} \} \qquad (14)$$

[M] and $\{F\}$ evaluated at time t

$$\{k_2\} = \frac{H}{2}^2 [M]^{-1} \{ \{F\} - [K] \{ \{w\} + \frac{H}{2} \{\dot{w}\} + \frac{1}{4} \{k_1\} \}$$

$$- [\bar{M}] \{ \{\dot{w}\} + \frac{1}{H} \{k_1\} \} \} \tag{15}$$

$[M]$ and $\{F\}$ evaluated at $t + \frac{H}{2}$

$$\{k_3\} = \frac{H}{2}^2 [M]^{-1} \{ \{F\} - [K] \{ \{w\} + \frac{H}{2} \{\dot{w}\} + \frac{1}{4} \{k_1\} \}$$

$$- [\bar{M}] \{ \{\dot{w}\} + \frac{1}{H} \{k_2\} \} \} \tag{16}$$

$[M]$ and $\{F\}$ evaluated at $t + \frac{H}{2}$

$$\{k_4\} = \frac{H}{2}^2 [M]^{-1} \{ \{F\} - [K] \{ \{w\} + H \{\dot{w}\} + \{k_3\} \}$$

$$- [\bar{M}] \{ \{\dot{w}\} + \frac{2}{H} \{k_3\} \} \} \tag{17}$$

$[M]$ and $\{F\}$ evaluated at $t + H$

The new displacement and velocity vectors for time $t + H$ can be calculated using Equations 12 and 13.

4.2 Condensed Matrix Formulation

If the system may be satisfactorily modeled using a smaller number of degrees of freedom per node, then it is advantageous to reduce the total number of degrees of freedom prior to

the integration of the equations of motion. Analysis could be undertaken assuming that rotational inertia terms contribute a negligible amount to the dynamic behavior of the system. The mass matrix will be singular if the rotational inertia terms are set equal to zero. It will not be possible to find the inverse of the mass matrix unless a condensation process is employed. The condensation process can be accomplished as follows (Ref. 10):

1. The equations of motion are

$$[M] \{\ddot{w}\} + [K] \{w\} = \{F\} \tag{18}$$

2. Partition the system so that the zero mass terms are separated,

$$\begin{bmatrix} [K_{pp}] & [K_{po}] \\ [K_{op}] & [K_{oo}] \end{bmatrix} \begin{Bmatrix} \{w_p\} \\ \{w_o\} \end{Bmatrix} + \begin{bmatrix} [M_p] & [0] \\ [0] & [0] \end{bmatrix} \begin{Bmatrix} \{\ddot{w}_p\} \\ \{\ddot{w}_o\} \end{Bmatrix} = \begin{Bmatrix} \{F_p\} \\ \{F_o\} \end{Bmatrix} \tag{19}$$

3. Form two separate sets of equations,

$$[K_{pp}] \{w_p\} + [K_{po}] \{w_o\} + [M_p] \{\ddot{w}_p\} = \{F_p\} \tag{20}$$

$$[K_{op}] \{w_p\} + [K_{oo}] \{w_o\} = \{F_o\} \tag{21}$$

4. Solve for $\{w_o\}$ from Equation 21,

$$\{w_o\} = [K_{oo}]^{-1} \{\{F_o\} - [K_{op}] \{w_p\}\} \tag{22}$$

-13-

5. Substitute $\{w_o\}$ from Equation 22 into Equation 20 and solve for the acceleration,

$$\{\ddot{w}_p\} = [M_p]^{-1} \left\{ \{F_p\} - [K_{pp}] \{w_p\} - [K_{po}] [K_{oo}]^{-1} \{F_o\} \right.$$

$$\left. + [K_{po}] [K_{oo}]^{-1} [K_{op}] \{w_p\} \right\} \tag{23}$$

The condensed set of equations of motion can be solved using the following procedure:

1. Obtain a solution for $\{w_p\}$ by applying the Runge-Kutta procedure to equation 23.

2. Substitute $\{w_p\}$ into Equation 22 and solve for $\{w_o\}$.

3. Increment the time and start a new cycle.

It is not necessary to solve for the displacements associated with the zero mass terms if only the displacements associated with the non-zero mass terms are of interest. Thus, the Runge-Kutta integration procedure need only be applied to Equation 23.

5. RESULTS

Theoretical analyses were made for the following cases:

Truck Position	Speed
Lane 3	25 mph
Lane 3	50 mph
Lane 3	300 mph
Lane 5	50 mph

Beam and lane numbering are shown in Fig. 4. A non-dimensional distance or time factor, defined by either the ratio of (front-wheel distance)/(bridge length) or the (time of front-wheel travel)/(time for front-wheel to cross the bridge), is used to locate the truck position. Displacements in the upward direction and moments that produce tension on the bottom fibers are considered positive. Table 1 gives a summary of the displacement and bending moment plots which are of the following types:

1. Displacement or Bending Moment Time Histories (D.T.H. or B.M.T.H.) which are response traces of a group of node points or of a single node point while the truck travels across the bridge.

2. Beam Displacement Diagrams for various load positions (D. Diag.).

3. Bending Moment Diagrams for various load positions (B.M. Diag.).

4. Midspan displacement diagrams.

5. Midspan bending moment diagrams.

6. Contours of displacements.

7. Contours of beam bending moments.

5.1 Lane 3 Runs

Figures 7 through 30 show the displacement and bending
moment time histories for the 25 mph and 50 mph cases of the
nodal point groups (2,3,4), (7,8,9), (12,13,14), (17,18,19),
(22,23,24), and (27,28,29) representing points on beams F,E,D,C,B
and A as shown in Fig. 4. The dynamic and static nodal point
responses are plotted on the same graph so that comparisons are
easily made. The dynamic response appears as an almost symmetric
oscillation about the smooth static response curve. At a dis-
tance ratio of 1.467 the rear axle of the vehicle leaves the
bridge span and the static response becomes zero. The dynamic
oscillations still persist and the analysis is stopped at approxi-
mately a distance ratio of 1.5. The period of forced vibration
for the 25 mph case and 50 mph case are approximately equal. It
should be noted that the figures corresponding to 25 mph cover a
time span of approximately 3 seconds. Those referring to 50 mph
cover approximately 1½ seconds.

The maximum computed deflection occurs at the midspan
node points for the grid used for any particular truck position
and beam as can be seen in Figs. 7,8,11,12,15,16,19,20,23,24,27

and 28. The maximum computed beam bending moments occur at the midspan node points for the grid used, as can be seen in Figs. 9,10,13,14,17,18,21,22,25,26,29 and 30. As expected, the point of maximum moment in those beams under the wheels moves along the beam as the vehicle moves across the bridge (Figs. 21,22,25 and 26). The points of maximum computed beam bending moments and corresponding distance ratios can be tabulated as follows:

Points of Maximum Moment	Distance Ratio
Nodes 17 and 22	0.0 to 0.51
Nodes 18 and 23	0.51 to 1.07
Nodes 19 and 24	1.07 to 1.467

Beams A,B,C,D and E have maximum deflections in the downward direction and maximum moments which produce tension in the bottom fibers. Beam F deflects upward and is under negative bending moment producing tension in the top fibers. This is caused primarily by the unsymmetrical lane 3 loading and the magnitude of the curb-beam stiffness which was twice the value used for an interior beam. The largest value from the envelopes of maximum moment and deflection are located at midspan. Figures 31 through 34 compare the maximum midspan response of all the beams. Maximum static responses occur at a distance ratio of 0.738 for the midspan node points, while the maximum dynamic responses occur between 0.707 and 0.831 depending on the particular node point and the vehicular speed involved.

The maximum deflection and moment of the bridge occurs at node point 23, located at the midspan of beam B, followed by node points 18,28,13,8 and 3 arranged in a decreasing order of magnitude. The value of the negative moment at node point 3 on the curb beam is approximately $\frac{1}{15}$ the magnitude of the maximum moment at node point 23, while the deflection is $\frac{1}{30}$ the maximum deflection at node point 23.

Figures 35 through 38 show the response of node point 3 for the 25 mph and 50 mph lane 3 cases plotted in an enlarged scale. A dynamic response with larger amplitudes are present for the 50 mph case as compared to the 25 mph run.

Figures 39 and 40 show the influence of excluding the (Ad^2) term of the composite section on the displacement time history of node points 23 and 3. Reducing the stiffness by assuming the modified beam plate superstructure to be symmetrically stiffened changes the deflection time histories as follows:

1. Node point 23 - Fig. 39

     a) Deflection increase of 40%

     b) Frequency decrease of 25%

2. Node point 3 - Fig. 40

     a) Static deflection shape reversed into the negative range

     b) Decrease in static deflection of 50%

     c) Increase in dynamic deflection of 250%

d) Decrease in frequency of 38%

A critical velocity of approximately 500 mph was calculated considering the entire bridge structure as a single beam (Ref. 8). Figures 41 through 44 show the displacement and bending moment time histories of the midspan node points for the 300 mph lane 3 loading. The dynamic load factor associated with the maximum deflection is 1.56 as opposed to 1.07 for the 25 mph and 50 mph cases.

Figures 43 and 44 show the response time histories of node point 3 for the 300 mph lane 3 case plotted in an enlarged scale. Nodal point 3 moves through one complete cycle while the truck is on the span and has an amplification factor equal to 2.49.

Figures 45 through 50 are plots of beam B displacement and bending moment diagrams. The diagrams are numbered in time sequence with a distance ratio interval between the diagrams of 0.1231. The figures include static lane 3, 25 mph lane 3, and 50 mph lane 3 cases. Figures 47 and 48 show beam B deflected upward and subjected to a negative internal moment.

The deflection and moment diagrams for the maximum dynamic state and the static state of beam B and the dynamic state of beam F are plotted for comparison in Figs. 51,52,53 and 54. These figures correspond to the 25 mph lane 3 case at a distance ratio of 0.738 and the 50 mph lane 3 case at a distance ratio of 0.707 respectively.

Figures 55 through 60 show the midspan deflection and moment diagrams for the static lane 3, the 25 mph lane 3, and the 50 mph lane 3 cases. The diagrams are numbered in sequence with a distance ratio interval between the diagrams of 0.1231. Node point 3 is located on the extreme left-hand side of the plots with node point 28 located on the right-hand side. Maximum deflection and moment occurs at node point 23 on beam B except for the case when the node line has a convex deflection shape upwards as shown in Figs. 57 and 59.

5.2 Lane 5 Runs

Fifty mph lane 5 plots are shown in Figs. 61 through 84. The lane 5 loading is symmetrical about the center-line of the bridge. However, due to the absence of a curb and parapet section on one side of the bridge non-symmetric response develops.

Figures 61 through 72 show the displacement and bending moment time histories of beams F,E,D,C,B and A. As indicated in the discussion of lane 3 runs, the dynamic response appears as an almost symmetric oscillation about the smooth static response. The maximum deflection of the beams occurs at midspan regardless of truck position. The maximum moment of beams A,B,E and F, which are not directly under the wheels, occur at midspan. The points of maximum computed beam bending moments and corresponding distance ratios for beams C and D which are directly under the truck wheels can be tabulated as follows:

Points of Maximum Moment	Distance Ratio
Nodes 12 and 17	0.0 to 0.51
Nodes 13 and 18	0.51 to 1.07
Nodes 14 and 19	1.07 to 1.467

The midspan beam deflection and bending moment time histories are plotted in Figs. 73 and 74. The maximum response occurs at node 18 on beam C. This is expected because node point 13 is influenced to a greater extent than node point 18 by the additional stiffness provided by the curb and parapet section. The maximum deflection of beam F is $\frac{1}{12}$ of that of beam C. There is a pronounced difference between the dynamic response of beams A and F. This difference is due to the existence of the curb and parapet section over beam F only. All nodal deflections are in the downward sense and nodal moments produce tension in the bottom fibers, except where dynamic oscillations near the end of the run produce positive deflections and negative moments.

Deflection and moment diagrams for beam C are plotted for distance ratio intervals of 0.1231 in Figs. 75 through 78, corresponding to the static and 50 mph lane 5 runs.

The deflection and moment diagrams at distance ratios of 0.707 and 0.676 for the maximum dynamic response and the static response of beam C and the dynamic response of beam F are given in Figs. 79 and 80. Figures 81 through 84 present the midspan deflection and moment diagrams corresponding to static and 50 mph lane 5 runs.

5.3 Contour Plots

Displacement and beam bending moment contours are plotted in the figures enumerated below:

Figure	Case
85 through 92	25 mph - lane 3
93 through 100	50 mph - lane 3
101 through 108	50 mph - lane 5

Contour values corresponding to the contour symbols used in the plots are given in Table 11.

Contours for the maximum displacement and bending moment states are shown in Figs. 85,86,93,94,101 and 102 for the three cases. Contour displacement sequences and corresponding bending moment sequences as the rear axle leaves the bridge are presented to illustrate the bridge vibration characteristics as the response of the superstructure approaches the state of free vibration. From the displacement contours, it is apparent that the bridge deck vibrates in elliptical dish shaped patterns with the major axis of the ellipse parallel to the bridge axis. This is expected since this shape corresponds to the first mode of a plate. A line parallel to the major axis of the ellipse is also seen to correspond to the first modal shape of a simply supported beam.

6. COMPARISON WITH EXPERIMENTAL RESULTS

The analytical (computed) results are compared to the Lehighton Bridge field test results (Ref. 14). Experimental and analytical static deflection and moment values for the transverse midspan node points are listed in Table 2. The maximum static lane 3 computed deflection is -0.1241 in. at node 23 with a corresponding moment of 3350 in-kip while the field test indicated a maximum deflection of -0.090 in. with a moment of 3530 in-kip. The maximum static lane 5 computed deflection and moment are -0.1185 in. and 3251 in-kip occurring at node 18 while the experimental maximums are -0.078 in. and 3401 in-kip occurring at node 13.

The ratio values which are defined as the analytical (computed) results divided by the experimental results are listed in Table 3. They indicate that the computed moments are much closer to the experimental values than the computed deflections. The computed moments have an average error of 10% while the computed deflections have an average error of 40%.

Theoretical results show beam F deflecting upward for a lane 3 loading, as in the case of an experimental lane 2 load, but opposite to an experimental lane 3 loading. Node 3 deflection ratio values of -0.67 and 0.43, corresponding to lane 3 and lane 5 loads respectively, indicate that the stiffness of beam F has been overestimated. Beams A,B,C,D and E exhibit deflection

-23-

ratios greater than 1.0 which indicate that the stiffness has been underestimated.

The neutral axis position and the degree of end restraint vary with the load position in the actual structure (Ref. 1, 14). Considering beams away from the loaded lane shows that the position of the neutral axis falls closer to that of the basic section as the distance from the loaded lane increases. This is reflected in the deflection ratio values which change with the location of the loaded lane and beam position. The deflection ratios for a particular beam should decrease as the distance between the loaded lane and the beam in question increases. This is shown in Table 4 where the deflection ratio values of beams A and B decrease while those of beams D,E and F increase when going from the lane 3 to lane 5 loading.

The midspan dynamic response for deflection (DEF) and moment (Mom.) with the corresponding dynamic load factors, $(DLF)_d$ and $(DLF)_m$, for lane 3 and lane 5 speed runs are listed in Tables 4 and 5 respectively. The total dynamic load factor, as defined in Table 4, provides a measure of the overall dynamic amplification. Beams which are not directly under the load tend to have higher amplification factors than those beams directly under the load. It should not be inferred from this that the maximum dynamic stress necessarily occurs at the beam with the maximum amplification factor. The maximum stress is, of course, a function of the maximum live load stress as well as the amplification factor.

The computed and experimental dynamic load factors for deflection and moment are listed in Tables 6 and 7. The experimental cases differ from the theoretical cases where noted. All computed amplification factors were greater than 1.0 while 16 out of the 36 experimental values were less than 1.0. The computed amplification factors were always maximum for beam F. This was usually the case for experimental results, although not always. Unlike the edge beams, the interior beams did not exceed the AASHO impact factor in both experimental and theoretical analyses.

Experimental and computed moment distribution coefficients are reported in Tables 8 and 9 for lanes 3 and 5 respectively. Moment distribution coefficients for the static lane 3 and lane 5 cases are plotted in Figs. 109 and 110. The largest discrepancies occur at beam F.

Experimental deflection time histories are shown in Figs. 111 and 112 for node 23 on beam B and in Fig. 113 for node 13 on beam D. These figures correspond to the loading cases of 24.4 mph lane 2, 52.6 mph lane 2, and 54.5 mph lane 6 respectively. Inaccuracies may exist in the horizontal time scale of the figures due to the uncertainties involved in reading the experimental oscillograph traces. All three figures show the tendency of the dynamic response to oscillate around the static response curve in an irregular manner. An irregular response time history, which corresponds to the actual behavior, could be analytically obtained by using a spring-mass vehicle system rather

than the constant force system which gave a symmetric response about the static deflection curve.

Frequencies of vibration are listed in Table 10. The natural unloaded frequency of vibration was estimated by considering the entire cross section of the superstructure as a single beam (Ref. 8). Experimental and theoretical loaded frequencies were calculated by finding the average loaded frequency of vibration of beams B or D, corresponding to a lane 3 or a lane 5 loading respectively.

For lane 3 loading, the estimated natural frequency, (see Table 10) gives a higher value while the theoretical loaded frequencies based on the finite element technique give a lower estimate to the experimental loaded frequencies. For lane 5 loading both the loaded theoretical and estimated natural frequencies form a lower value to the experimental frequency. It may be noted that the lumped mass matrix idealization, as used in the reported study, may give either an upper or lower estimate to the true frequency of vibration depending on the particular problem (Ref. 2).

7. CONCLUSIONS AND RECOMMENDATIONS

A procedure for the dynamic analysis of highway bridges using the finite element method has been presented. The finite element program that was used in the theoretical analysis is applicable to symmetrically stiffened plates. Eccentricity of the beams was incorporated by the employment of a modified beam stiffness as mentioned in Section 3.1.

Comparisons between the experimental and theoretical behavior indicate differences of 40% for beam deflections and 10% for beam moments. The assumption of a constant force vehicle model rather than a spring-mass vehicle model produced almost symmetrical dynamic oscillations around the static response curve, unlike the more irregular experimental oscillations. Differences between the theoretical and experimental frequencies ranged from 4% to 28%.

Possible future research may include the following:

1. Idealization of the vehicle as a spring-mass system.

2. Modification of the finite element program to include unsymmetrically stiffened plates in a more refined manner.

3. Assessment of the effect of bridge end restraint, such as the neoprene pads, on the dynamic behavior.

4. Assessment of the effect of neglecting the rotary inertia terms in the formulation of the equations of motion.

5. Evaluation of the effect of vehicle position on bridge properties.

6. Investigation of the effect of discretization on the static and dynamic results.

8. APPENDIX - MASS MATRICES

A. Interior Slab Element
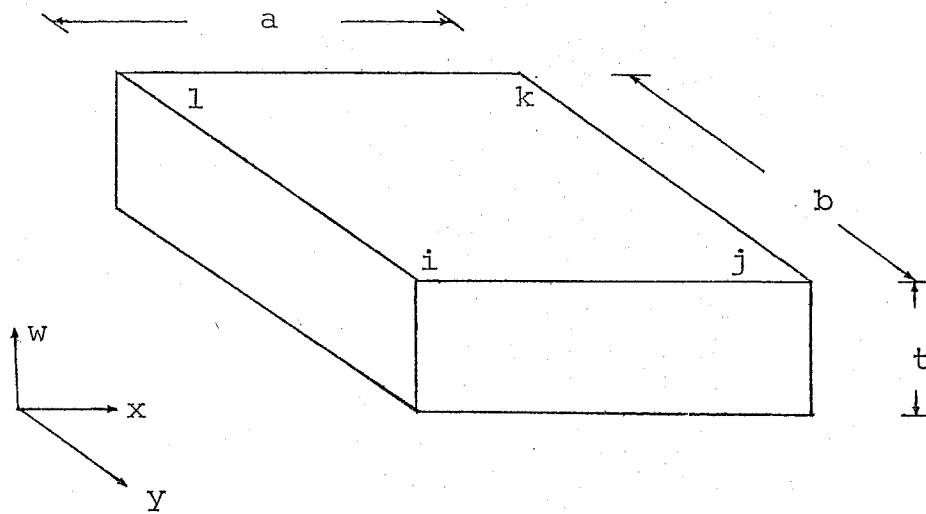
The lumped mass contribution to node i, j, k, or l:

$$\frac{1}{4} \begin{bmatrix} M_w & 0 & 0 \\ 0 & Im_x & 0 \\ 0 & 0 & Im_x \end{bmatrix}$$

$$M_w = p \ a \ b \ t$$

$$Im_x = p \ b \ I_x$$

$$Im_y = p \ a \ I_y$$

where   p   =   the density

a   =   the x dimension

b   =   the y dimension

t   =   the thickness

I_x =   the moment of inertia around the x-axis

I_y =   the moment of inertia around the y-axis

B.   Beam Element
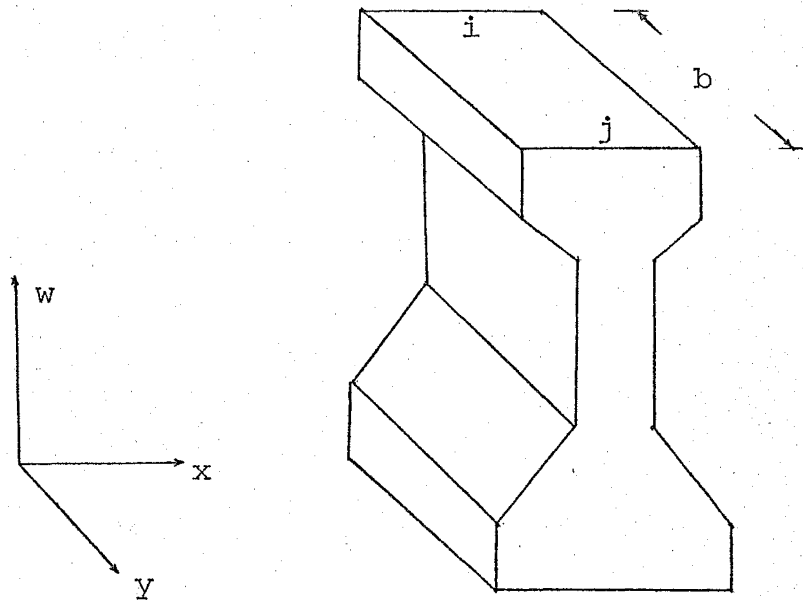
The lumped mass contribution to node i and j:

$$\frac{1}{2} \begin{bmatrix} M_w & 0 & 0 \\ 0 & Im_x & 0 \\ 0 & 0 & Im_y \end{bmatrix}$$

$$M_w = p \ vol$$

$$Im_x = p \ b \ I_x$$

$$Im_y = p \ b \ J$$

where   vol = the volume

         J   = the polar moment of inertia

C. Truck

The lumped mass contribution to node i:

$$\begin{bmatrix} (Mt)_i & 0 & 0 \\ 0 & 0 & 0 \\ 0 & 0 & 0 \end{bmatrix}$$

$$(Mt)_i = (Ft/g)_i$$

where   Ft = the external truck force at node i

         g = the acceleration due to gravity

-31-

9. ACKNOWLEDGMENTS

10. TABLES

TABLE 1   SUMMARY OF RESPONSE FIGURES

Figure	Beam (Nodal Points)	Description of Figure	Case: MPH – Lane
7		D.T.H.	25 – 3
8	F(2,3,4)	D.T.H.	50 – 3
9		B.M.T.H.	25 – 3
10		B.M.T.H.	50 – 3
11		D.T.H.	25 – 3
12	E(7,8,9)	D.T.H.	50 – 3
13		B.M.T.H.	25 – 3
14		B.M.T.H.	50 – 3
15		D.T.H.	25 – 3
16	D(12,13,14)	D.T.H.	50 – 3
17		B.M.T.H.	25 – 3
18		B.M.T.H.	50 – 3
19		D.T.H.	25 – 3
20	C(17,18,19)	D.T.H.	50 – 3
21		B.M.T.H.	25 – 3
22		B.M.T.H.	50 – 3
23		D.T.H.	25 – 3
24	B(22,23,24)	D.T.H.	50 – 3
25		B.M.T.H.	25 – 3
26		B.M.T.H.	30 – 3
27		D.T.H.	25 – 3
28	A(27,28,29)	D.T.H.	50 – 3
29		B.M.T.H.	25 – 3
30		B.M.T.H.	50 – 3

TABLE 1   SUMMARY OF RESPONSE FIGURES
(Continued)

Figure	Beam (Nodal Points)	Description of Figure	Case: MPH – Lane
31		Midspan D.T.H.	25 – 3
32	(3,8,13,18,23,28)	Midspan D.T.H.	50 – 3
33		Midspan B.M.T.H.	25 – 3
34		Midspan B.M.T.H.	50 – 3
35		D.T.H.	25 – 3
36	F(3)	D.T.H.	50 – 3
37		B.M.T.H.	25 – 3
38		B.M.T.H.	50 – 3
39	B(23)	D.T.H.	50 – 3
40	F(3)	D.T.H.	50 – 3
41	(3,8,13,18,23,28)	Midspan D.T.H.	300 – 3
42	(3,8,13,18,23,28)	Midspan B.M.T.H.	300 – 3
43	F(3)	D.T.H.	300 – 3
44	F(3)	B.M.T.H.	300 – 3
45		D. Diag.	Static – 3
46		B.M. Diag.	Static – 3
47	B(21,22,23,24,25)	D. Diag.	25 – 3
48		B.M. Diag.	25 – 3
49		D. Diag.	50 – 3
50		B.M. Diag.	50 – 3

TABLE 1   SUMMARY OF RESPONSE FIGURES
(Continued)

Figure	Beam (Nodal Points)	Description of Figure	Case: MPH – Lane
51		D. Diag.	Static and 25 – 3
52	B and F	B.M. Diag.	Static and 25 – 3
53		D. Diag.	Static and 50 – 3
54		B.M. Diag.	Static and 50 – 3
55		Midspan D. Diag.	Static – 3
56		Midspan B.M. Diag.	Static – 3
57	(3,8,13,18,23,28)	Midspan D. Diag.	25 – 3
58		Midspan B.M. Diag.	25 – 3
59		Midspan D. Diag.	50 – 3
60		Midspan B.M. Diag.	50 – 3
61	F(2,3,4)	D.T.H.	50 – 5
62		B.M.T.H.	50 – 5
63	E(7,8,9)	D.T.H.	50 – 5
64		B.M.T.H.	50 – 5
65	D(12,13,14)	D.T.H.	50 – 5
66		B.M.T.H.	50 – 5
67	C(17,18,19)	D.T.H.	50 – 5
68		B.M.T.H.	50 – 5
69	B(22,23,24)	D.T.H.	50 – 5
70		B.M.T.H.	50 – 5

TABLE 1   SUMMARY OF RESPONSE FIGURES
(Continued)

Figure	Beam (Nodal Points)	Description of Figure	Case: MPH – Lane
71	A(27,28,29)	D.T.H.	50 – 5
72		B.M.T.H.	50 – 5
73	(3,8,13,18,23,28)	Midspan D.T.H.	50 – 5
74		Midspan B.M.T.H.	50 – 5
75	C(16,17,18,19,20)	D. Diag.	Static – 5
76		B.M. Diag.	Static – 5
77		D. Diag.	50 – 5
78		B.M. Diag.	50 – 5
79	C and F	D. Diag.	Static and 50 – 5
80		B.M. Diag.	Static and 50 – 5
81	(3,8,13,18,23,28)	Midspan D. Diag.	Static – 5
82		Midspan B.M. Diag.	Static – 5
83		Midspan D. Diag.	50 – 5
84		Midspan B.M. Diag.	50 – 5
85	(Contour Plot)	Displ. at 0.738	25 – 3
86		B.M. at 0.738	25 – 3
87		Displ. at 1.446	25 – 3
88		Displ. at 1.476	25 – 3
89		Displ. at 1.507	25 – 3
90		B.M. at 1.446	25 – 3
91		B.M. at 1.476	25 – 3
92		B.M. at 1.507	25 – 3

TABLE 1   SUMMARY OF RESPONSE FIGURES
(Continued)

Figure	Beam (Nodal Points)	Description of Figure	Case: MPH – Lane
93		Displ. at 0.707	50 – 3
94		B.M. at 0.707	50 – 3
95		Displ. at 1.415	50 – 3
96		Displ. at 1.446	50 – 3
97	(Contour Plot)	Displ. at 1.476	50 – 3
98		B.M. at 1.415	50 – 3
99		B.M. at 1.446	50 – 3
100		B.M. at 1.476	50 – 3
101		Displ. at 0.707	50 – 5
102		B.M. at 0.707	50 – 5
103		Displ. at 1.446	50 – 5
104	(Contour Plot)	Displ. at 1.476	50 – 5
105		Displ. at 1.507	50 – 5
106		B.M. at 1.446	50 – 5
107		B.M. at 1.476	50 – 5
108		B.M. at 1.507	50 – 5
111	B(23)	Experimental D.T.H.	24.4 – 2
112	B(23)	Experimental D.T.H.	52.6 – 2
113	D(13)	Experimental D.T.H.	54.5 – 6

TABLE 2   EXPERIMENTAL AND COMPUTED STATIC MIDSPAN

GIRDER DEFLECTIONS AND MOMENTS

| Beam (Node) | Deflections (in) | | | | Moments (in-kip) | | | |
| | Static – Lane 3 | | Static – Lane 5 | | Static – Lane 3 | | Static – Lane 5 | |
	Comp.	Exper.	Comp.	Exper.	Comp.	Exper.	Comp.	Exper.
A(28)	-.0842	-.068	-.0186	-.026	+2107.	+1905.	+465.	+541.
B(23)	-.1241	-.090	-.0705	-.053	+3350.	+3530.	+1887.	+1763.
C(18)	-.1188	-.080	-.1185	-.075	+3259.	+3168.	+3251.	+3048.
D(13)	-.0702	-.052	-.1174	-.078	+1879.	+1922.	+3224.	+3401.
E(8)	-.0260	-.021	-.0666	-.047	+699.	+772.	+1782.	+1747.
F(3)	+.0027	-.004	-.0104	-.024	-150.	+184.	+572.	+1003.

TABLE 3 STATIC MIDSPAN GIRDER DEFLECTION AND MOMENT RATIOS

$$\text{Deflection Ratio} = \frac{\text{Computed Deflection}}{\text{Experimental Deflection}}$$

$$\text{Moment Ratio} = \frac{\text{Computed Moment}}{\text{Experimental Moment}}$$

Beam (Node)	Deflection Ratio		Moment Ratio	
	Lane 3	Lane 5	Lane 3	Lane 5
A(28)	+1.24	+0.72	+1.11	+0.86
B(23)	+1.34	+1.33	+0.95	+1.07
C(18)	+1.48	+1.58	+1.03	+1.07
D(13)	+1.35	+1.51	+0.98	+0.95
E(8)	+1.24	+1.42	+0.91	+1.02
F(3)	−0.67	+0.43	−0.82	+0.57
Average % Error	34.5	44.8	8.0	13.0

TABLE 4 LANE 3 COMPUTED MIDSPAN GIRDER DEFLECTIONS (DEF.), MOMENTS (MOM),

AND CORRESPONDING DYNAMIC LOAD FACTORS (DLF)[1]

Beam (Node)	25 MPH – Lane 3				50 MPH – Lane 3			
	DEF. (in)	$(DLF)_d$	MOM. (in-kip)	$(DLF)_m$	DEF. (in)	$(DLF)_d$	MOM. (in-kip)	$(DLF)_m$
A(28)	-0.0925	1.098	+2321.	1.102	-0.0910	1.081	+2282.	1.083
B(23)	-0.1324	1.067	+3523.	1.052	-0.1321	1.064	+3573.	1.067
C(18)	-0.1260	1.060	+3345.	1.026	-0.1261	1.061	+3431.	1.053
D(13)	-0.0751	1.010	+2011.	1.010	-0.0749	1.067	+2011.	1.070
E(8)	-0.0287	1.104	+772.	1.104	-0.0289	1.108	+773.	1.106
F(3)	+0.0036	1.334	-202.	1.347	+0.0046	1.704	-256.	1.707
Total[2,3,4] (DLF)		1.076		1.06		1.075		1.08

[1] $(DLF) = \dfrac{\text{Maximum Dynamic Response}}{\text{Maximum Static Response}}$

[2] $\Sigma^{*} = 0.86\ D_A + D_B + D_C + D_D + D_E + 1.41\ D_F$ (Ref. 2)

[3] $\text{Total } (DLF)_d = \dfrac{\Sigma^{*}\ \text{Dynamic DEF.}}{\Sigma^{*}\ \text{Static DEF.}}$

[4] $\text{Total } (DLF)_m = \dfrac{\Sigma\ \text{Dynamic MOM.}}{\Sigma\ \text{Static MOM.}}$

TABLE 5 LANE 5 COMPUTED MIDSPAN GIRDER DEFLECTIONS (DEF),

MOMENTS (MOM.), AND CORRESPONDING DYNAMIC LOAD FACTORS (DLF)

50 MPH - Lane 5

Beam (Node)	DEF. (in)	$(DLF)_d$	MOM. (in-kip)	$(DLF)_m$
A(28)	-0.0242	1.301	+604.	1.299
B(23)	-0.0756	1.072	+2029.	1.075
C(18)	-0.1246	1.051	+3411.	1.049
D(13)	-0.1225	1.043	+3334.	1.034
E(8)	-0.0791	1.188	+1901.	1.067
F(3)	-0.0152	1.461	+835.	1.460
Total (DLF)		1.1		1.08

TABLE 6 EXPERIMENTAL AND COMPUTED DEFLECTION DYNAMIC LOAD FACTORS, $(DLF)_d$

$$\text{AASHO Impact Factor } \left(1 + \frac{50}{125 + L}\right) = 1.255$$

Beam (Node)	25 MPH - Lane 3 Comp. $(DLF)_d$	25 MPH - Lane 3 Exper.[1] $(DLF)_d$	50 MPH - Lane 3 Comp. $(DLF)_d$	50 MPH - Lane 3 Exper.[2] $(DLF)_d$	50 MPH - Lane 5 Comp. $(DLF)_d$	50 MPH - Lane 5 Exper.[3] $(DLF)_d$
A(28)	1.098	0.92	1.081	0.93	1.301	1.08
B(23)	1.067	1.00*	1.064	1.02*	1.072	1.00
C(18)	1.060	0.93	1.061	0.96	1.051	0.99
D(13)	1.070	0.92	1.067	0.97	1.043	0.93
E(8)	1.104	0.73	1.108	1.00	1.188	0.95
F(3)	1.333	1.99*	1.704	1.33*	1.461	0.94
Total	1.076	0.93	1.075	0.96	1.10	0.96

[1] Experimental was for 24.4 MPH - Lane 2

[2] Experimental was for 52.6 MPH - Lane 2

[3] Experimental was for 54.5 MPH - Lane 6

* These values were calculated by the authors and are different from those reported in Ref. (2).

TABLE 7 EXPERIMENTAL AND COMPUTED MOMENT DYNAMIC LOAD FACTORS, $(DLF)_m$

$$\text{AASHO Impact Factor} = (1 + \frac{50}{125 + L}) = 1.255$$

Beam (Node)	25 MPH – Lane 3		50 MPH – Lane 3		50 MPH – Lane 5	
	Comp. $(DLF)_m$	Exper.[1] $(DLF)_m$	Comp. $(DLF)_m$	Exper.[2] $(DLF)_m$	Comp. $(DLF)_m$	Exper.[3] $(DLF)_m$
A(28)	1.102	1.08	1.083	1.06	1.299	1.08
B(23)	1.052	1.04	1.067	1.05	1.075	0.96
C(18)	1.026	1.05	1.053	1.03	1.049	0.98
D(13)	1.070	0.98	1.070	1.02	1.034	0.95
E(8)	1.104	1.21	1.106	1.21	1.067	0.88
F(3)	1.347	-4.24	1.707	-2.24	1.460	1.10
Total	1.06	1.07	1.08	1.06	1.08	.97

[1] Experimental was for 25.8 MPH – Lane 2

[2] Experimental was for 50.7 MPH – Lane 2

[3] Experimental was for 49.3 MPH – Lane 5

TABLE 8   EXPERIMENTAL AND COMPUTED LANE 3 MOMENT DISTRIBUTION COEFFICIENTS

$$\text{Distribution Coefficient (Computed)} = \frac{\text{Moment} \times 100}{\Sigma \text{ Moments}}$$

$$\text{Distribution Coefficient (Experimental)} = \frac{\text{Moment Coefficient} \times 100}{\Sigma \text{ Moment Coefficients}}$$

Beam (Node)	Static Lane 3		25 MPH Lane 3	50 MPH Lane 3
	Comp.	Exper.	Comp.	Comp.
A(28)	18.4	16.6	19.1	18.5
B(23)	29.3	30.7	29.1	29.0
C(18)	28.5	27.6	27.6	27.8
D(13)	16.4	16.7	16.6	16.3
E(8)	6.1	6.7	6.4	6.3
F(3)	-1.3	1.6	-1.7	-2.1

TABLE 9 EXPERIMENTAL AND COMPUTED LANE 5 MOMENT DISTRIBUTION COEFFICIENTS

Beam (Node)	Static - Lane 5		50 MPH - Lane 5	
	Comp.	Exper.	Comp.	Exper.[1]
A(28)	4.2	4.7	5.0	5.2
B(23)	16.9	15.3	16.7	15.2
C(18)	29.1	26.5	28.2	26.8
D(13)	28.8	29.6	27.5	29.1
E(8)	15.9	15.2	15.7	13.9
F(3)	5.1	8.7	6.9	9.8

[1] Experimental was for 49.3 MPH - Lane 5

TABLE 10   FREQUENCIES OF VIBRATION (CYCLES/SECOND)

Case Source	Lane 3		Lane 5
	25 MPH	50 MPH	50 MPH
Theoretical[1] (Single Beam Model)	5.7	5.7	5.7
Experimental[2,3]	5.4	5.5	6.8
Theoretical[2] (Finite Element)	5.2	4.9	4.9

[1] $f \text{ (cps)} = \dfrac{\pi}{2L^2} \sqrt{\dfrac{EI}{m}}$ (Ref. 8)

[2] Loaded frequency

[3] Experimental values correspond to the following cases:

    24.4 MPH — Lane 2
    52.6 MPH — Lane 2
    54.5 MPH — Lane 6

-47-

TABLE 11   CONTOUR VALUES

(Deflections in inches, Moments in inch-kips)

FIGURE 85

FIGURE 86

CONTOUR VALUE	CONTOUR SYMBOL	CONTOUR VALUE	CONTOUR SYMBOL
0.	1	3.5234736E+03	1
-1.0000000E-02	2	3.1955385E+03	2
-2.0000000E-02	3	2.8676037E+03	3
-3.0000000E-02	4	2.5396689E+03	4
-4.0000000E-02	5	2.2117341E+03	5
-5.0000000E-02	6	1.8837993E+03	6
-6.0000000E-02	7	1.5558646E+03	7
-7.0000000E-02	8	1.2279298E+03	8
-8.0000000E-02	9	8.9999500E+02	9
-9.0000000E-02	A	5.7200022E+02	A
-1.0000000E-01	B	2.4412544E+02	B
-1.1000000E-01	C	-8.3809329E+01	C
-1.2000000E-01	D		
-1.3000000E-01	E		

TABLE 11 CONTOUR VALUES

(Continued)

FIGURE 87

FIGURE 88

CONTOUR VALUE   CONTOUR SYMBOL

CONTOUR VALUE   CONTOUR SYMBOL

CONTOUR VALUE	CONTOUR SYMBOL	CONTOUR VALUE	CONTOUR SYMBOL
$1.1293612E-03$	•••••••••1	$8.0008359E-03$	•••••••••1
$8.0105770E-04$	•••••••••2	$7.4293469E-03$	•••••••••2
$4.7275437E-04$	•••••••••3	$6.8578587E-03$	•••••••••3
$1.4445103E-04$	•••••••••4	$6.2863705E-03$	•••••••••4
$-1.6385231E-04$	•••••••••5	$5.7148822E-03$	•••••••••5
$-5.1215565E-04$	•••••••••6	$5.1433940E-03$	•••••••••6
$-8.4045898E-04$	•••••••••7	$4.5719058E-03$	•••••••••7
$-1.1687623E-03$	•••••••••8	$4.0004176E-03$	•••••••••8
$-1.4970557E-03$	•••••••••9	$3.4289293E-03$	•••••••••9
$-1.8253690E-03$	•••••••••A	$2.8574411E-03$	•••••••••A
$-2.1536723E-03$	•••••••••B	$2.2859529E-03$	•••••••••B
$-2.4819757E-03$	•••••••••C	$1.7144647E-03$	•••••••••C
$-2.8102790E-03$	•••••••••D	$1.1429764E-03$	•••••••••D
$-3.1385823E-03$	•••••••••E	$5.7148822E-04$	•••••••••E
$-3.4668853E-03$	•••••••••F	$0.$	•••••••••F

TABLE 11   CONTOUR VALUES

(Continued)

FIGURE 89   FIGURE 90

CONTOUR VALUE   CONTOUR SYMBOL   CONTOUR VALUE   CONTOUR SYMBOL

CONTOUR VALUE	CONTOUR SYMBOL	CONTOUR VALUE	CONTOUR SYMBOL
0.	∗∗∗∗∗∗∗∗∗1	1.1715894E+02	∗∗∗∗∗∗∗∗∗1
-5.3234207E-04	∗∗∗∗∗∗∗∗∗2	1.0434283E+02	∗∗∗∗∗∗∗∗∗2
-1.0646841E-03	∗∗∗∗∗∗∗∗∗3	9.1526725E+01	∗∗∗∗∗∗∗∗∗3
-1.5970262E-03	∗∗∗∗∗∗∗∗∗4	7.8710622E+01	∗∗∗∗∗∗∗∗∗4
-2.1293683E-03	∗∗∗∗∗∗∗∗∗5	6.5894518E+01	∗∗∗∗∗∗∗∗∗5
-2.6617103E-03	∗∗∗∗∗∗∗∗∗6	5.3078415E+01	∗∗∗∗∗∗∗∗∗6
-3.1940524E-03	∗∗∗∗∗∗∗∗∗7	4.0262312E+01	∗∗∗∗∗∗∗∗∗7
-3.7263945E-03	∗∗∗∗∗∗∗∗∗8	2.7446208E+01	∗∗∗∗∗∗∗∗∗8
-4.2587366E-03	∗∗∗∗∗∗∗∗∗9	1.4630105E+01	∗∗∗∗∗∗∗∗∗9
-4.7910786E-03	∗∗∗∗∗∗∗∗∗A	1.8140015E+00	∗∗∗∗∗∗∗∗∗A
-5.3234207E-03	∗∗∗∗∗∗∗∗∗B	-1.1002102E+01	∗∗∗∗∗∗∗∗∗B
-5.8557628E-03	∗∗∗∗∗∗∗∗∗C	-2.3818205E-01	∗∗∗∗∗∗∗∗∗C
-6.3881048E-03	∗∗∗∗∗∗∗∗∗D	-3.6634309E+01	∗∗∗∗∗∗∗∗∗D
-6.9204469E-03	∗∗∗∗∗∗∗∗∗E	-4.9450412E+01	∗∗∗∗∗∗∗∗∗E
-7.4527882E-03	∗∗∗∗∗∗∗∗∗F	-0.2266509E+01	∗∗∗∗∗∗∗∗∗F

TABLE 11   CONTOUR VALUES

(Continued)

FIGURE   91

CONTOUR VALUE	CONTOUR SYMBOL
0.	+++++++++1
-2.0000000E+01	+++++++++2
-4.0000000E+01	+++++++++3
-6.0000000E+01	+++++++++4
-8.0000000E+01	+++++++++5
-1.0000000E+02	+++++++++6
-1.2000000E+02	+++++++++7
-1.4000000E+02	+++++++++8
-1.6000000E+02	+++++++++9
-1.8000000E+02	+++++++++A
-2.0000000E+02	+++++++++B

FIGURE   92

CONTOUR VALUE	CONTOUR SYMBOL
2.0023907E+02	+++++++++1
1.8589632E+02	+++++++++2
1.7155159E+02	+++++++++3
1.5720785E+02	+++++++++4
1.4286413E+02	+++++++++5
1.2852040E+02	+++++++++6
1.1417667E+02	+++++++++7
9.9832934E+01	+++++++++8
8.5465040E+01	+++++++++9
7.1145473E-01	+++++++++7
5.0017426E-01	+++++++++8
4.2458016E-01	+++++++++0
2.6142816E-01	+++++++++D
1.3700550E-01	+++++++++E
-5.7316266E-01	+++++++++F

TABLE 11 CONTOUR VALUES

(Continued)

FIGURE 93

CONTOUR VALUE	CONTOUR SYMBOL
0.	1
-1.0000000E-02	2
-2.0000000E-02	3
-3.0000000E-02	4
-4.0000000E-02	5
-5.0000000E-02	6
-6.0000000E-02	7
-7.0000000E-02	8
-8.0000000E-02	9
-9.0000000E-02	...........A
-1.0000000E-01	...........B
-1.1000000E-01	C
-1.2000000E-01	...........D
-1.3000000E-01	...........E

FIGURE 94

CONTOUR VALUE	CONTOUR SYMBOL
0.	1
2.7000000E+02	2
5.4000000E+02	3
8.1000000E+02	4
1.0800000E+03	5
1.3500000E+03	6
1.6200000E+03	7
1.8900000E+03	8
2.1600000E+03	9
2.4300000E+03	...........A
2.7000000E+03	...........B
2.9700000E+03	C
3.2400000E+03	...........D
3.5100000E+03	...........E

TABLE 11   CONTOUR VALUES

(Continued)

FIGURE   95   FIGURE   96

CONTOUR VALUE   CONTOUR SYMBOL   CONTOUR VALUE   CONTOUR SYMBOL

CONTOUR VALUE	CONTOUR SYMBOL	CONTOUR VALUE	CONTOUR SYMBOL
4.2917833E-03	＊＊＊＊＊＊＊＊＊1	-8.1000000E-04	＊＊＊＊＊＊＊＊＊1
3.7020801E-03	＊＊＊＊＊＊＊＊＊2	-5.4000000E-04	＊＊＊＊＊＊＊＊＊2
3.1123774E-03	＊＊＊＊＊＊＊＊＊3	-2.7000000E-04	＊＊＊＊＊＊＊＊＊3
2.5226747E-03	＊＊＊＊＊＊＊＊＊4	0.	＊＊＊＊＊＊＊＊＊4
1.9329720E-03	＊＊＊＊＊＊＊＊＊5	2.7000000E-04	＊＊＊＊＊＊＊＊＊5
1.3432693E-03	＊＊＊＊＊＊＊＊＊6	5.4000000E-04	＊＊＊＊＊＊＊＊＊6
7.3356587E-04	＊＊＊＊＊＊＊＊＊7	8.1000000E-04	＊＊＊＊＊＊＊＊＊7
1.4386380E-04	＊＊＊＊＊＊＊＊＊8	1.0800000E-03	＊＊＊＊＊＊＊＊＊8
-4.2685366E-04	＊＊＊＊＊＊＊＊＊9	1.3500000E-03	＊＊＊＊＊＊＊＊＊9
-1.0158410E-03	＊＊＊＊＊＊＊＊＊A	1.6200000E-03	＊＊＊＊＊＊＊＊＊A
-1.6052443E-03	＊＊＊＊＊＊＊＊＊B	1.8900000E-03	＊＊＊＊＊＊＊＊＊B
-2.1949470E-03	＊＊＊＊＊＊＊＊＊C	2.1600000E-03	＊＊＊＊＊＊＊＊＊C
-2.7846497E-03	＊＊＊＊＊＊＊＊＊D		
-3.3743524E-03	＊＊＊＊＊＊＊＊＊E		
-3.9640547E-03	＊＊＊＊＊＊＊＊＊F		

TABLE 11   CONTOUR VALUES

(Continued)

FIGURE 97		FIGURE 98	
CONTOUR VALUE	CONTOUR SYMBOL	CONTOUR VALUE	CONTOUR SYMBOL
0.	▲▲▲▲▲▲▲▲▲1	2.6718949E+02	▲▲▲▲▲▲▲▲▲1
-3.4180549E-04	▲▲▲▲▲▲▲▲▲2	2.4005650E+02	▲▲▲▲▲▲▲▲▲2
-6.8301098E-04	▲▲▲▲▲▲▲▲▲3	2.1292165E+02	▲▲▲▲▲▲▲▲▲3
-1.0254106E-03	▲▲▲▲▲▲▲▲▲4	1.8578759E+02	▲▲▲▲▲▲▲▲▲4
-1.3672220E-03	▲▲▲▲▲▲▲▲▲5	1.5865363E+02	▲▲▲▲▲▲▲▲▲5
-1.7090274E-03	▲▲▲▲▲▲▲▲▲6	1.3151907E+02	▲▲▲▲▲▲▲▲▲6
-2.0608329E-03	▲▲▲▲▲▲▲▲▲7	1.0438572E+02	▲▲▲▲▲▲▲▲▲7
-2.3926364E-03	▲▲▲▲▲▲▲▲▲8	7.7251759E+01	▲▲▲▲▲▲▲▲▲8
-2.7344439E-03	▲▲▲▲▲▲▲▲▲9	5.0117801E+01	▲▲▲▲▲▲▲▲▲9
-3.0762494E-03	▲▲▲▲▲▲▲▲▲A	2.2983843E+01	▲▲▲▲▲▲▲▲▲A
-3.4180549E-03	▲▲▲▲▲▲▲▲▲B	-4.1501144E+00	▲▲▲▲▲▲▲▲▲B
-3.7598604E-03	▲▲▲▲▲▲▲▲▲C	-3.1284072E+01	▲▲▲▲▲▲▲▲▲C
-4.1016659E-03	▲▲▲▲▲▲▲▲▲D	-5.8418030E+01	▲▲▲▲▲▲▲▲▲D
-4.4434714E-03	▲▲▲▲▲▲▲▲▲E	-8.5551987E+01	▲▲▲▲▲▲▲▲▲E
-4.7852704E-03	▲▲▲▲▲▲▲▲▲F	-1.1268593E+02	▲▲▲▲▲▲▲▲▲F

TABLE 11 CONTOUR VALUES

(Continued)

FIGURE 99

CONTOUR VALUE	CONTOUR SYMBOL
5.0000000E+01	⋯⋯1
4.0000000E+01	⋯⋯2
3.0000000E+01	⋯⋯3
2.0000000E+01	⋯⋯4
1.0000000E+01	⋯⋯5
0.	⋯⋯6
-1.0000000E+01	⋯⋯7
-2.0000000E+01	⋯⋯8
-3.0000000E+01	⋯⋯9
-4.0000000E+01	⋯⋯A
-5.0000000E+01	⋯⋯B
-6.0000000E+01	⋯⋯C
-7.0000000E+01	⋯⋯D
-8.0000000E+01	⋯⋯E

FIGURE 100

CONTOUR VALUE	CONTOUR SYMBOL
1.5048271E+02	⋯⋯1
1.4512019E+02	⋯⋯2
1.3378769E+02	⋯⋯3
1.2245516E+02	⋯⋯4
1.1112208E+02	⋯⋯5
9.9790178E+01	⋯⋯C
8.8457670E+01	⋯⋯7
7.7125173E+01	⋯⋯8
6.5792670E+01	⋯⋯9
5.4460167E+01	⋯⋯A
4.3127665E+01	⋯⋯9
3.1795162E+01	⋯⋯C
2.0462659E+01	⋯⋯D
9.1301564E+00	⋯⋯E
-2.2023461E+00	⋯⋯F

TABLE 11   CONTOUR VALUES

(Continued)

FIGURE 101

CONTOUR VALUE	CONTOUR SYMBOL
0.	▲▲▲▲▲▲▲▲▲1
-1.1000000E-02	▲▲▲▲▲▲▲▲▲2
-2.2000000E-02	▲▲▲▲▲▲▲▲▲3
-3.3000000E-02	▲▲▲▲▲▲▲▲▲4
-4.4000000E-02	▲▲▲▲▲▲▲▲▲5
-5.5000000E-02	▲▲▲▲▲▲▲▲▲6
-6.6000000E-02	▲▲▲▲▲▲▲▲▲7
-7.7000000E-02	▲▲▲▲▲▲▲▲▲8
-8.8000000E-02	▲▲▲▲▲▲▲▲▲9
-9.9000000E-02	▲▲▲▲▲▲▲▲▲A
-1.1000000E-01	▲▲▲▲▲▲▲▲▲B
-1.2100000E-01	▲▲▲▲▲▲▲▲▲C

FIGURE 102

CONTOUR VALUE	CONTOUR SYMBOL
3.3672549E+03	▲▲▲▲▲▲▲▲▲1
3.0564621E+03	▲▲▲▲▲▲▲▲▲2
2.7456696E+03	▲▲▲▲▲▲▲▲▲3
2.4348771E+03	▲▲▲▲▲▲▲▲▲4
2.1240847E+03	▲▲▲▲▲▲▲▲▲5
1.8132922E+03	▲▲▲▲▲▲▲▲▲6
1.5024997E+03	▲▲▲▲▲▲▲▲▲7
1.1917073E+03	▲▲▲▲▲▲▲▲▲8
8.8091478E+02	▲▲▲▲▲▲▲▲▲9
5.7012231E+02	▲▲▲▲▲▲▲▲▲A
2.5932984E+02	▲▲▲▲▲▲▲▲▲B
-5.1462631E+01	▲▲▲▲▲▲▲▲▲C

TABLE 11   CONTOUR VALUES

(Continued)

FIGURE 103

CONTOUR VALUE   CONTOUR SYMBOL

CONTOUR VALUE	CONTOUR SYMBOL
-4.9500000E-03	1
-4.4000000E-03	2
-3.8500000E-03	3
-3.3000000E-03	4
-2.7500000E-03	5
-2.2000000E-03	6
-1.6500000E-03	7
-1.1000000E-03	8
-5.5000000E-04	9
0.	..........A
5.5000000E-04	..........B
1.1000000E-03	C
1.6500000E-03	..........D
2.2000000E-03	..........E

FIGURE 104

CONTOUR VALUE   CONTOUR SYMBOL

CONTOUR VALUE	CONTOUR SYMBOL
1.5127416E-03	1
1.0252525E-03	2
5.3776354E-04	3
5.0274599E-05	4
-4.3721434E-04	5
-9.2470328E-04	6
-1.4121922E-03	7
-1.8996811E-03	8
-2.3871701E-03	9
-2.8746590E-03	..........A
-3.3621480E-03	..........H
-3.8496369E-03	C
-4.3371258E-03	..........D
-4.8246148E-03	..........E
-5.3121032E-03	..........F

TABLE 11   CONTOUR VALUES

(Continued)

FIGURE 105

CONTOUR VALUE	CONTOUR SYMBOL
5.0421430E-03	▲▲▲▲▲▲▲▲▲1
4.3052883E-03	▲▲▲▲▲▲▲▲▲2
3.5684340E-03	▲▲▲▲▲▲▲▲▲3
2.8315798E-03	▲▲▲▲▲▲▲▲▲4
2.0947255E-03	▲▲▲▲▲▲▲▲▲5
1.3578713E-03	▲▲▲▲▲▲▲▲▲6
6.2101704E-04	▲▲▲▲▲▲▲▲▲7
-1.1583721E-04	▲▲▲▲▲▲▲▲▲8
-8.5269147E-04	▲▲▲▲▲▲▲▲▲9
-1.5894457E-03	▲▲▲▲▲▲▲▲▲A
-2.3264000E-03	▲▲▲▲▲▲▲▲▲B
-3.0632842E-03	▲▲▲▲▲▲▲▲▲C
-3.8001088E-03	▲▲▲▲▲▲▲▲▲D
-4.5369627E-03	▲▲▲▲▲▲▲▲▲E
-5.2738164E-03	▲▲▲▲▲▲▲▲▲F

FIGURE 106

CONTOUR VALUE	CONTOUR SYMBOL
-9.0000000E+01	▲▲▲▲▲▲▲▲▲1
-6.0000000E+01	▲▲▲▲▲▲▲▲▲2
-3.0000000E+01	▲▲▲▲▲▲▲▲▲3
0.	▲▲▲▲▲▲▲▲▲4
3.0000000E+01	▲▲▲▲▲▲▲▲▲5
6.0000000E+01	▲▲▲▲▲▲▲▲▲6
9.0000000E+01	▲▲▲▲▲▲▲▲▲7
1.2000000E+02	▲▲▲▲▲▲▲▲▲8
1.5000000E+02	▲▲▲▲▲▲▲▲▲9
1.8000000E+02	▲▲▲▲▲▲▲▲▲A
2.1000000E+02	▲▲▲▲▲▲▲▲▲B
2.4000000E+02	▲▲▲▲▲▲▲▲▲C
2.7000000E+02	▲▲▲▲▲▲▲▲▲D

TABLE 11   CONTOUR VALUES

(Continued)

FIGURE 107

CONTOUR VALUE	CONTOUR SYMBOL
1.5271752E+02	▲▲▲▲▲▲▲▲▲1
1.3614998E+02	▲▲▲▲▲▲▲▲▲2
1.1958246E+02	▲▲▲▲▲▲▲▲▲3
1.0301493E+02	▲▲▲▲▲▲▲▲▲4
8.6447411E+01	▲▲▲▲▲▲▲▲▲5
6.9879888E+01	▲▲▲▲▲▲▲▲▲6
5.3312368E+01	▲▲▲▲▲▲▲▲▲7
3.6744841E+01	▲▲▲▲▲▲▲▲▲8
2.0177318E+01	▲▲▲▲▲▲▲▲▲9
3.6097943E+00	▲▲▲▲▲▲▲▲▲A
-1.2957729E+01	▲▲▲▲▲▲▲▲▲B
-2.9525252E+01	▲▲▲▲▲▲▲▲▲C
-4.6092778E+01	▲▲▲▲▲▲▲▲▲D
-6.2660249E+01	▲▲▲▲▲▲▲▲▲E
-7.9227814E+01	▲▲▲▲▲▲▲▲▲F

FIGURE 108

CONTOUR VALUE	CONTOUR SYMBOL
1.2811916E+02	▲▲▲▲▲▲▲▲▲1
9.9047842E+01	▲▲▲▲▲▲▲▲▲2
6.9978540E+01	▲▲▲▲▲▲▲▲▲3
4.0905239E+01	▲▲▲▲▲▲▲▲▲4
1.1833937E+01	▲▲▲▲▲▲▲▲▲5
-1.7237365E+01	▲▲▲▲▲▲▲▲▲6
-4.6308667E+01	▲▲▲▲▲▲▲▲▲7
-7.5379968E+01	▲▲▲▲▲▲▲▲▲8
-1.0445127E+02	▲▲▲▲▲▲▲▲▲9
-1.3352257E+02	▲▲▲▲▲▲▲▲▲A
-1.6259387E+02	▲▲▲▲▲▲▲▲▲B
-1.9166518E+02	▲▲▲▲▲▲▲▲▲C
-2.2073648E+02	▲▲▲▲▲▲▲▲▲D
-2.4980778E+02	▲▲▲▲▲▲▲▲▲E
-2.7887905E+02	▲▲▲▲▲▲▲▲▲F

11. <u>FIGURES</u>
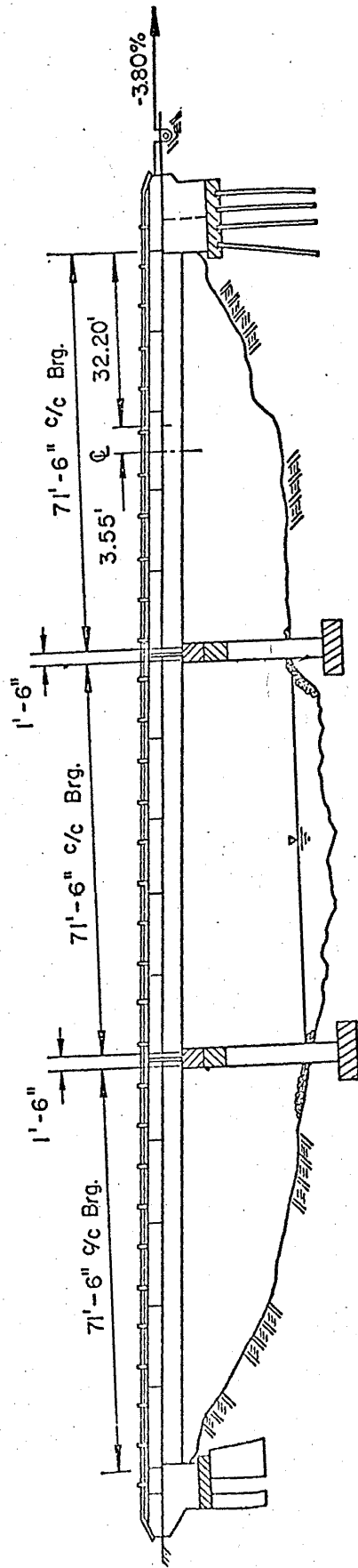
Fig. 1 Elevation of Test Bridge

37'-11½"

35'-11½"

2'-0"

1'-11½"   12'-0"   12'-0"   10'-0"   9" 1'-3"

1/8"per Ft.   Point of   1/8" per ft.   7½"   3/8" per ft.   5¼" 1'-0"
              Profile Grade   Nominal   1'-1"

3'-1¾"

2'-1"   6-²⁴/₄₅ P/s I-Beams @ 6'-9" C/c=33'-9"   2'-1½"
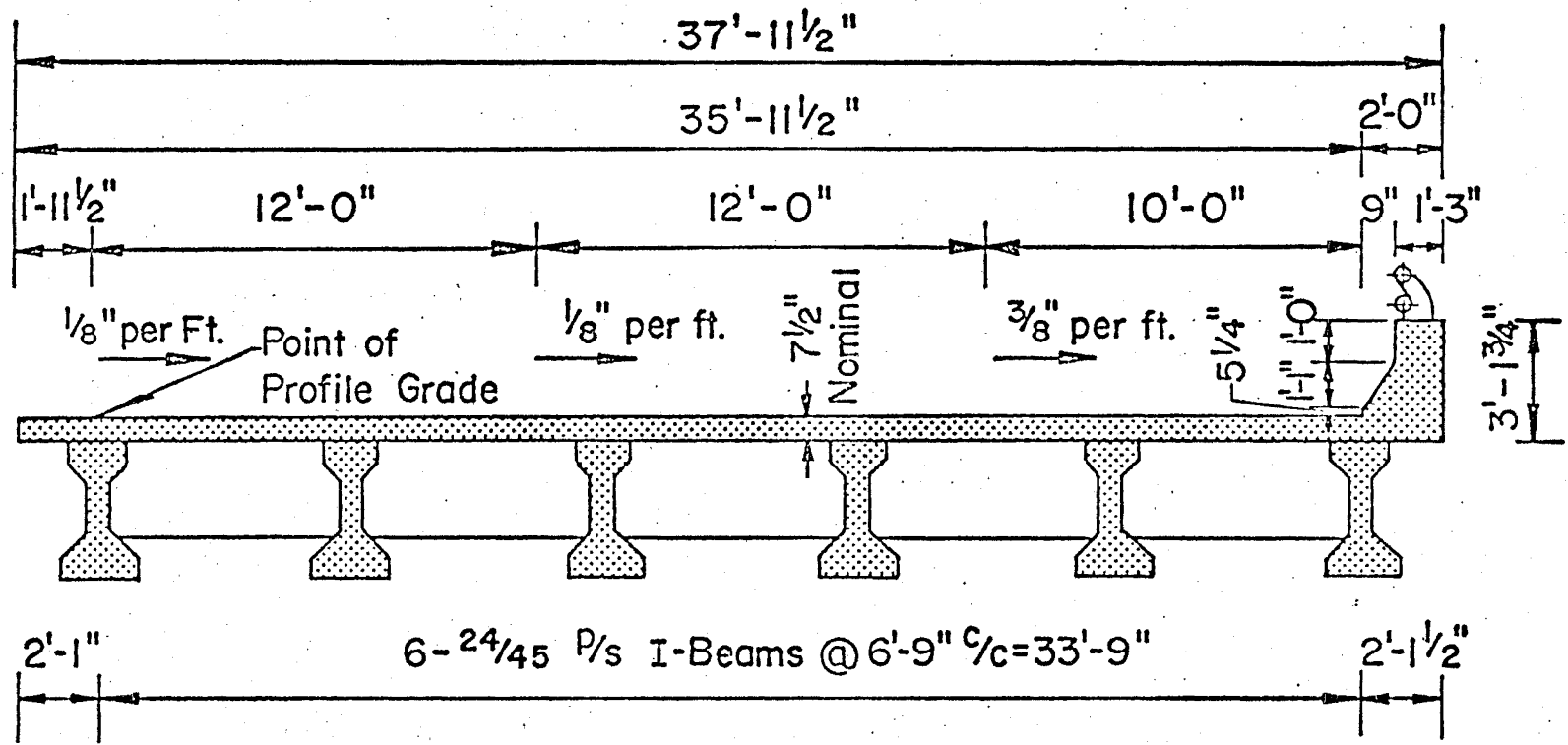
Fig. 2   Cross-Section of Test Bridge

#4 @ 12"

#5 @ 6 ½"

#5 @ 10"

2"

7 ½"

1¼" 1¼" 1¼" 1¼"

5"

Corrugated
Steel
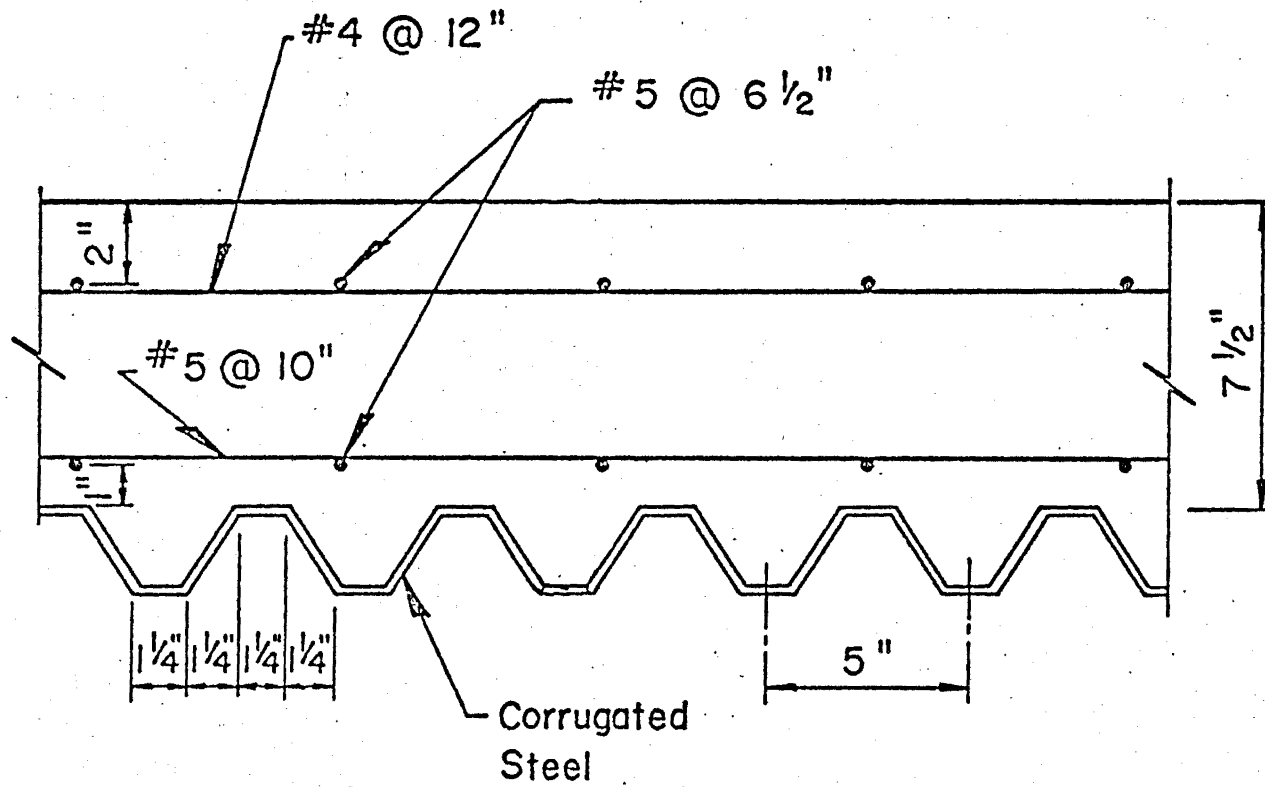
Fig. 3 Transverse Cross-Section of Slab
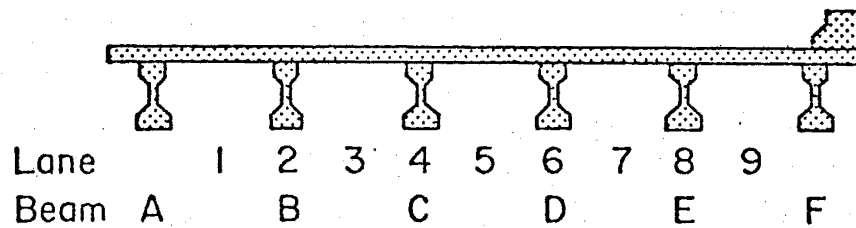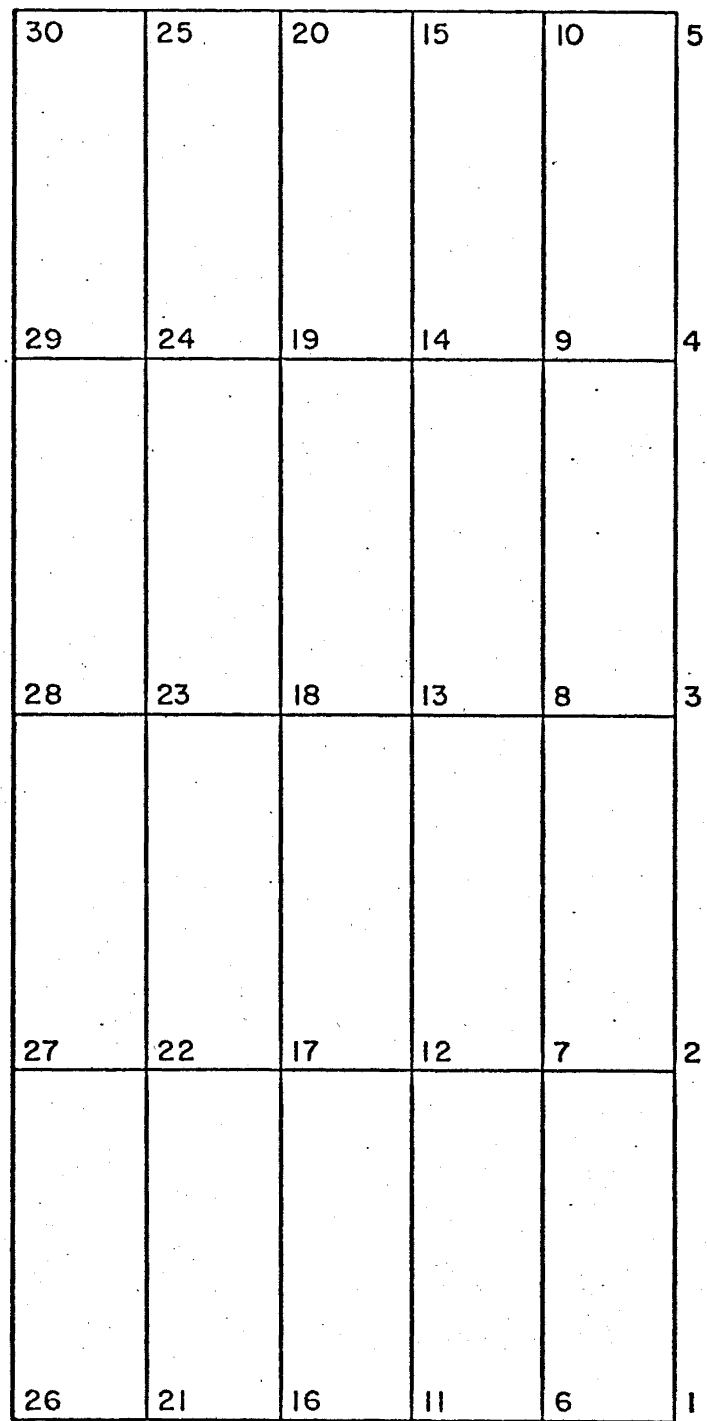
Fig. 4 Finite Element Mesh

ASSEMBLED
LCCT-12 ELEMENT
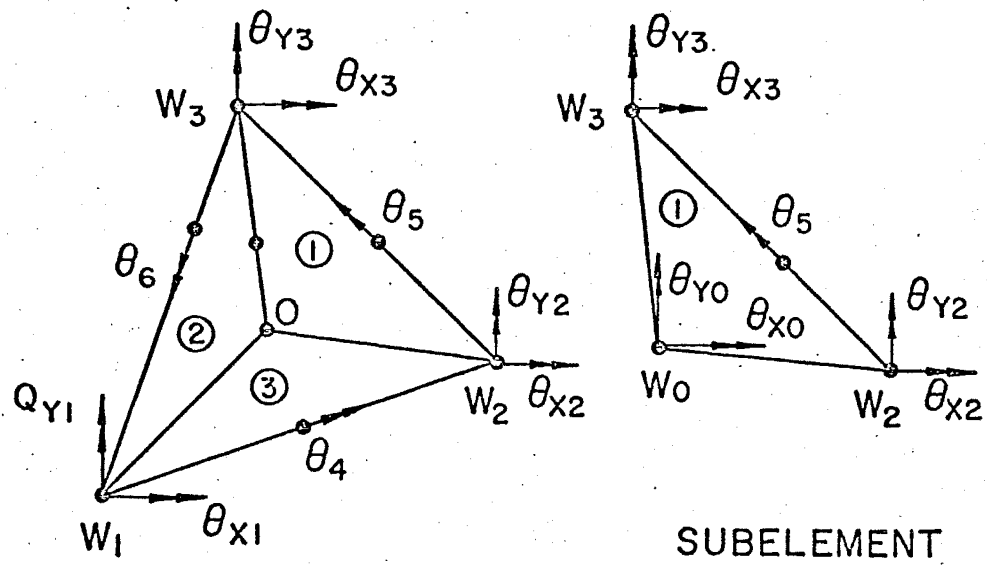
Fig. 5A
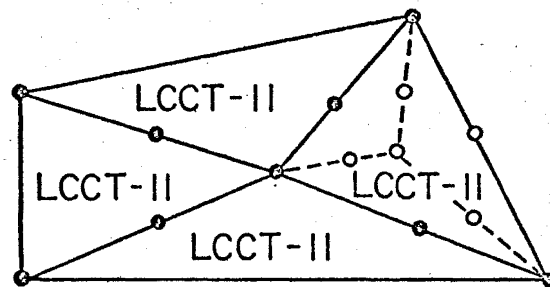
QUADRILATERAL
ELEMENT (Q-19)

Fig. 5B Quadrilateral Element (Q-19)
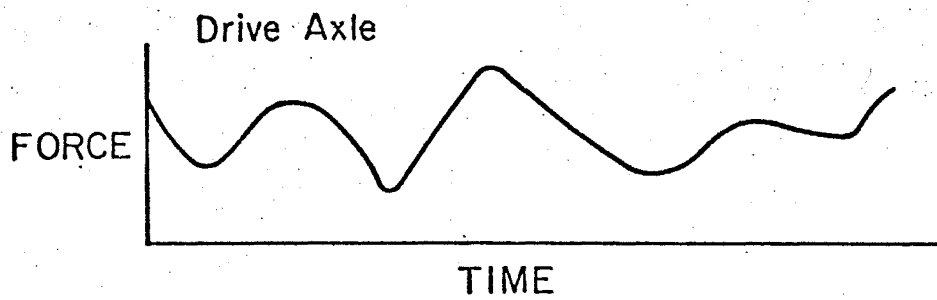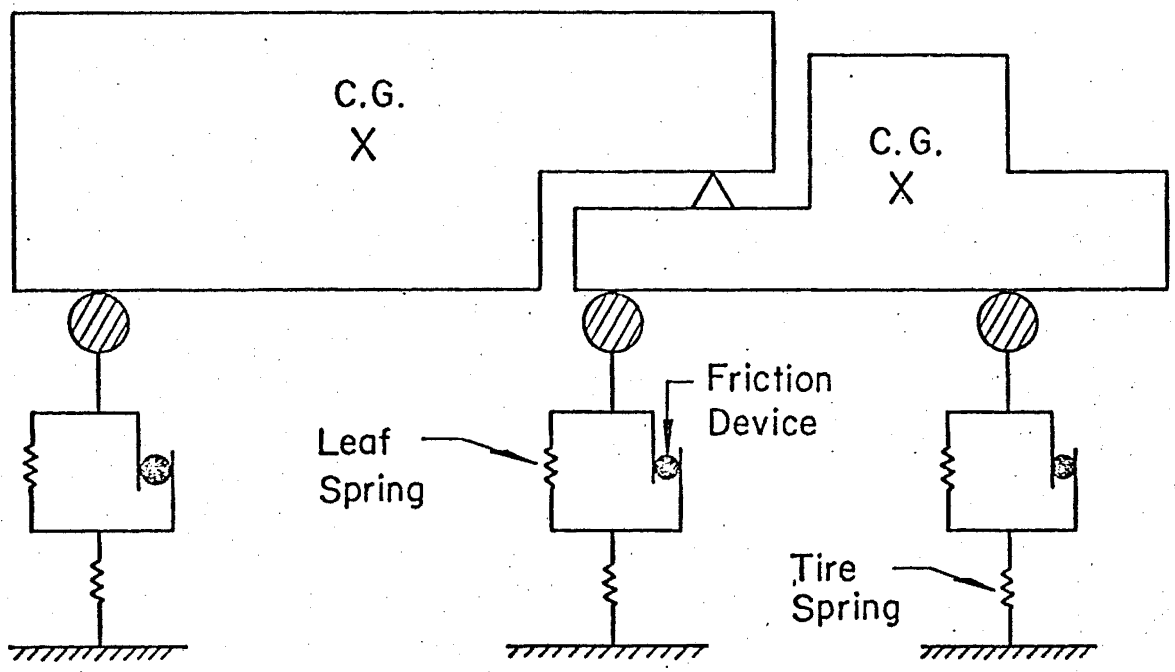
Fig. 6A Spring-Mass Truck Model

13.0'   20.4'
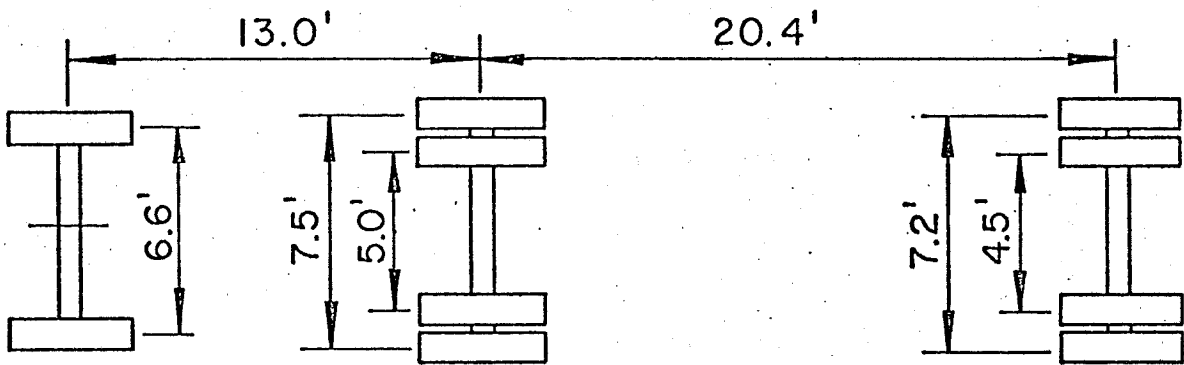
Axle and Wheel Spacing

Total
Front
Load
↓
10.200^k

Total
Drive
Load
↓
32.200^k

Total
Rear
Load
↓
32.675^k

Axle Loads
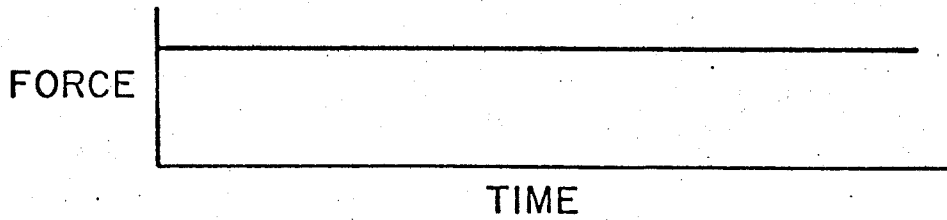
FORCE

TIME

Fig. 6B   Constant-Force Truck Model

FIGURE   7-25MPH-LANE 3

DISPLACEMENT TIME HISTORY
BEAM F-NODE POINTS 2,3,4

DISPLACEMENT (IN.)
X (10⁻²)

FR-WHEEL DIST./BRIDGE LENGTH
X (10⁻¹)
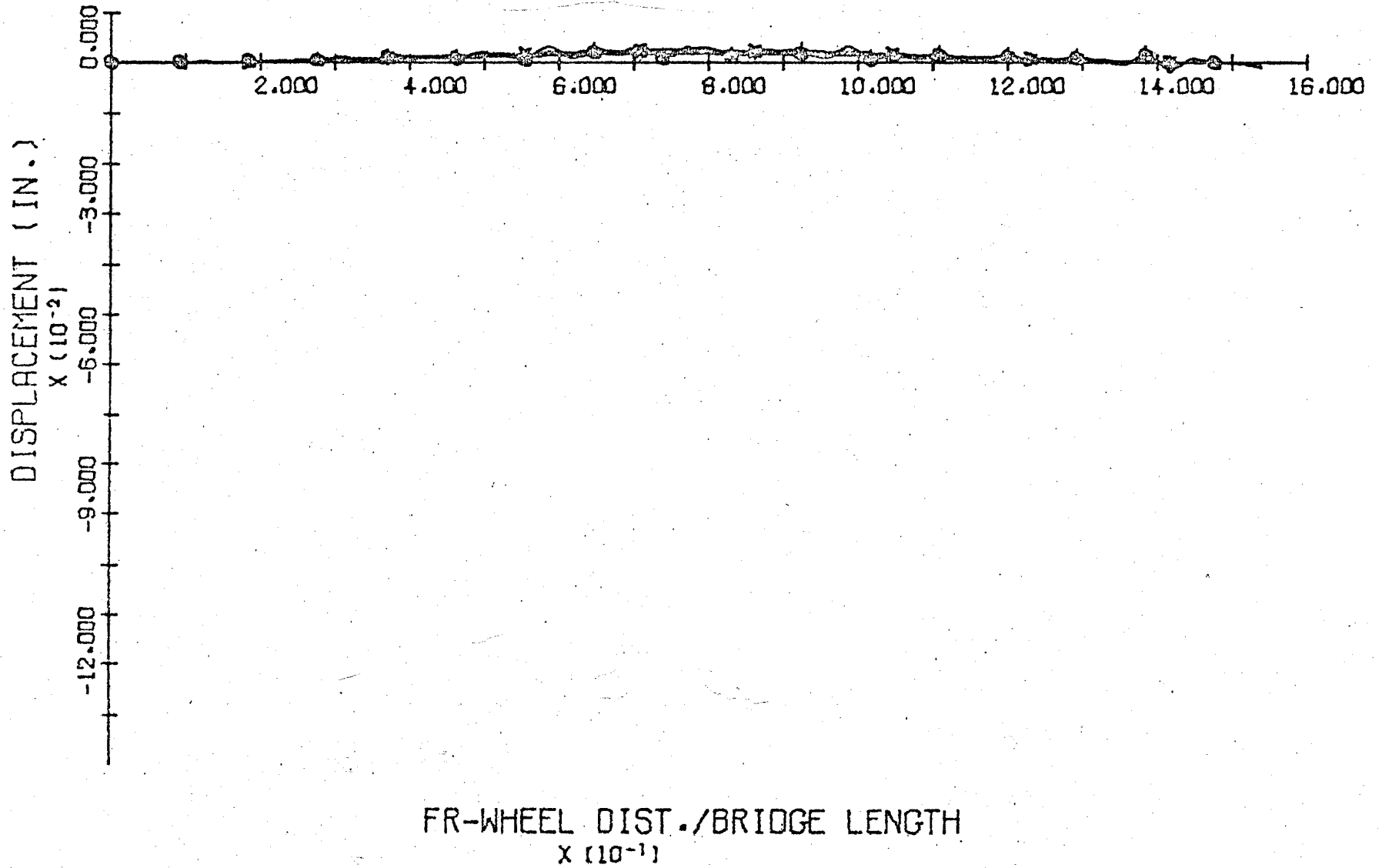
FIGURE   8 50MPH-LANE 3
DISPLACEMENT TIME HISTORY
BEAM F-NODE POINTS 2.3.4

DISPLACEMENT (IN.)
X (10⁻²)

FR-WHEEL DIST./BRIDGE LENGTH
X (10⁻¹)
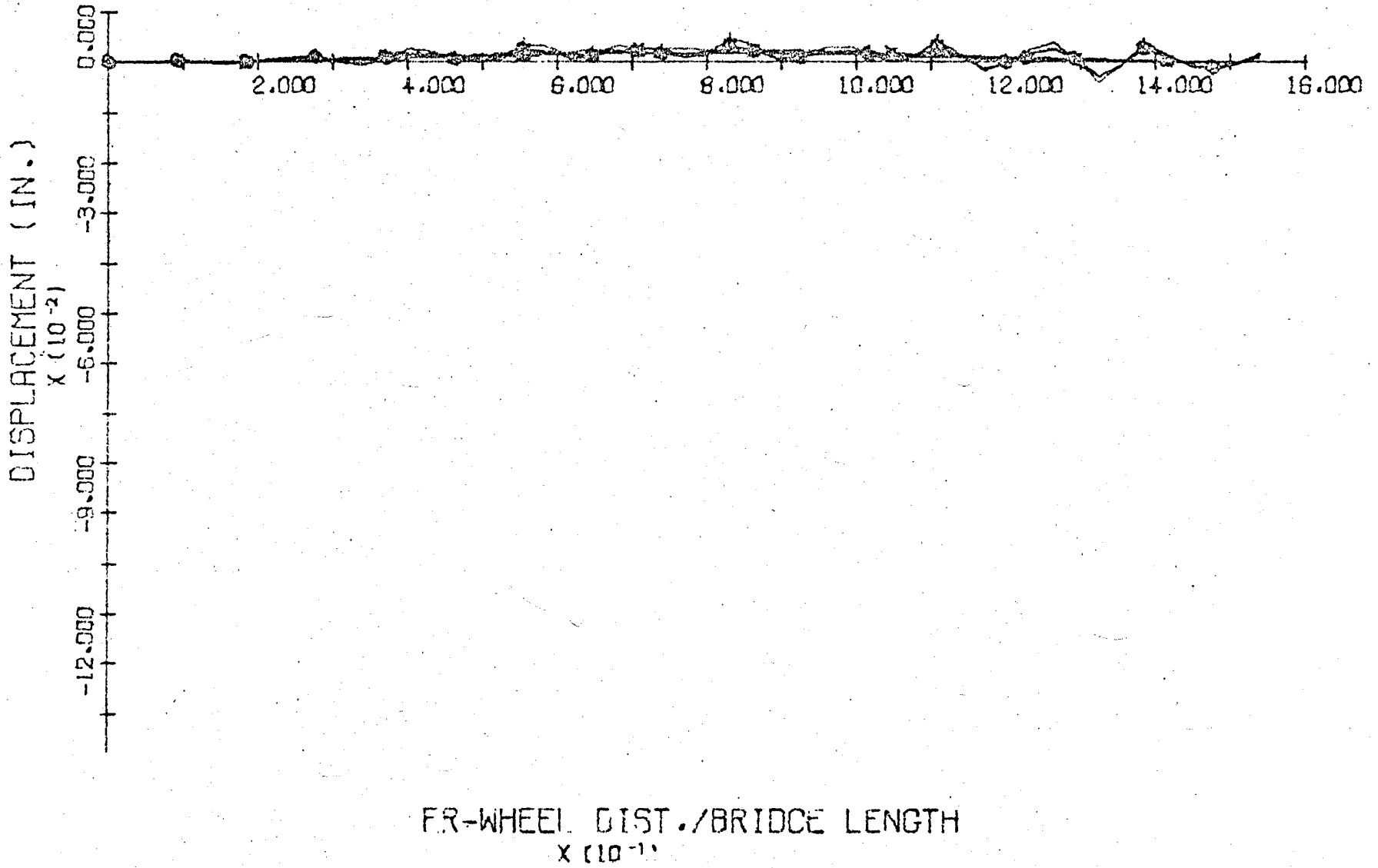
FIGURE 9 25MPH-LANE 3

BENDING MOMENT TIME HISTORY

BEAM F-NODE POINTS 2,3,4

FR-WHEEL DIST./BRIDGE LENGTH
X (10⁻¹)

BENDING MOMENT (IN.-KIP.)
X (10⁻²)
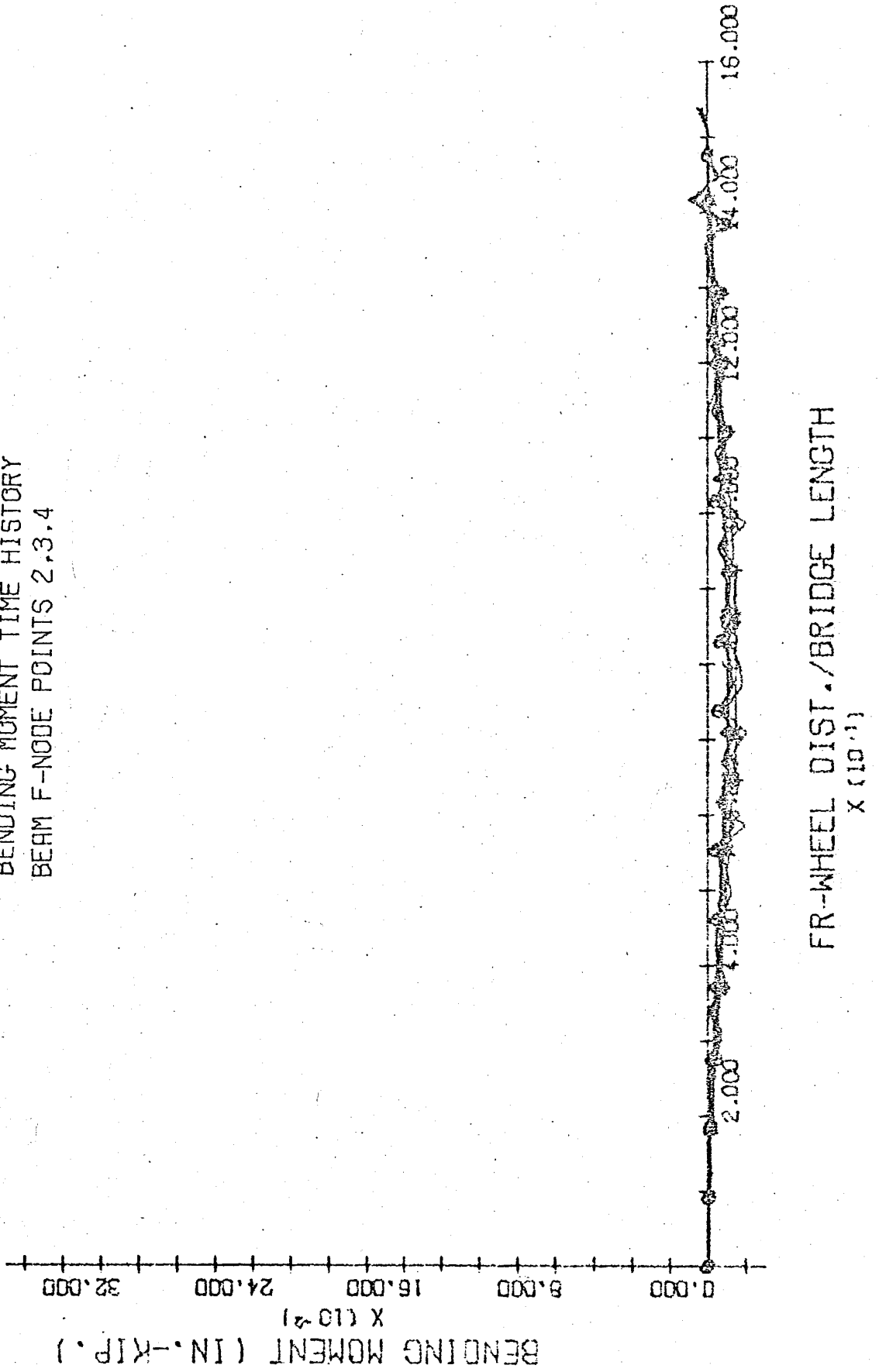
FIGURE 10 50MPH-LANE 3
BENDING MOMENT TIME HISTORY
BEAM F-NODE POINTS 2,3,4
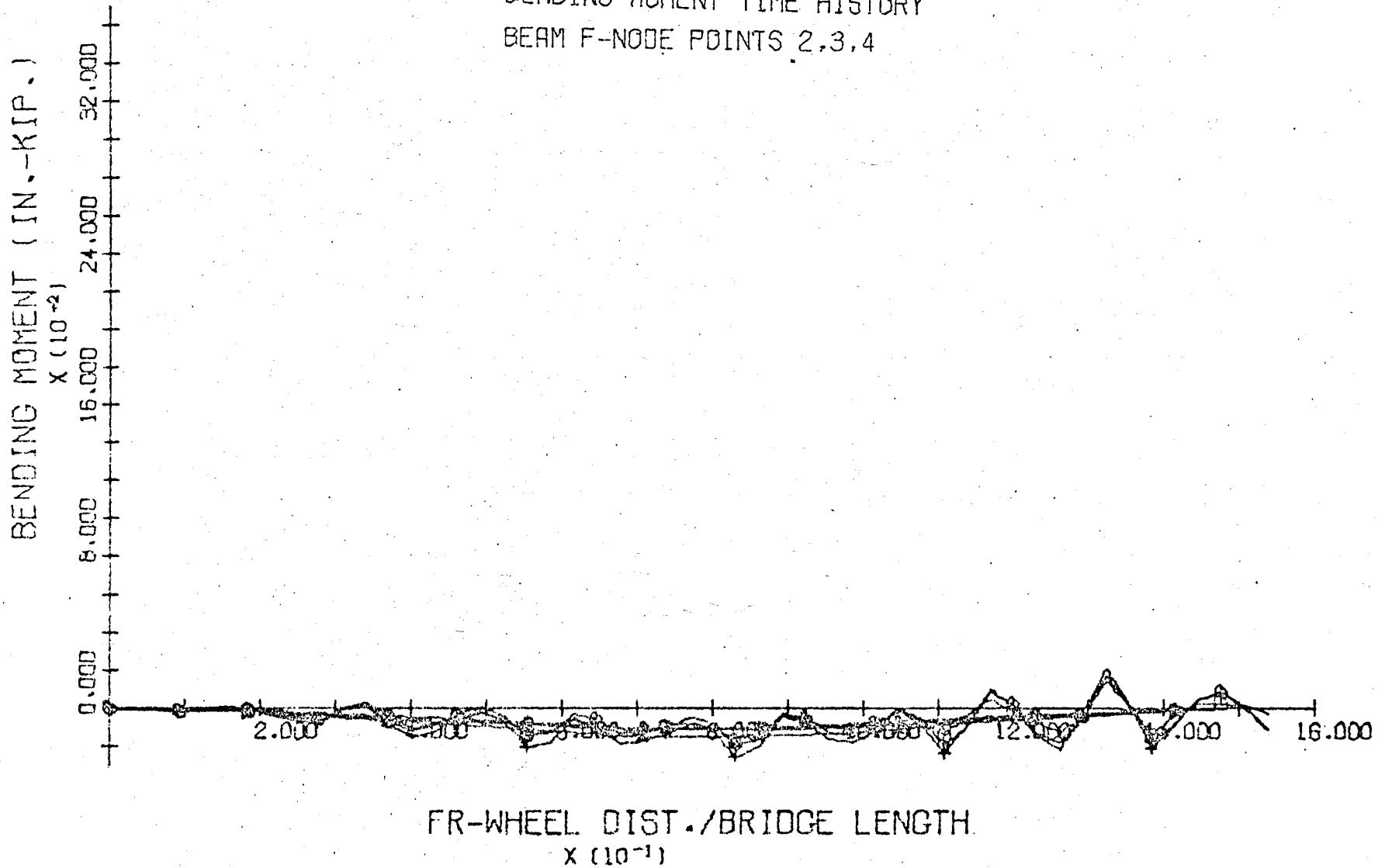
FIGURE 11 25MPH-LANE 3
DISPLACEMENT TIME HISTORY
BEAM E-NODE POINTS 7,8,9

FR-WHEEL DIST./BRIDGE LENGTH
X (10⁻¹)
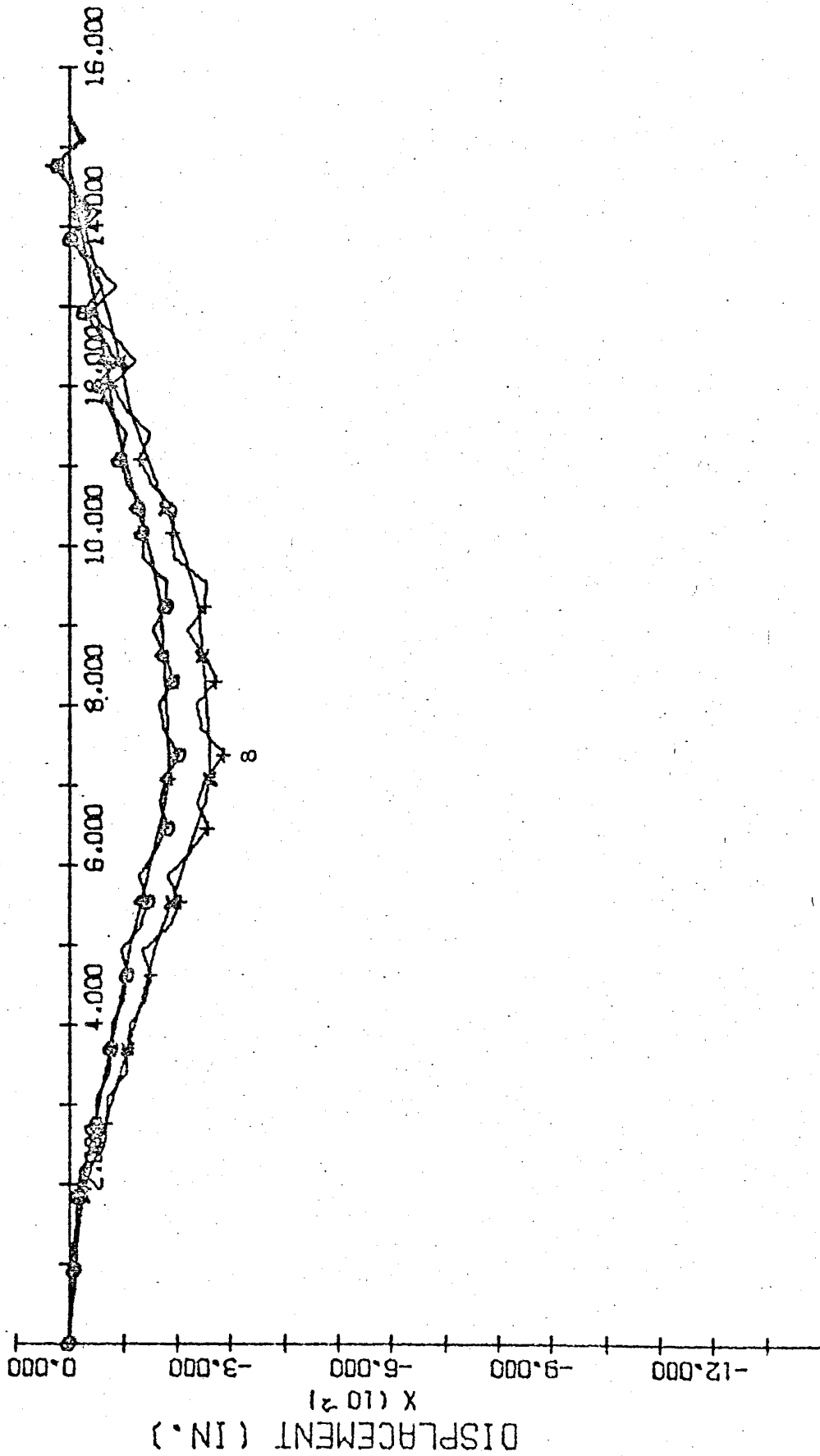
DISPLACEMENT (IN.)
X (10²)

FIGURE 12 50MPH-LANE 3
DISPLACEMENT TIME HISTORY
BEAM E-NODE POINTS 7,8,9

FR-WHEEL DIST./BRIDGE LENGTH
X (10⁻¹)
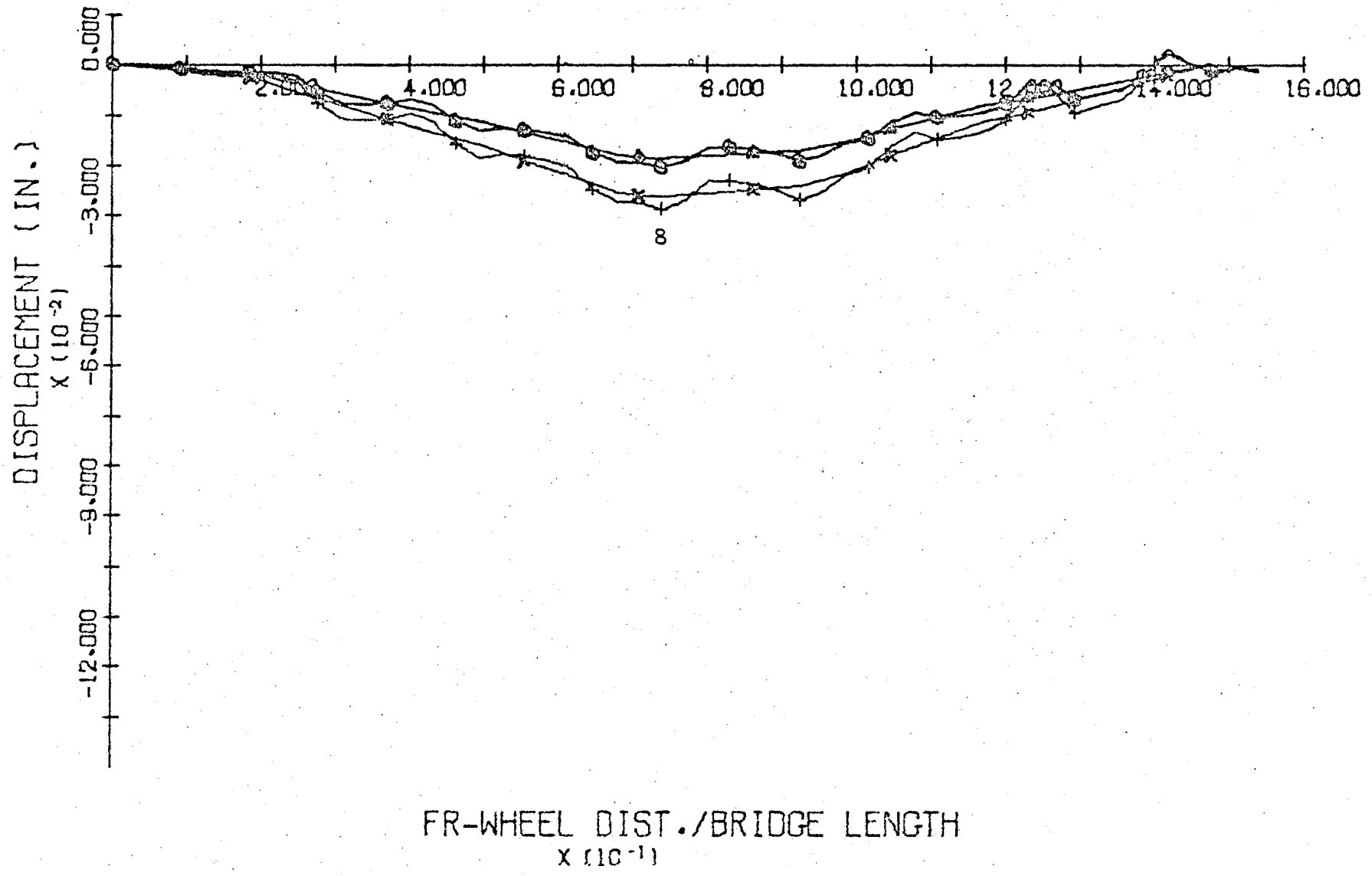
FIGURE 13 25MPH-LANE 3
BENDING MOMENT TIME HISTORY
BEAM E-NODE POINTS 7,8,9

FR-WHEEL DIST./BRIDGE LENGTH
X (10⁻¹)
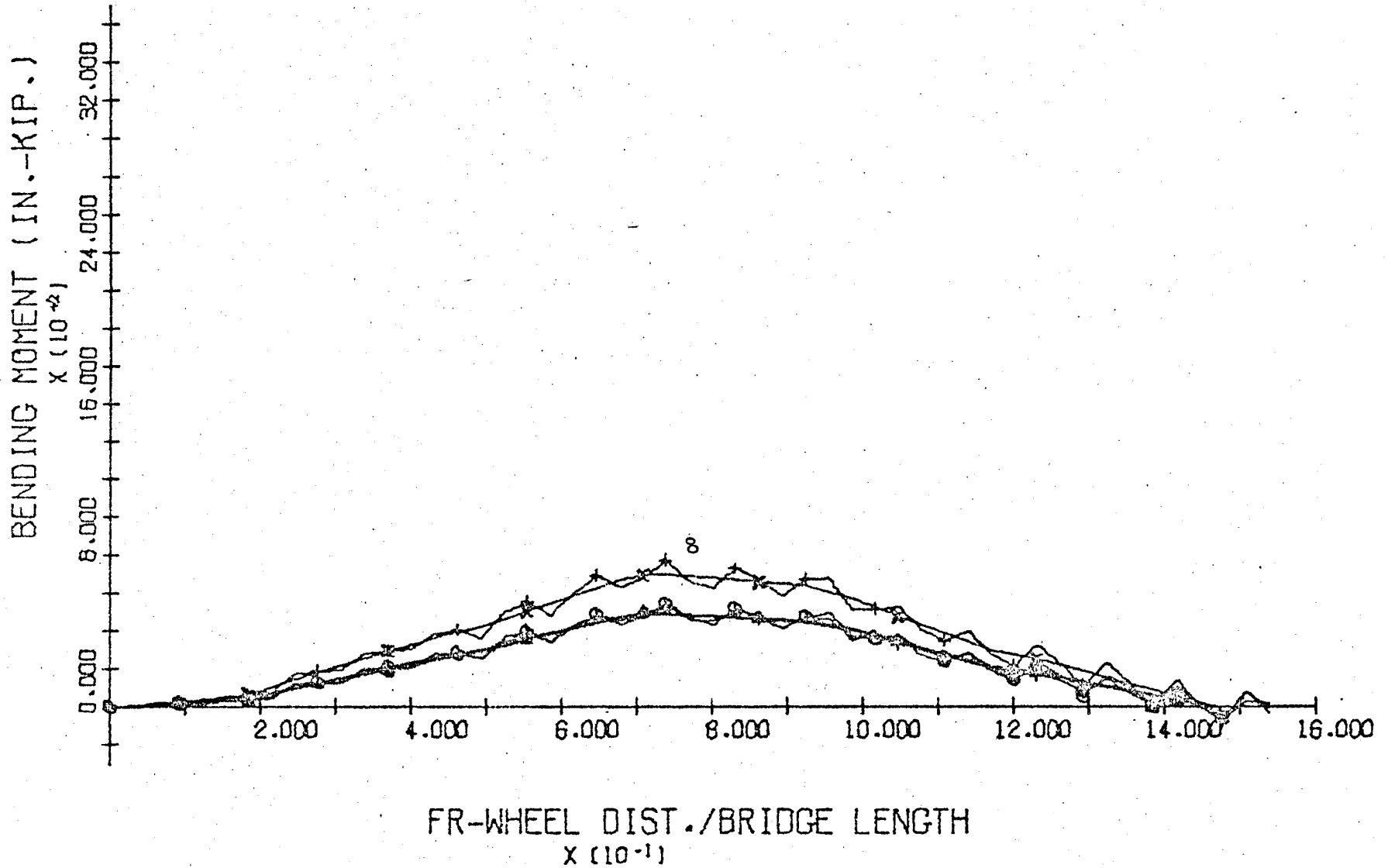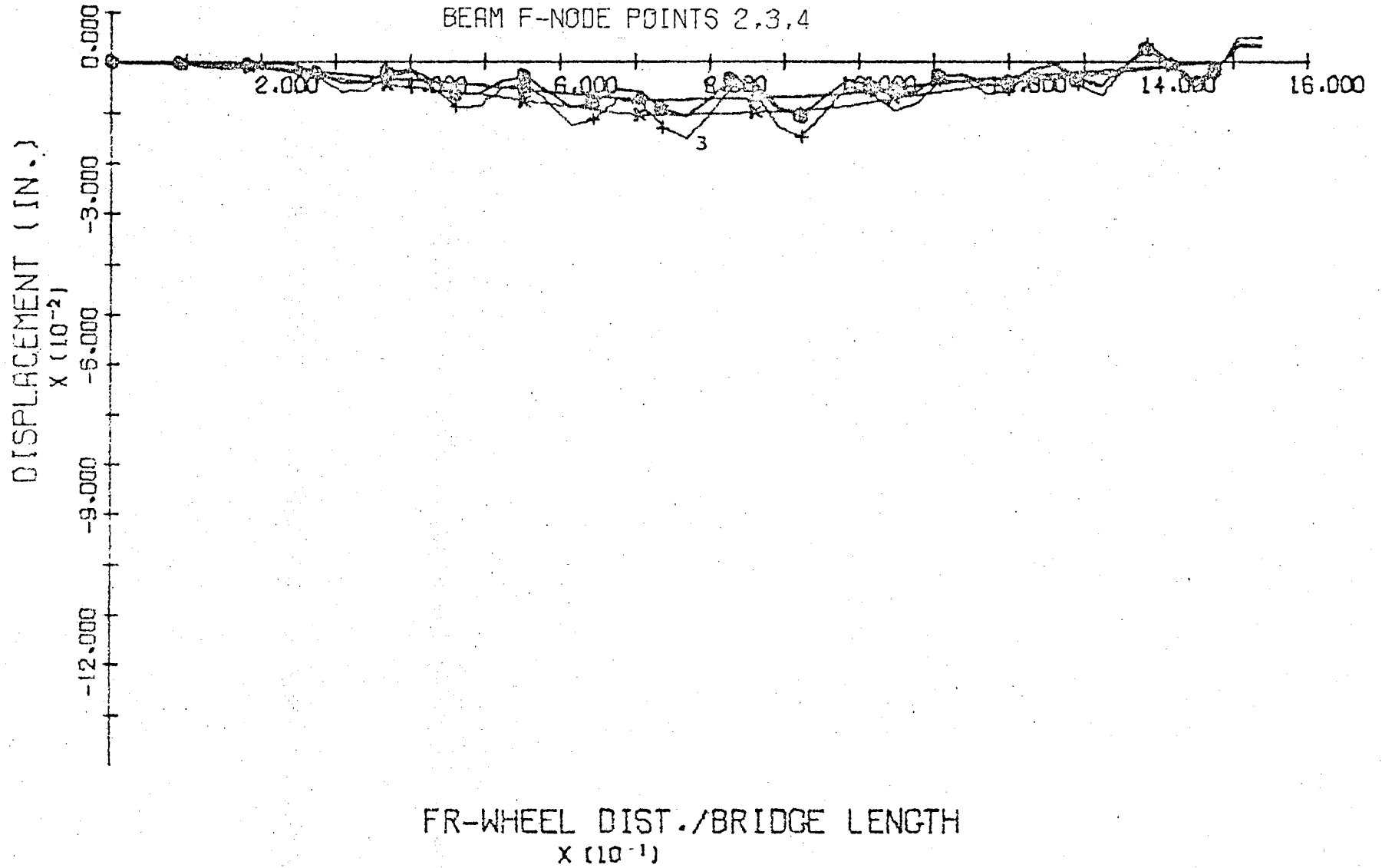
FIGURE 14 50MPH-LANE 3
BENDING MOMENT TIME HISTORY
BEAM E-NODE POINTS 7,8,9
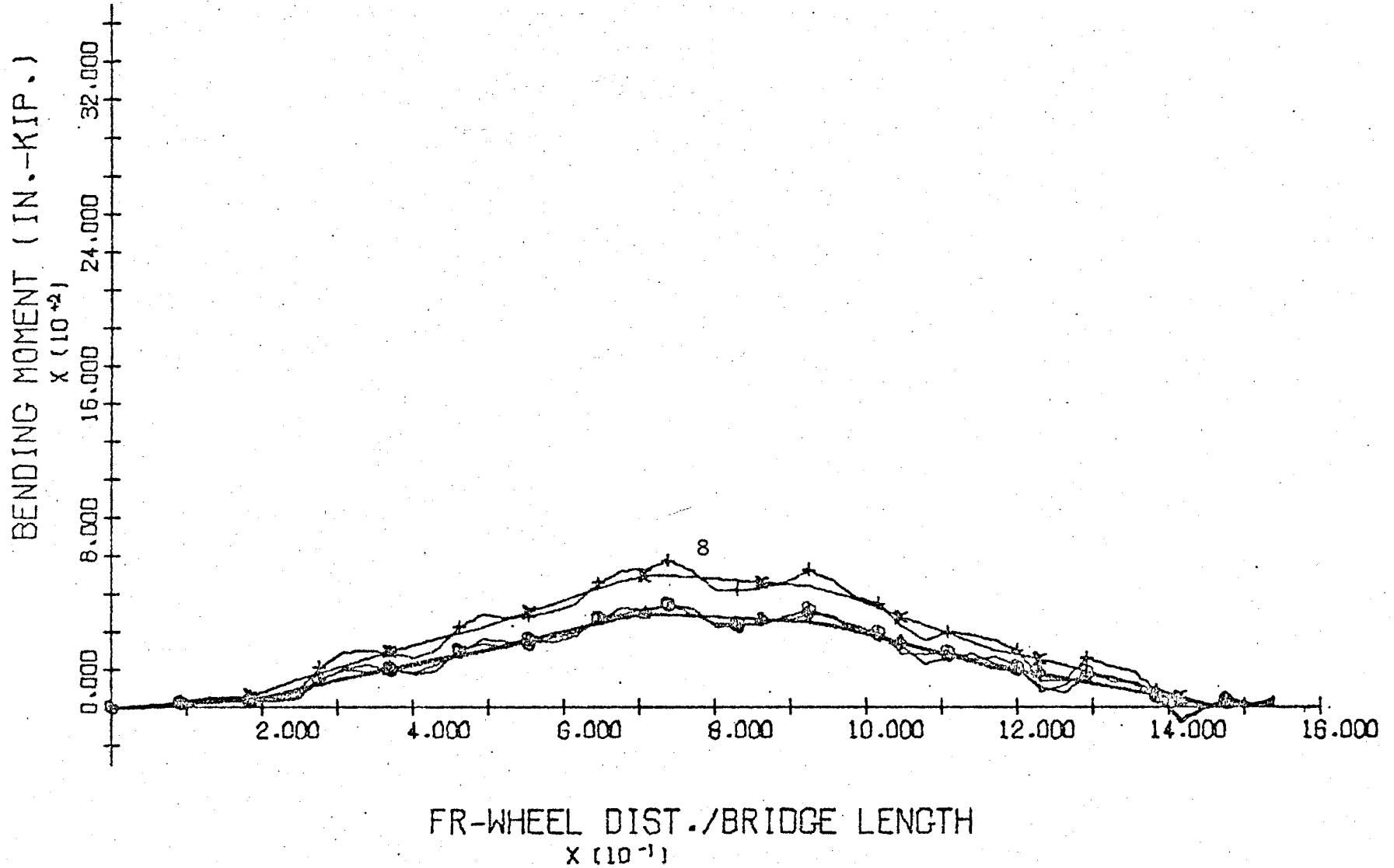
FIGURE 15 25MPH-LANE 3
DISPLACEMENT TIME HISTORY
BEAM D-NODE POINTS 12.13.14

FR-WHEEL DIST./BRIDGE LENGTH
X (10⁻¹)
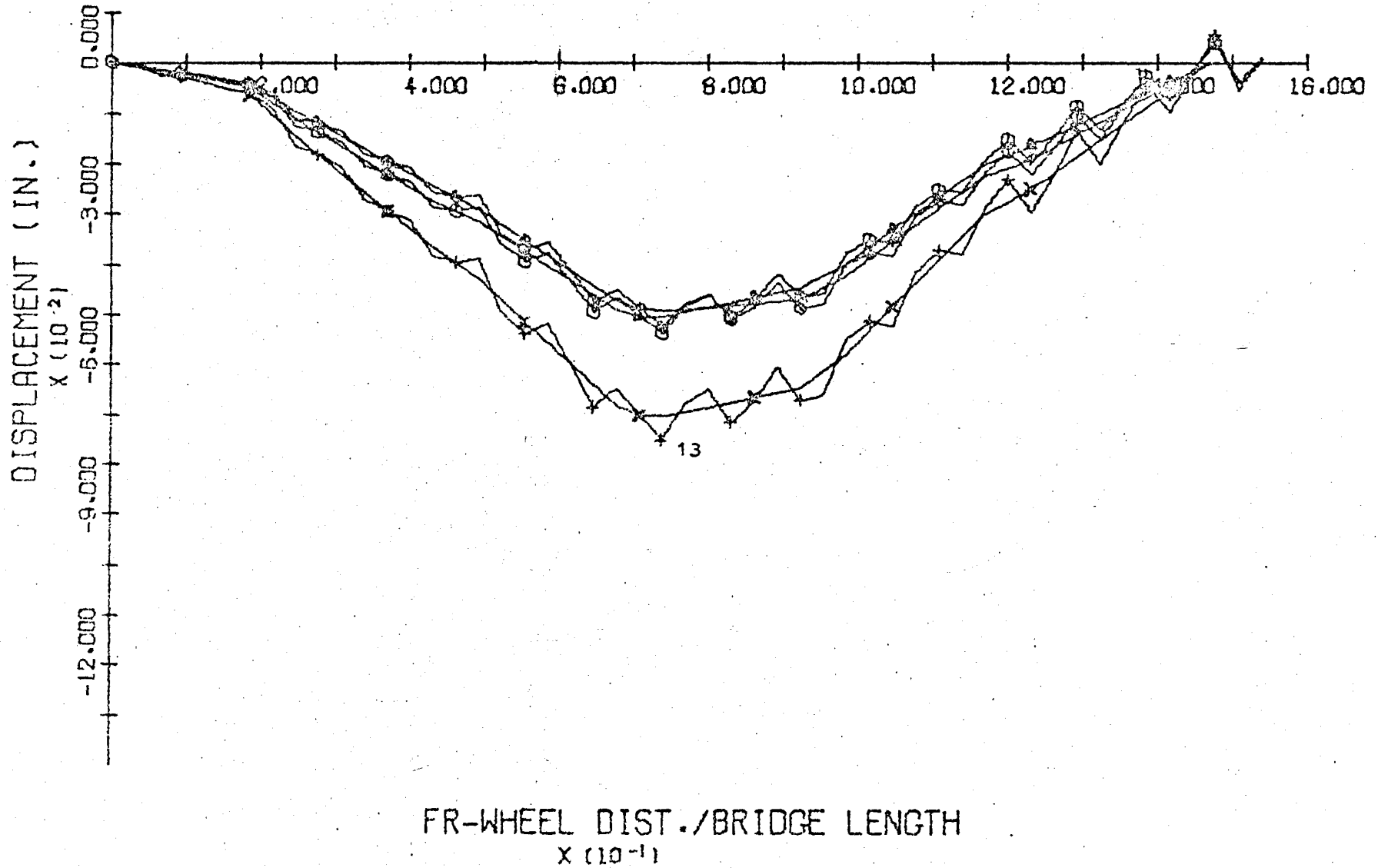
FIGURE 16 50MPH-LANE 3
DISPLACEMENT TIME HISTORY
BEAM D-NODE POINTS 12.13.14

DISPLACEMENT (IN.)
X (10⁻²)
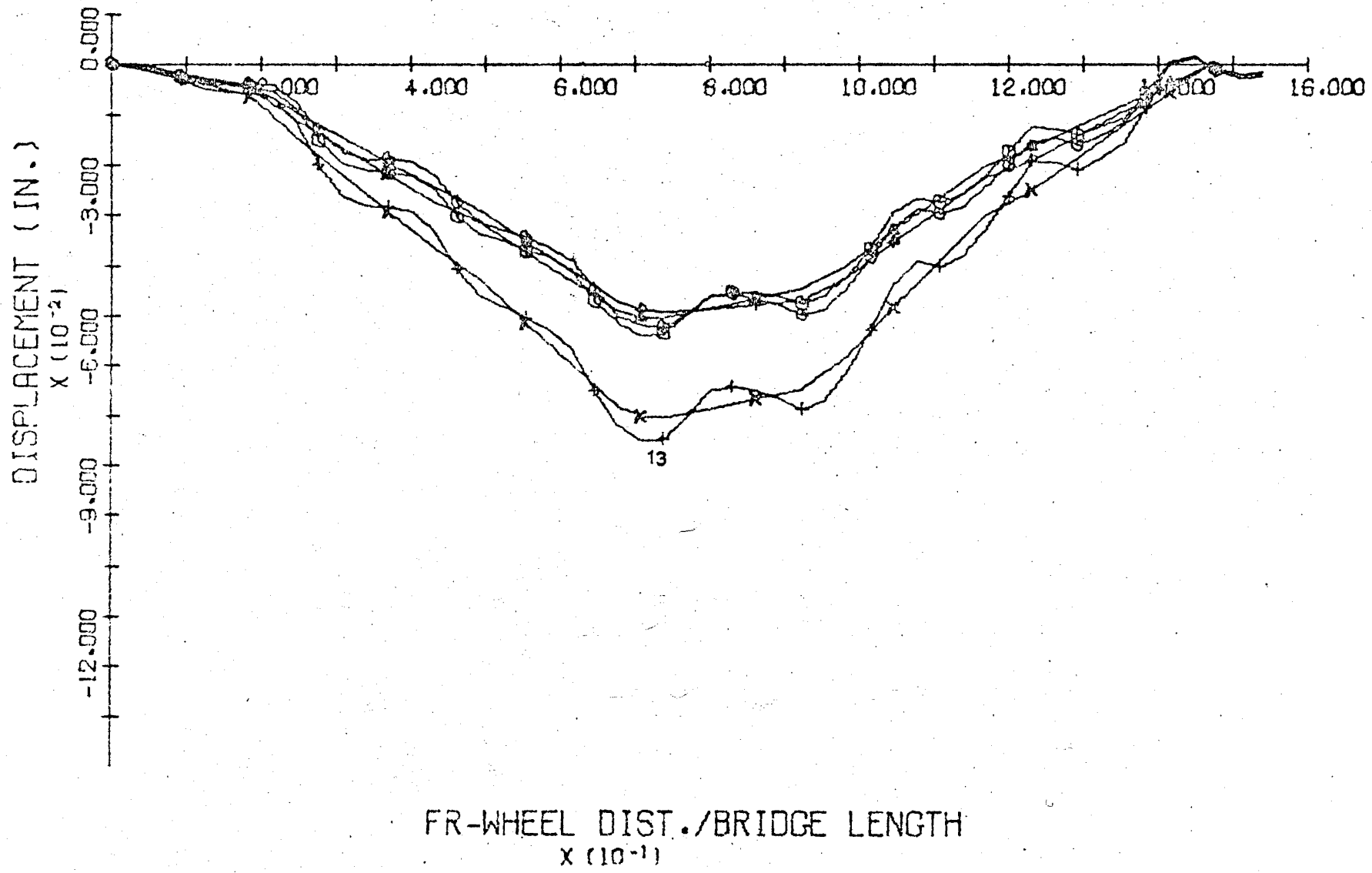
FR-WHEEL DIST./BRIDGE LENGTH
X (10⁻¹)

FIGURE 17 25MPH-LANE 3
BENDING MOMENT TIME HISTORY
BEAM D-NODE POINTS 12,13,14

BENDING MOMENT (IN.-KIP.)
X (10 +2)

FR-WHEEL DIST./BRIDGE LENGTH
X (10 -1)
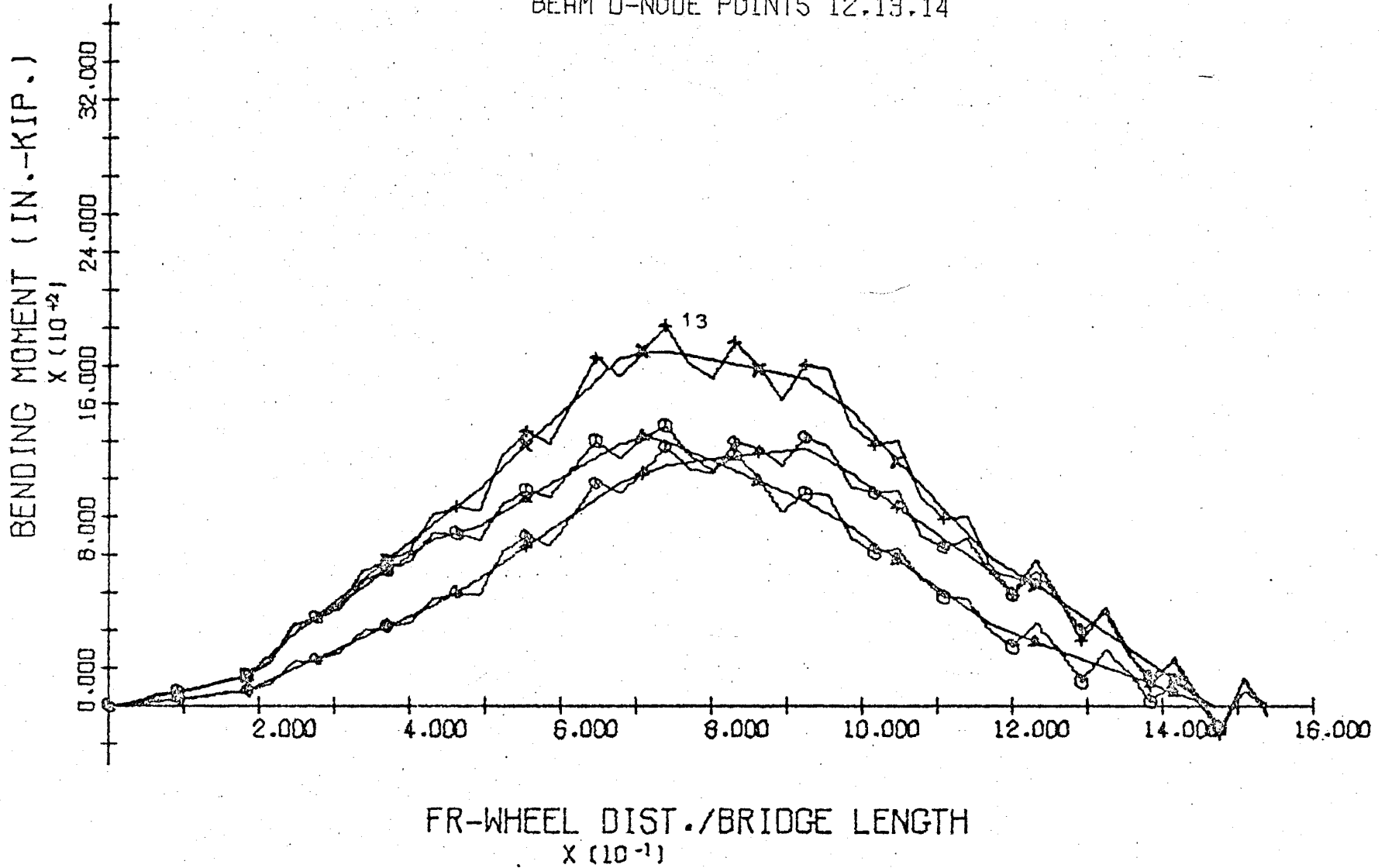
FIGURE 18 50MPH-LANE 3
BENDING MOMENT TIME HISTORY
BEAM 0-NODE POINTS 12,13,14

BENDING MOMENT (IN.-KIP.)
X (10⁻²)
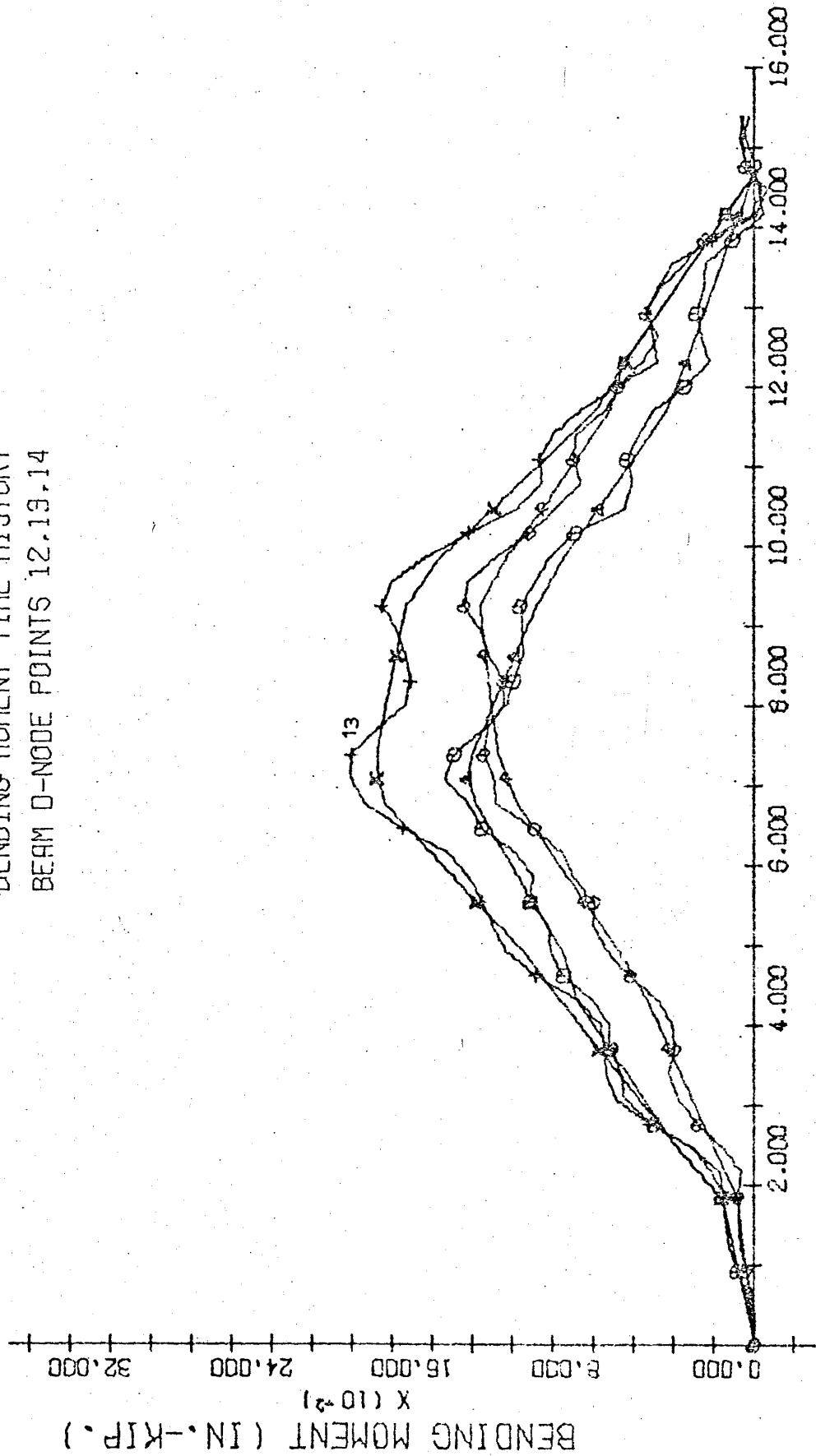
FR-WHEEL DIST./BRIDGE LENGTH
X (10⁻¹)

FIGURE 19 25MPH-LANE 3
DISPLACEMENT TIME HISTORY
BEAM C-NODE POINTS 17,18,19

DISPLACEMENT (IN.)
X (10⁻²)
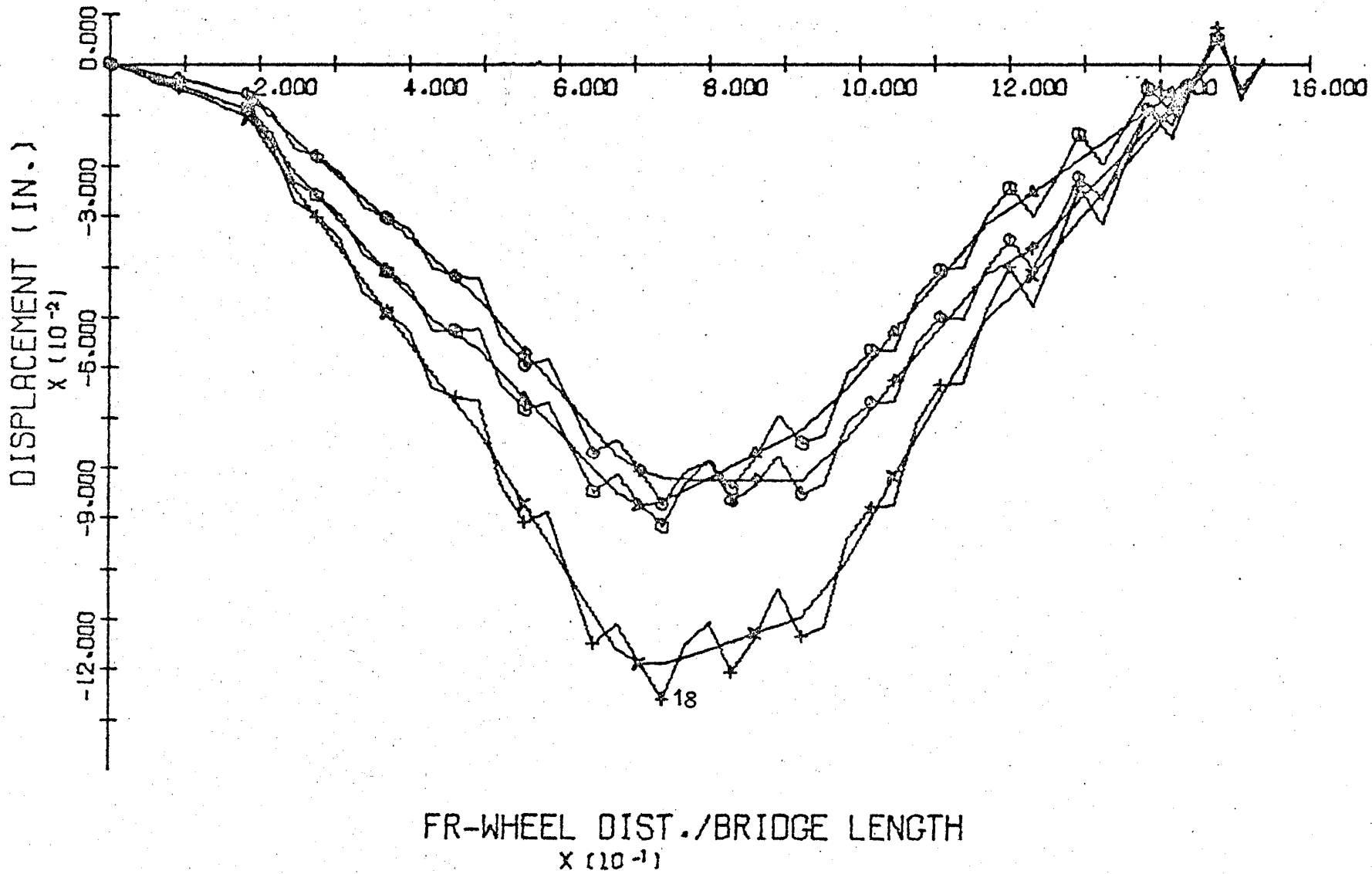
FR-WHEEL DIST./BRIDGE LENGTH
X (10⁻¹)

FIGURE 20 50MPH-LANE 3
DISPLACEMENT TIME HISTORY
BEAM C-NODE POINTS 17,18,19

FR-WHEEL DIST./BRIDGE LENGTH
X (10⁻¹)
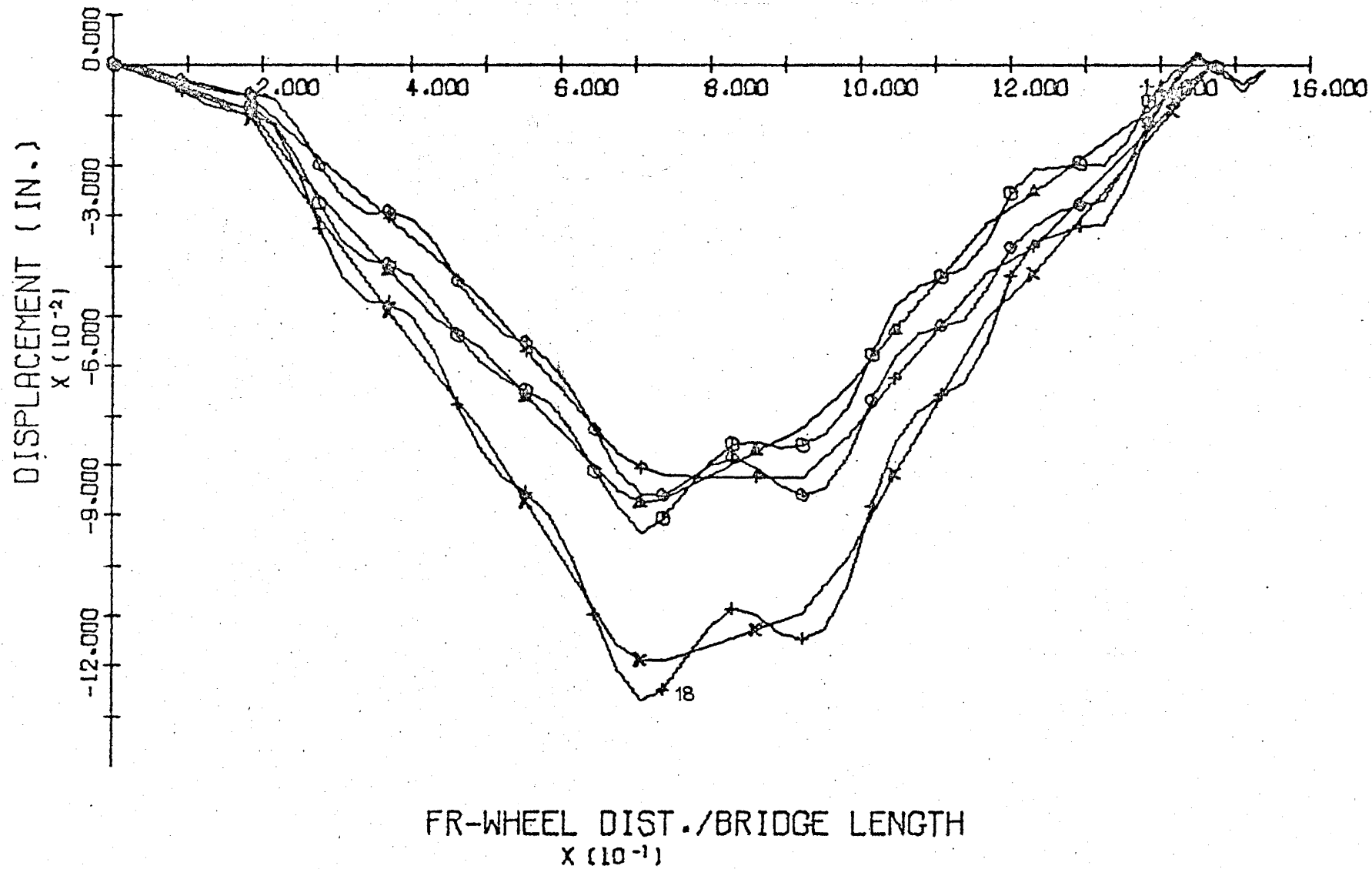
FIGURE 21 25MPH-LANE 3
BENDING MOMENT TIME HISTORY
BEAM C-NODE POINTS 17.18.19
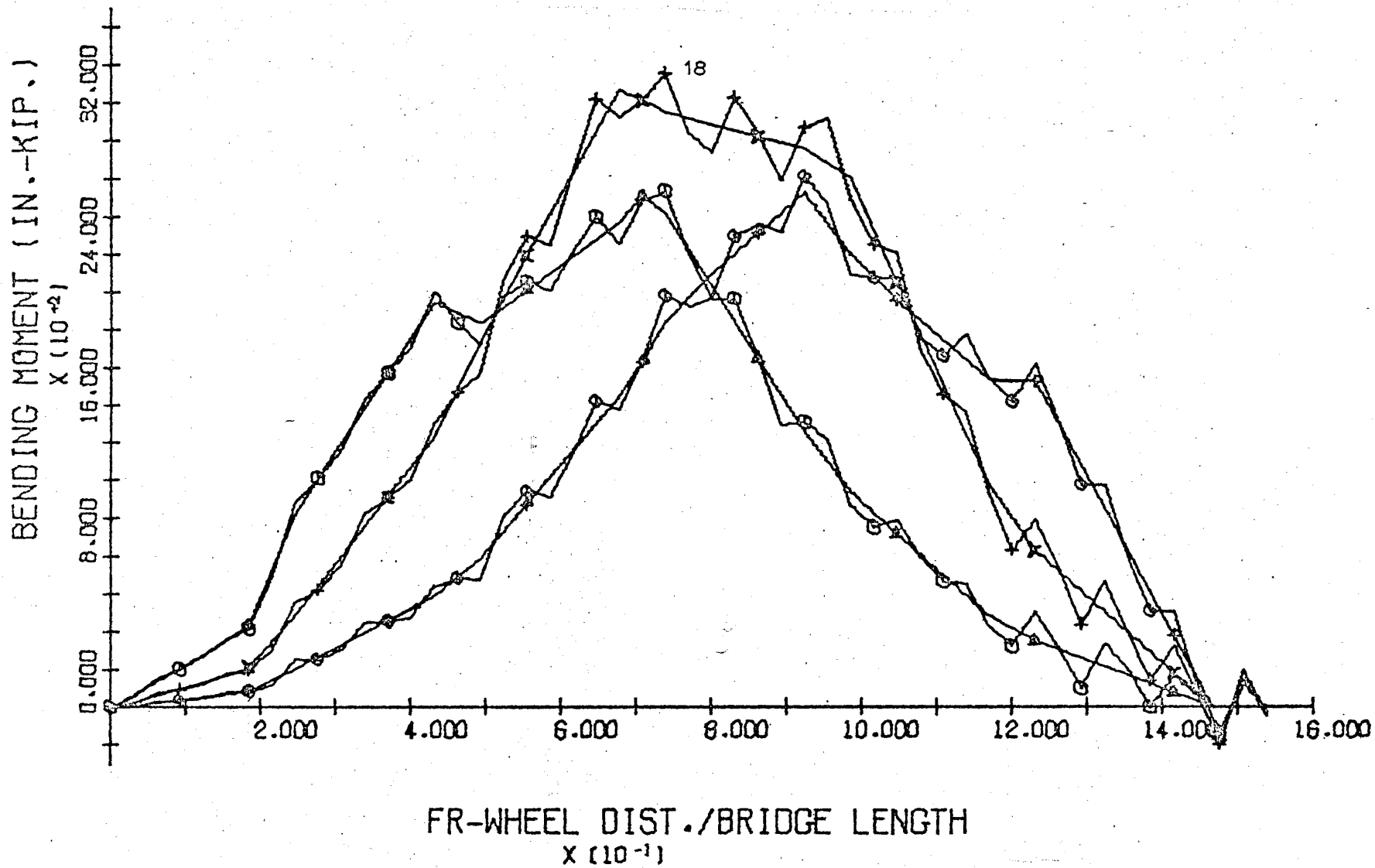
FIGURE 22 50MPH-LANE 3
BENDING MOMENT TIME HISTORY
BEAM C-NODE POINTS 17.18.19
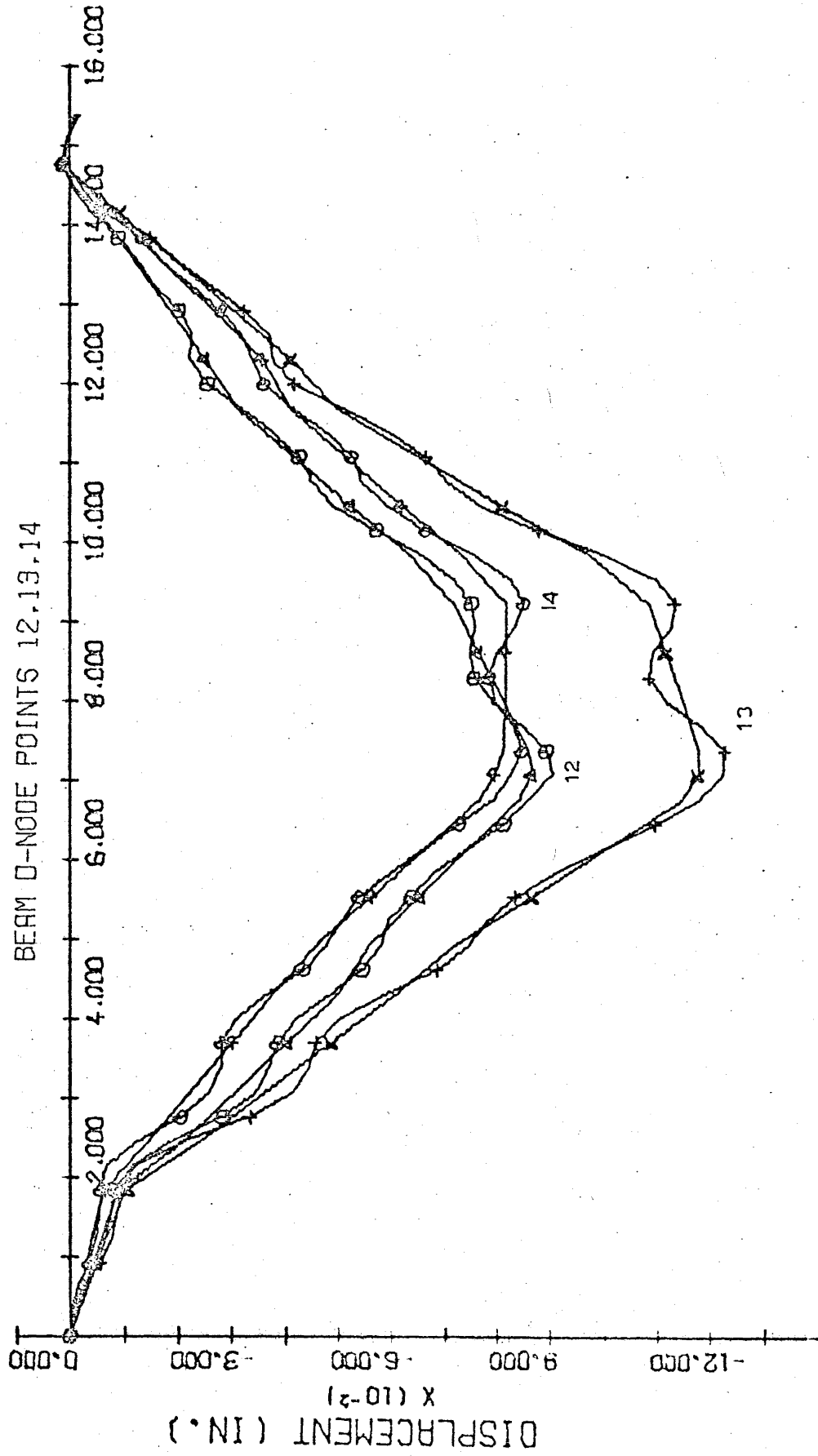
FR-WHEEL DIST./BRIDGE LENGTH
X (10⁻¹)
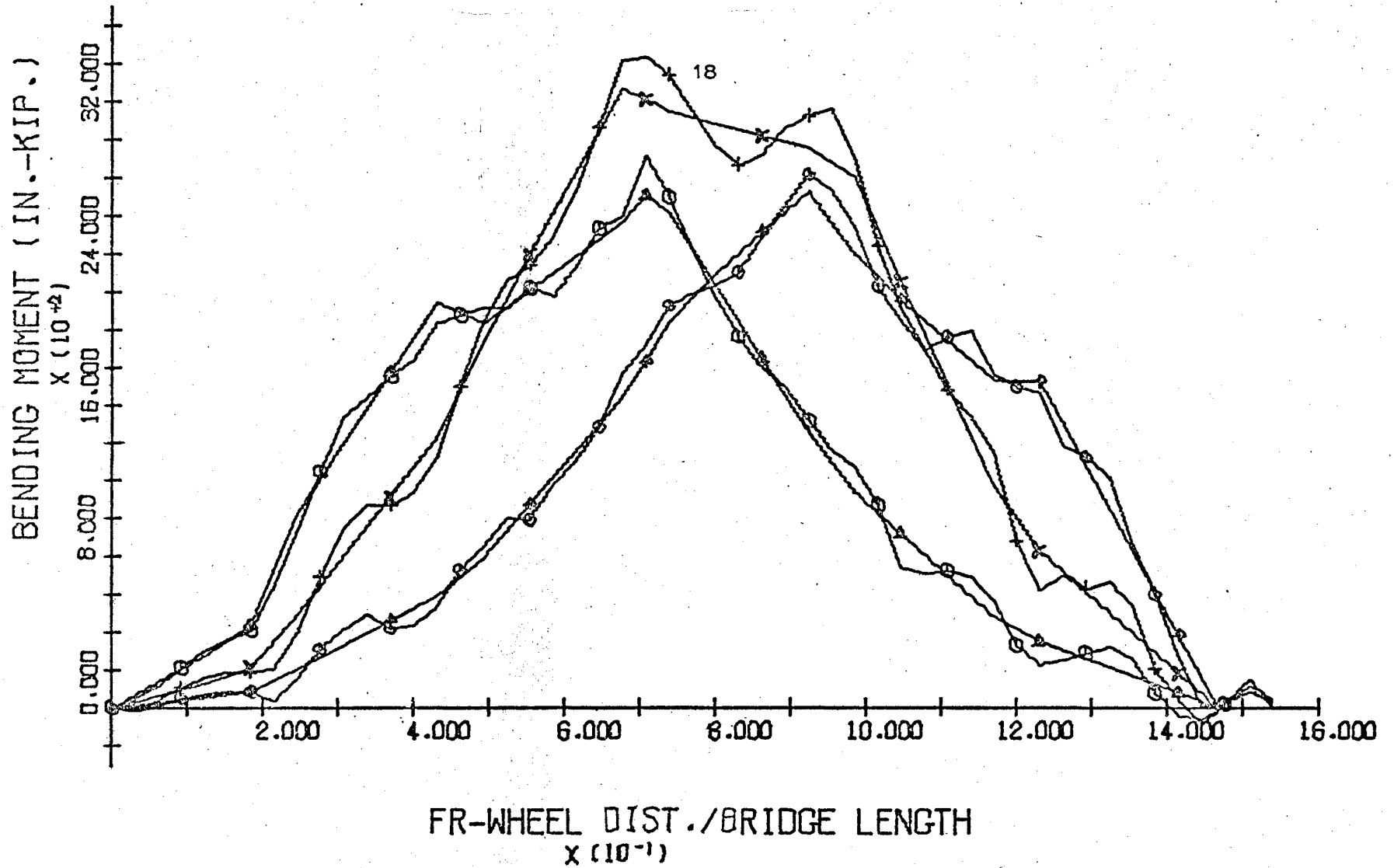
FIGURE 23 25MPH-LANE 3
DISPLACEMENT TIME HISTORY
BEAM 6-NODE POINTS 22,23,24

DISPLACEMENT (IN.) X (10⁻²)
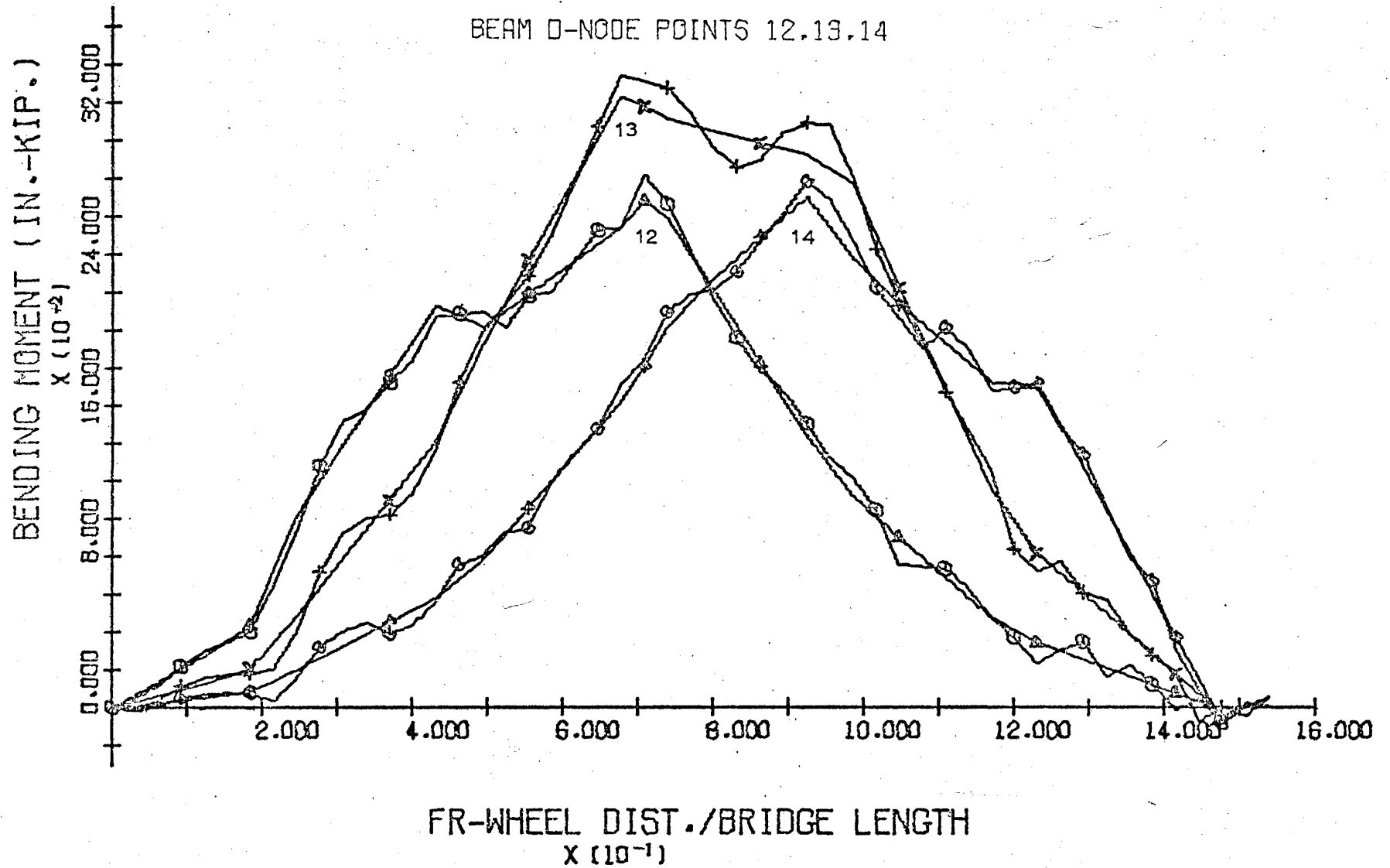
FR-WHEEL DIST./BRIDGE LENGTH
X (10⁻¹)
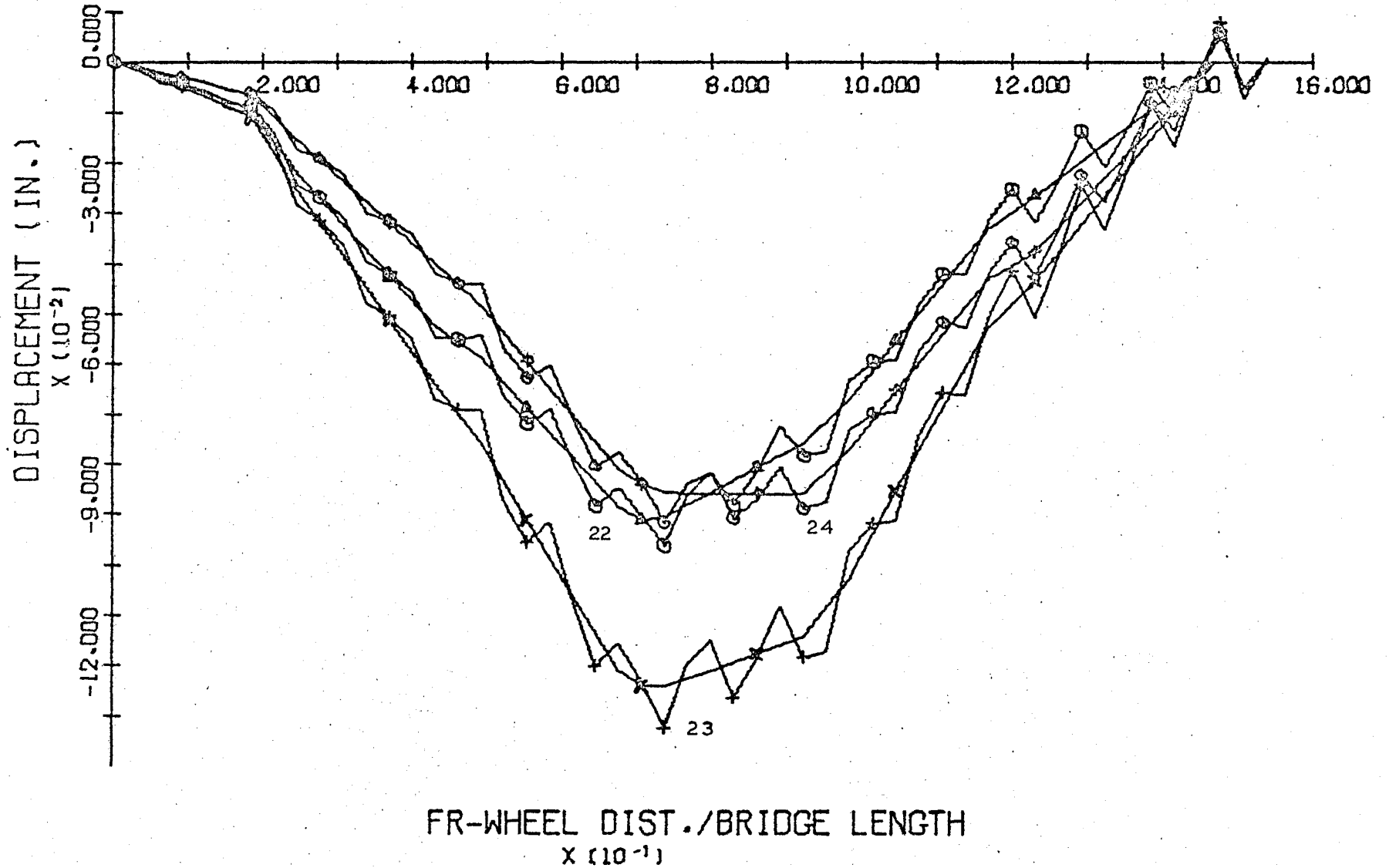
FIGURE 24 50MPH-LANE 3
DISPLACEMENT TIME HISTORY
BEAM B-NODE POINTS 22,23,24
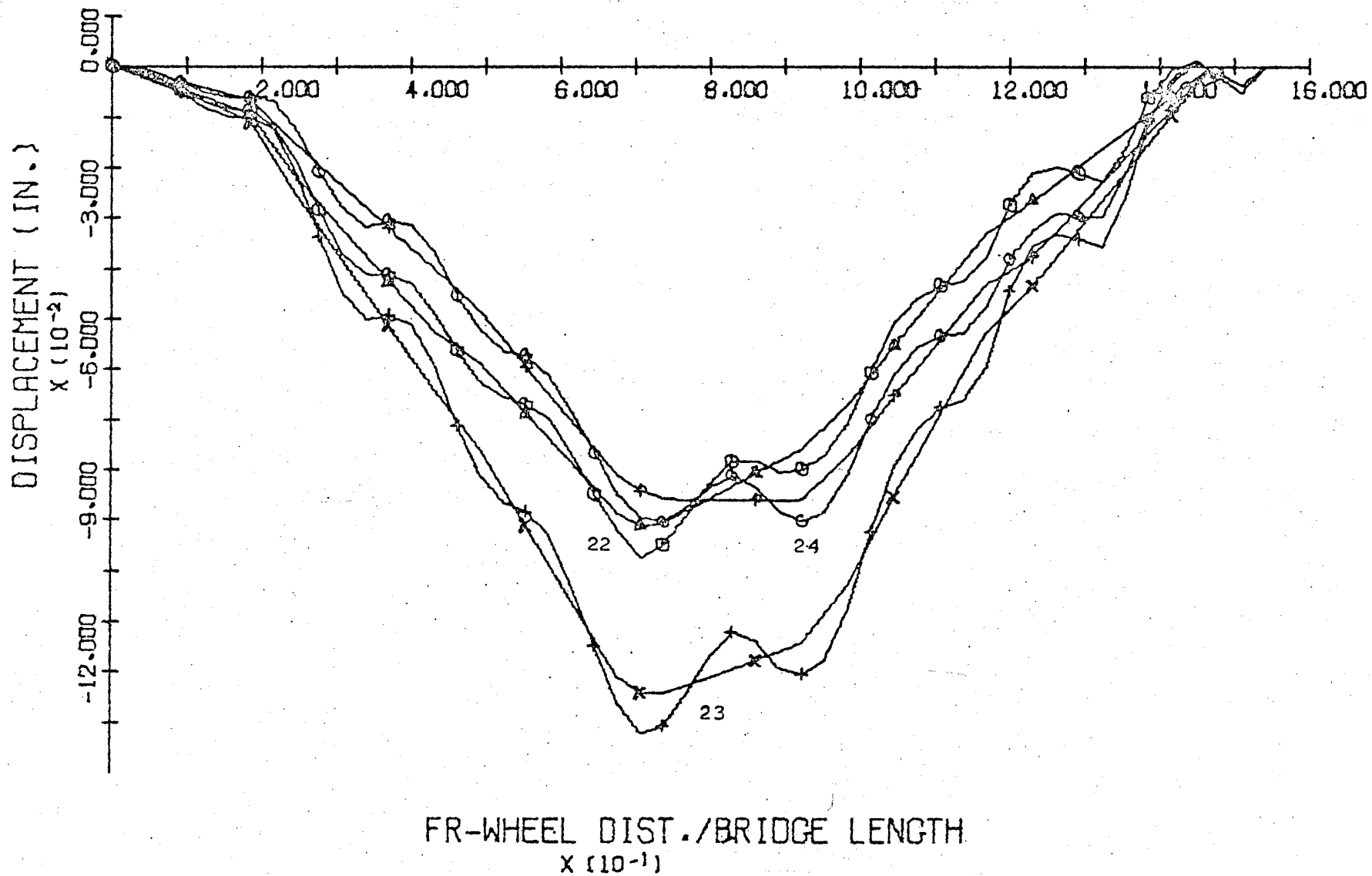
FIGURE 25 25MPH-LANE 3
BENDING MOMENT TIME HISTORY
BEAM 6-NODE POINTS 22,23,24

BENDING MOMENT (IN.-KIP.)
X (10⁺²)

FR-WHEEL DIST./BRIDGE LENGTH
X (10⁻¹)
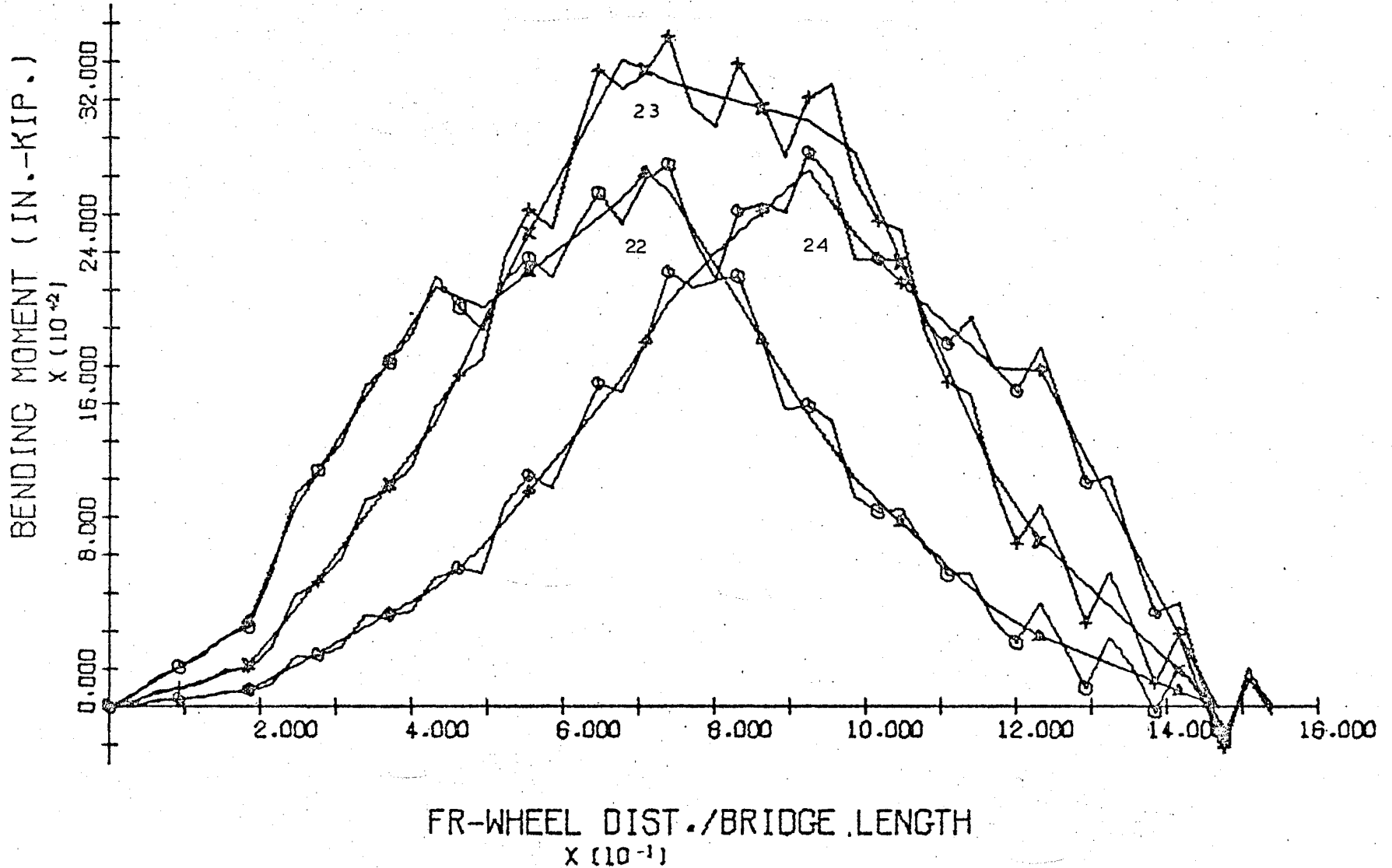
FIGURE 26 50MPH-LANE 3
BENDING MOMENT TIME HISTORY
BEAM B-NODE POINTS 22,23,24

BENDING MOMENT (IN.-KIP.) X (10⁻²)

FR-WHEEL DIST./BRIDGE LENGTH
X (10⁻¹)
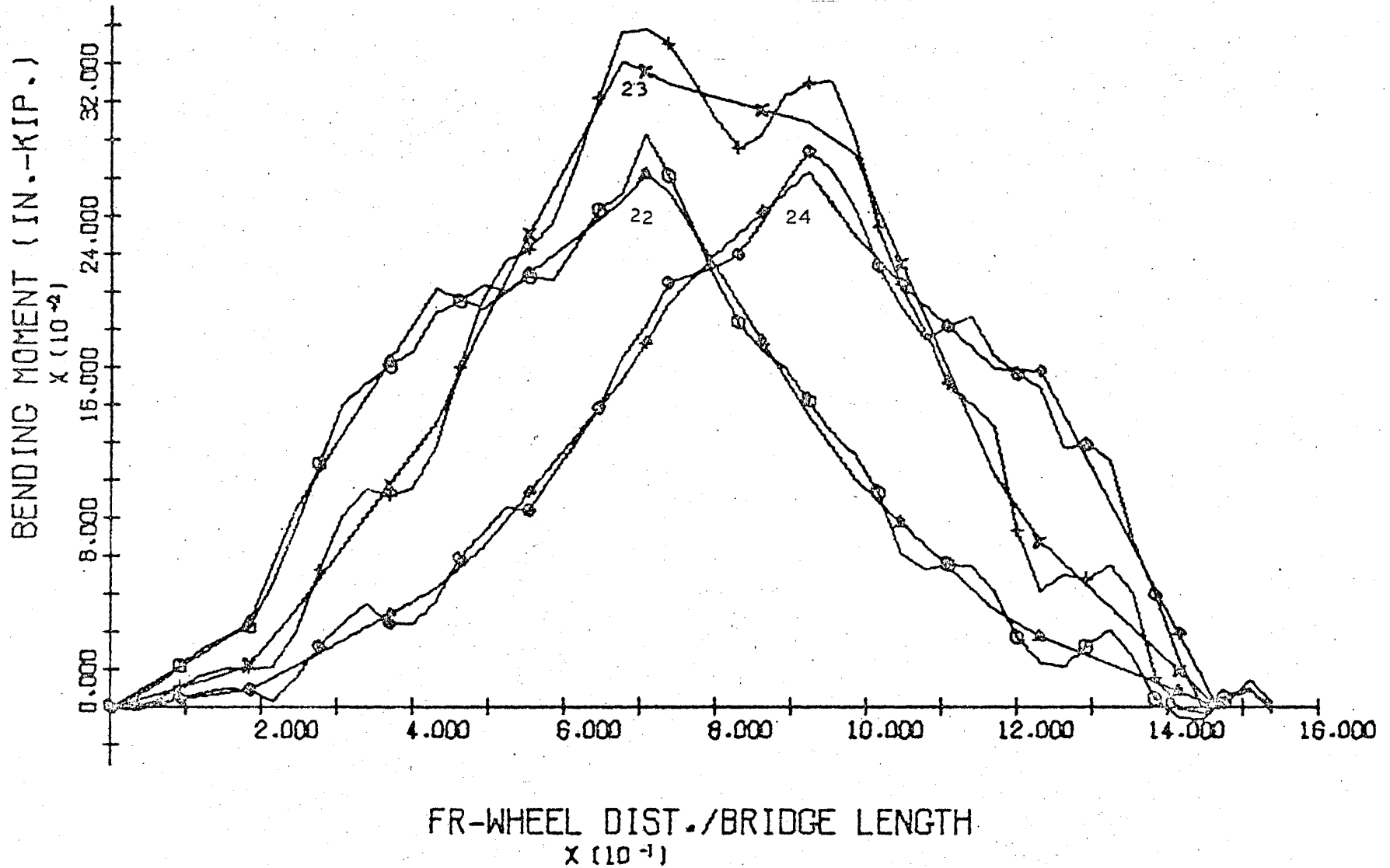
FIGURE 27 25MPH-LANE 3
DISPLACEMENT TIME HISTORY
BEAM A-NODE POINTS 27,28,29

FR-WHEEL DIST./BRIDGE LENGTH
X (10⁻¹)

DISPLACEMENT (IN.)
X (10⁻²)
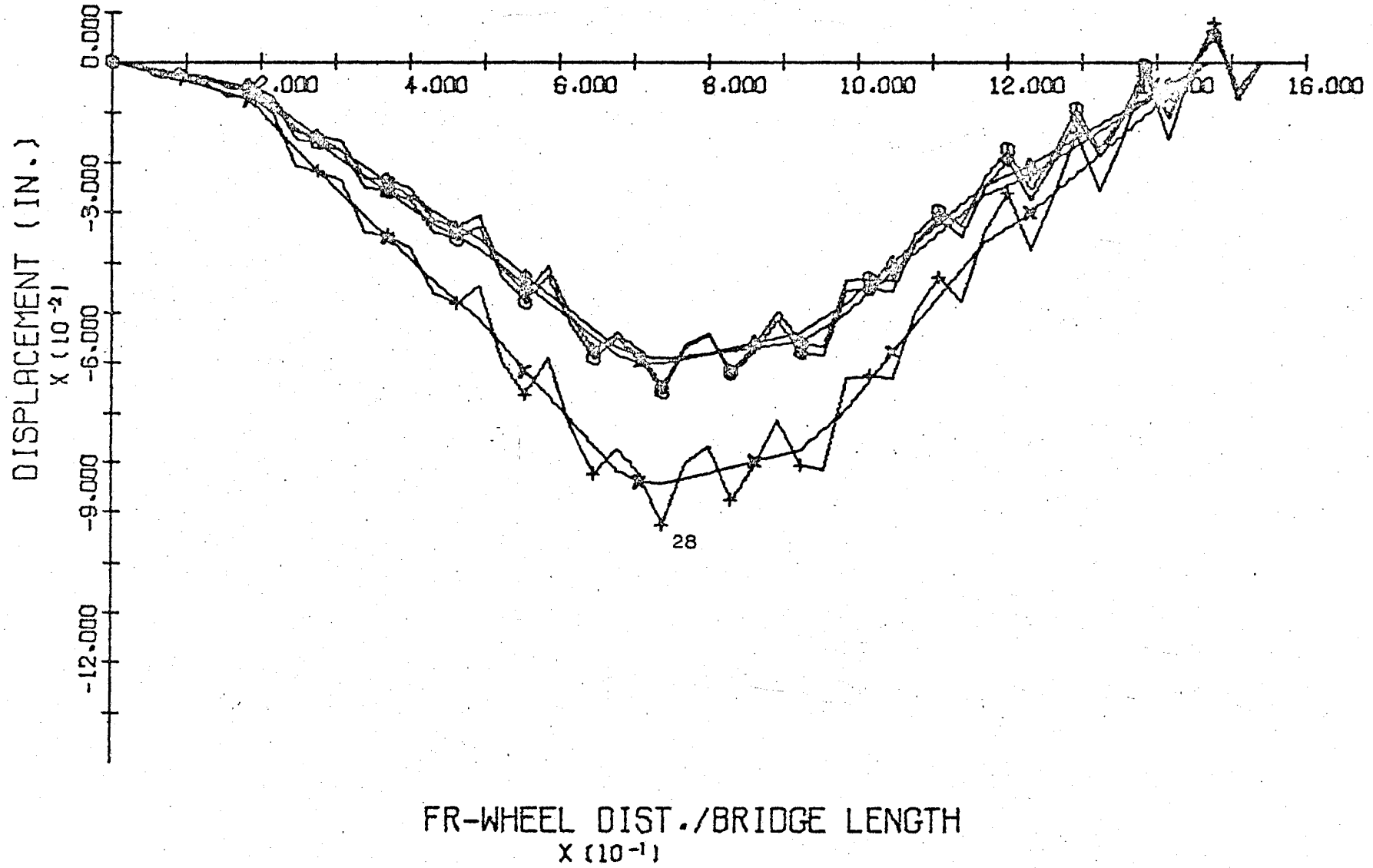
FIGURE 28 50MPH-LANE 3
DISPLACEMENT TIME HISTORY
BEAM A-NODE POINTS 27,28,29

FR-WHEEL DIST./BRIDGE LENGTH
X (10⁻¹)

-68-
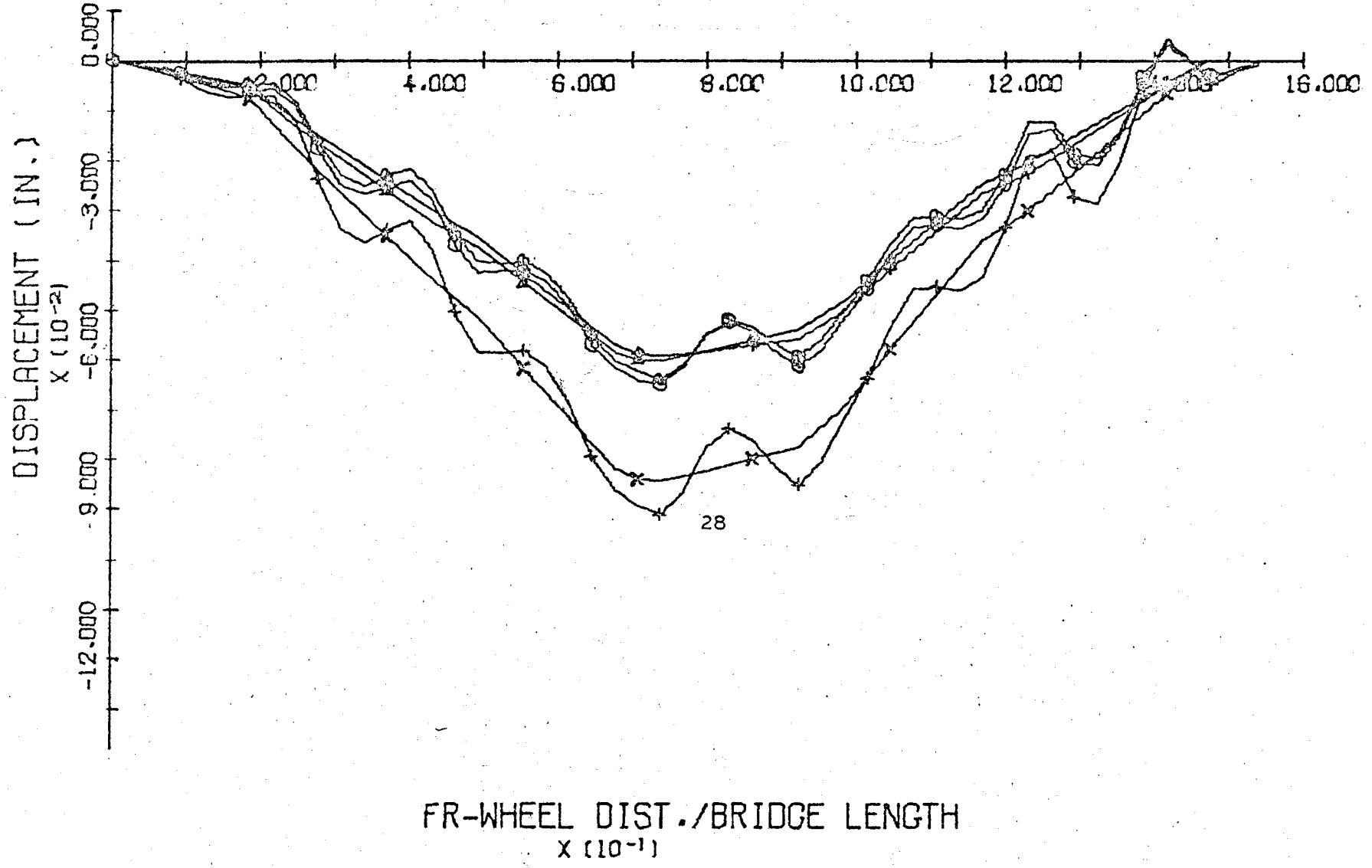
FIGURE 29 25MPH-LANE 3
BENDING MOMENT TIME HISTORY
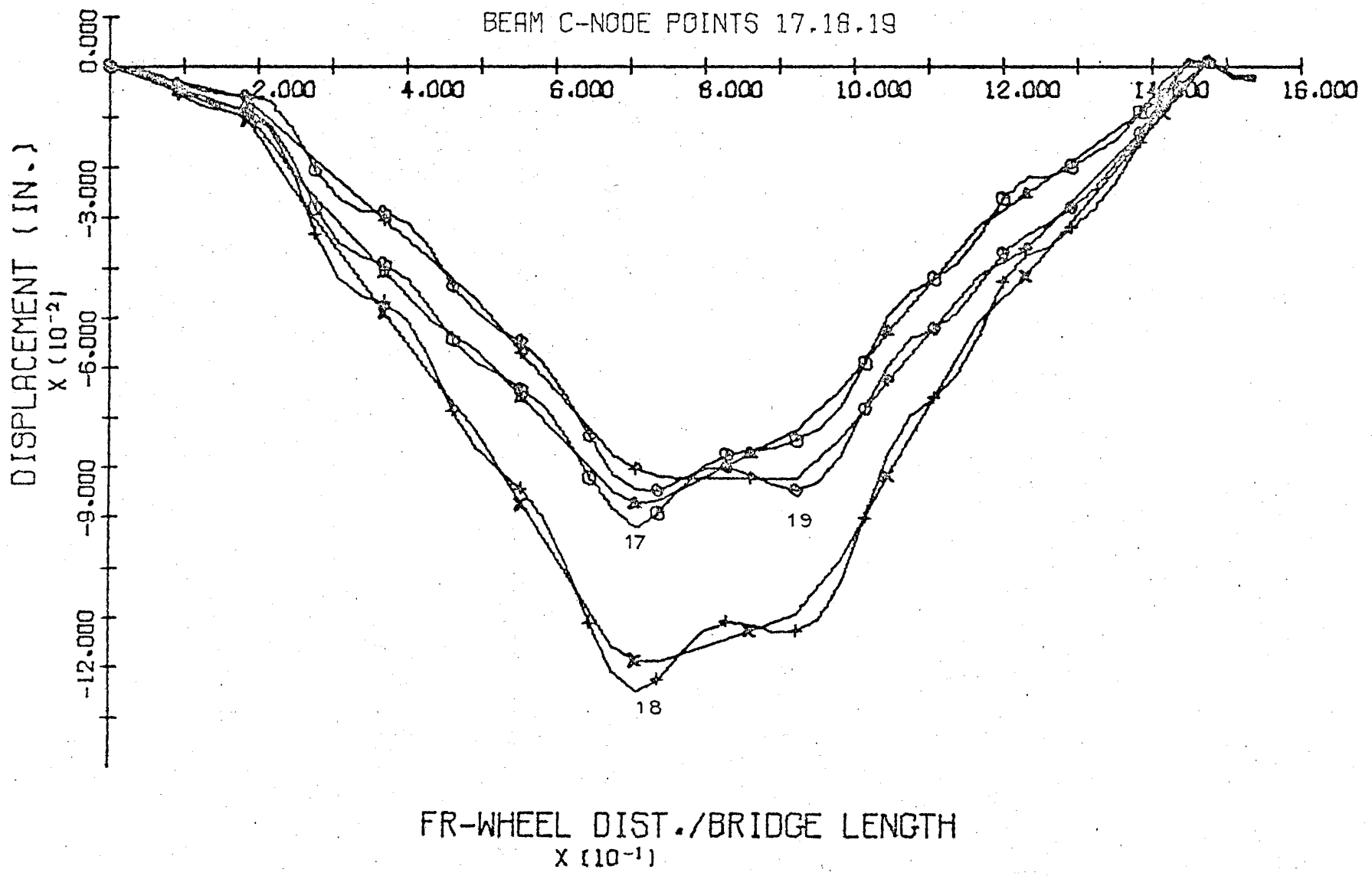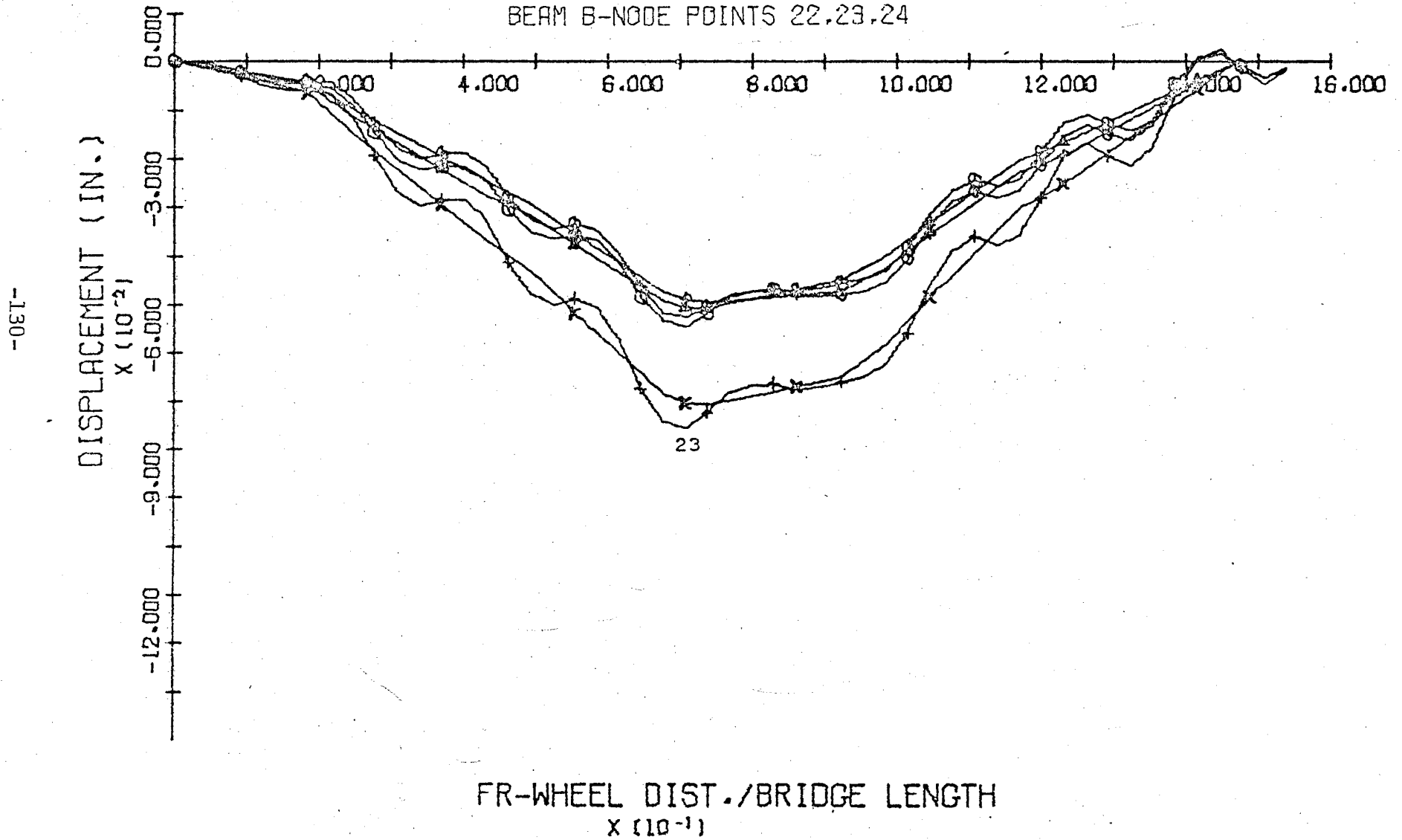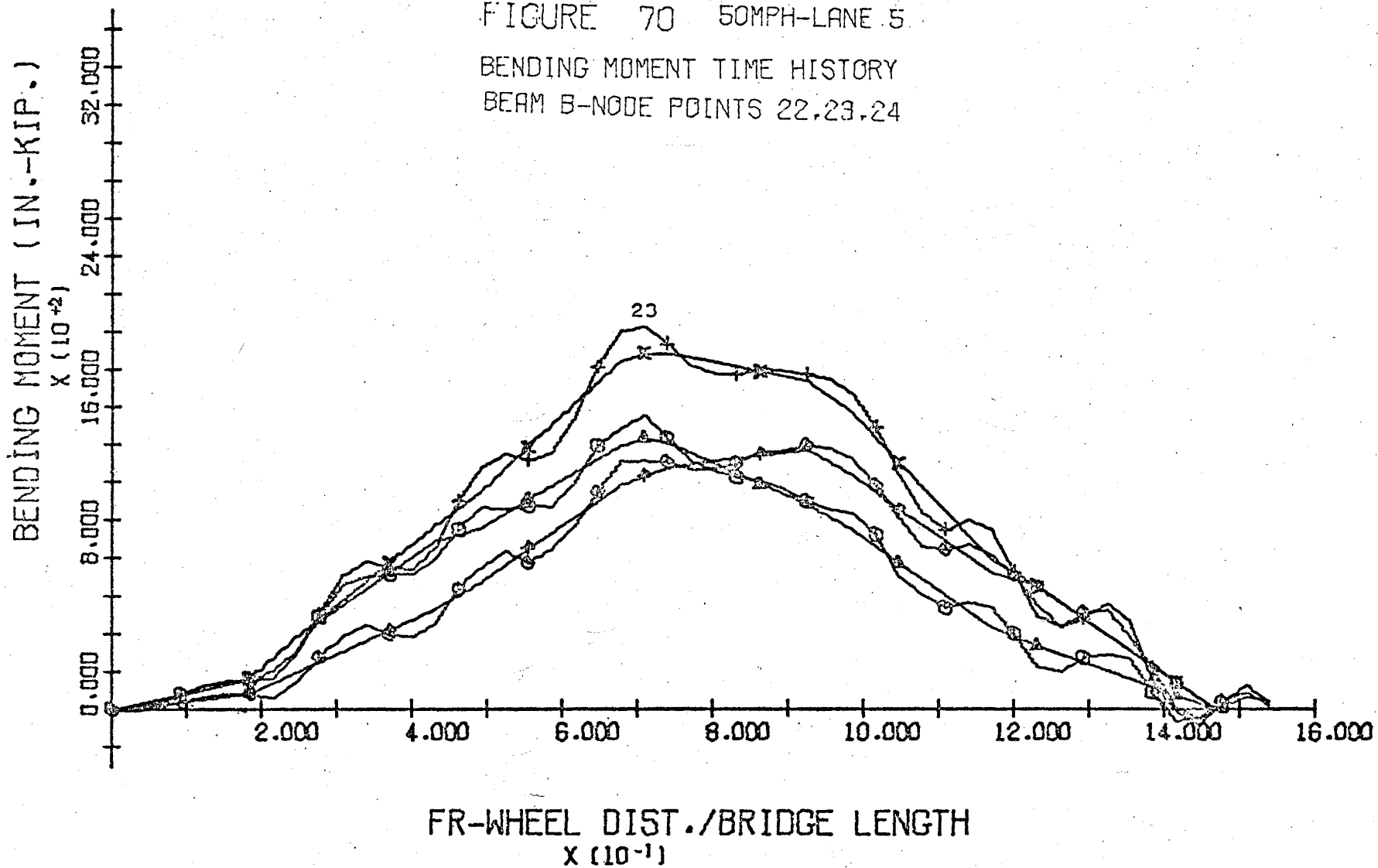BEAM A-NODE POINTS 27,28,29

FR-WHEEL DIST./BRIDGE LENGTH
X [10⁻¹]
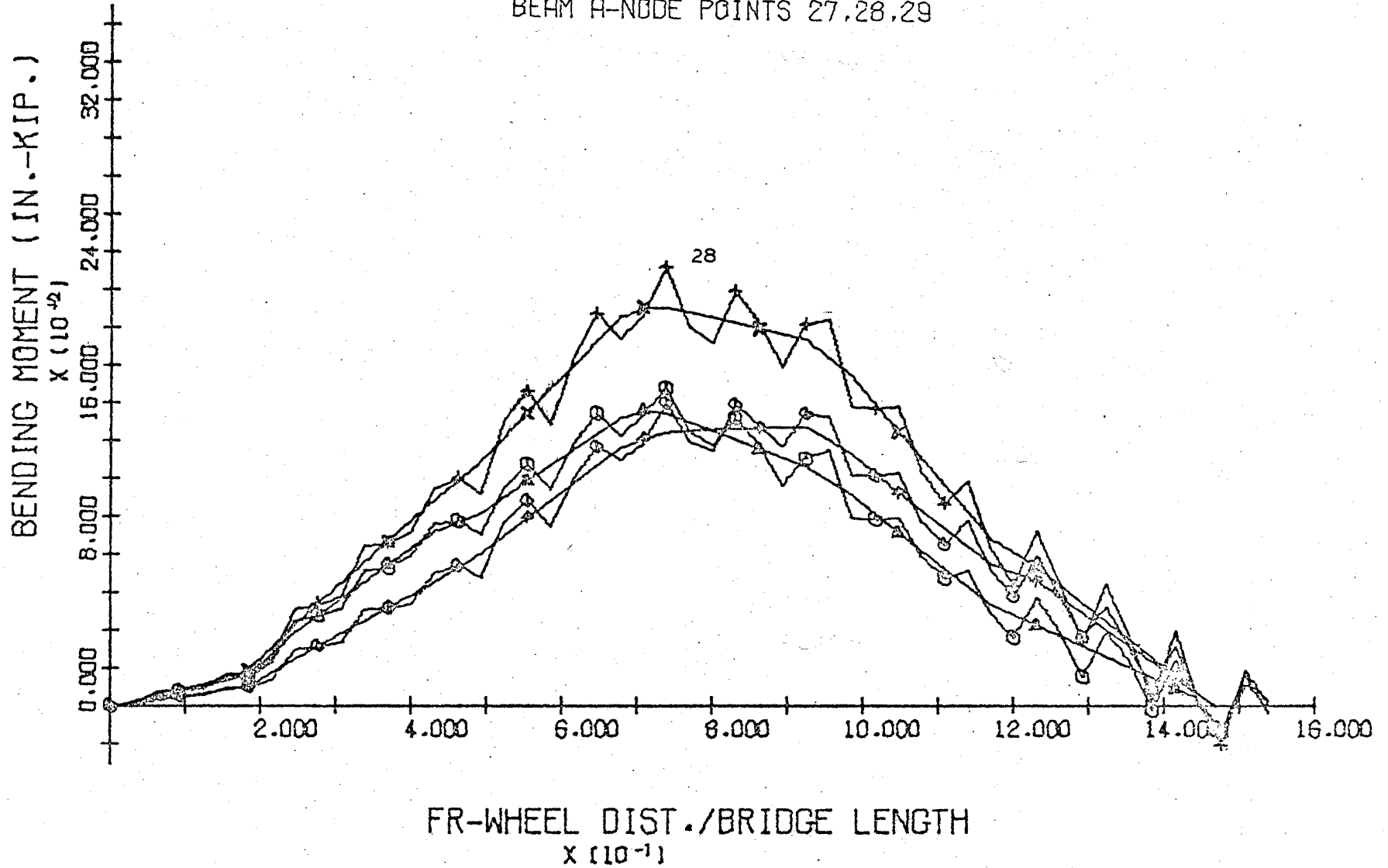
FIGURE 30 50MPH-LANE 3
BENDING MOMENT TIME HISTORY
BEAM A-NODE POINTS 27,28,29
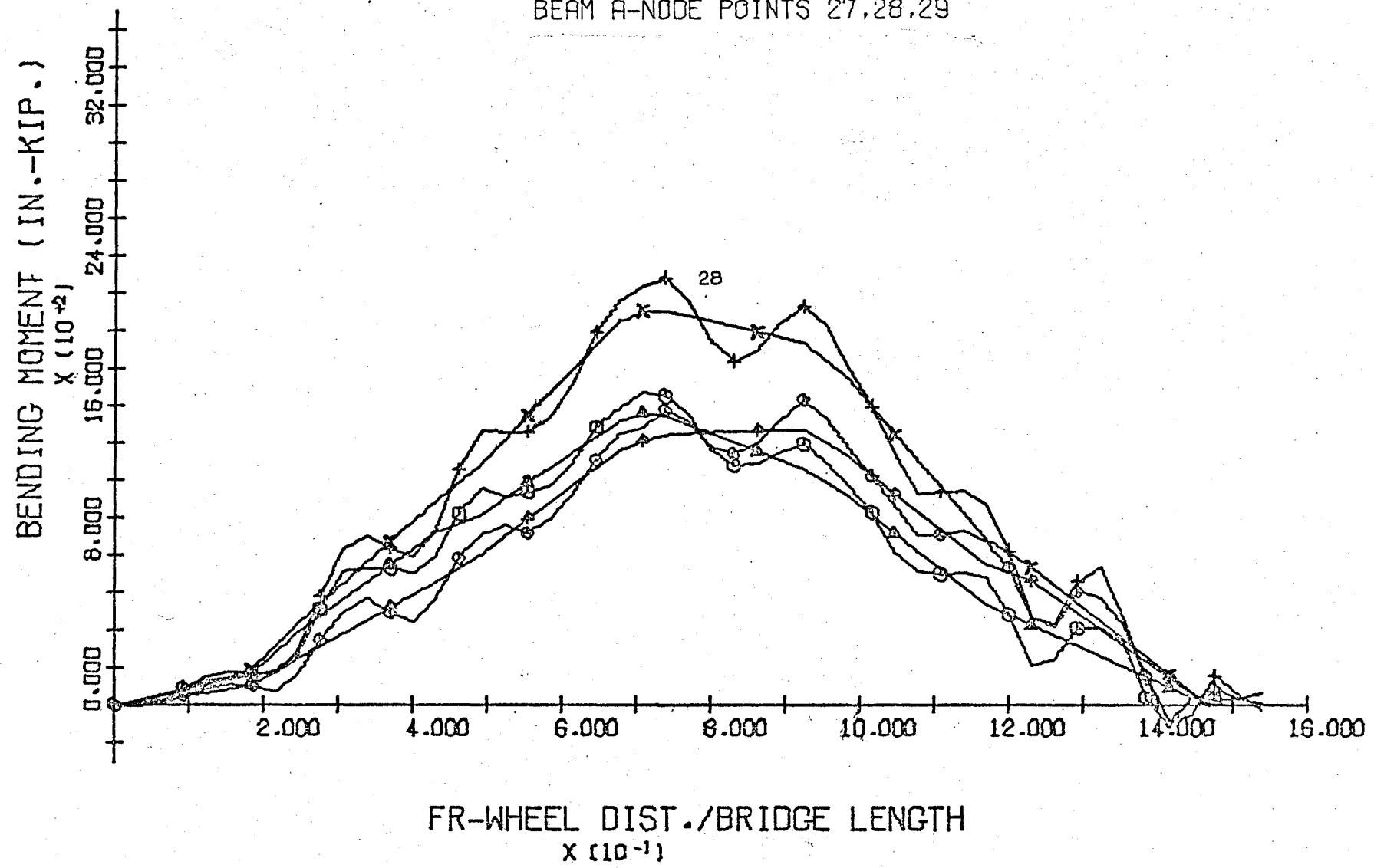
FIGURE 31 25MPH-LANE 3
DISPLACEMENT TIME HISTORY
NODE POINTS 3,8,13,18,23,28

FR-WHEEL DIST./BRIDGE LENGTH
X (10⁻¹)

FIGURE 32 50MPH-LANE 3
DISPLACEMENT TIME HISTORY

NODE POINTS 3,8,13,18,23,28

FR-WHEEL DIST./BRIDGE LENGTH
X (10⁻¹)
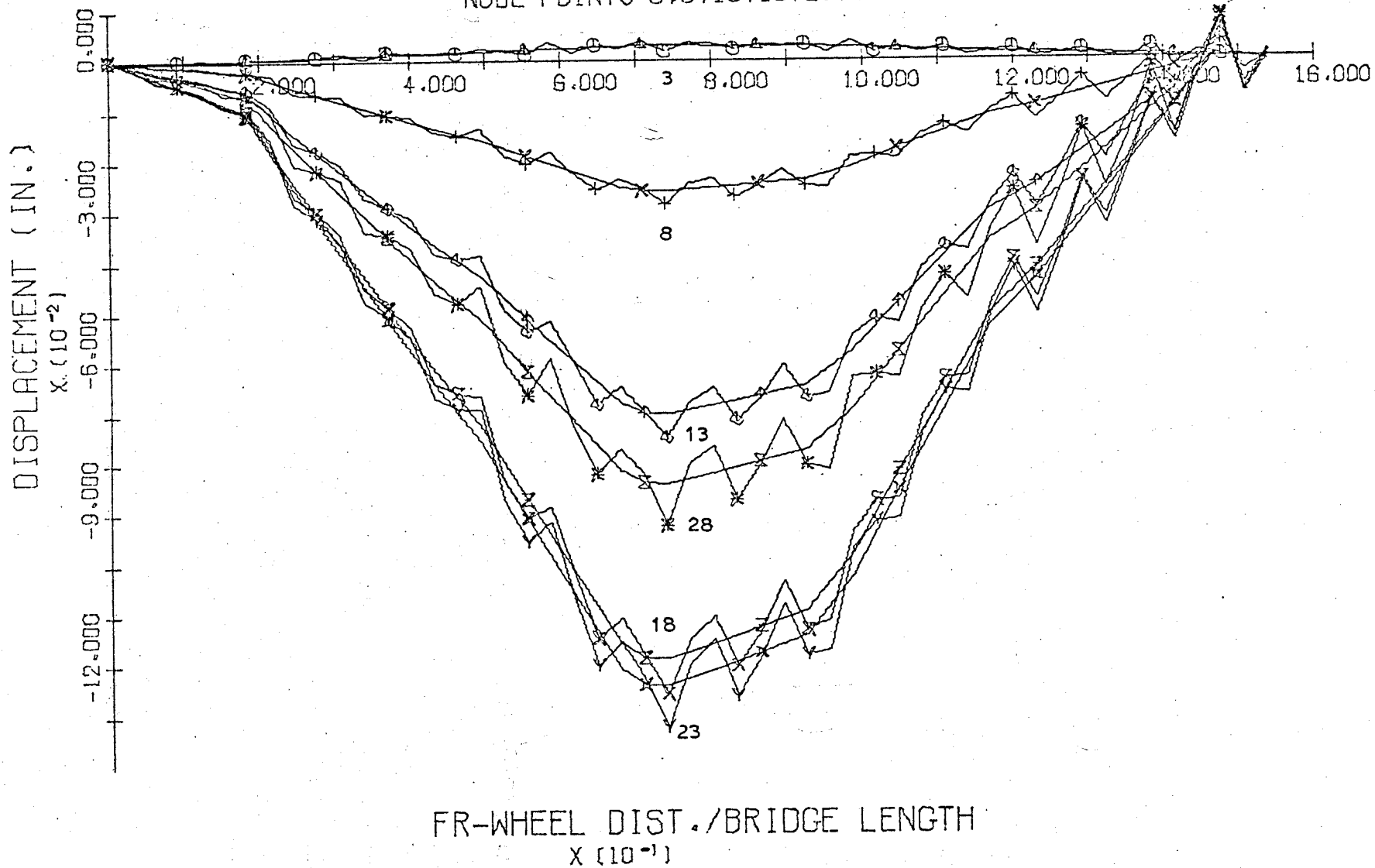
FIGURE 33 25MPH-LANE 3
BENDING MOMENT TIME HISTORY
NODE POINTS 3,8,13,18,23,28

BENDING MOMENT (IN.-KIP.)
X (10^2)

FR-WHEEL DIST./BRIDGE LENGTH
X (10^-1)

FIGURE 34 50MPH-LANE 3
BENDING MOMENT TIME HISTORY

NODE POINTS 3,8,13,18,23,28

FR-WHEEL DIST./BRIDGE LENGTH
X (10⁻¹)
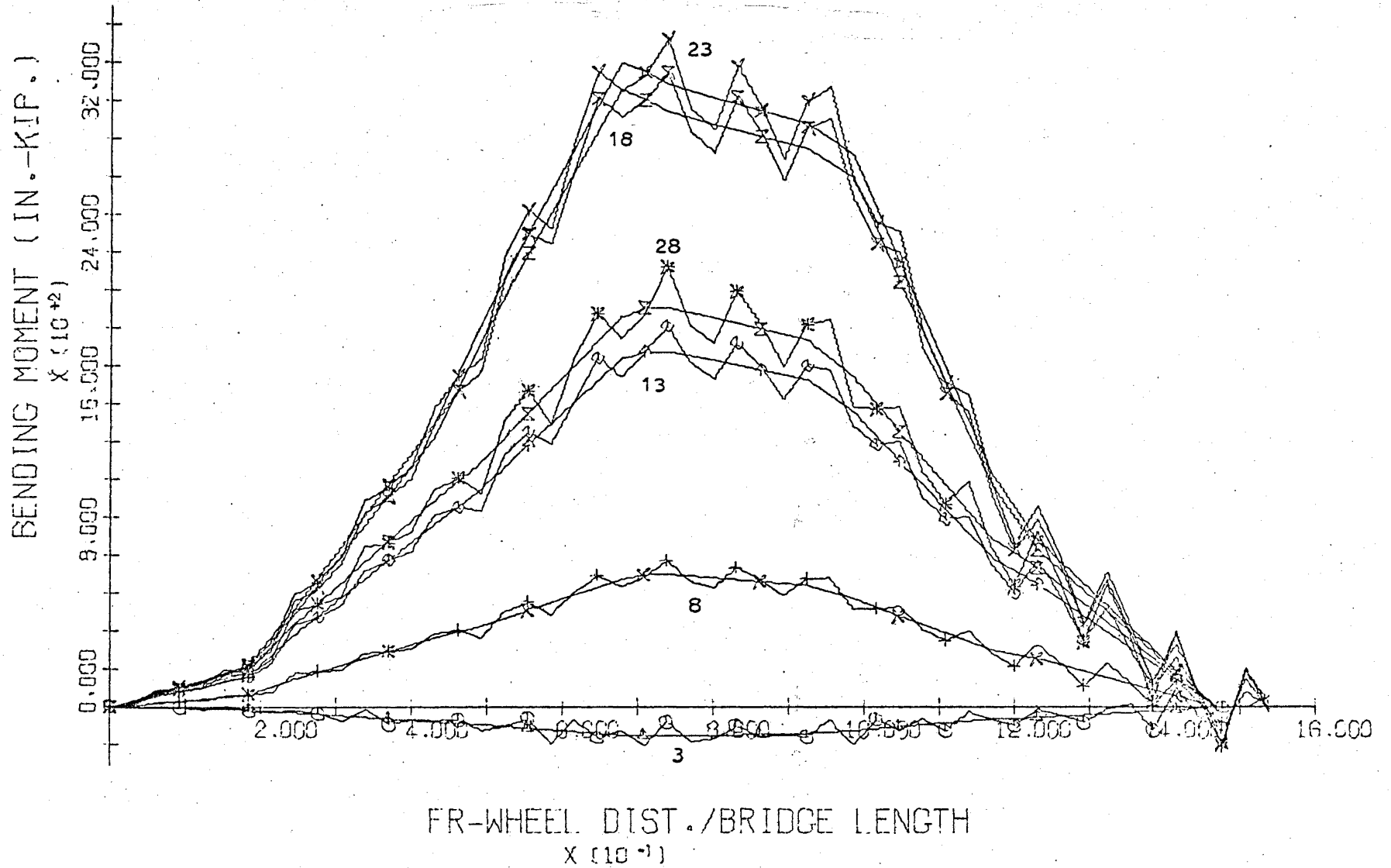
FIGURE 35 25MPH-LANE 3
DISPLACEMENT TIME HISTORY
BEAM F - NODE POINT 3
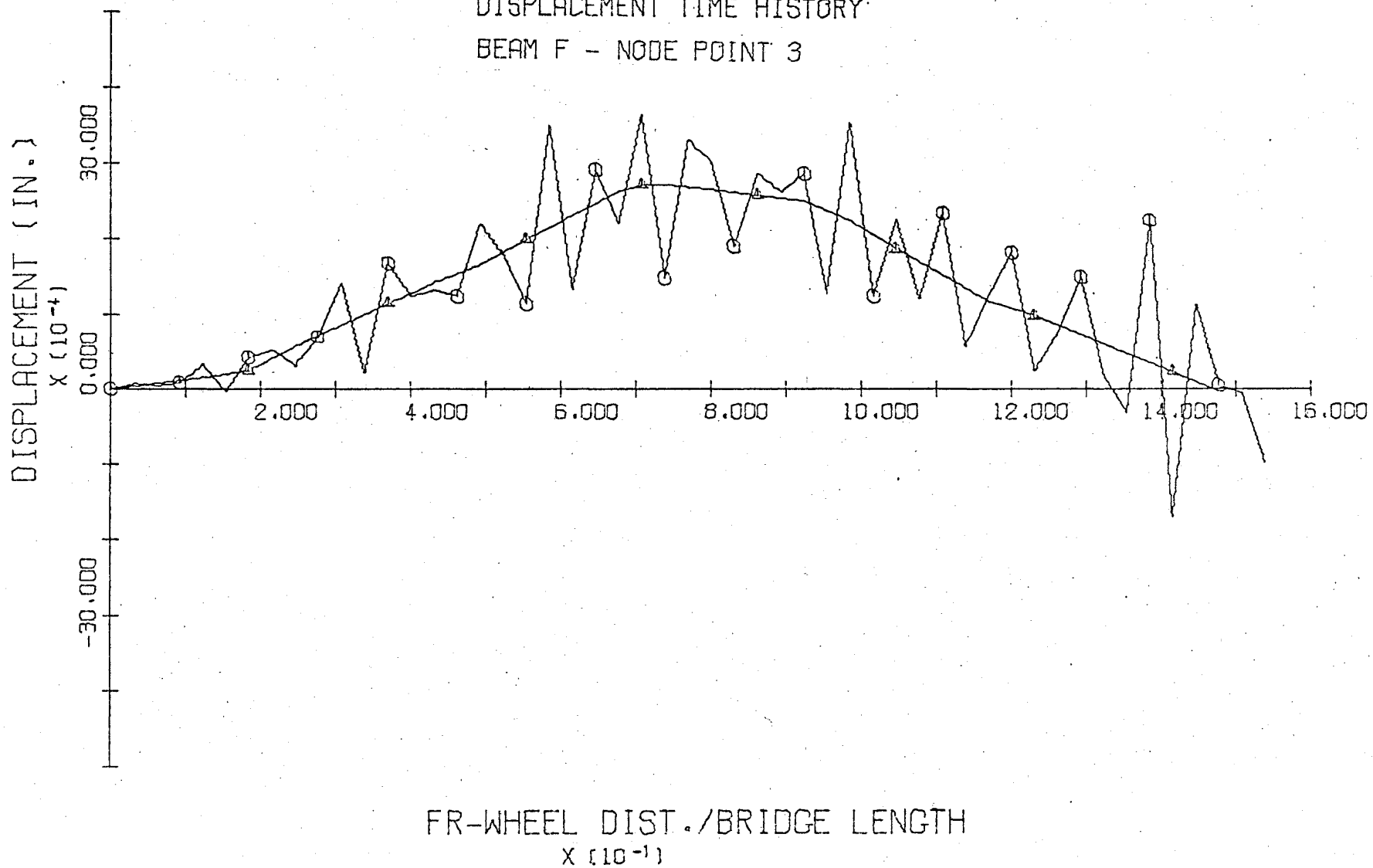
DISPLACEMENT (IN.)
X (10⁻⁴)

FR-WHEEL DIST./BRIDGE LENGTH
X (10⁻¹)

FICURE 36 50MPH-LANE 3
DISPLACEMENT TIME HISTORY
BEAM F - NODE POINT 3

DISPLACEMENT (IN.)
X (10⁻⁴)

FR-WHEEL DIST./BRIDGE LENGTH
X (10⁻¹)

FIGURE 37 25MPH-LANE 3
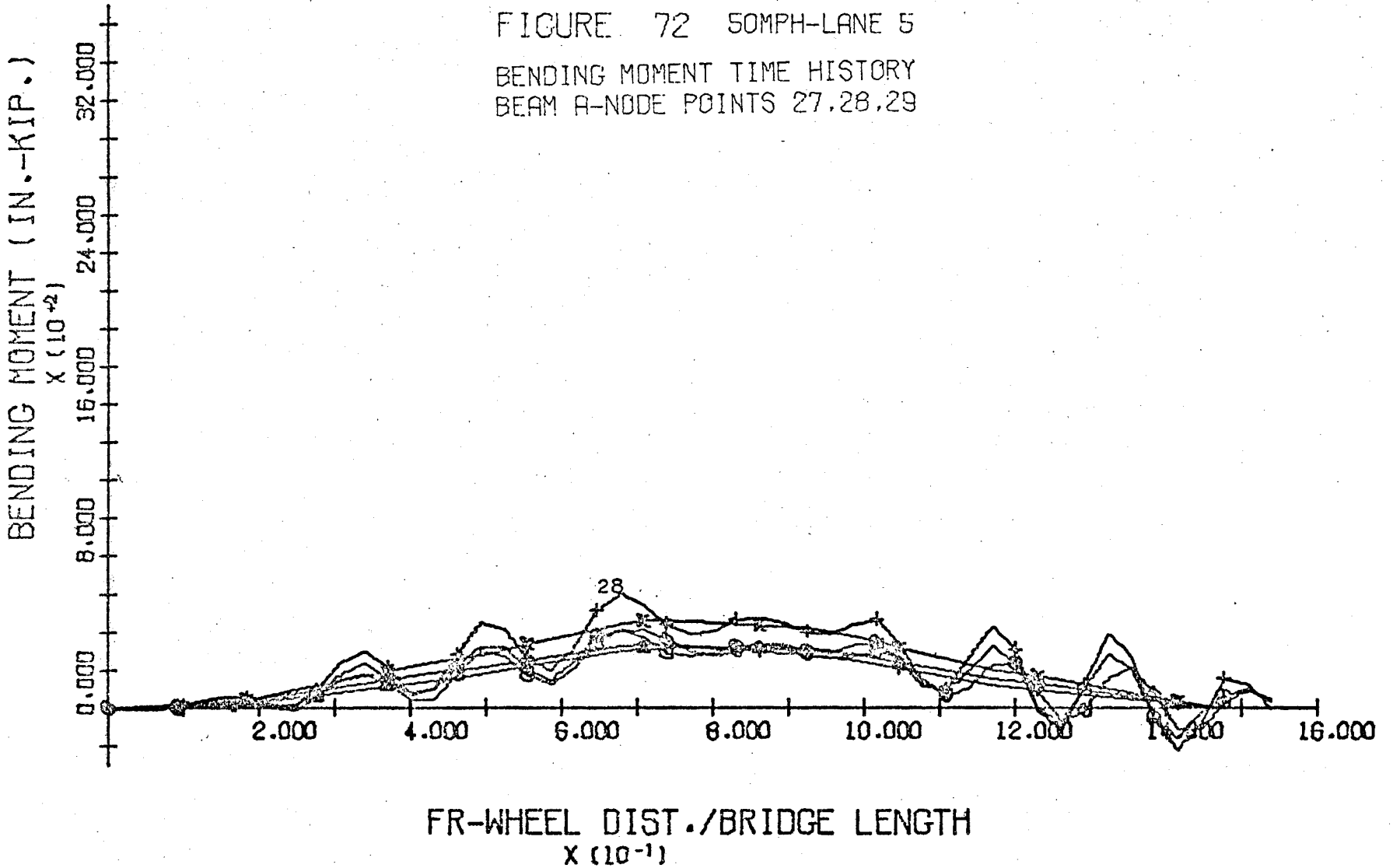BENDING MOMENT TIME HISTORY
BEAM F - NODE POINT 3

BENDING MOMENT (IN.-KIP.)
X (10⁺¹)

FR-WHEEL DIST./BRIDGE LENGTH
X (10⁻¹)
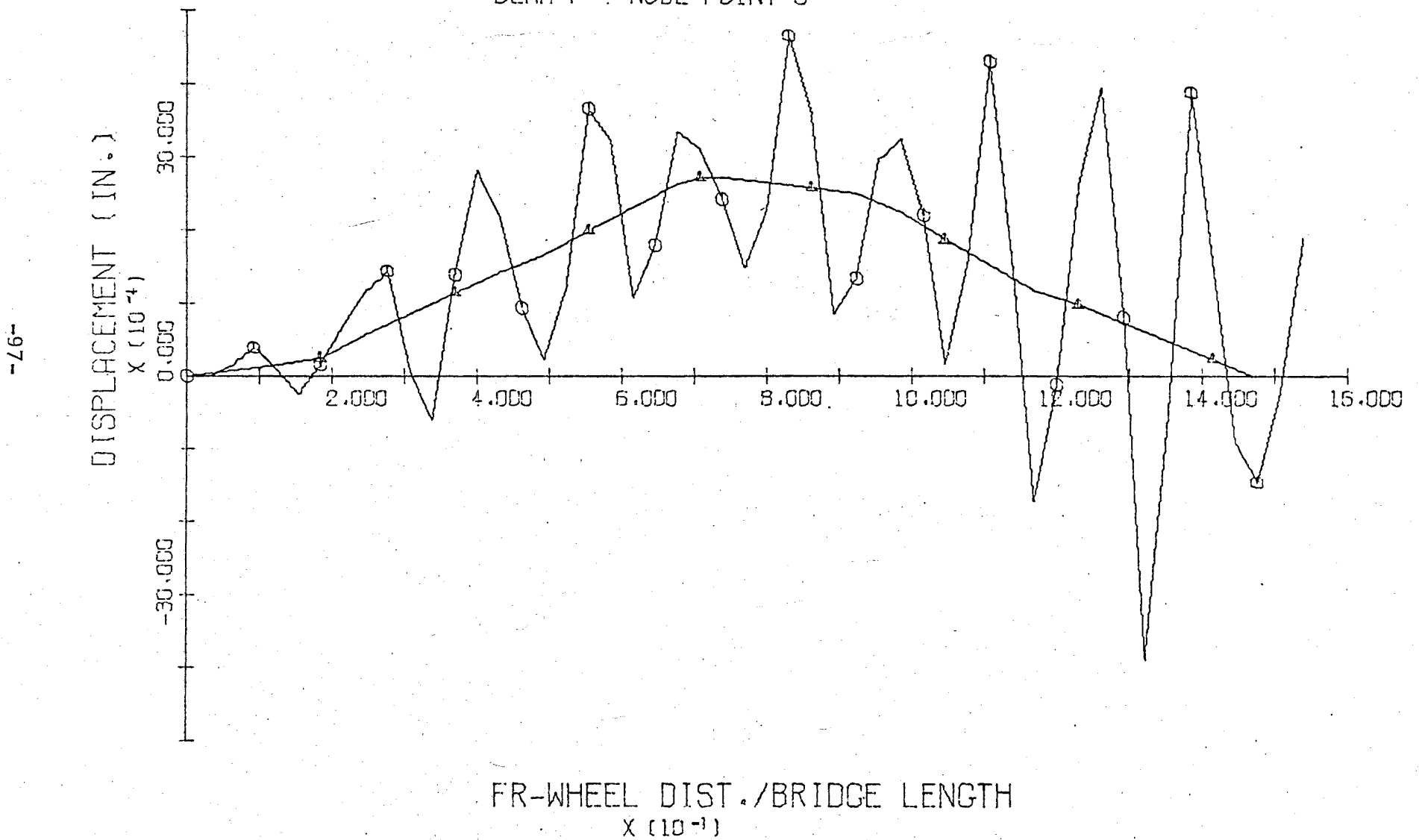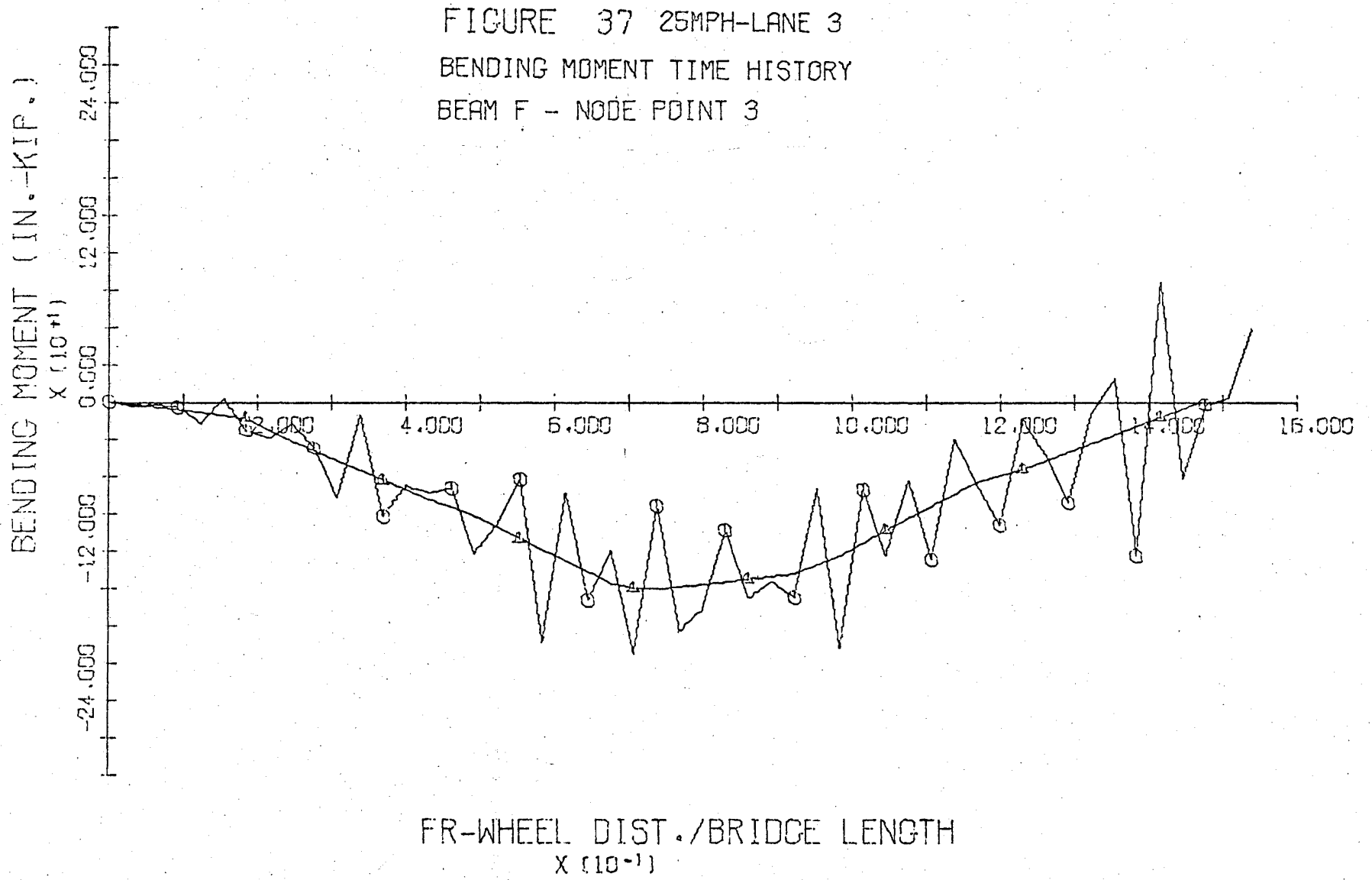
FIGURE 38 50MPH-LANE 3
BENDING MOMENT TIME HISTORY
BEAM F - NODE POINT 3

FR-WHEEL DIST./BRIDGE LENGTH
X (10⁻¹)

BENDING MOMENT (IN.-KIP.)
X (10⁻¹)

-99-
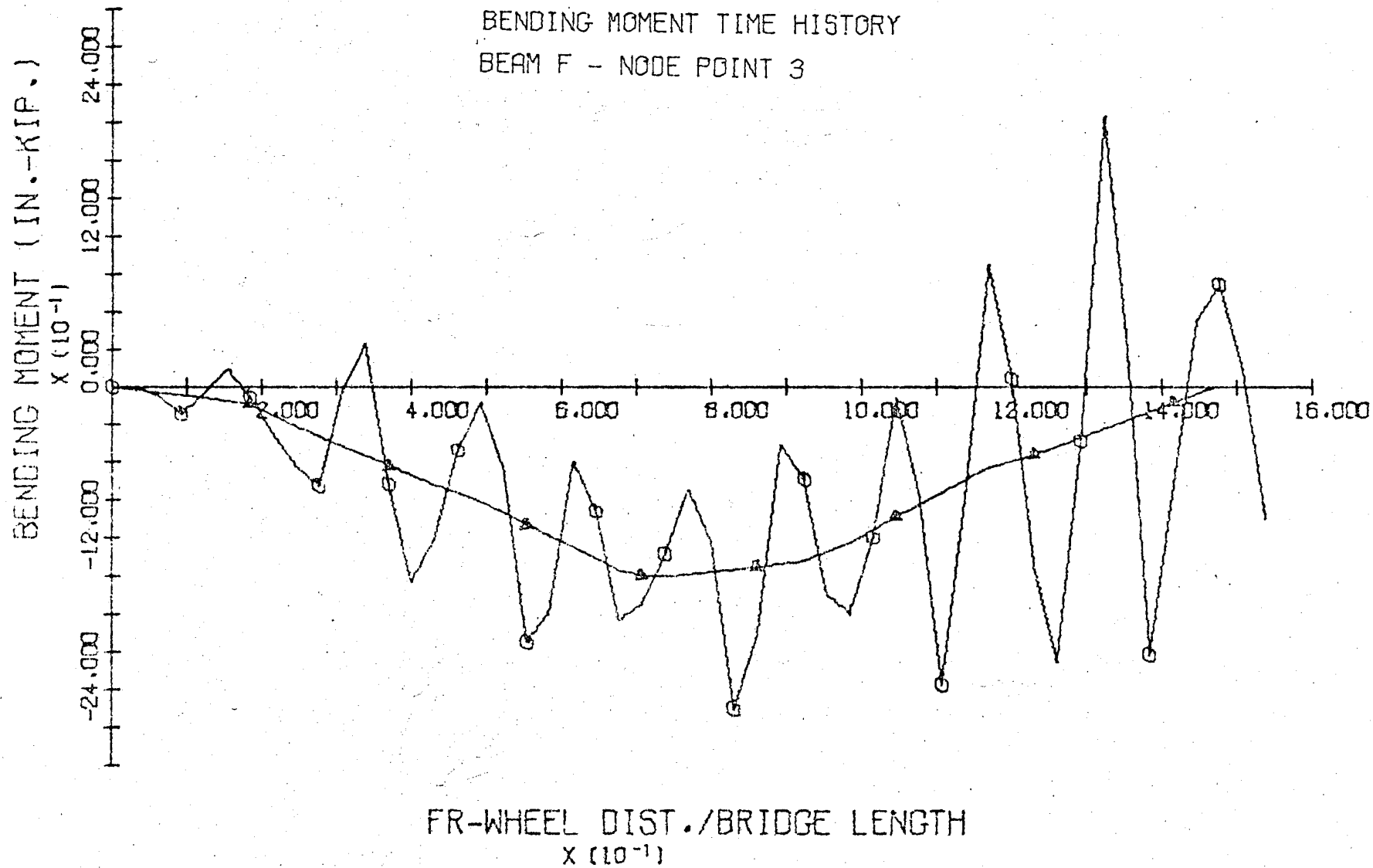
FIGURE 39 50MPH-LANE 3
DISPLACEMENT TIME HISTORY
BEAM B-NODE POINT 23

FR-WHEEL DIST./BRIDGE LENGTH
X (10⁻¹)
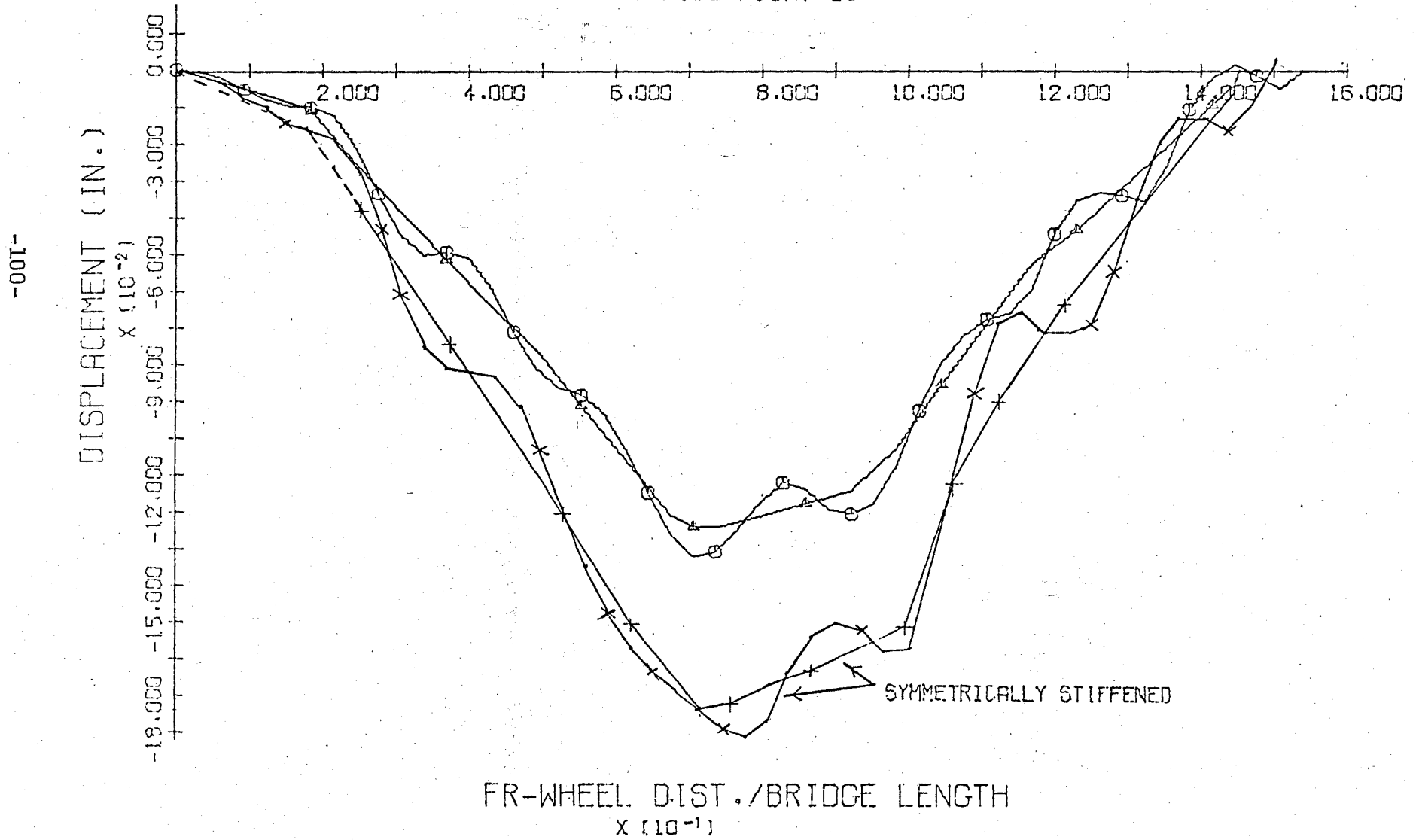
FIGURE 40 50MPH-LANE 3
DISPLACEMENT TIME HISTORY
BEAM F - NODE POINT 3
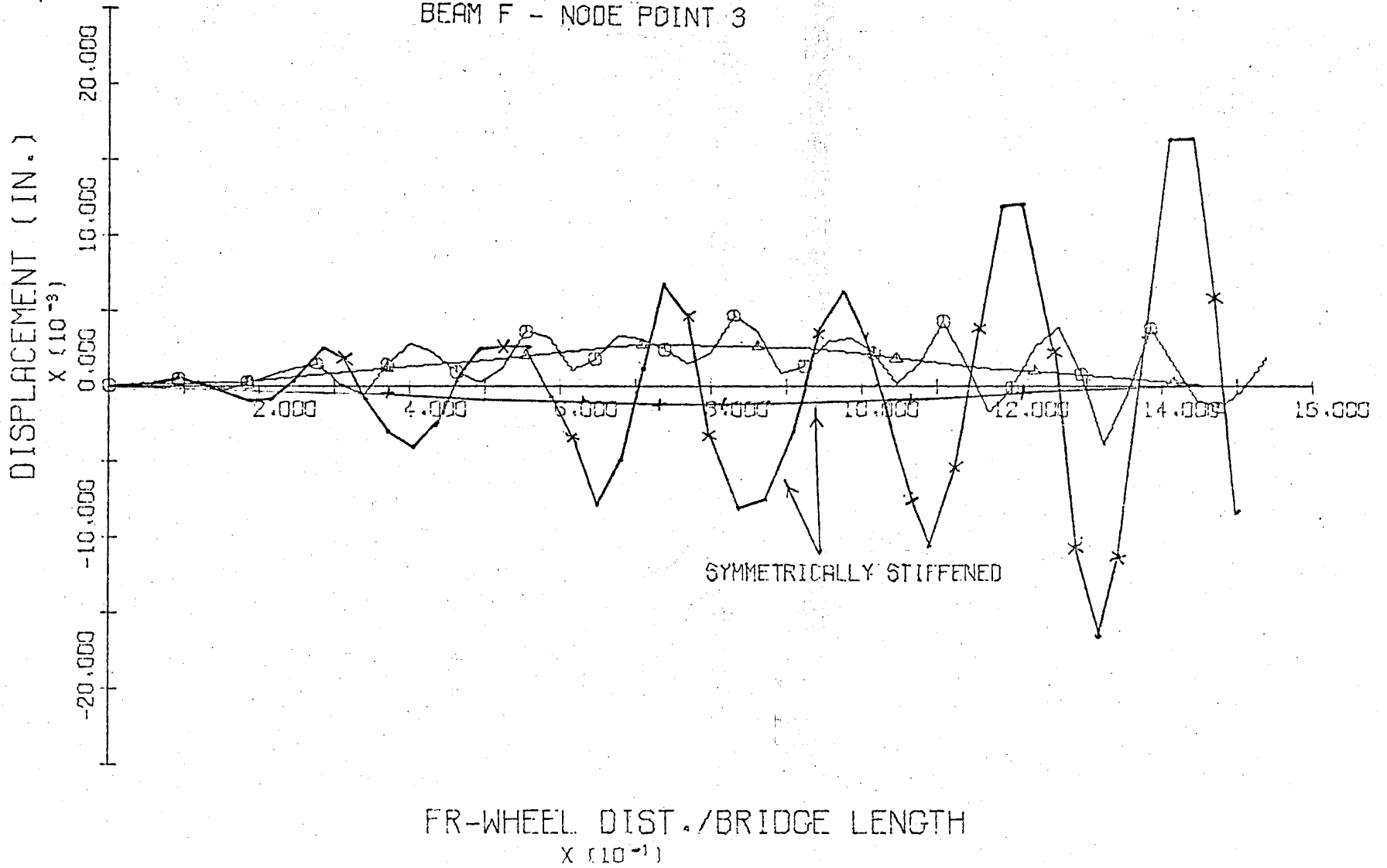
-101-

DISPLACEMENT (IN.)
X (10⁻³)

FR-WHEEL DIST./BRIDGE LENGTH
X (10⁻¹)

SYMMETRICALLY STIFFENED

FIGURE 41 300MPH-LANE 3
DISPLACEMENT TIME HISTORY
NODE POINTS 3,8,13,18,23,28
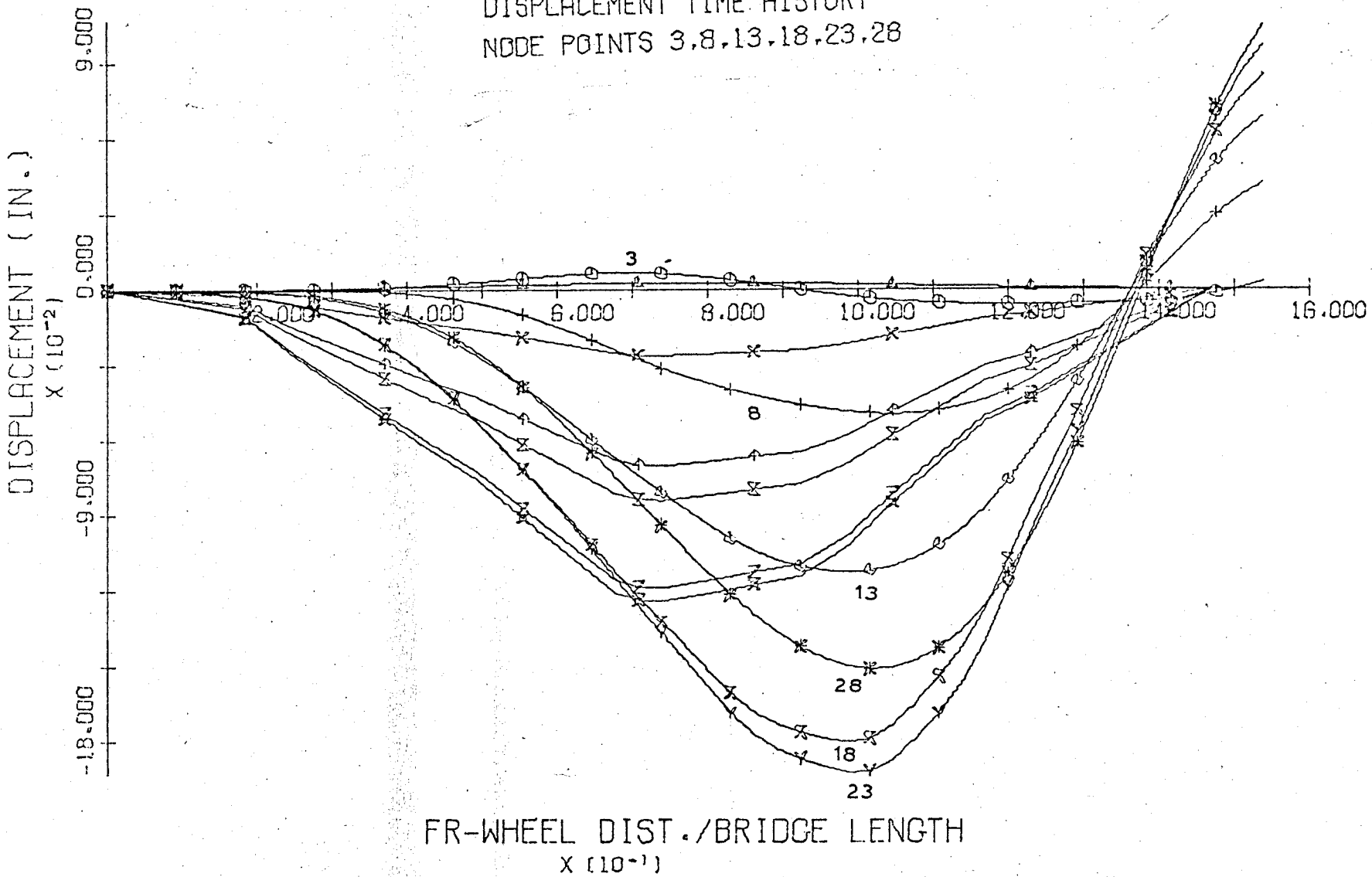
FIGURE 42 300MPH-LANE 3
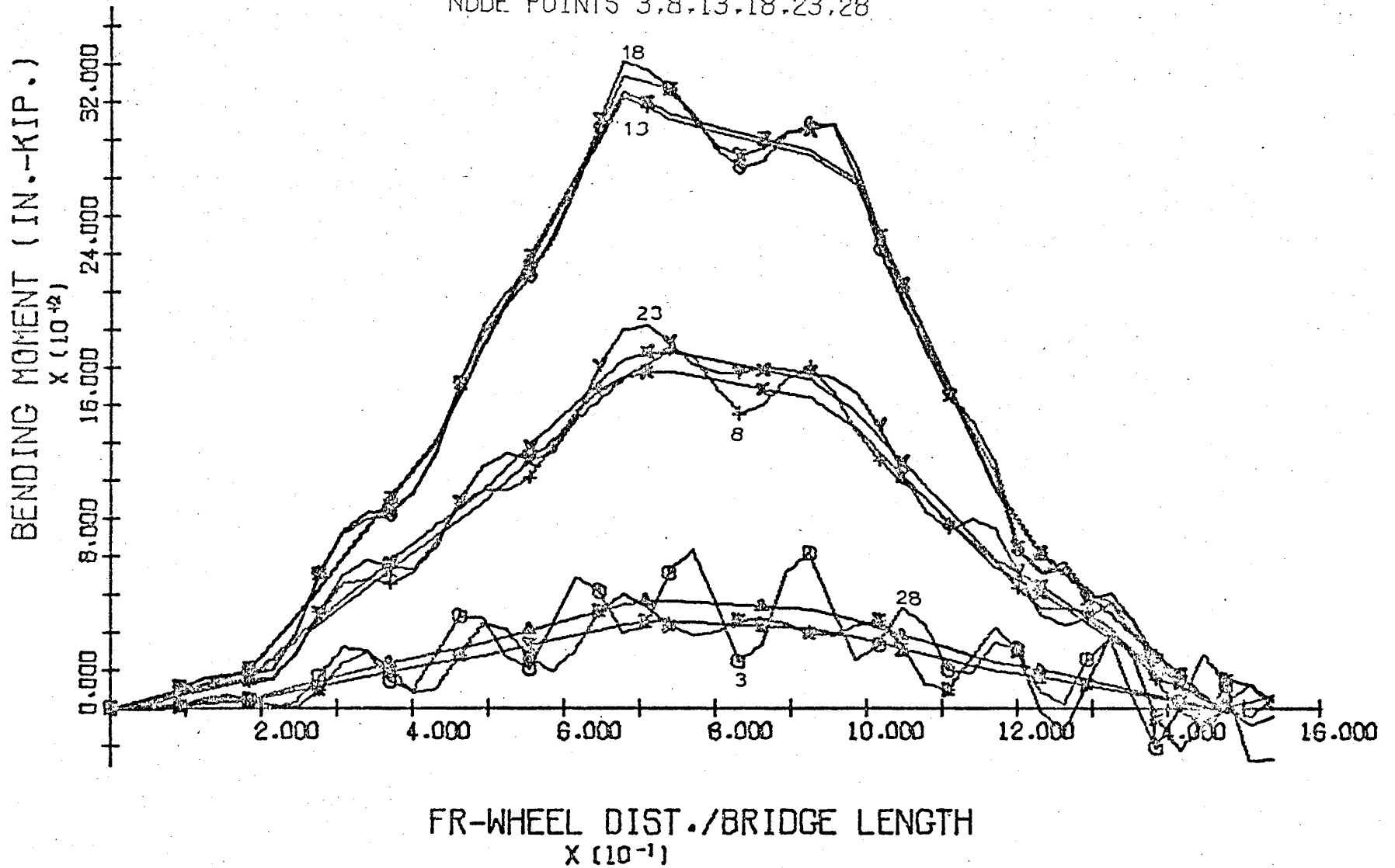BENDING MOMENT TIME HISTORY
NODE POINTS 3,8,13,18,23,28

BENDING MOMENT (IN.-KIP.) X (10^{+2})

23
18
28
13
8
3

2.000   4.000   6.000   8.000   10.000   12.000   14.000   16.000

50.000
40.000
20.000
0.000
-20.000

FR-WHEEL DIST./BRIDGE LENGTH
X (10^{-1})
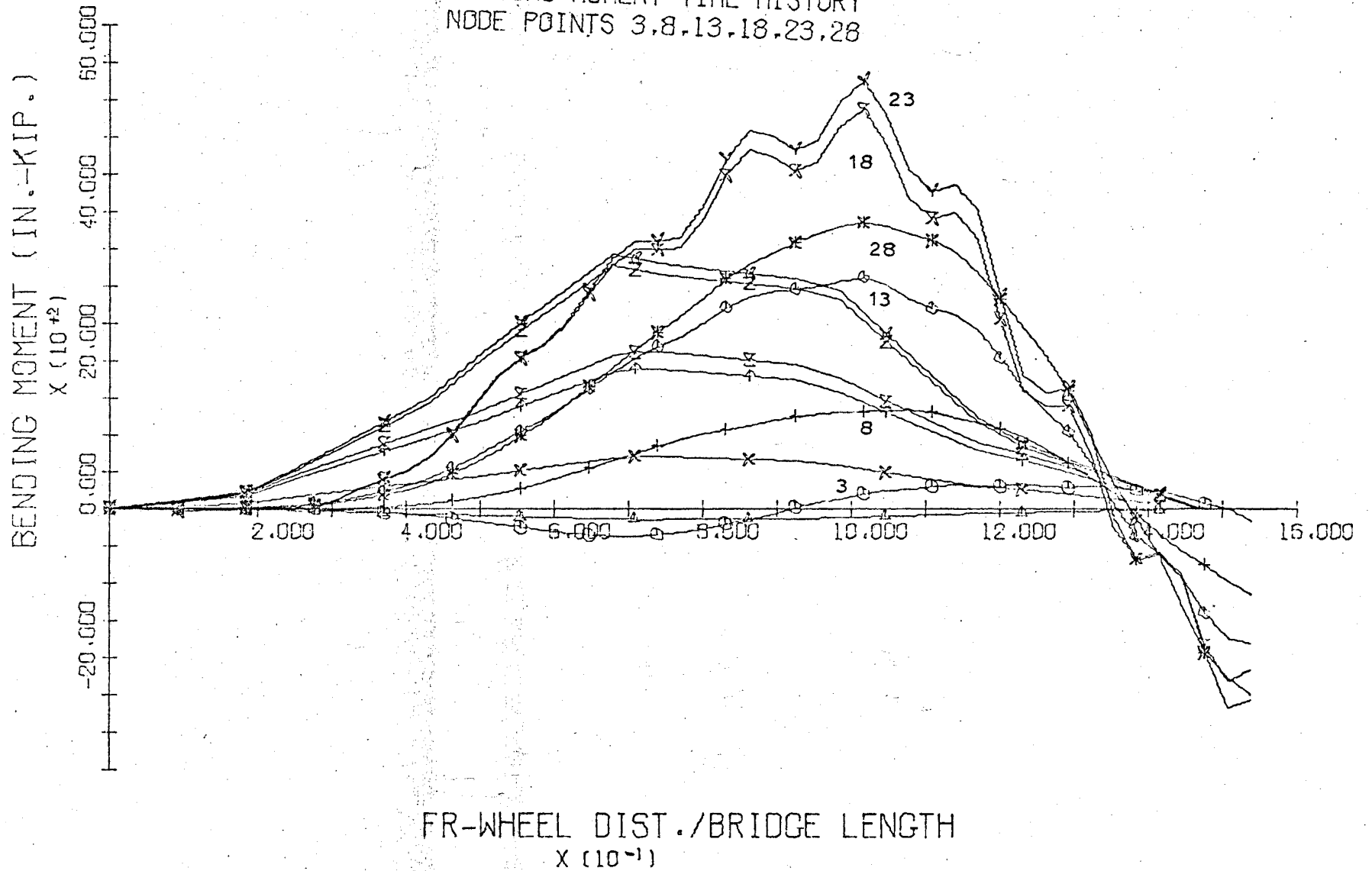
FIGURE 43 300MPH-LANE 3
DISPLACEMENT TIME HISTORY
BEAM F - NODE POINT 3

DISPLACEMENT (IN.)
X (10⁻¹)

FR-WHEEL DIST./BRIDGE LENGTH
X (10⁻¹)
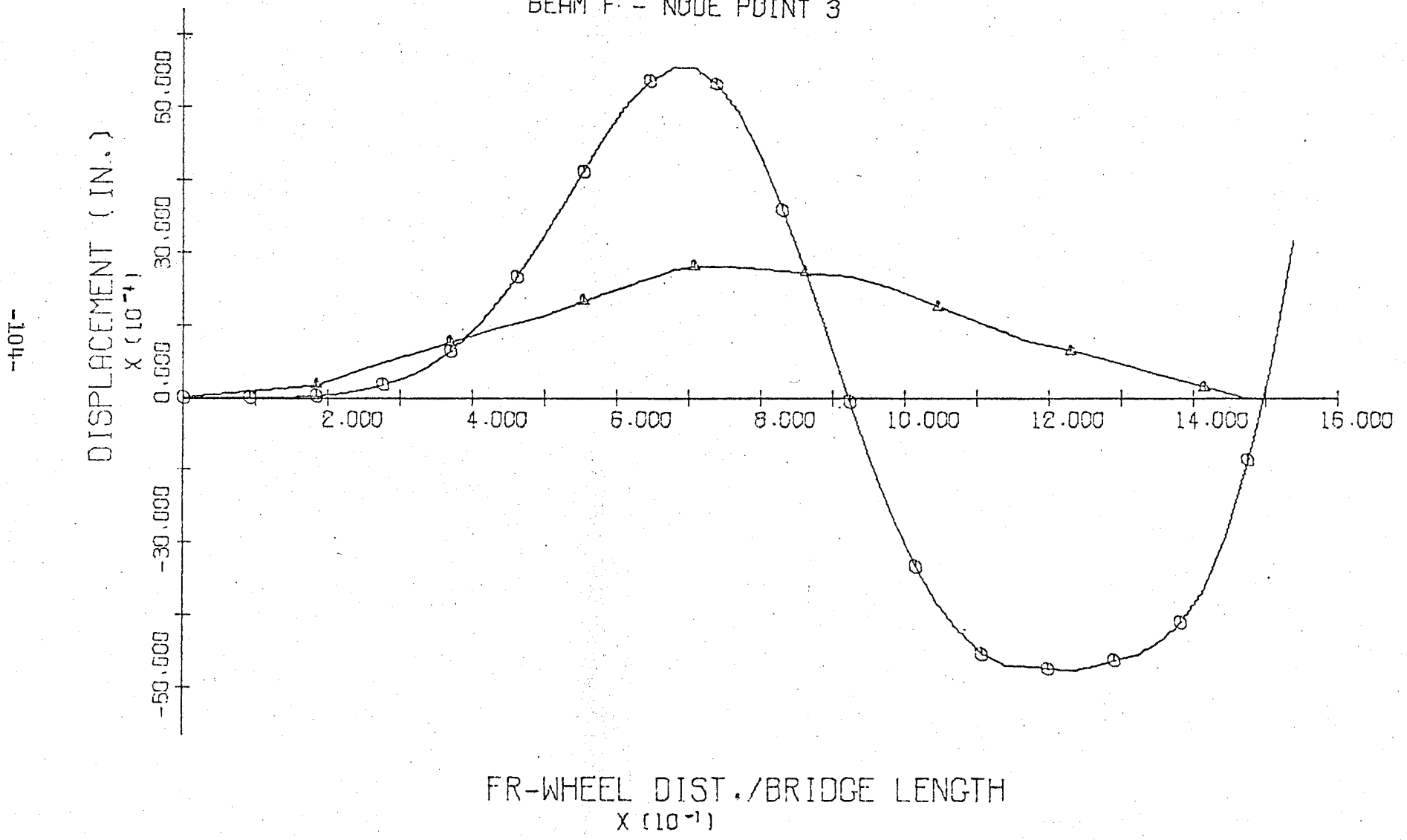
FIGURE 44. 300MPH-LANE 3
BENDING MOMENT TIME HISTORY
BEAM F-NODE POINT 3

BENDING MOMENT (IN.-KIP.)
X (10⁺¹)

FR-WHEEL DIST./BRIDGE LENGTH
X (10⁻¹)
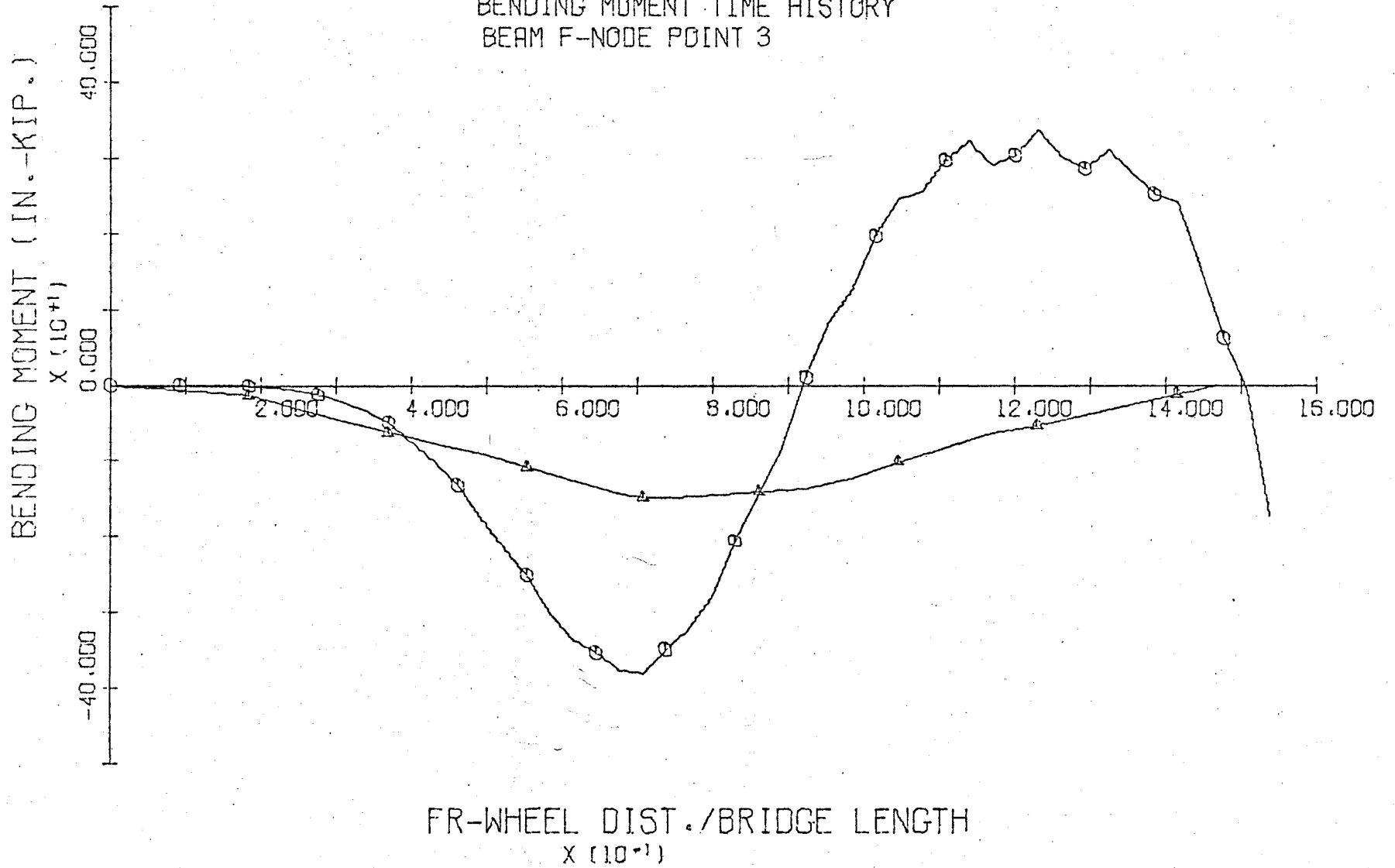
FIGURE 45 STATIC-LANE 3
DISPLACEMENT DIAGRAMS
BEAM B- NODE POINTS 21-22-23-24-25
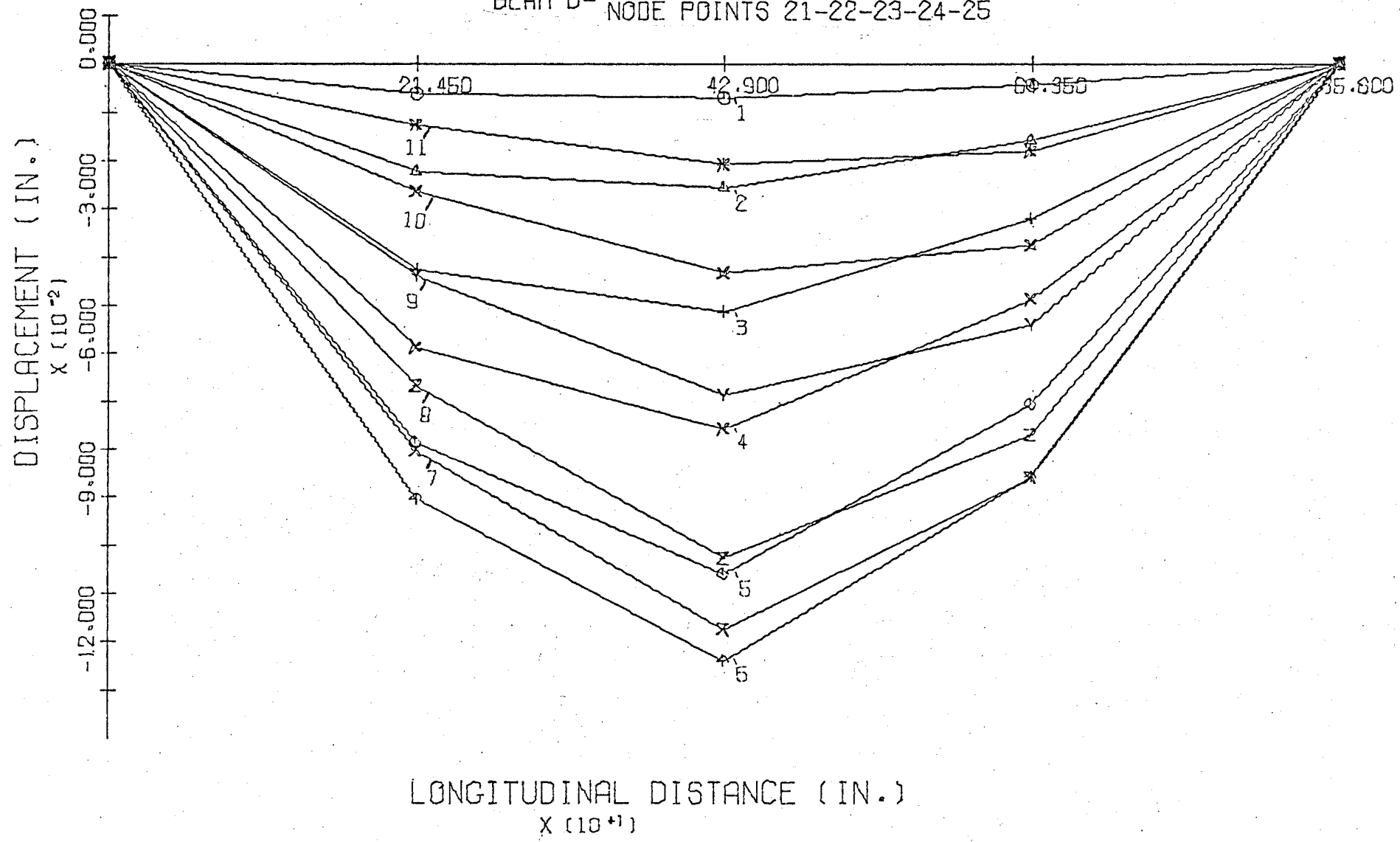
FIGURE 46 STATIC-LANE 3
BENDING MOMENT DIAGRAMS
BEAM B- NODE POINTS 21-22-23-24-25

BENDING MOMENT (IN.-KIP.)
X (10⁻²)

LONGITUDINAL DISTANCE (IN.)
X (10⁺¹)

-107-
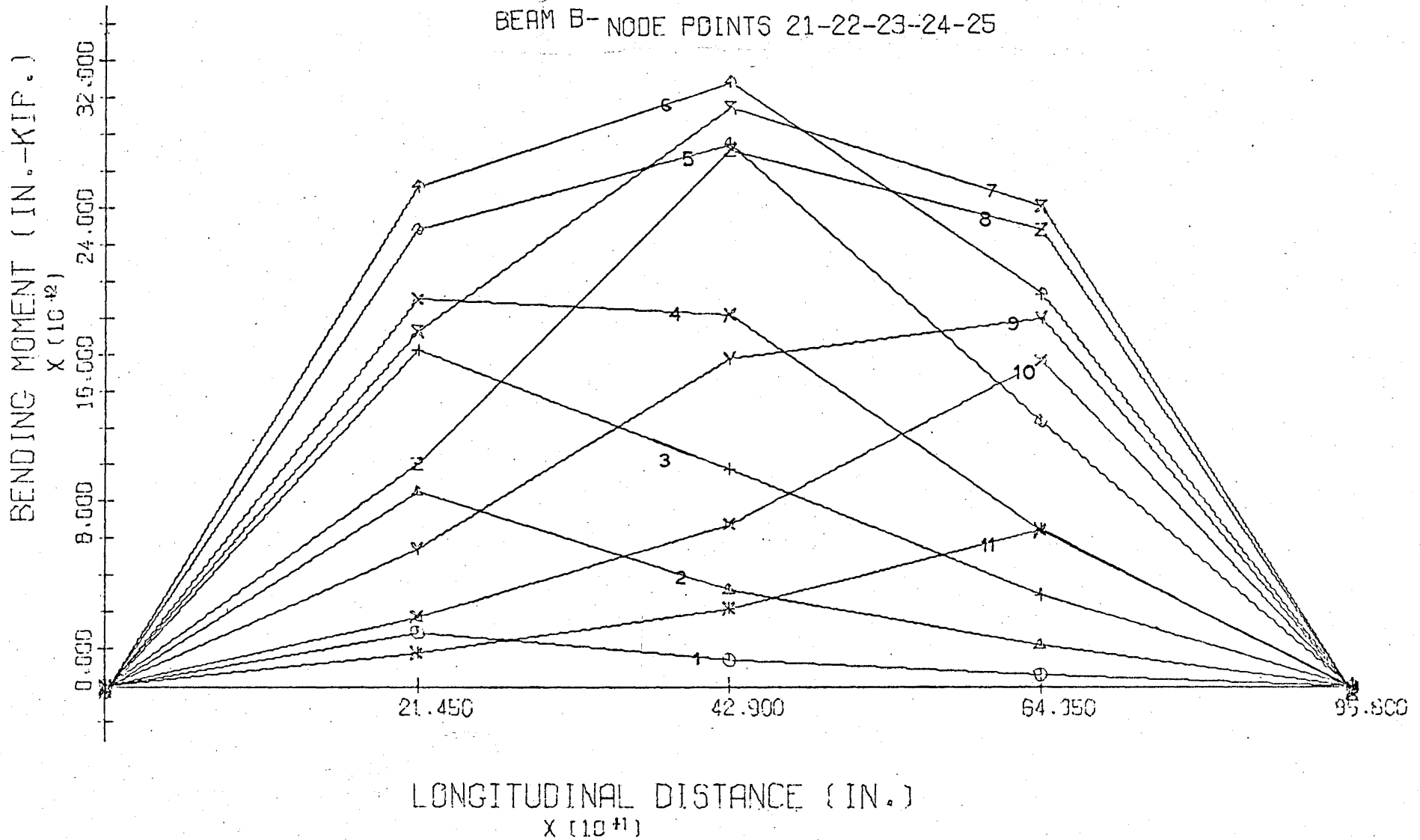
FIGURE 47 25MPH-LANE 3
DISPLACEMENT DIAGRAMS
BEAM B- NODE POINTS 21-22-23-24-25

LONGITUDINAL DISTANCE (IN.)
X (10 *1)

DISPLACEMENT (IN.)
X (10 *2)

-108-
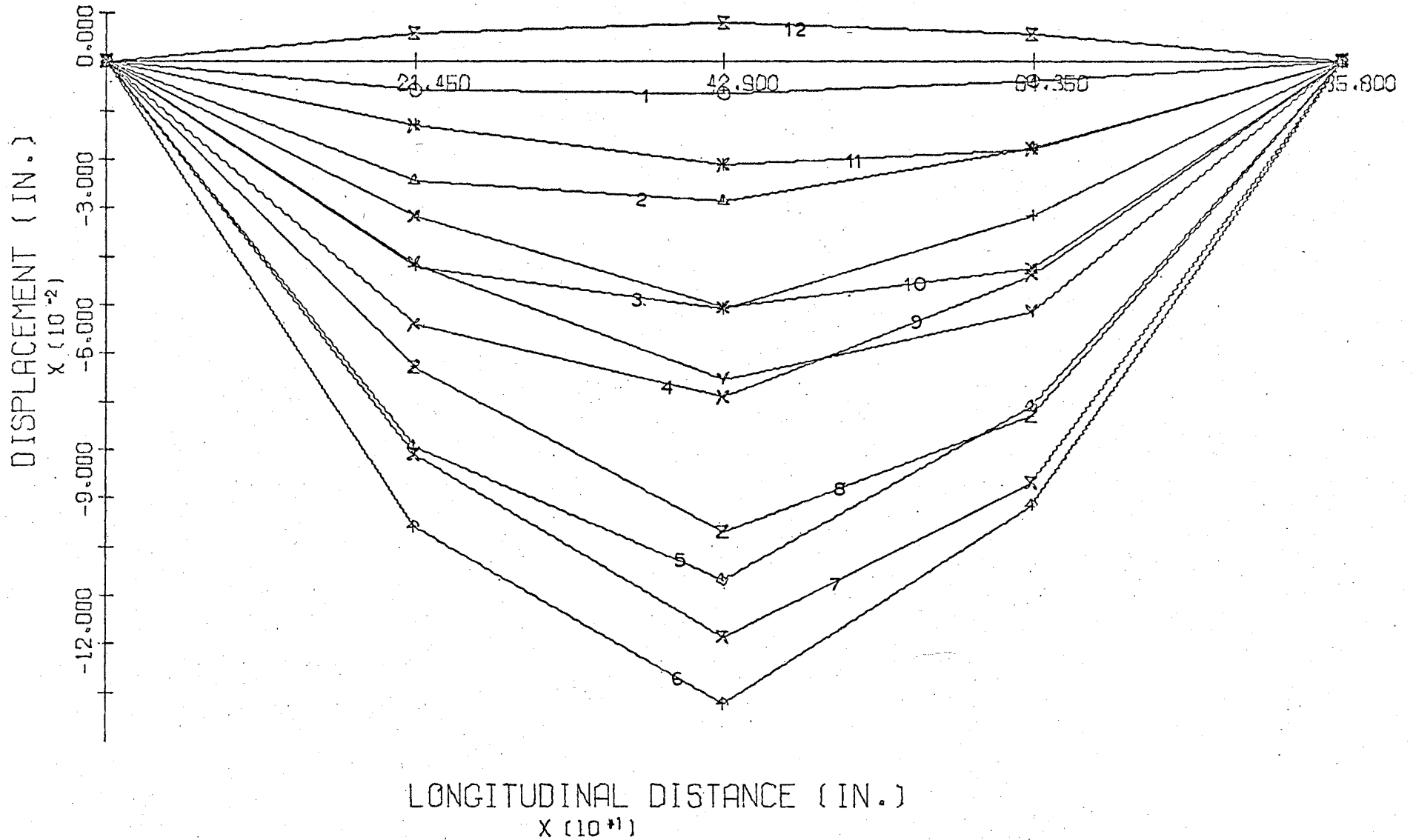
FIGURE 48 25MPH-LANE 3

BENDING MOMENT DIAGRAMS
BEAM B- NODE POINTS 21-22-23-24-25
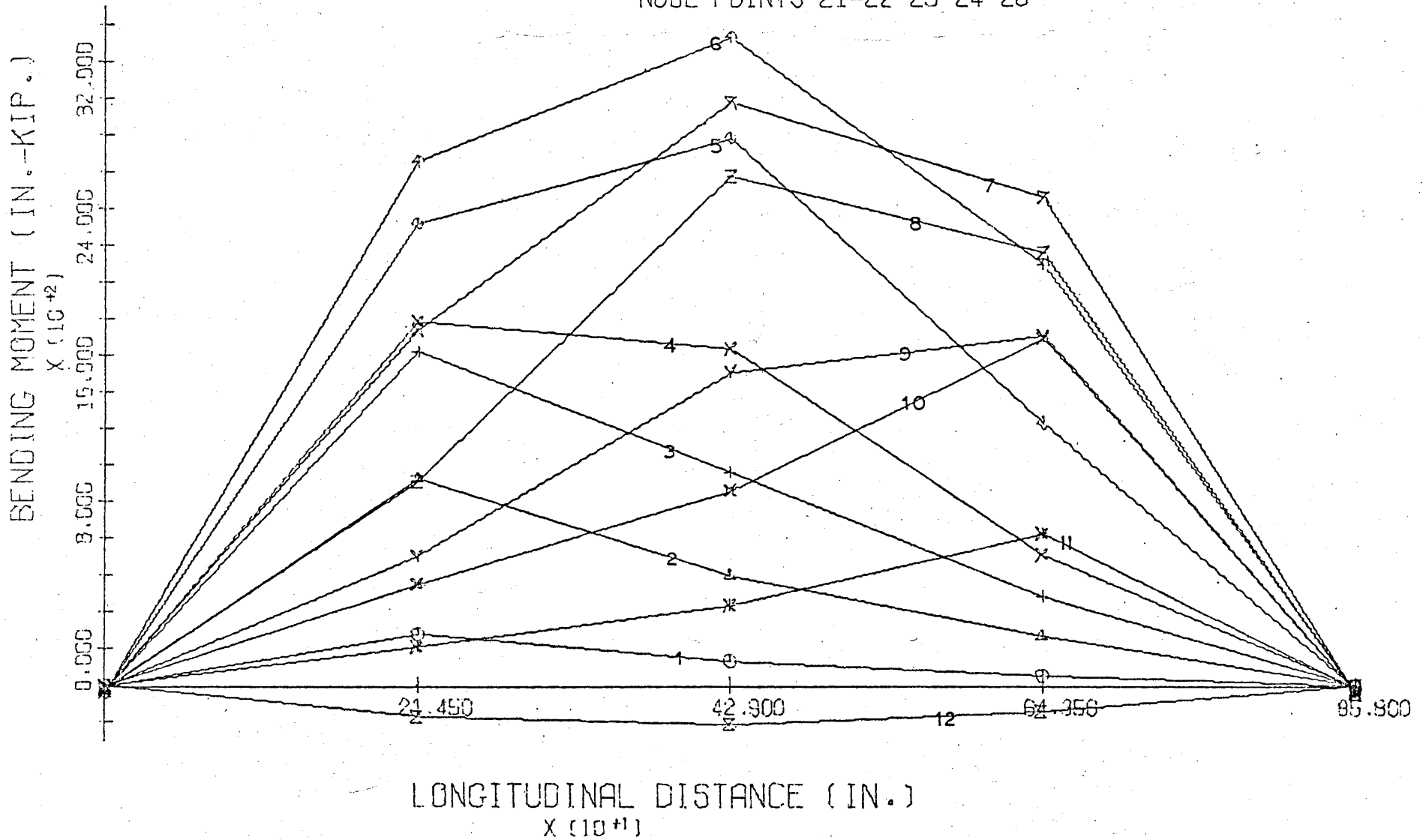
FIGURE 49 50MPH-LANE 3
DISPLACEMENT DIAGRAMS
BEAM B- NODE POINTS 21-22-23-24-25

LONGITUDINAL DISTANCE (IN.)
X (10 +1)

DISPLACEMENT (IN.)
X (10 -2)

-110-
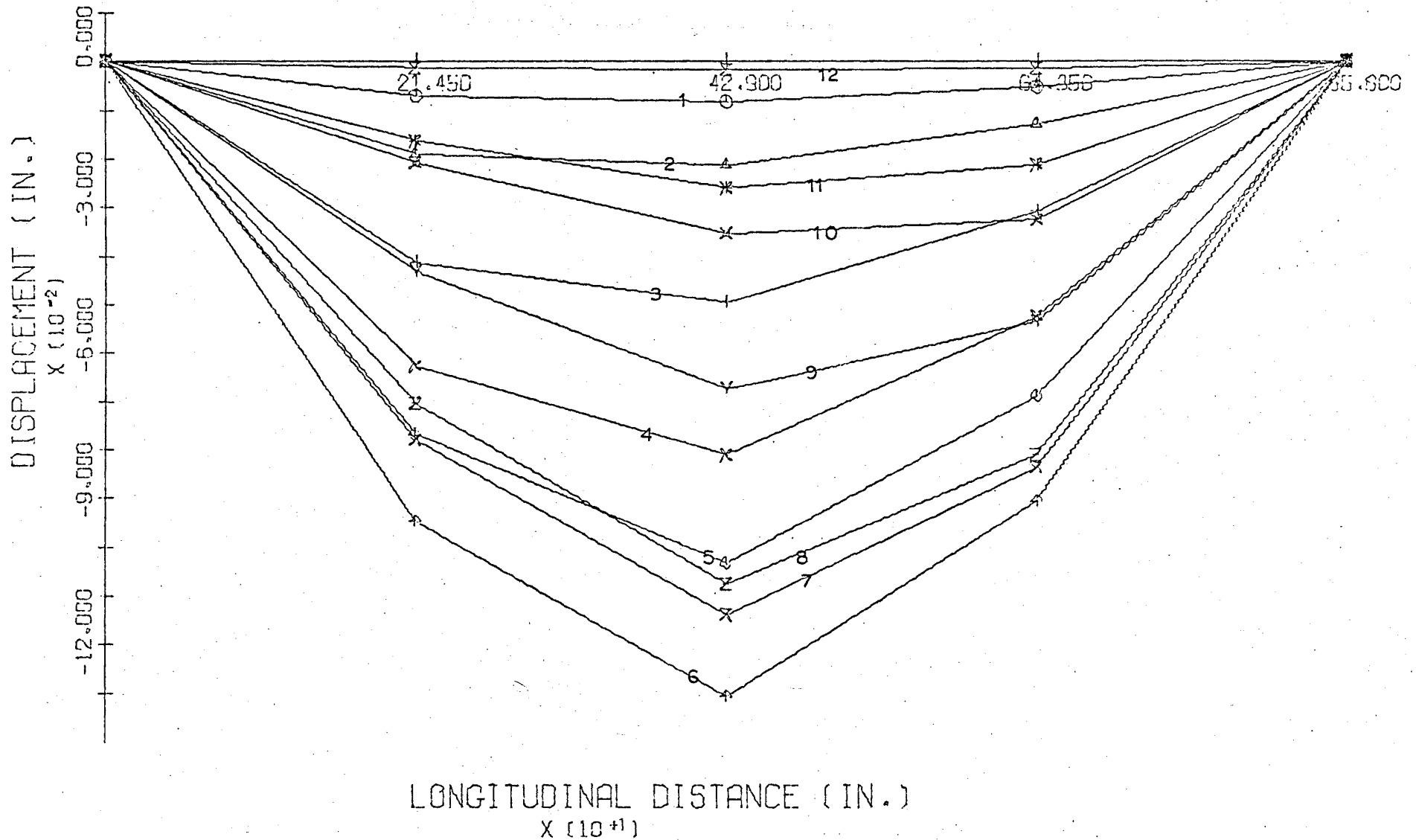
FIGURE 50 50MPH-LANE 3

BENDING MOMENT DIAGRAMS

BEAM B- NODE POINTS 21-22-23-24-25
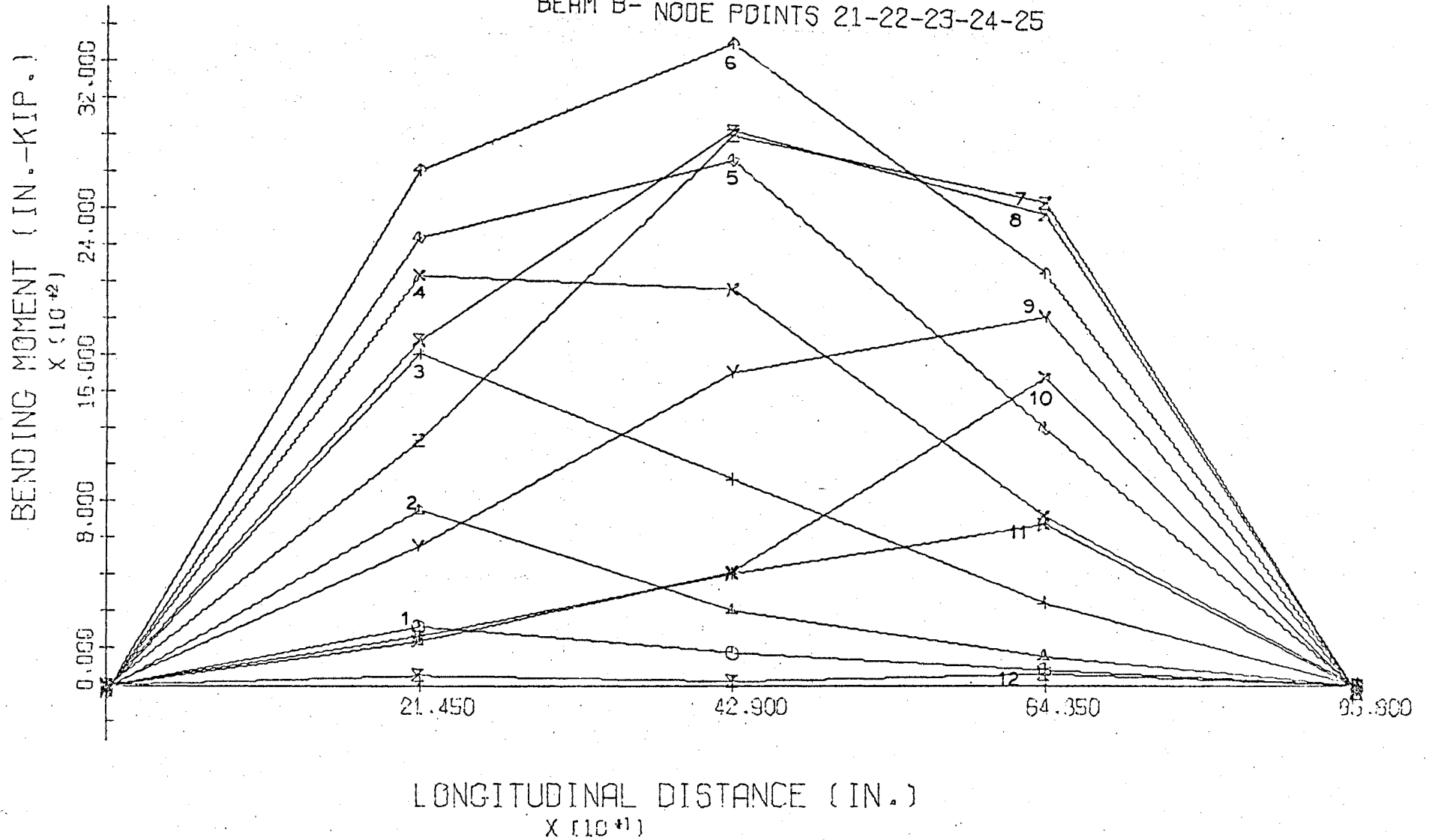
FIGURE 51 25MPH-LANE 3
DISPLACEMENT DIAGRAMS

7.38462E-01

BEAM F-DYNAMIC

BEAM B-STATIC

BEAM B-DYNAMIC

DISPLACEMENT (IN.)
X (10⁻²)

LONGITUDINAL DISTANCE (IN.)
X (10⁺¹)
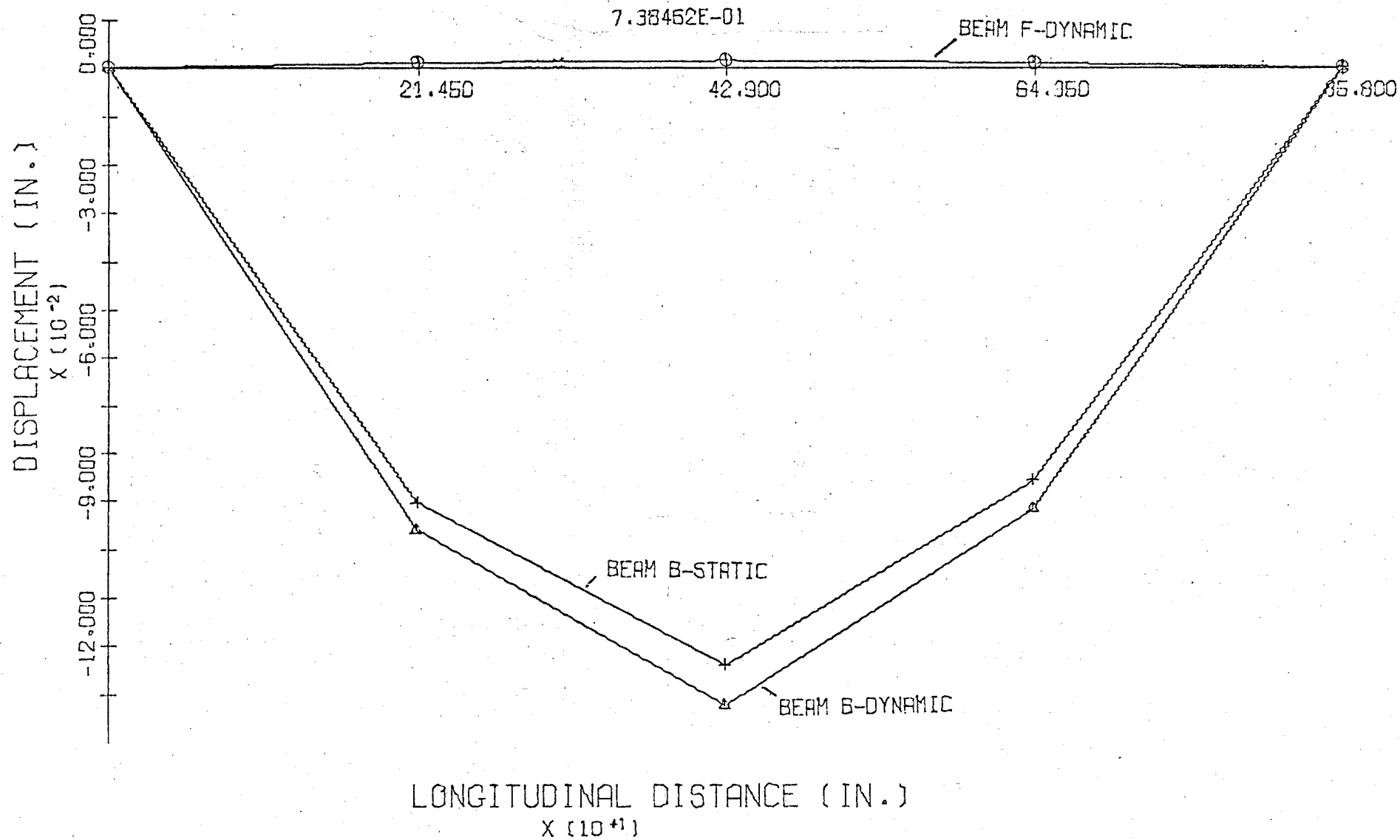
FIGURE 52 25MPH-LANE 3
BENDING MOMENT DIAGRAMS
7.38452E-01

BEAM B-DYNAMIC

BEAM B-STATIC

BEAM F-DYNAMIC

BENDING MOMENT (IN.-KIP.)
X (10+2)

32.000   24.000   16.000   8.000   0.000

LONGITUDINAL DISTANCE (IN.)
X (10+1)

21.450   42.300   64.350   85.500
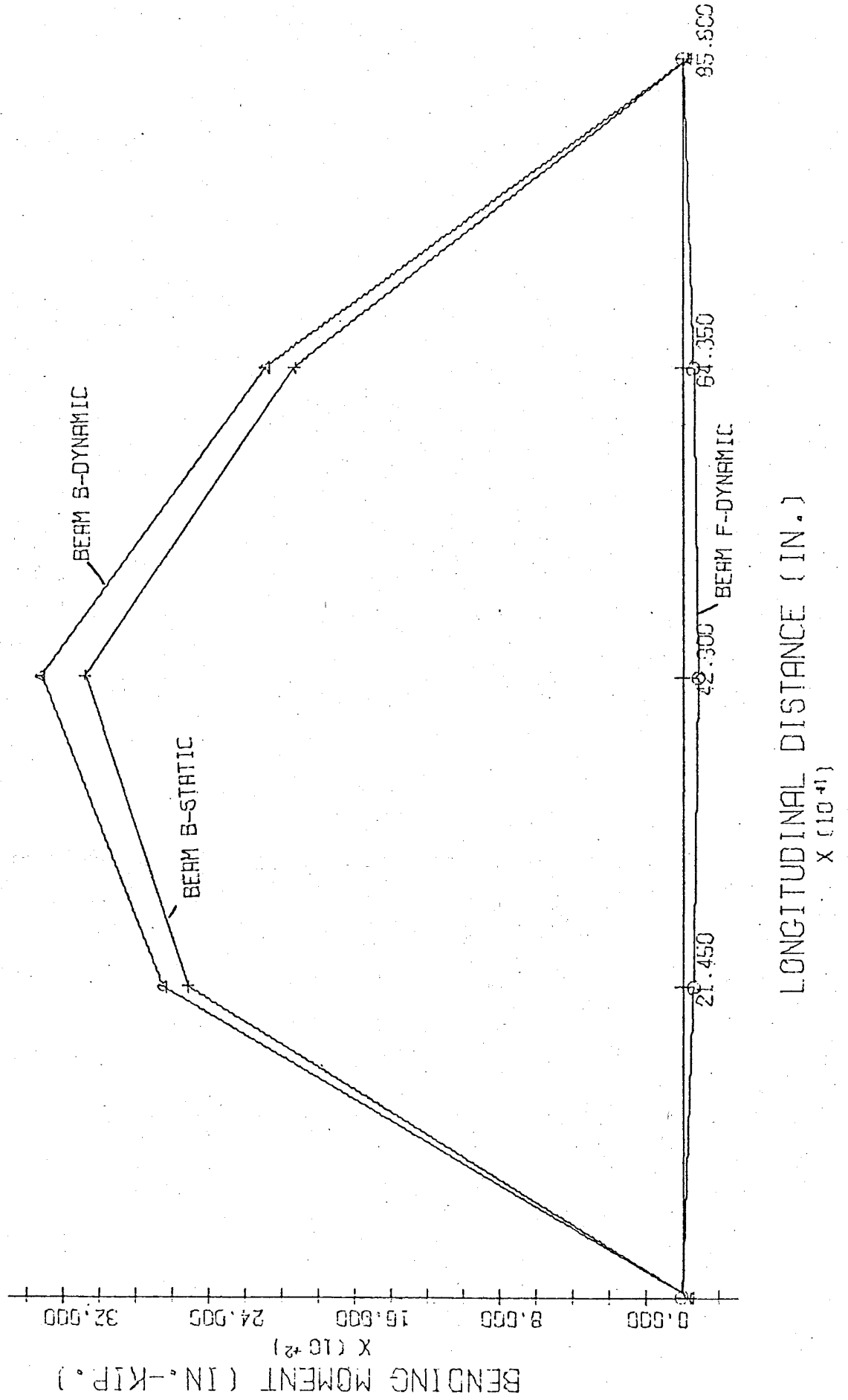
FIGURE 53 50MPH-LANE 3
DISPLACEMENT DIAGRAMS
7.07692E-01
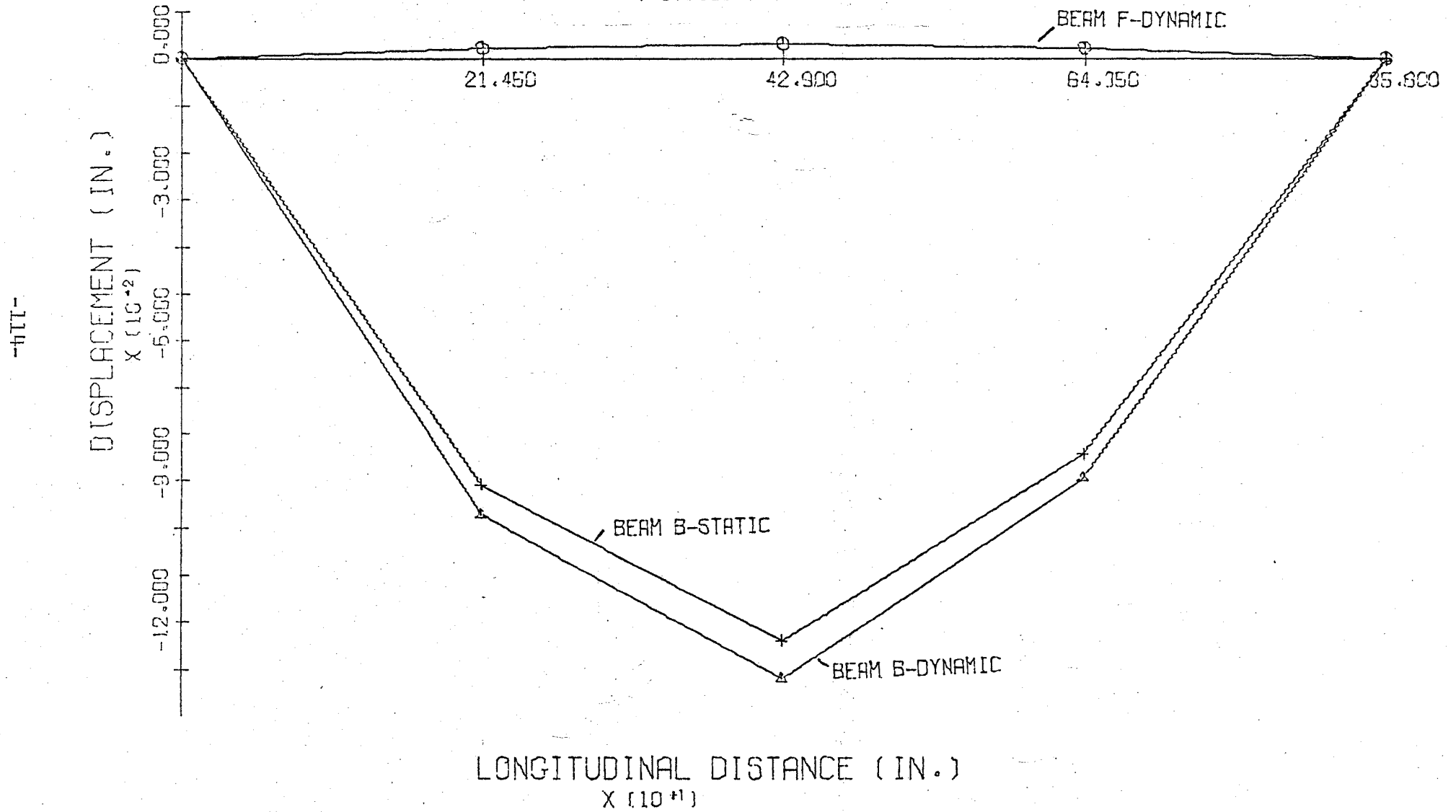
FIGURE 54 50MPH-LANE 3

BENDING MOMENT DIAGRAMS
7.07692E-01

BEAM B-DYNAMIC

BEAM B-STATIC

BEAM F-DYNAMIC

BENDING MOMENT (IN.-KIP.)
X (10^{+2})

LONGITUDINAL DISTANCE (IN.)
X (10^{+1})
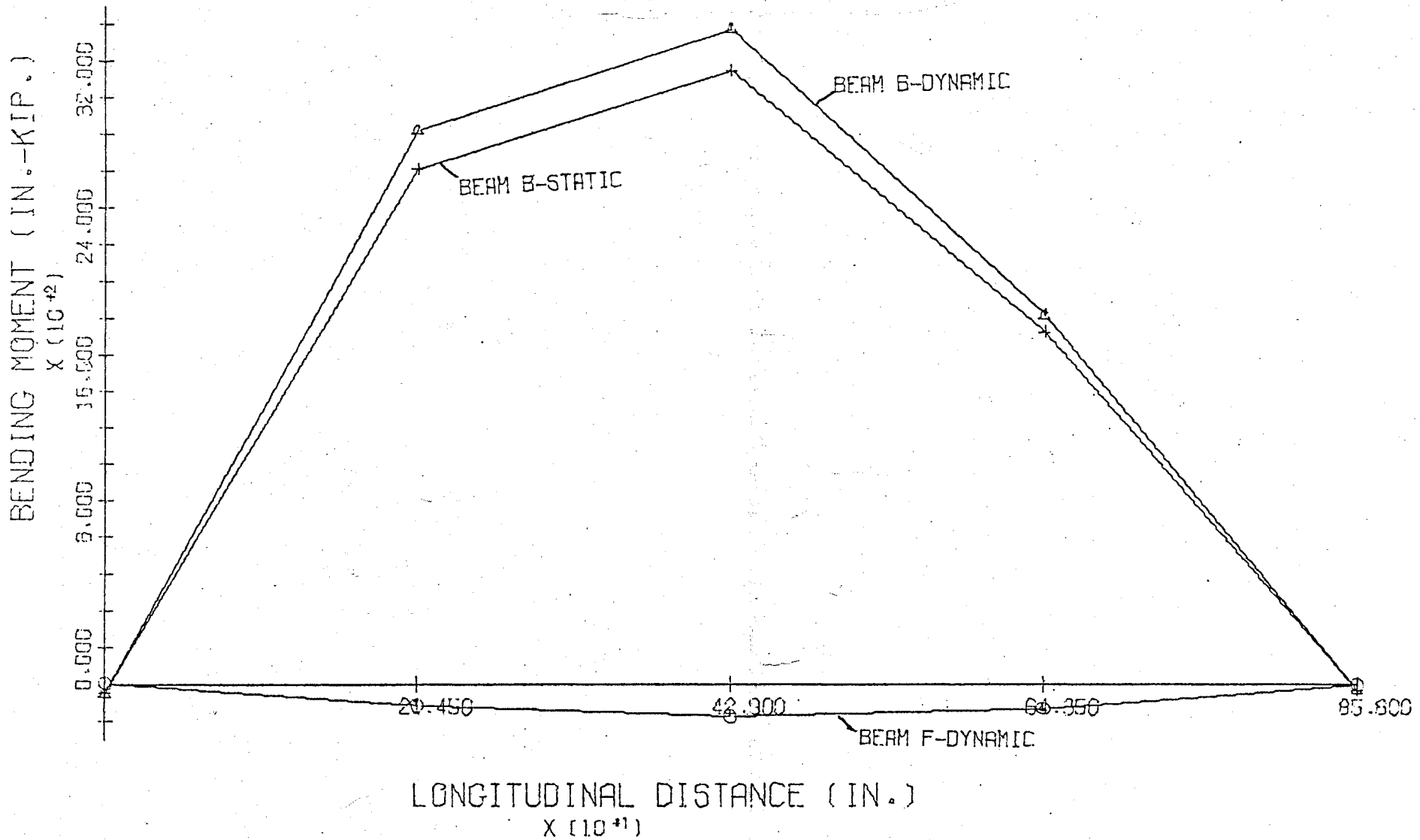
FIGURE 55 STATIC-LANE 3
DISPLACEMENT DIAGRAMS
NODE POINTS -3-8-13-18-23-28
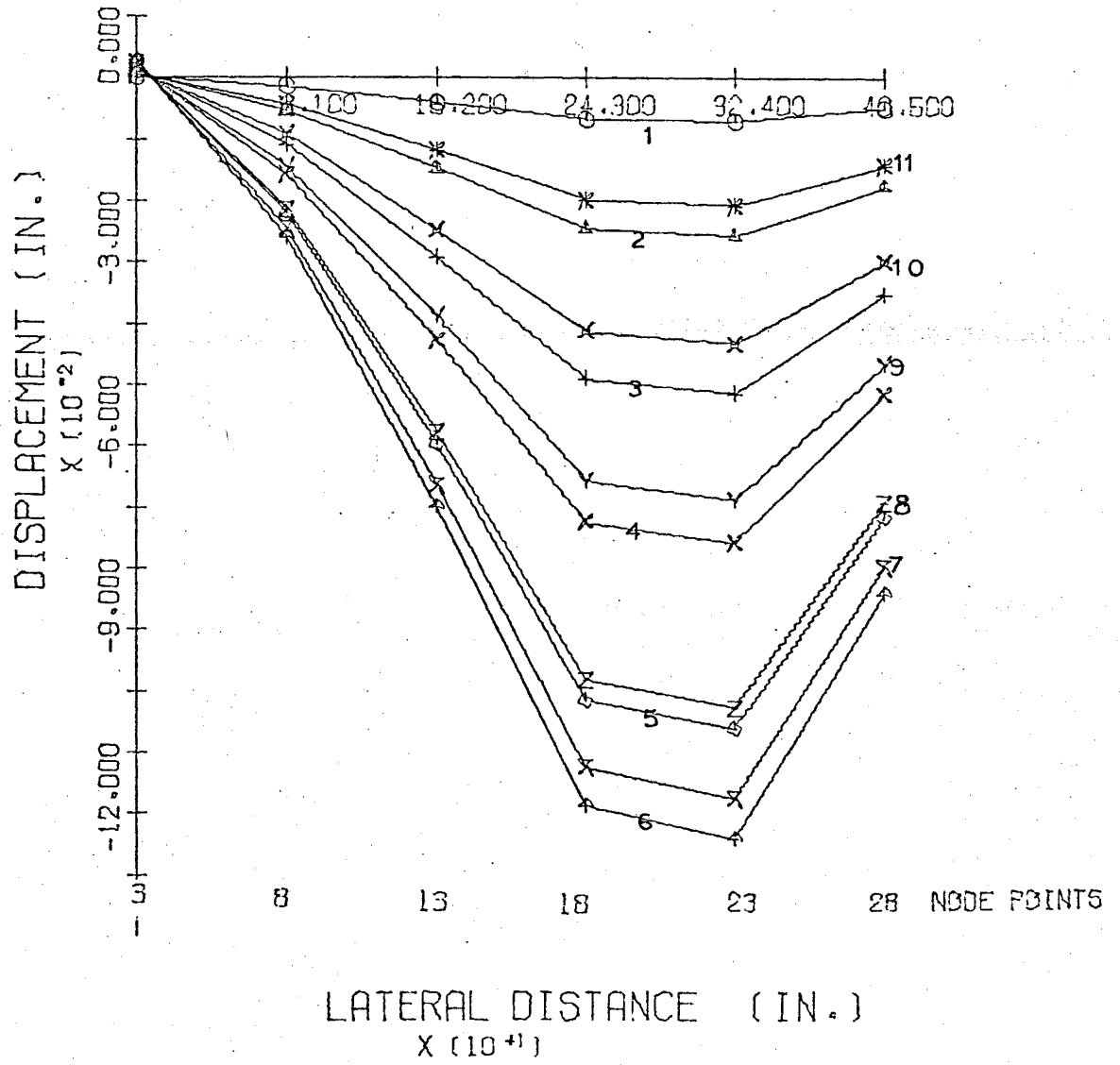
LATERAL DISTANCE (IN.)
X (10^{+1})

-116-

FIGURE 56 STATIC-LANE 3
BENDING MOMENT DIAGRAMS
NODE POINTS -3- 8-13-18-23-28
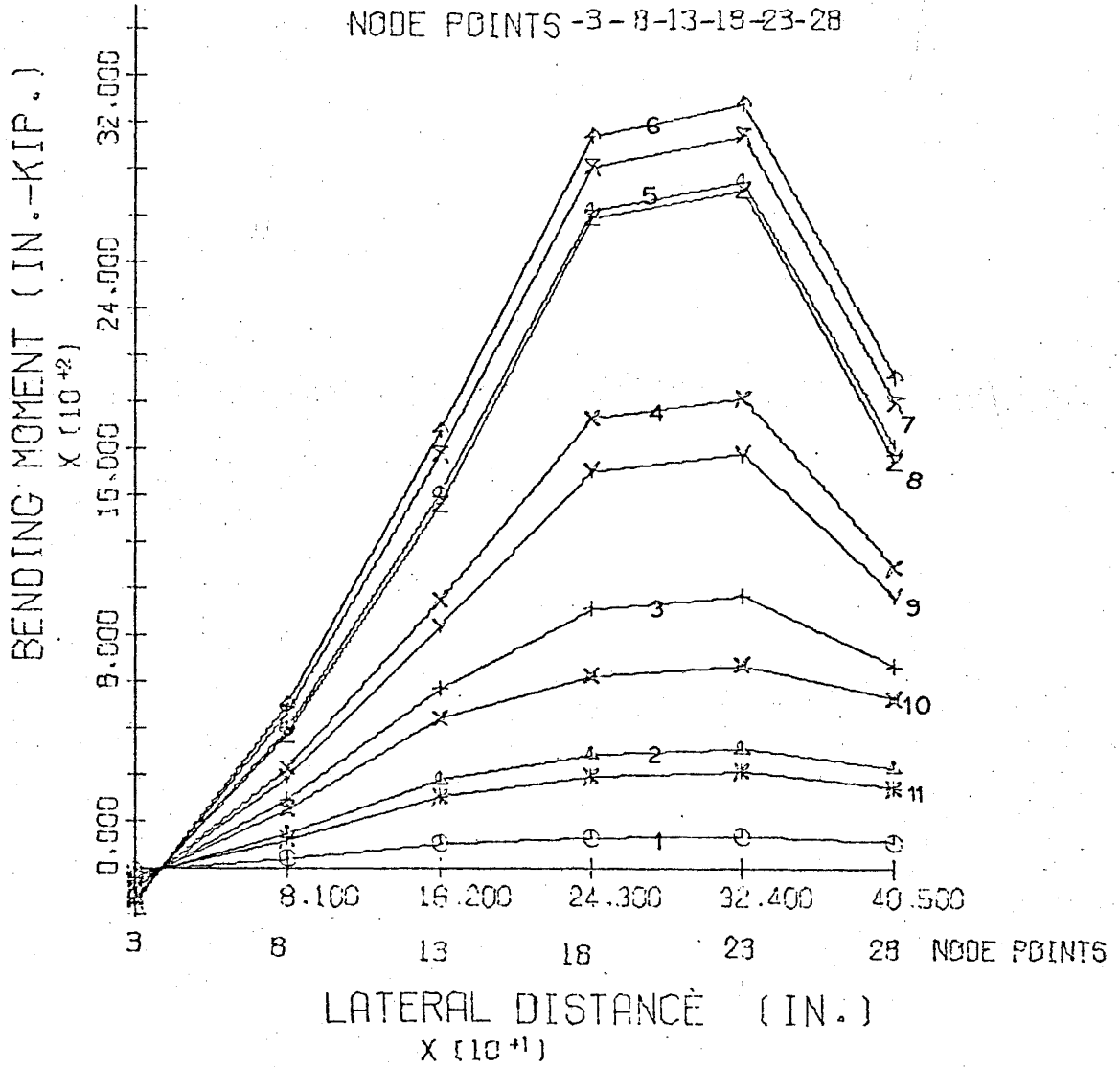
FICURE 57 25MPH-LANE 3
DISPLACEMENT DIAGRAMS
NODE POINTS -3—8-13-18-23-28
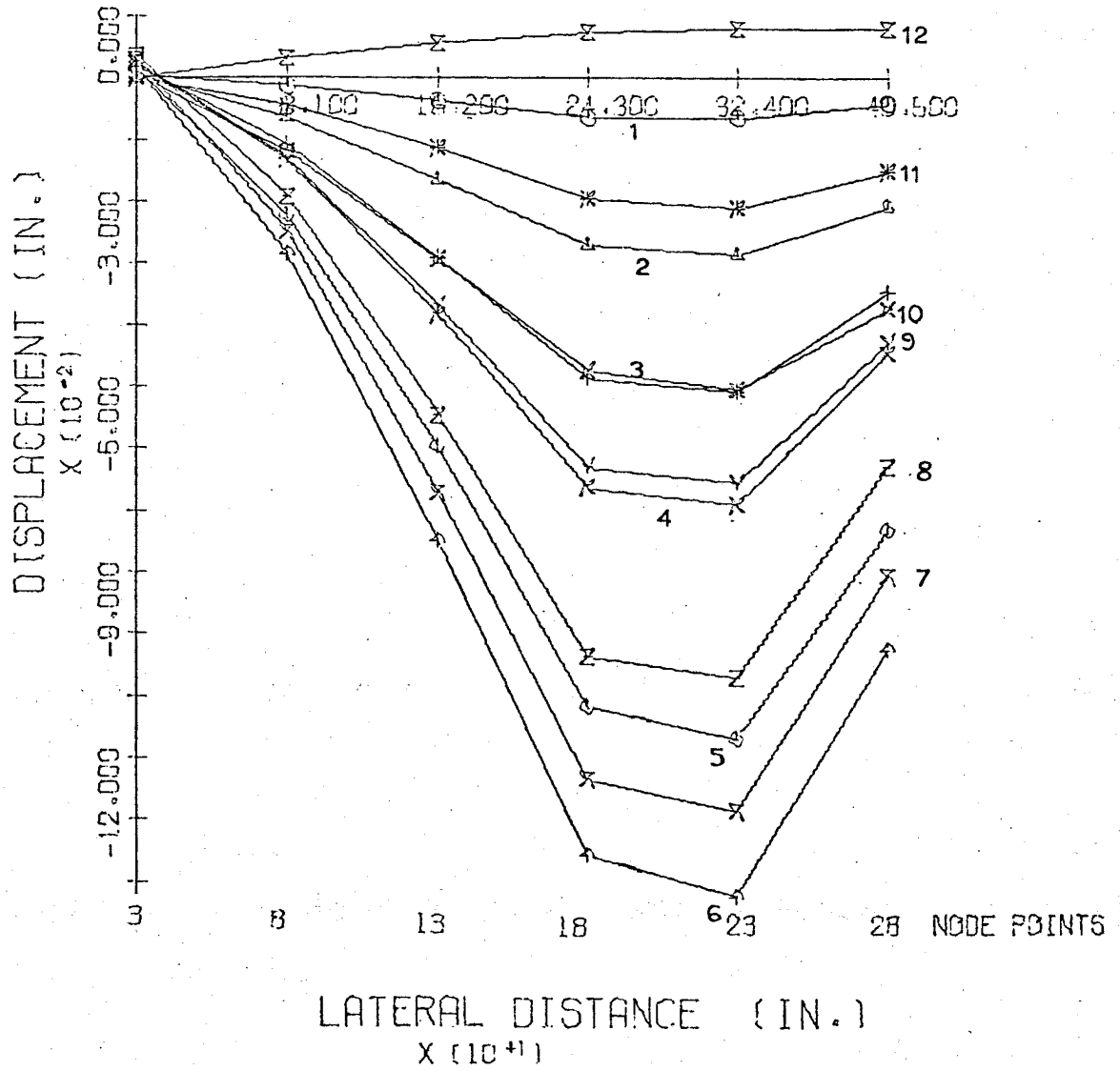
FIGURE 58 25MPH-LANE 3
BENDING MOMENT DIAGRAMS
NODE POINTS -3- 8 13-18-23-28
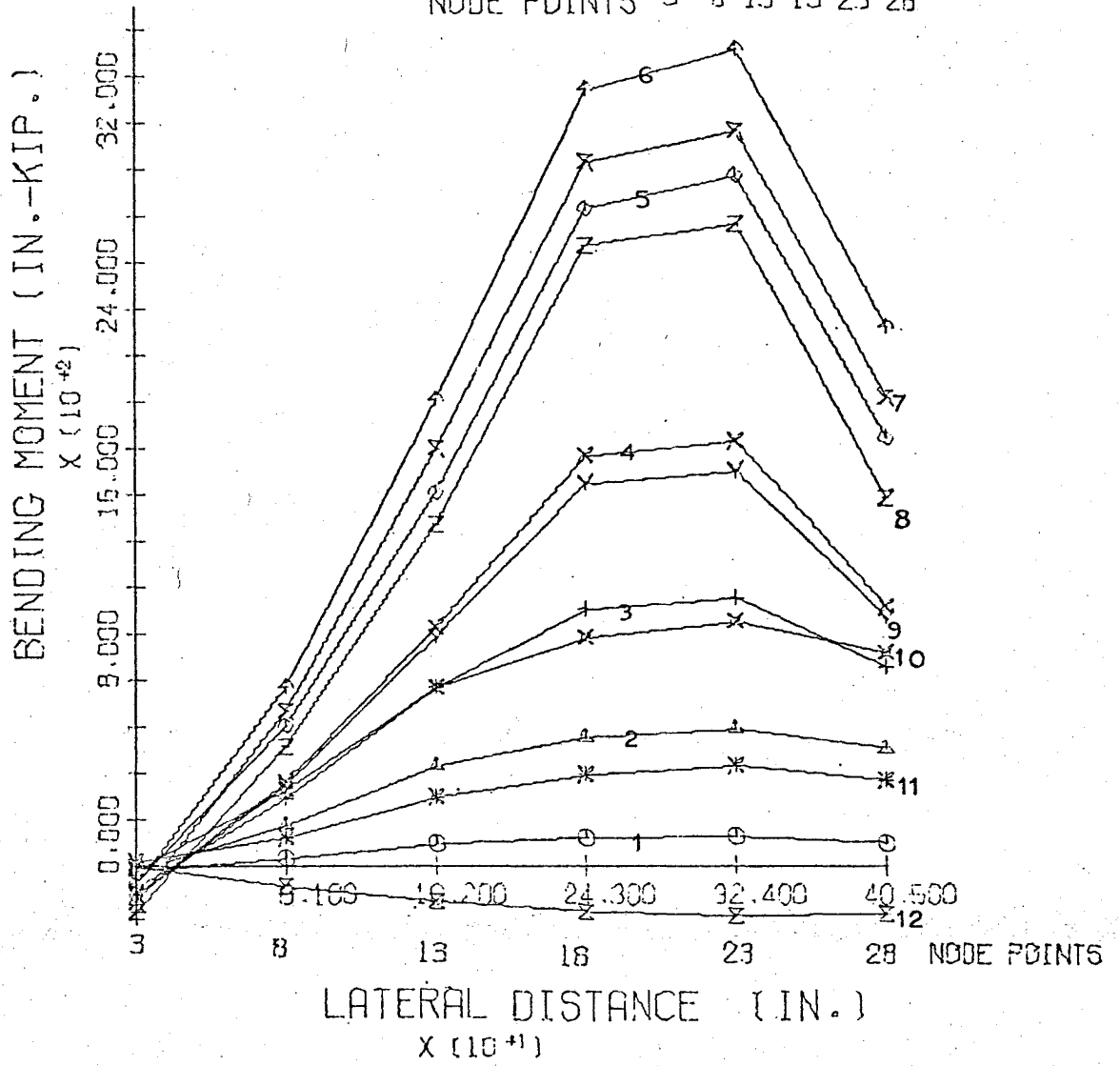
FIGURE 59 50MPH-LANE 3
DISPLACEMENT DIAGRAMS
NODE POINTS -3-8-13-18-23-28
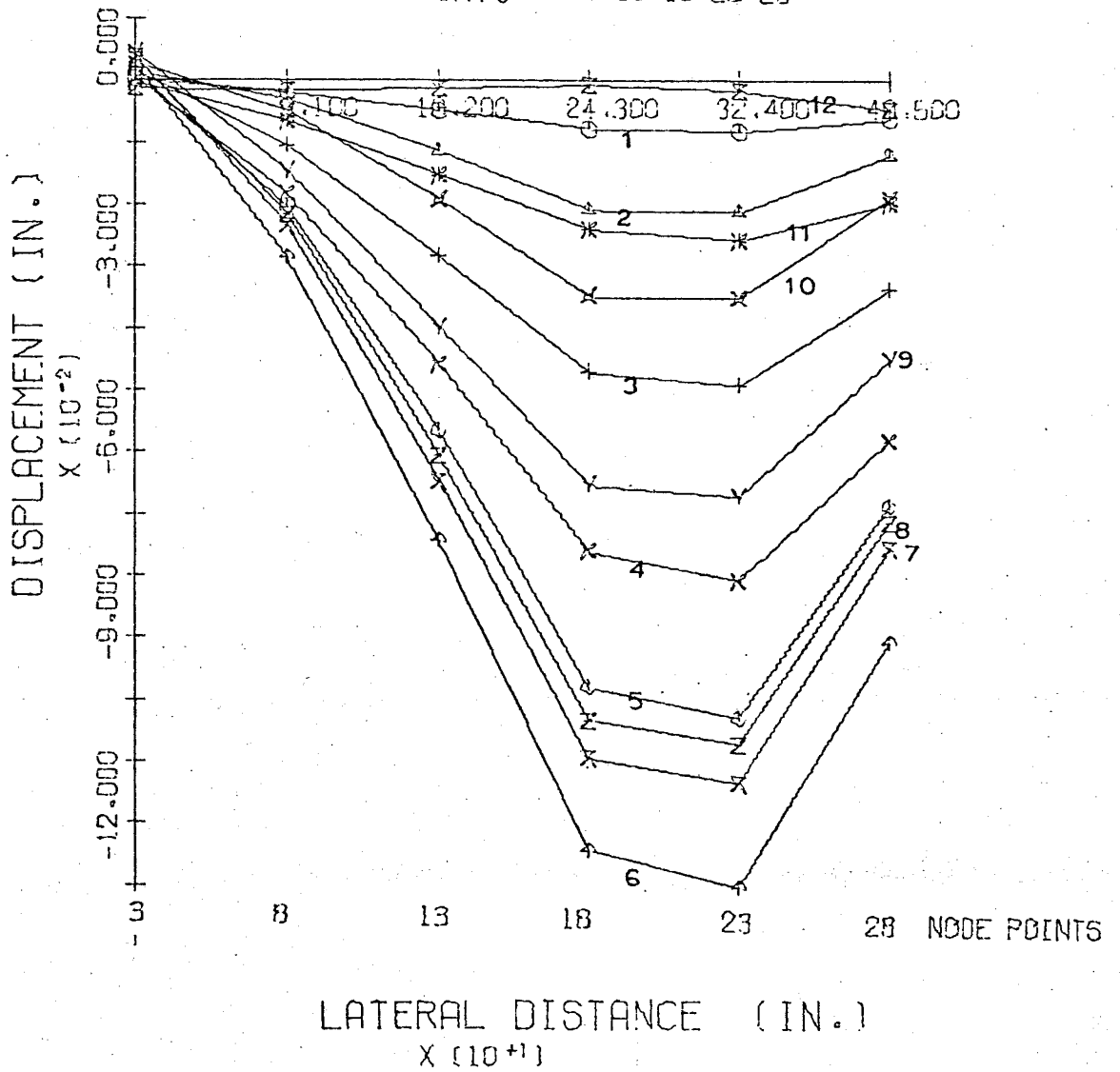
FIGURE 60 50MPH-LANE 3

BENDING MOMENT DIAGRAMS
NODE POINTS -3-8-13-18-23-28

-121-
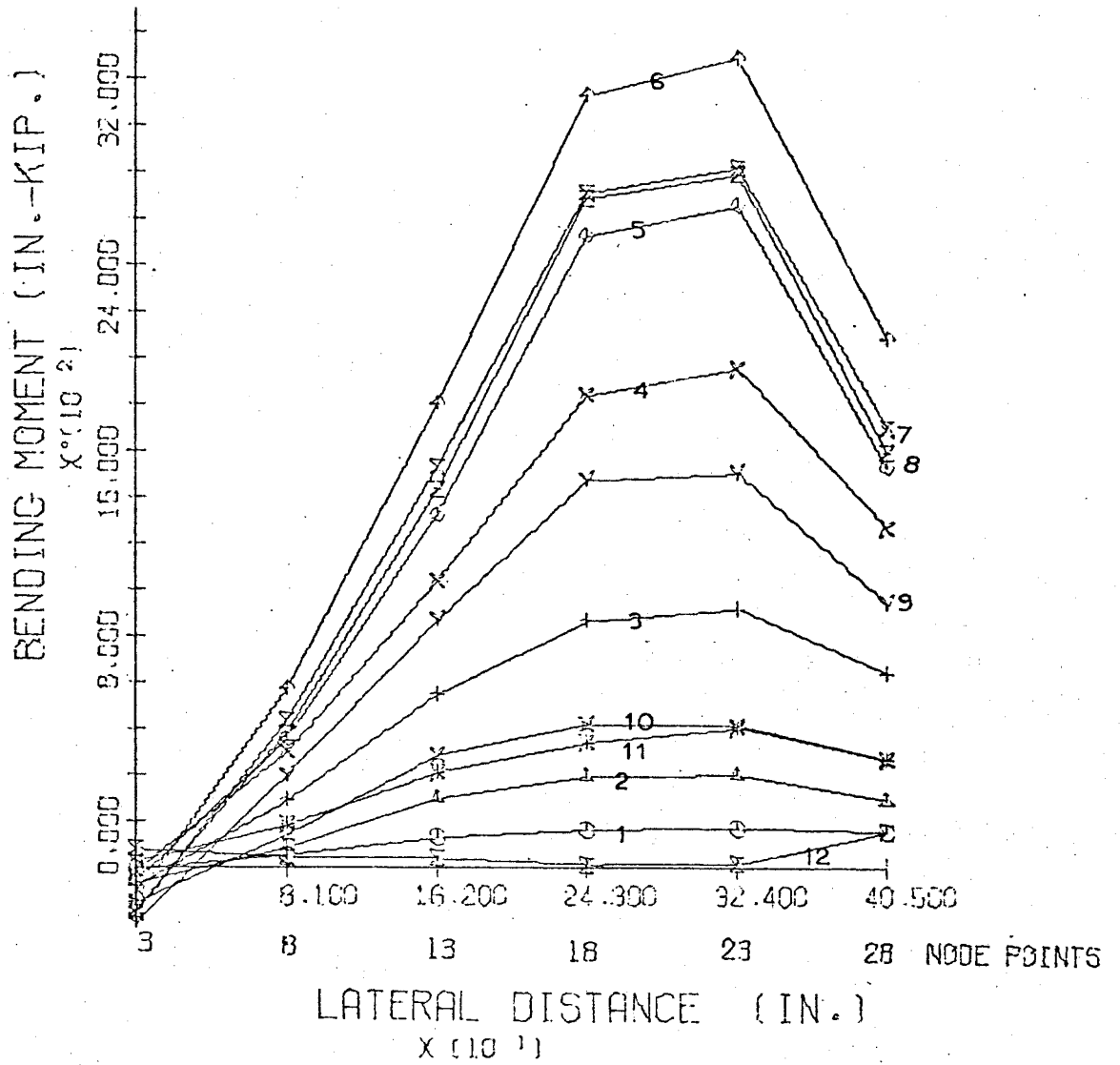
FIGURE 61 50MPH-LANE 5
DISPLACEMENT TIME HISTORY
BEAM F-NODE POINTS 2,3,4

DISPLACEMENT (IN.)
X (10⁻²)

FR-WHEEL DIST./BRIDGE LENGTH
X (10⁻¹)

FIGURE 62   50MPH-LANE 5

BENDING MOMENT TIME HISTORY
BEAM F-NODE POINTS 2,3,4

BENDING MOMENT (IN.-KIP.)
X (10⁺²)

FR-WHEEL DIST./BRIDGE LENGTH
X (10⁻¹)
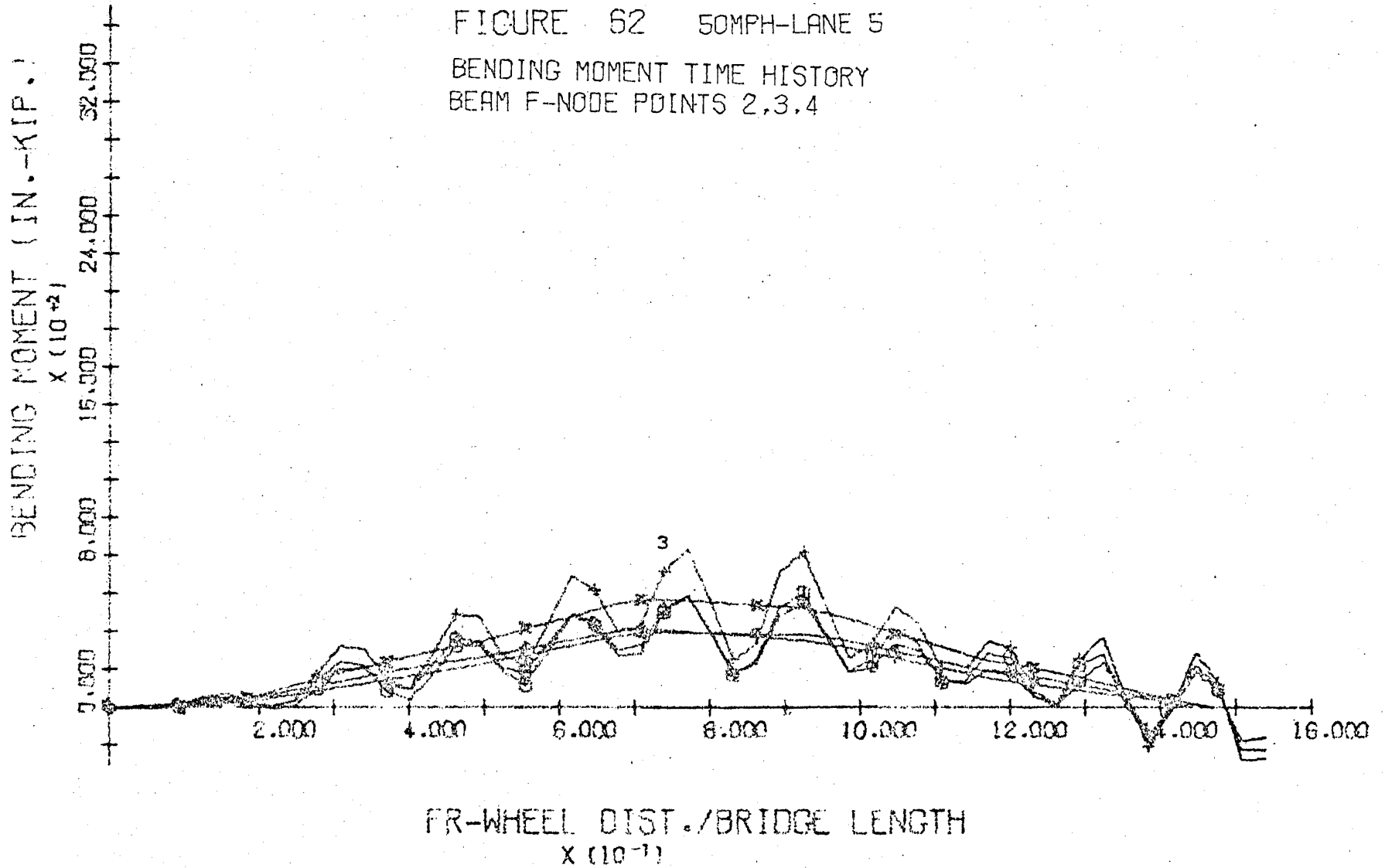
FIGURE 63 50MPH-LANE 5
DISPLACEMENT TIME HISTORY
BEAM E-NODE POINTS 7,8,9

-124-

FIGURE 64   50MPH-LANE 5
BENDING MOMENT TIME HISTORY
BEAM E-NODE POINTS 7,8,9

BENDING MOMENT (IN.-KIP.) X (10^{+2})

FR-WHEEL DIST./BRIDGE LENGTH
X (10^{-1})

FIGURE 65 50MPH-LANE 5
DISPLACEMENT TIME HISTORY

BEAM D-NODE POINTS 12,13,14

FR-WHEEL DIST./BRIDGE LENGTH
X (10⁻¹)
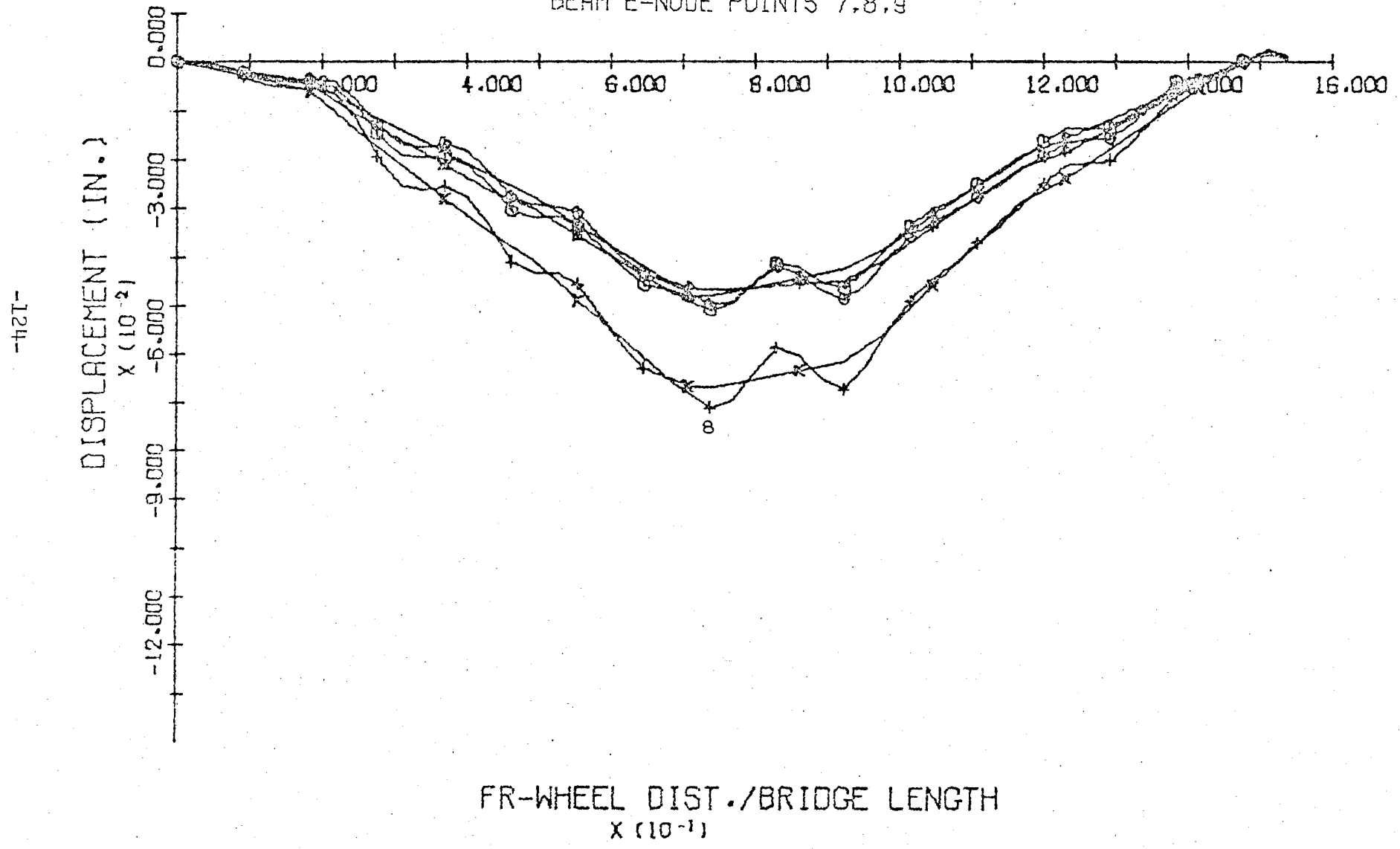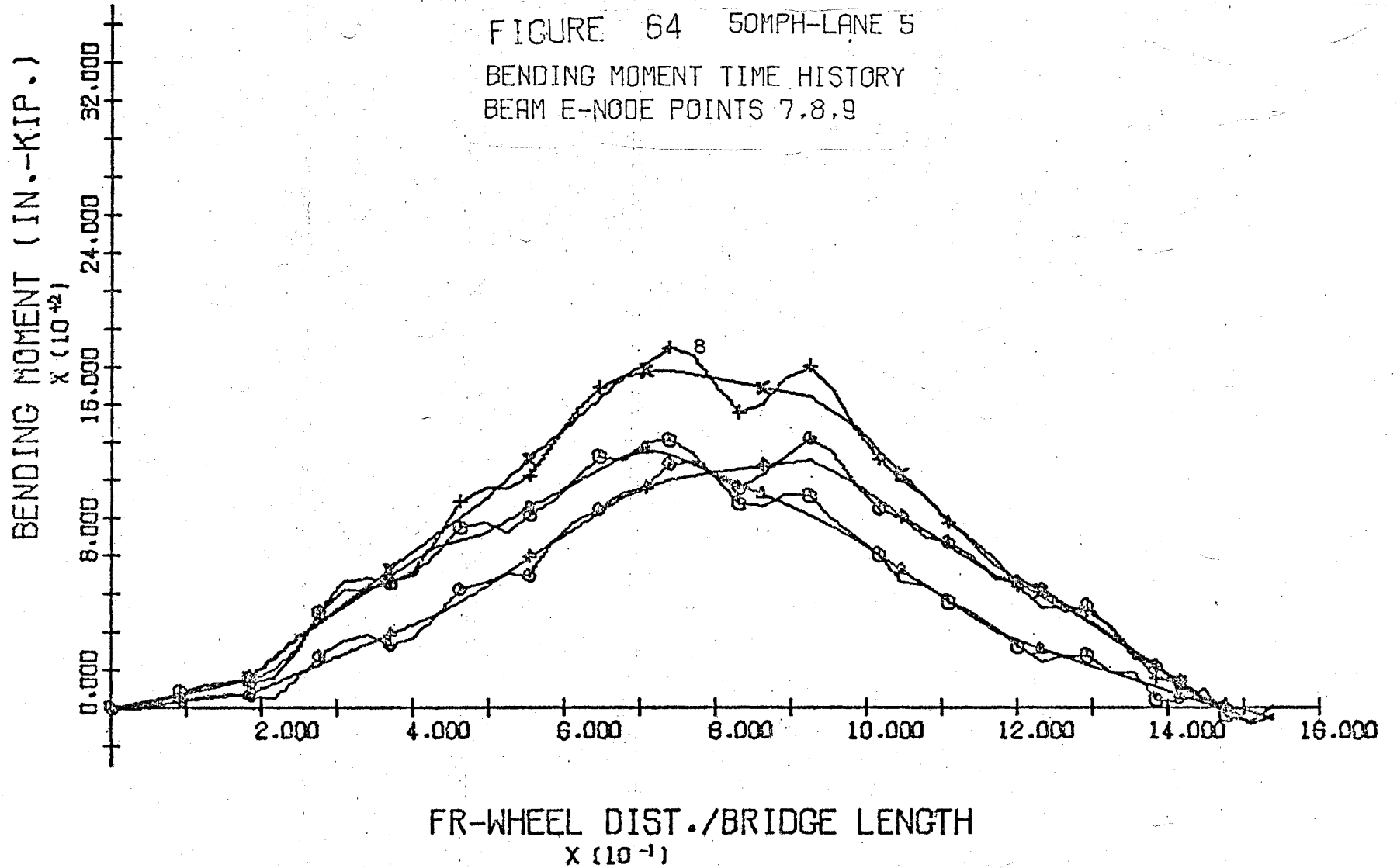
DISPLACEMENT (IN.)
X (10⁻²)

FIGURE 66   50MPH-LANE 5
BENDING MOMENT TIME HISTORY
BEAM D-NODE POINTS 12.13.14

BENDING MOMENT (IN.-KIP.)
X (10⁻²)

FR-WHEEL DIST./BRIDGE LENGTH
X (10⁻¹)

FIGURE 67 50MPH-LANE 5
DISPLACEMENT TIME HISTORY
BEAM C-NODE POINTS 17.18.19

DISPLACEMENT (IN.)
X (10⁻²)

FR-WHEEL DIST./BRIDGE LENGTH
X (10⁻¹)

FIGURE 68 50MPH-LANE 5
BENDING MOMENT TIME HISTORY
BEAM C-NODE POINTS 17,18,19
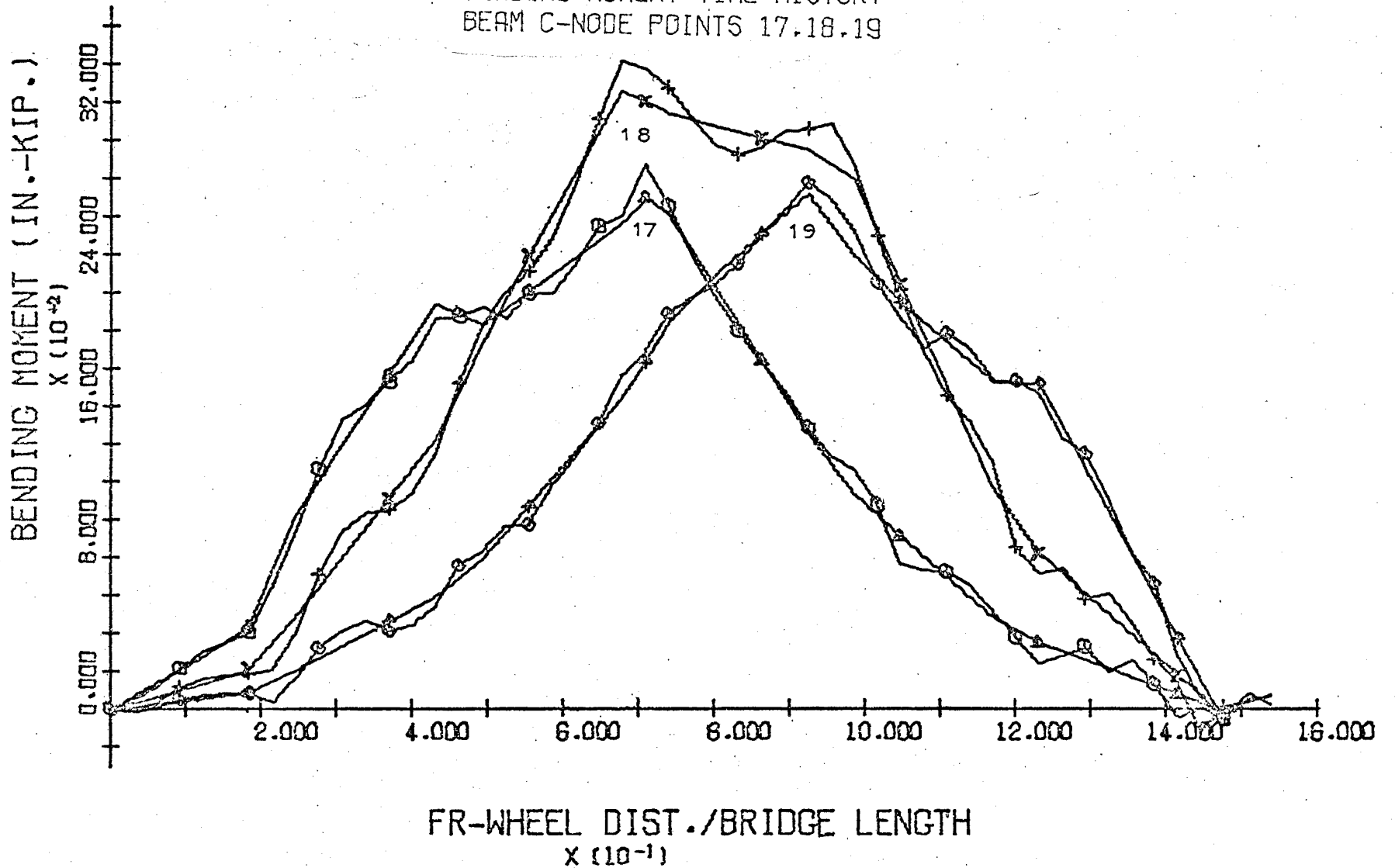
FIGURE 69 50MPH-LANE 5
DISPLACEMENT TIME HISTORY
BEAM 6-NODE POINTS 22,23,24

FR-WHEEL DIST./BRIDGE LENGTH
X (10⁻¹)

DISPLACEMENT (IN.)
X (10⁻²)

23

-130-

FIGURE 70 50MPH-LANE 5

BENDING MOMENT TIME HISTORY
BEAM B-NODE POINTS 22.23.24

FIGURE 71 50MPH-LANE 5
DISPLACEMENT TIME HISTORY
BEAM A-NODE POINTS 27,28,29

DISPLACEMENT (IN.)
X (.01)

FR-WHEEL DIST./BRIDGE LENGTH
X (10⁻¹)

FIGURE 72 50MPH-LANE 5

BENDING MOMENT TIME HISTORY
BEAM A-NODE POINTS 27,28,29
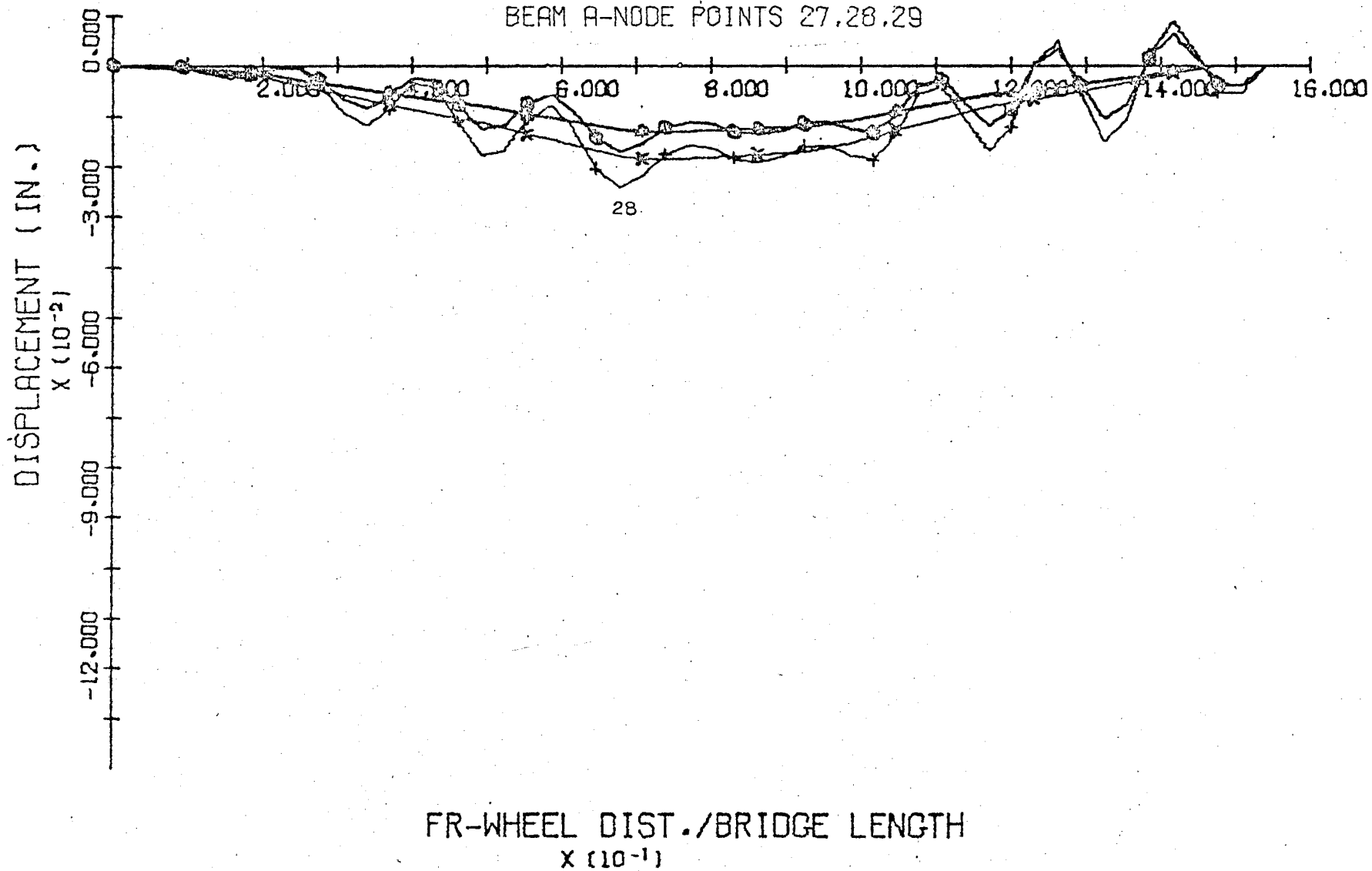
FIGURE 73 50MPH-LANE 5
DISPLACEMENT TIME HISTORY
NODE POINTS 3,8,13,18,23,28

FR-WHEEL DIST./BRIDGE LENGTH
X (10⁻¹)
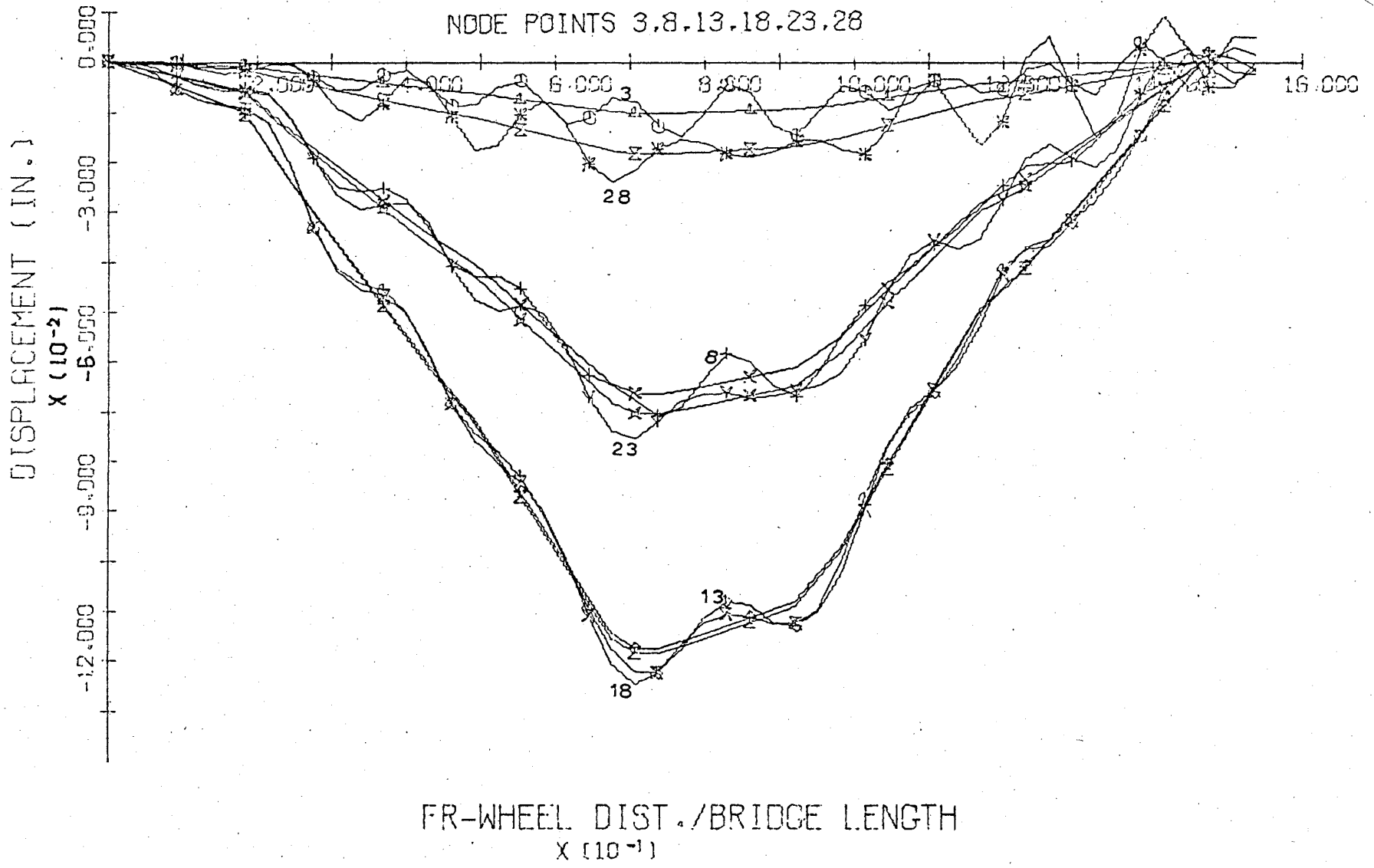
FIGURE 74 50MPH-LANE 5
BENDING MOMENT TIME HISTORY
NODE POINTS 3,8,13,18,23,28

BENDING MOMENT (IN.-KIP.) X (10⁺²)

FR-WHEEL DIST./BRIDGE LENGTH
X (10⁻¹)

FIGURE 75 STATIC-LANE 5
DISPLACEMENT DIAGRAMS

BEAM C- NODE POINTS 16-17-18-19-20

FIGURE 75 STATIC-LANE 5
BENDING MOMENT DIAGRAMS
BEAM C- NODE POINTS 16-17-18-19-20

BENDING MOMENT (IN.-KIP.) X (10⁺²)

LONGITUDINAL DISTANCE (IN.)
X (10⁺¹)

-137-
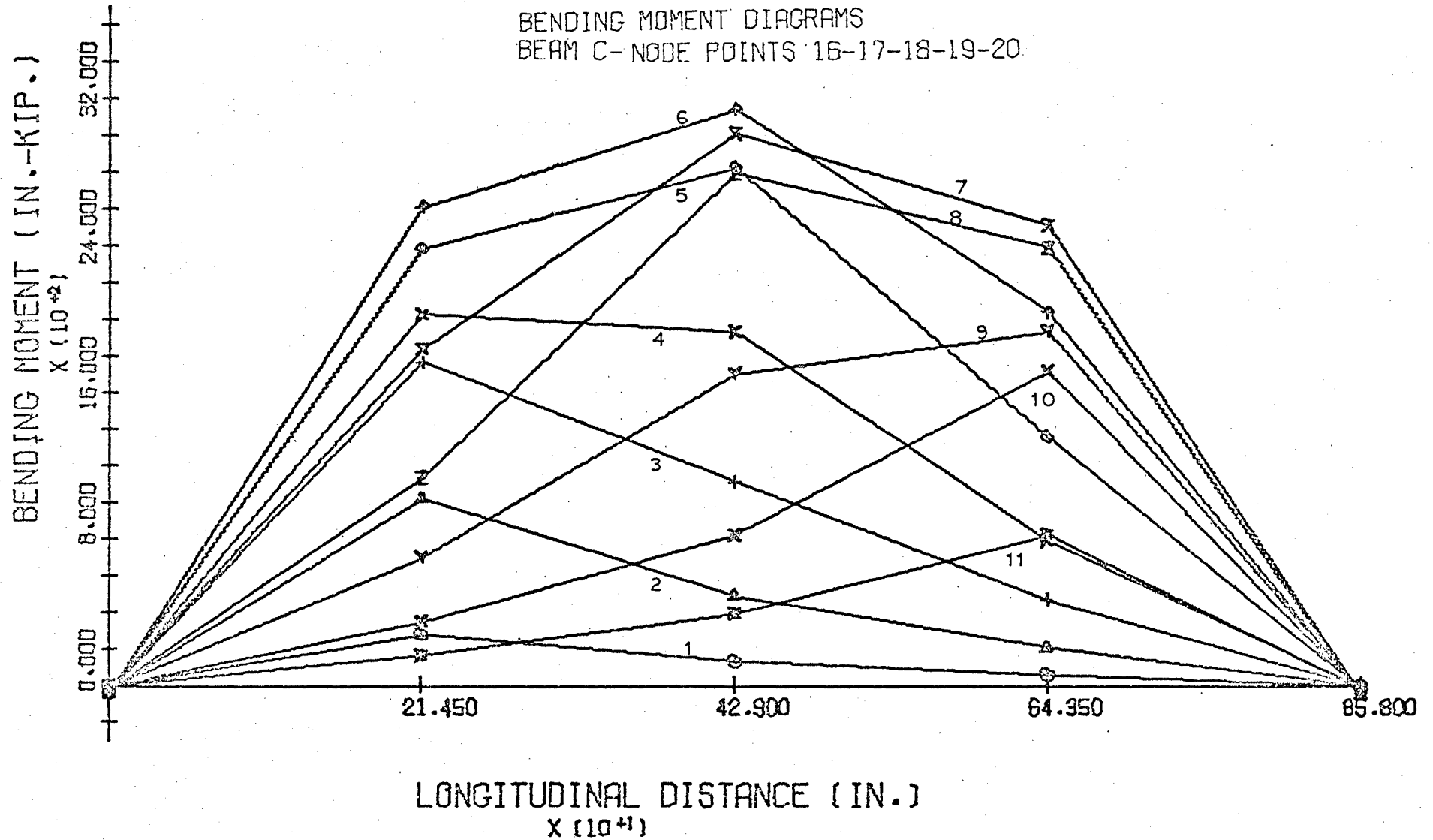
FIGURE 77 50MPH-LANE 5
DISPLACEMENT DIAGRAMS
BEAM C- NODE POINTS 16-17-18-19-20

LONGITUDINAL DISTANCE (IN.)
X (10⁺¹)
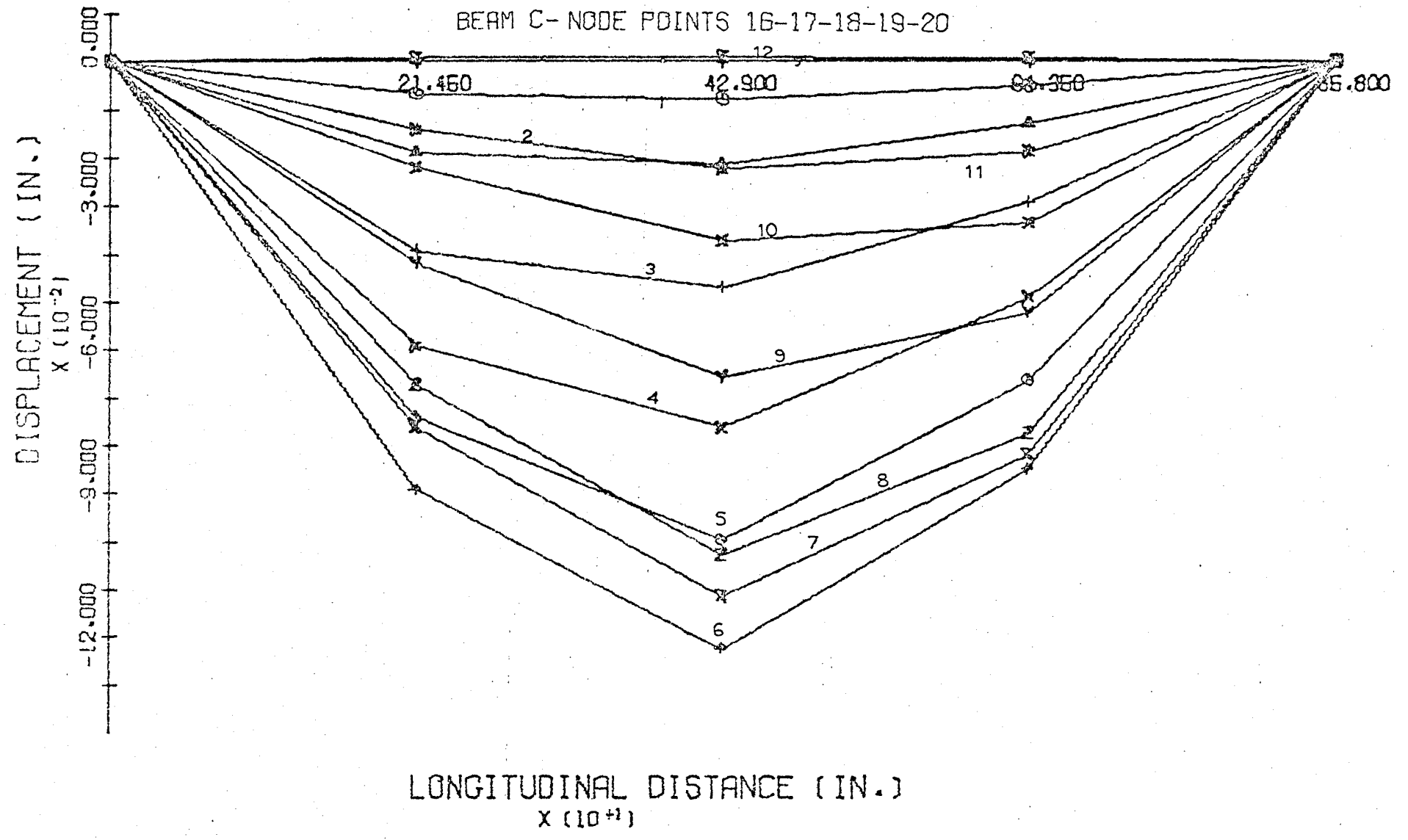
FIGURE 78 50MPH–LANE 5

BENDING MOMENT DIAGRAMS
BEAM C– NODE POINTS 16-17-18-19-20

LONGITUDINAL DISTANCE (IN.)
X (10⁺¹)
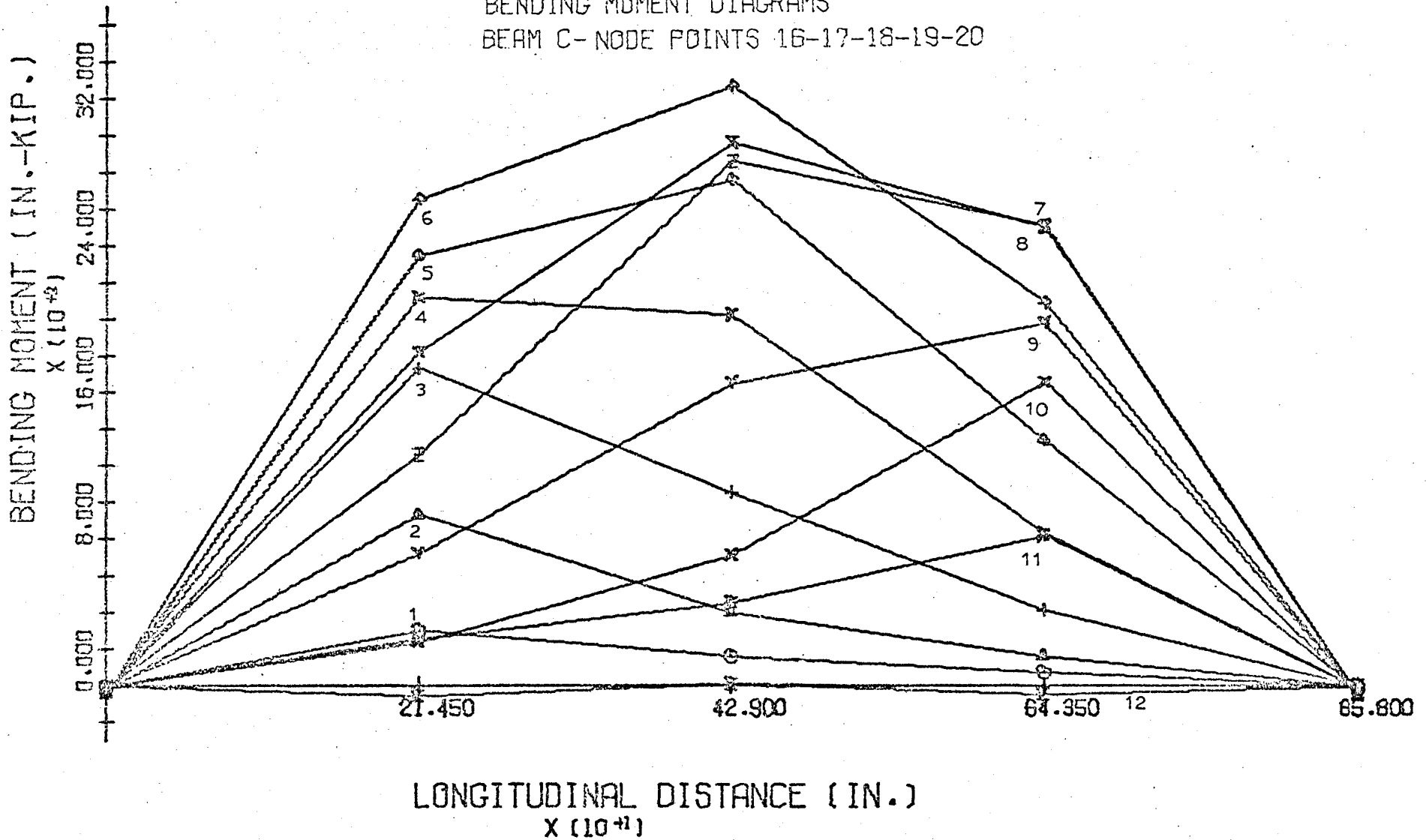
FIGURE 79 50MPH-LANE 5
DISPLACEMENT DIAGRAMS
7.07692E-01
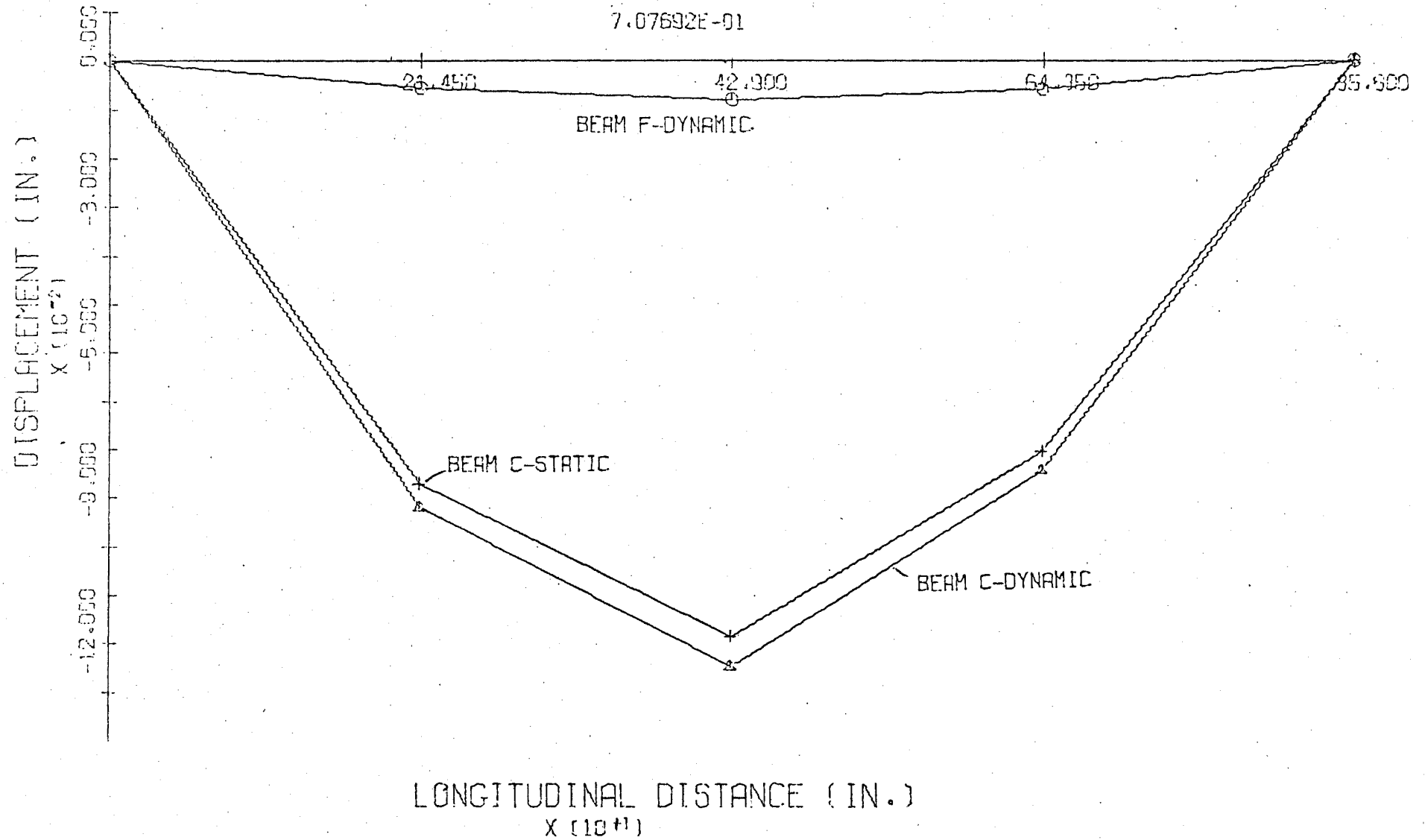
FICURE 8C 50MPH-LANE 5
BENDING MOMENT DIAGRAMS
6.76923E-01
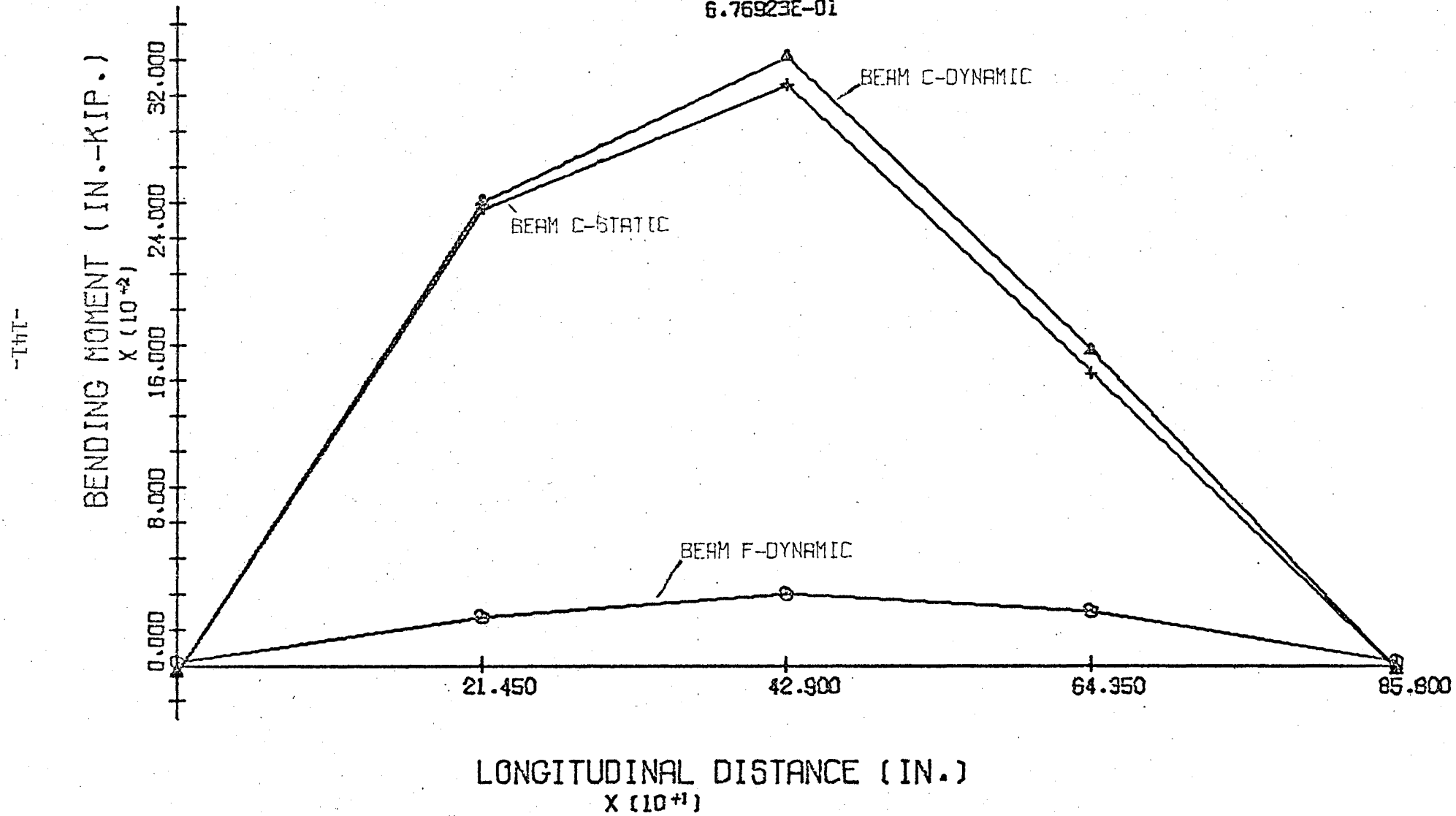
FIGURE 81 STATIC-LANE 5
DISPLACEMENT DIAGRAMS
NODE POINTS-3 -8-13-18-23-28
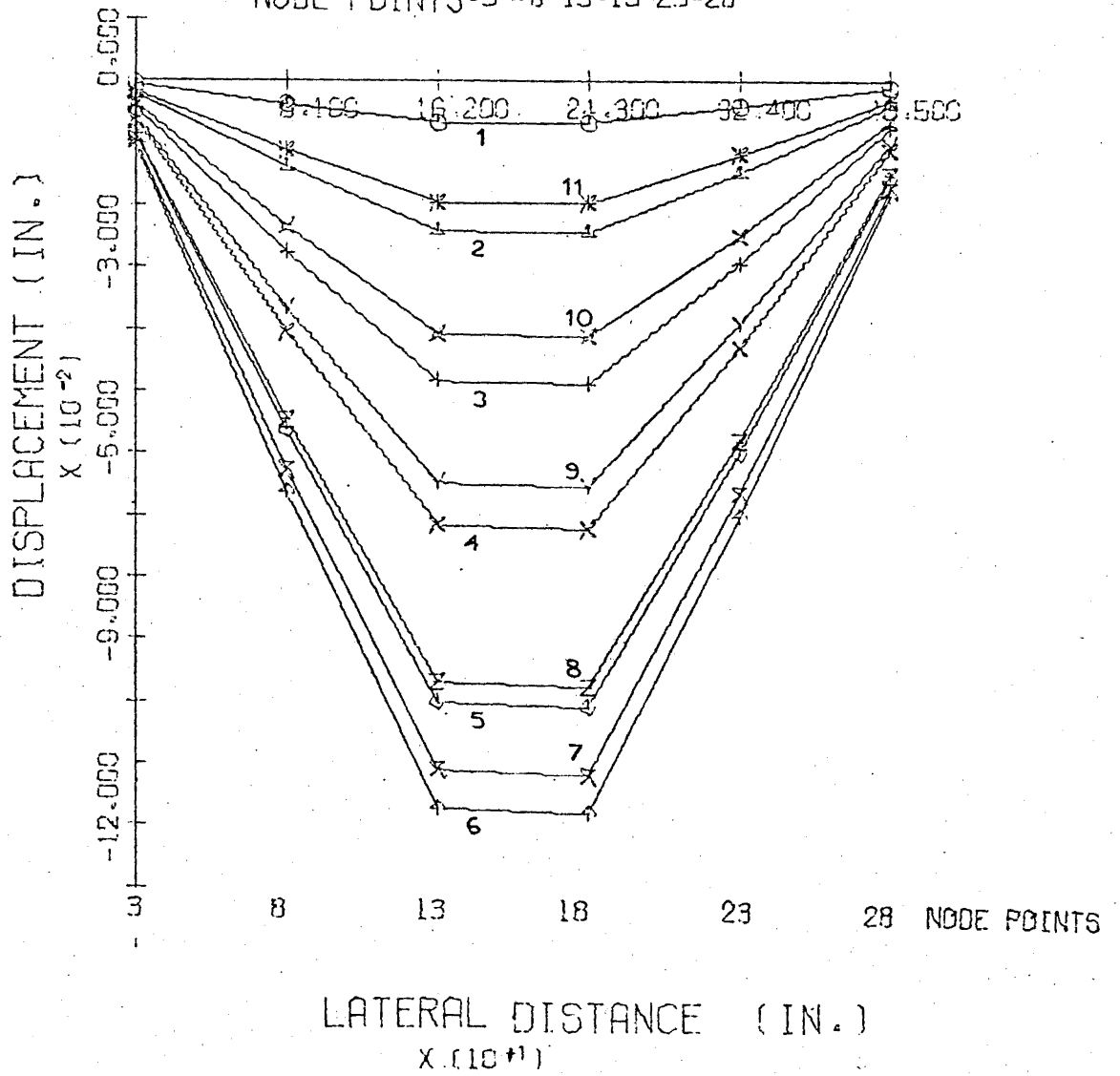
FIGURE 82 STATIC-LANE 5
BENDING MOMENT DIAGRAMS
NODE POINTS -3- 8-13-18-23-28
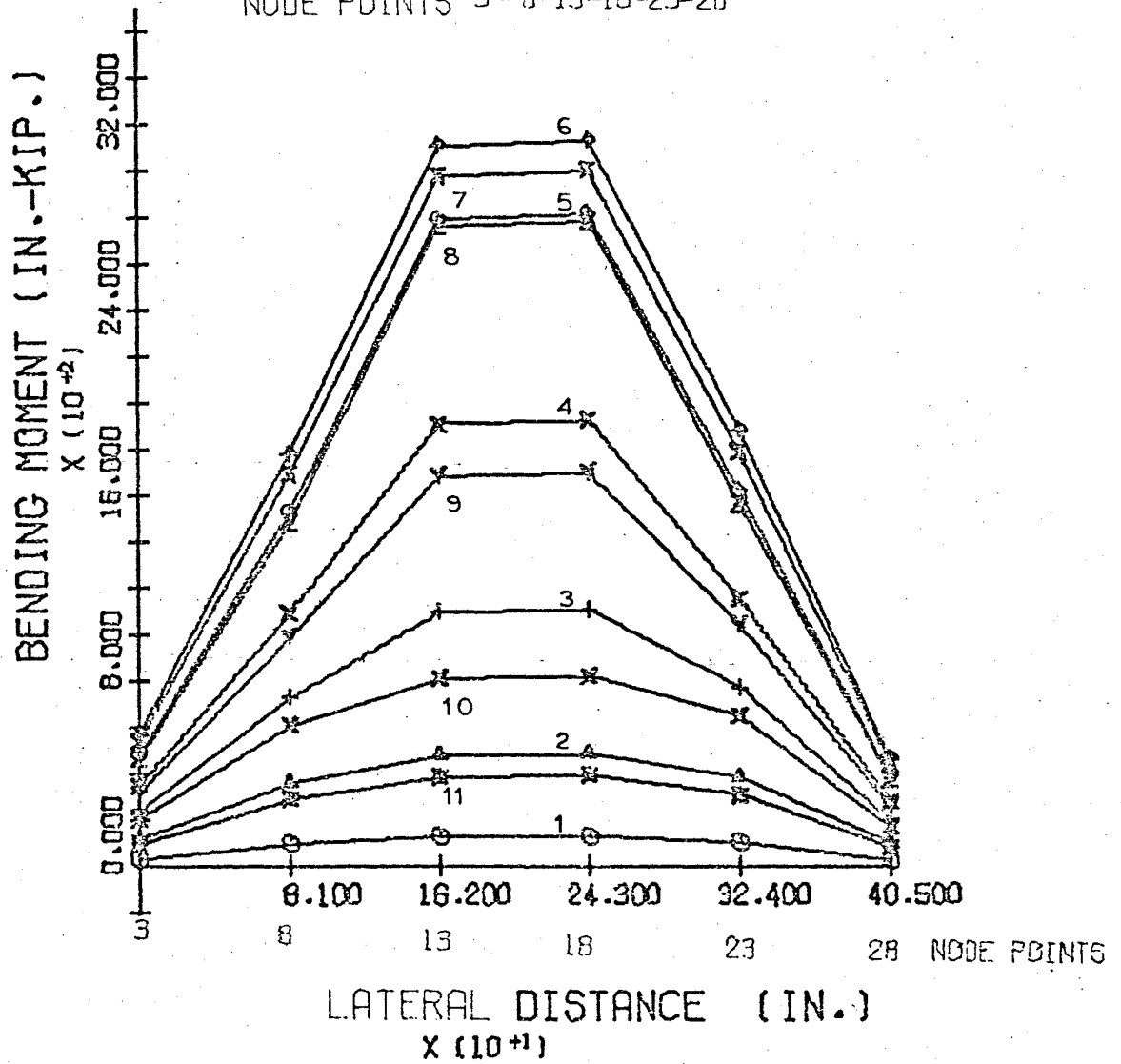
FIGURE 83 50MPH-LANE 5
DISPLACEMENT DIAGRAMS
NODE POINTS -3- 8-13-18-23-28
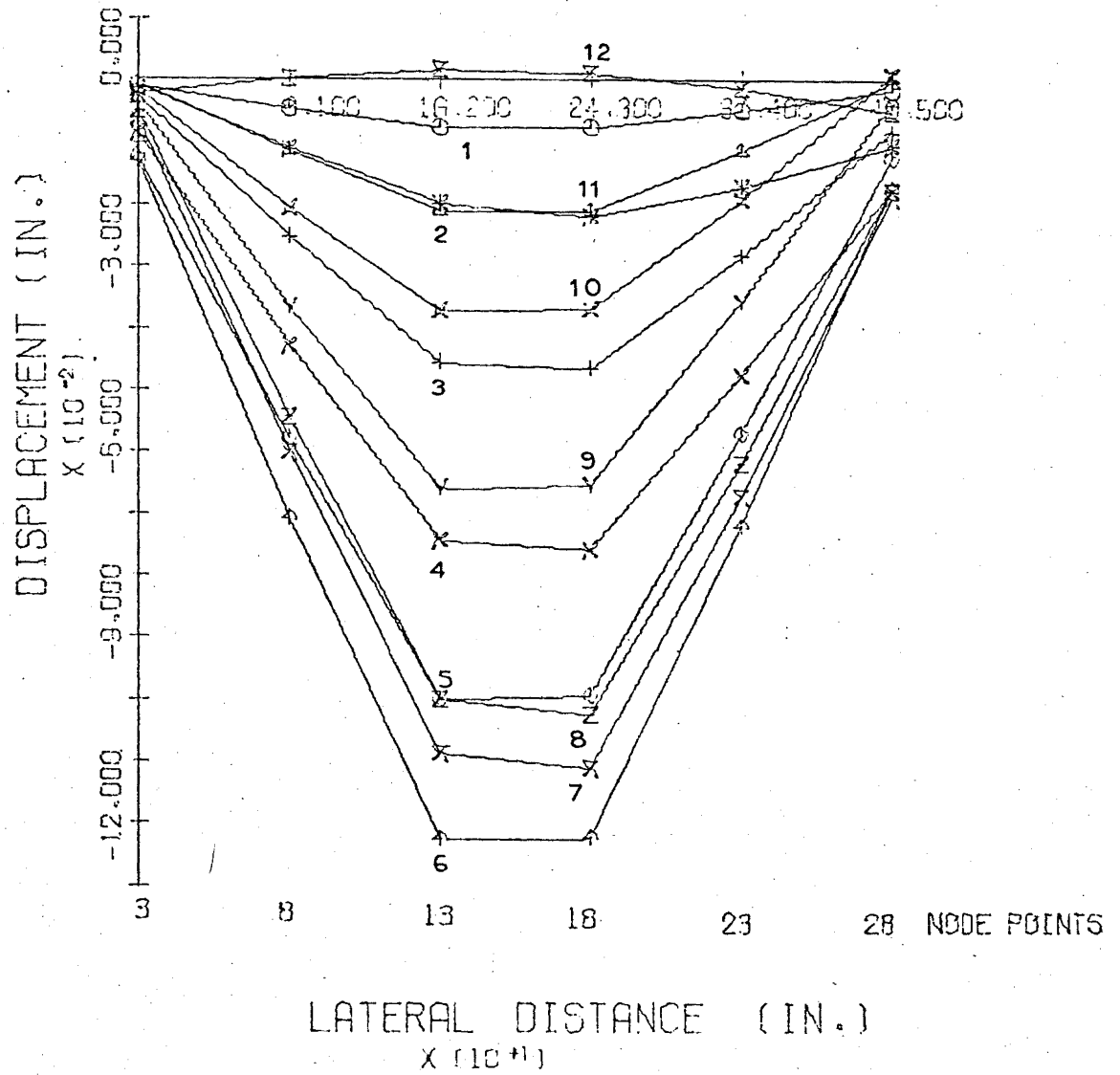
FIGURE 84 50MPH-LANE 5
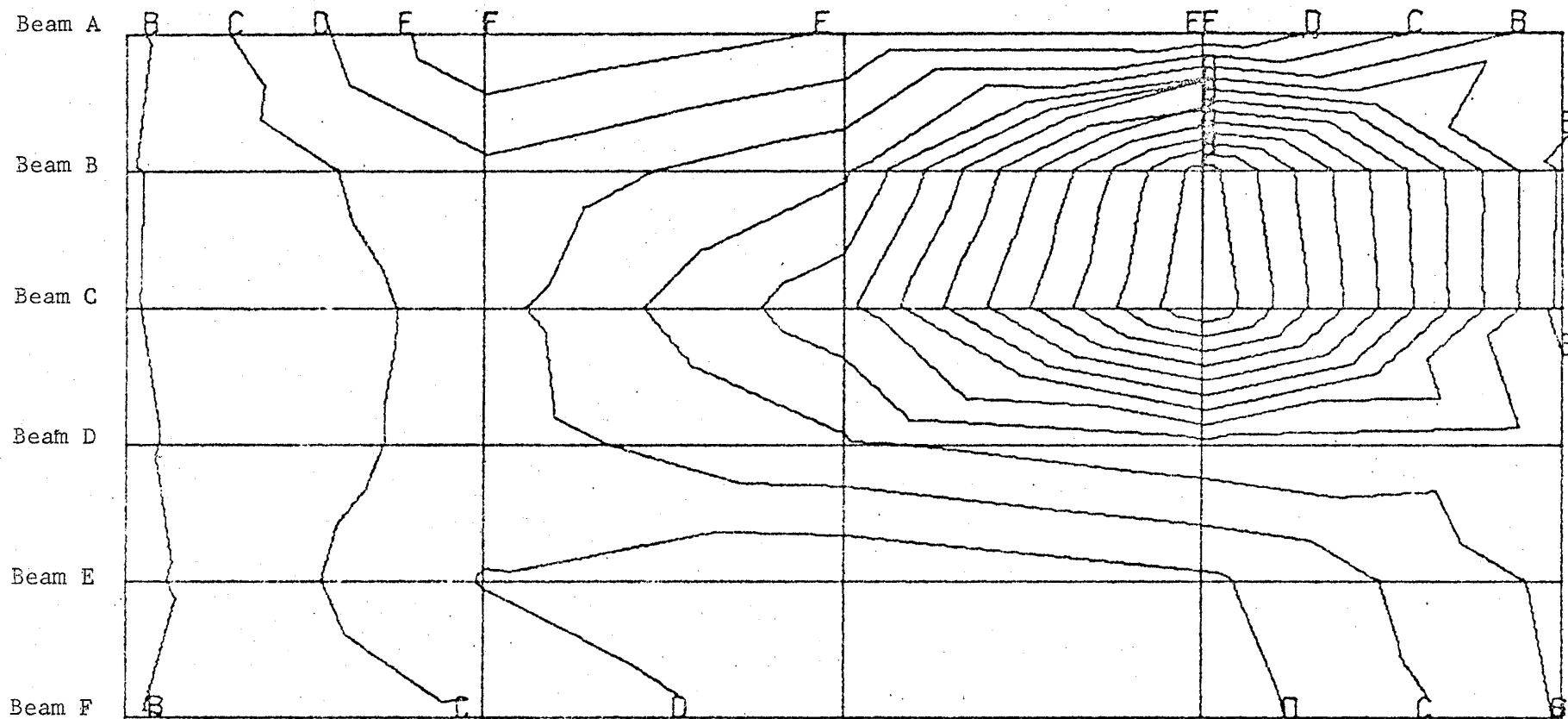BENDING MOMENT DIAGRAMS
NODE POINTS -3 -8 -13 -18 -23 -28

-145-
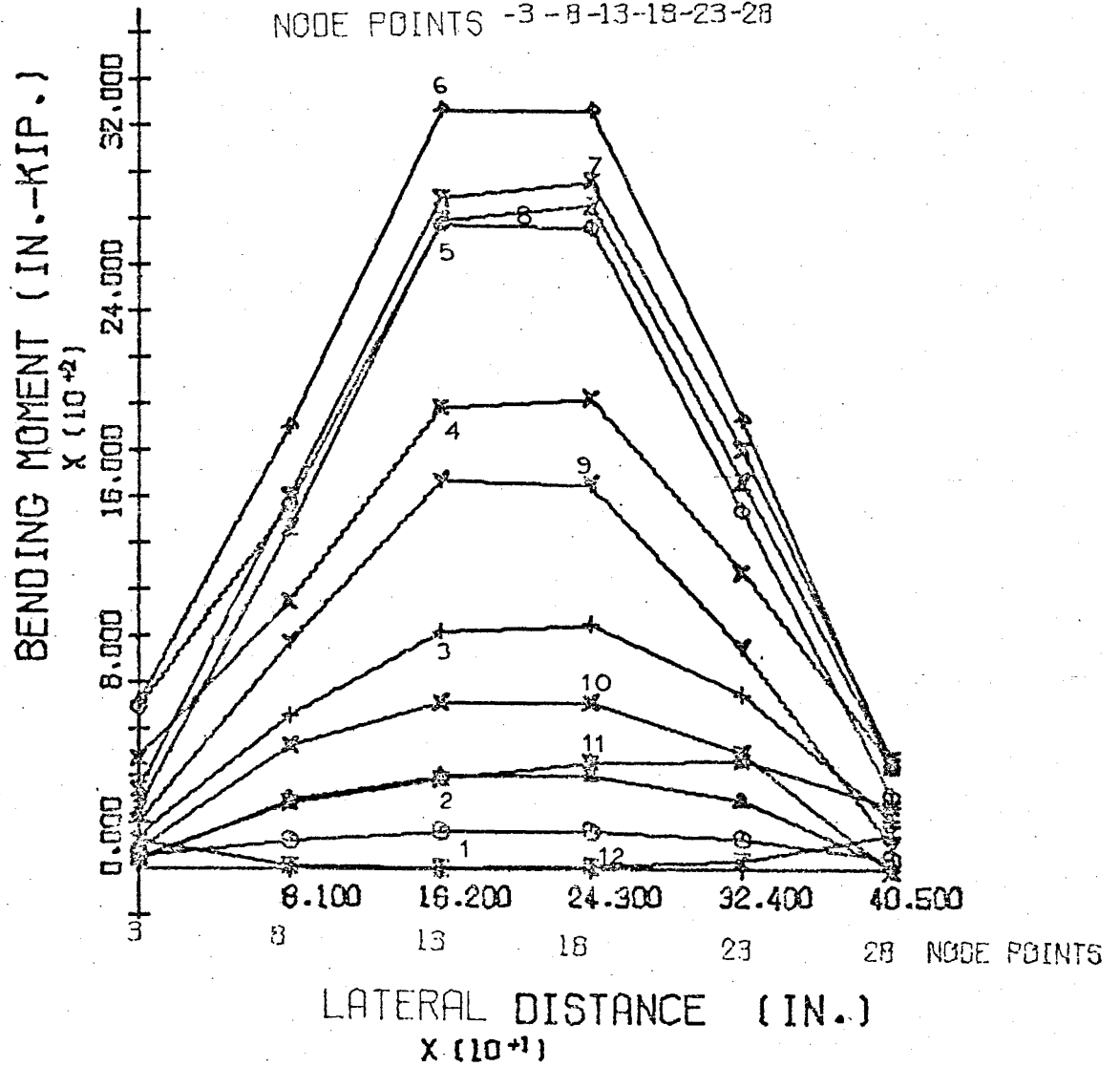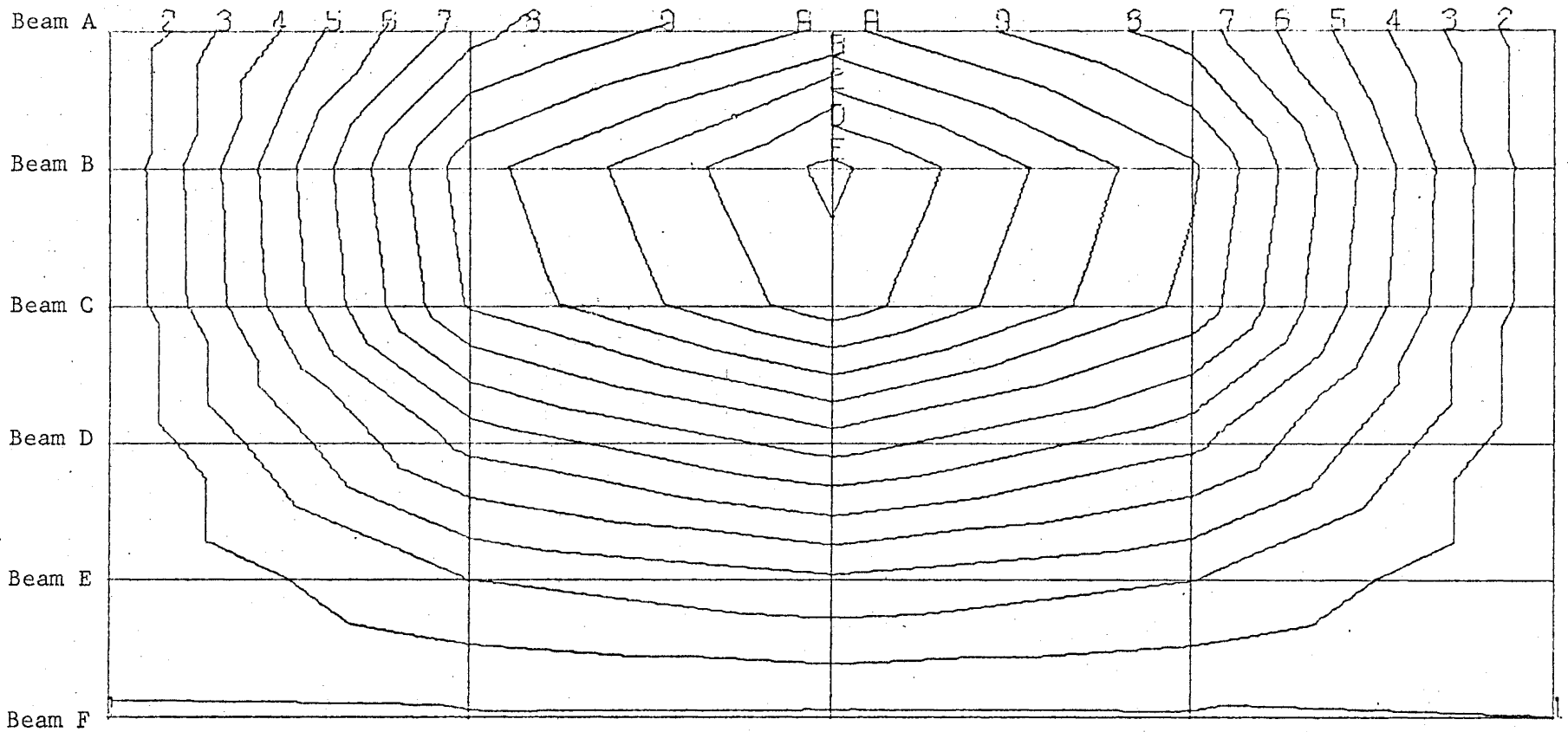
DISPLACEMENT(IN.) CONTOURS
CASE - 25 MPH LANE 3
FR-WHEEL DIST./BRIDGE LENGTH = 0.73945
FIGURE 85
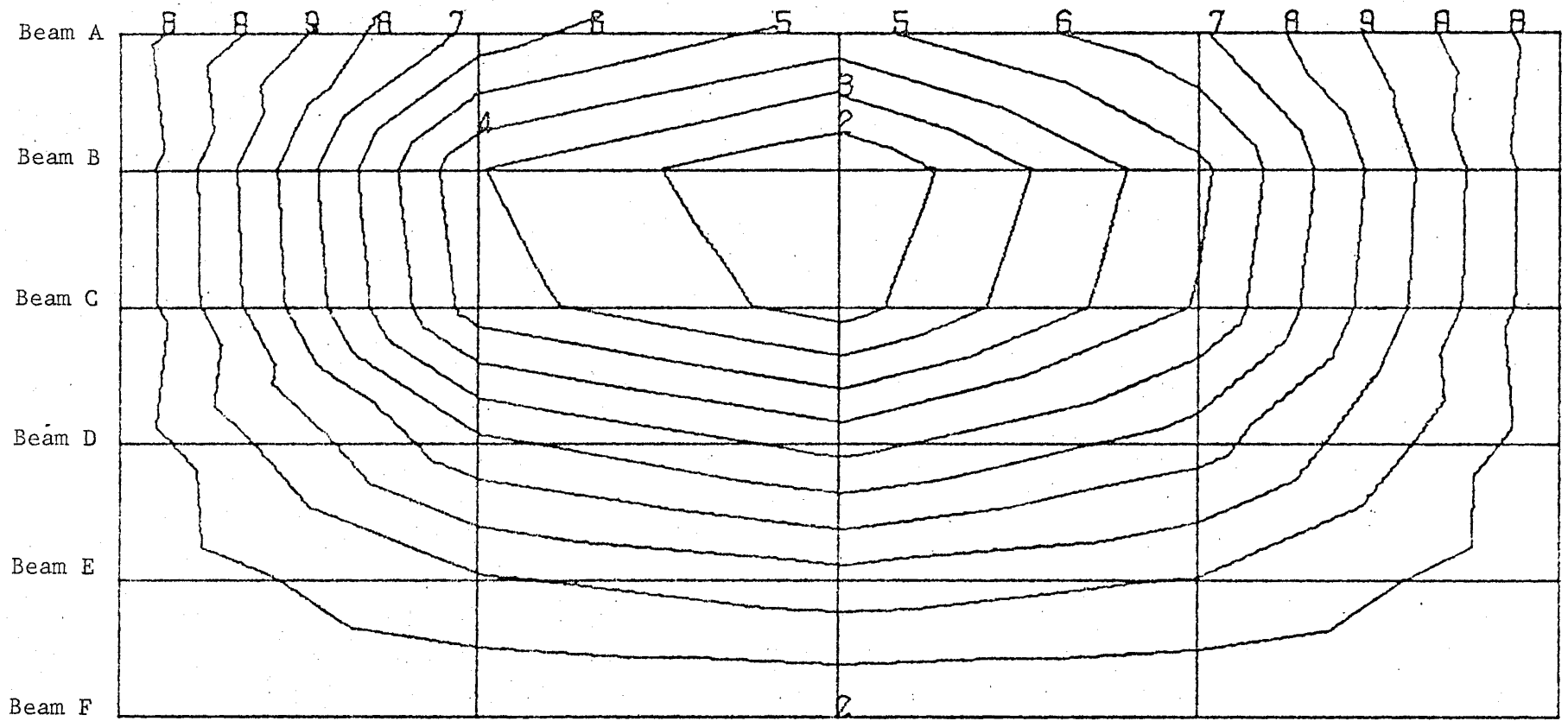
BENDING MOMENT(IN.-KIP) CONTOURS
CASE- 25 MPH LANE 3
FR-WHEEL DIST./BRIDGE LENGTH = 0.7385
FIGURE 86
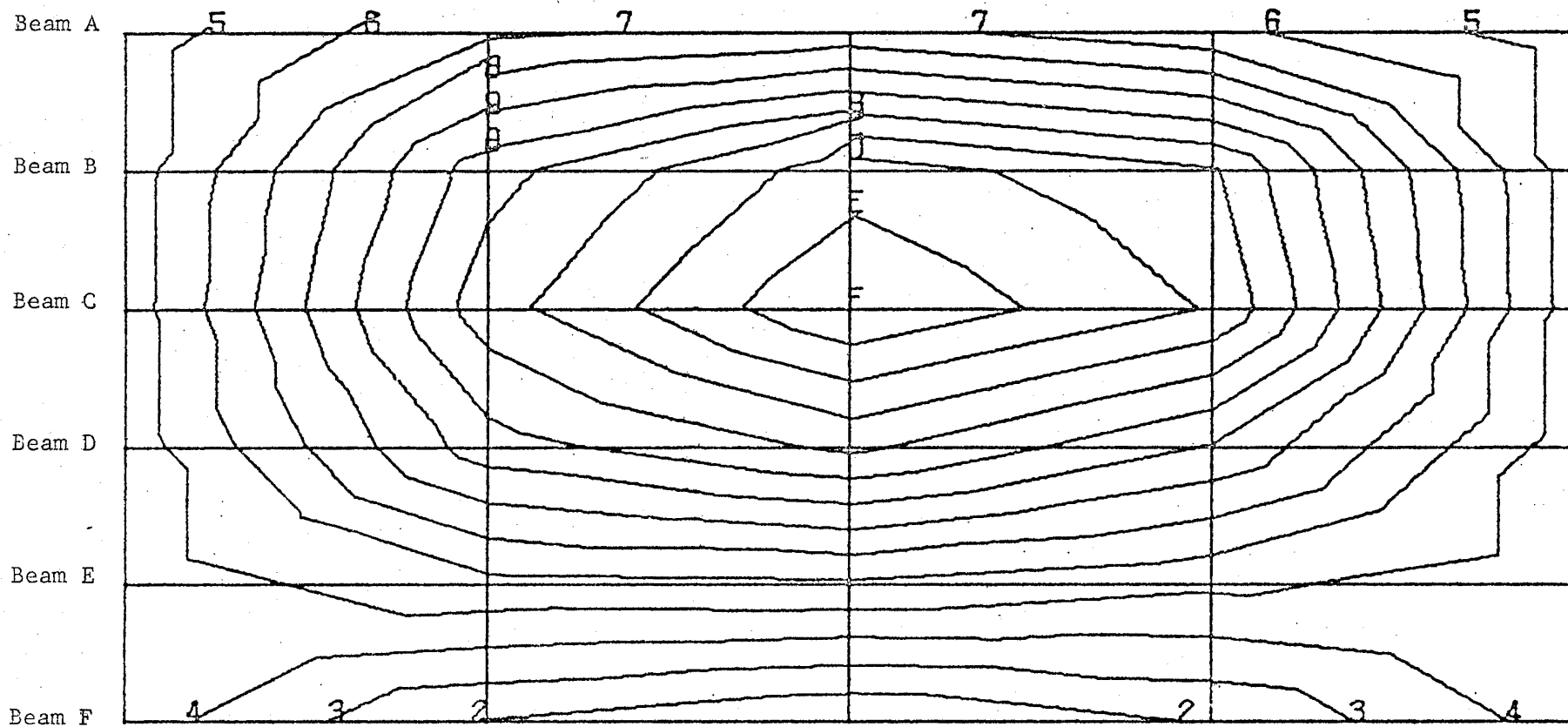
-147-

DISPLACEMENT(IN.) CONTOURS

CASE- 25 MPH LANE 3

FR-WHEEL DIST./BRIDGE LENGTH = 1.4462

FIGURE 87
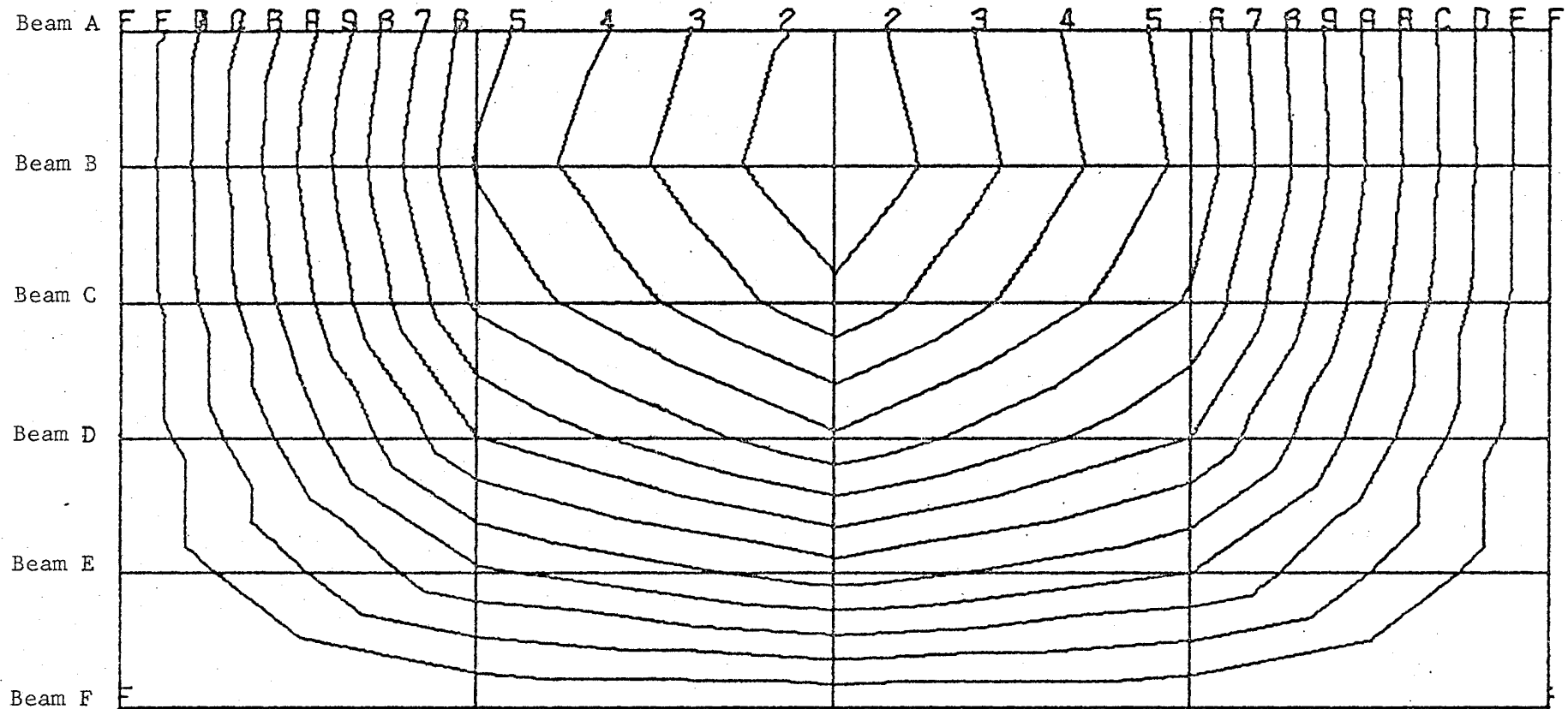
DISPLACEMENT(IN.) CONTOURS
CASE- 25 MPH LANE 3
FR-WHEEL DIST./BRIDGE LENGTH = 1.4769
FIGURE 86
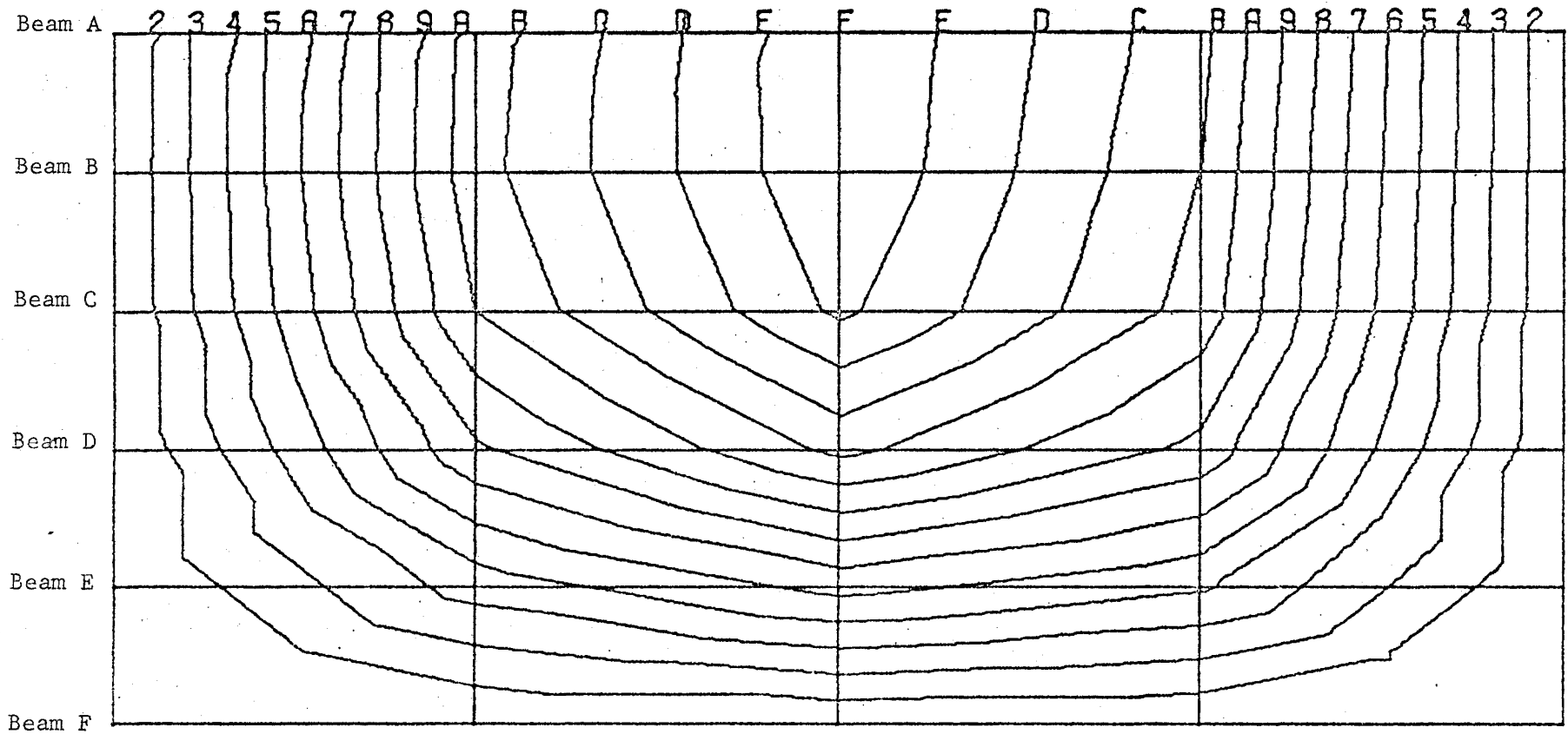
Beam A

Beam B

Beam C

Beam D

Beam E

Beam F

2 3 4 5 6 7 8 9 A B C D E F F D C B A 9 8 7 6 5 4 3 2

DISPLACEMENT(IN.) CONTOURS
CASE- 25 MPH LANE 3
FR-WHEEL DIST./BRIDGE LENGTH = 1.5077
FIGURE 89

BENDING MOMENT(IN.-KIP) CONTOURS
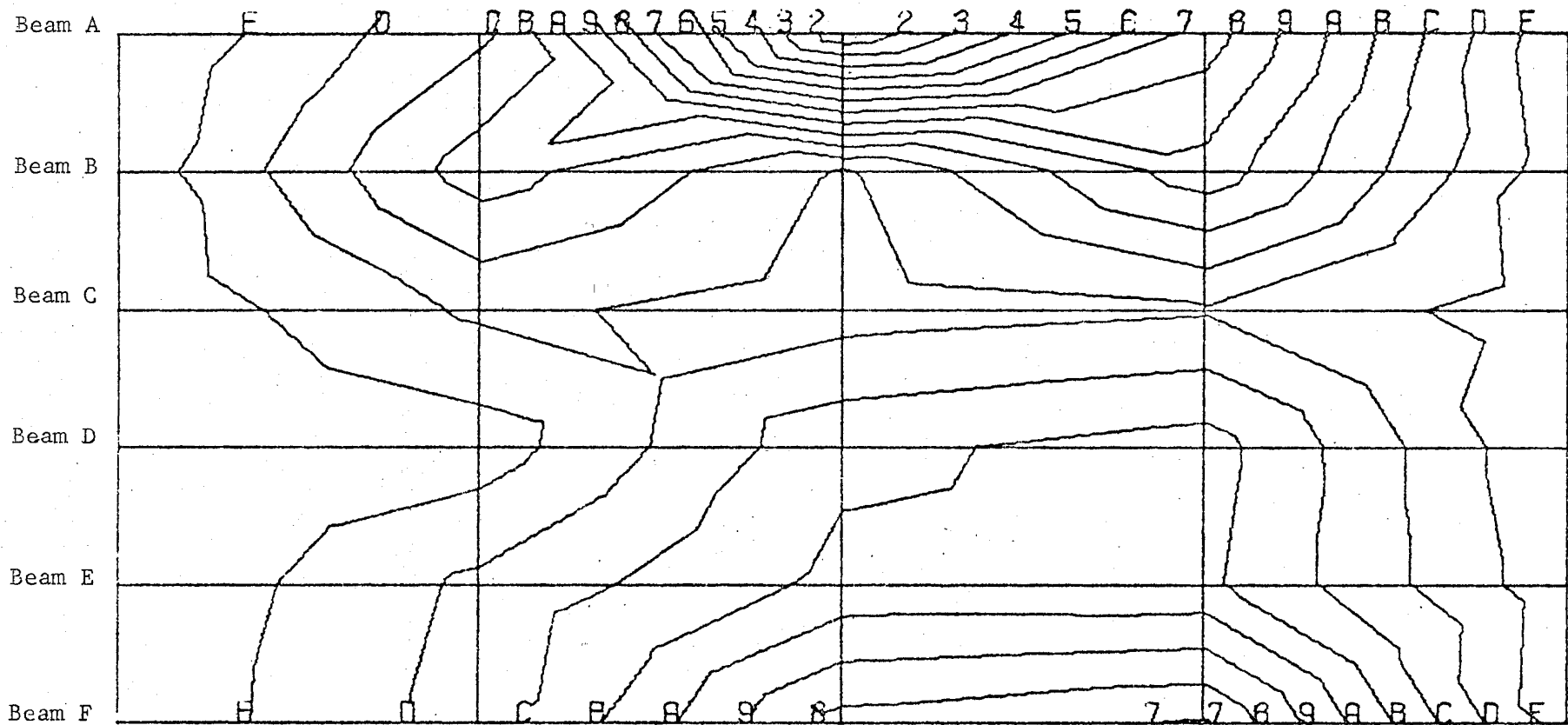CASE- 25 MPH LANE 3
FR-WHEEL DIST./BRIDGE LENGTH = 1.4462
FIGURE 90
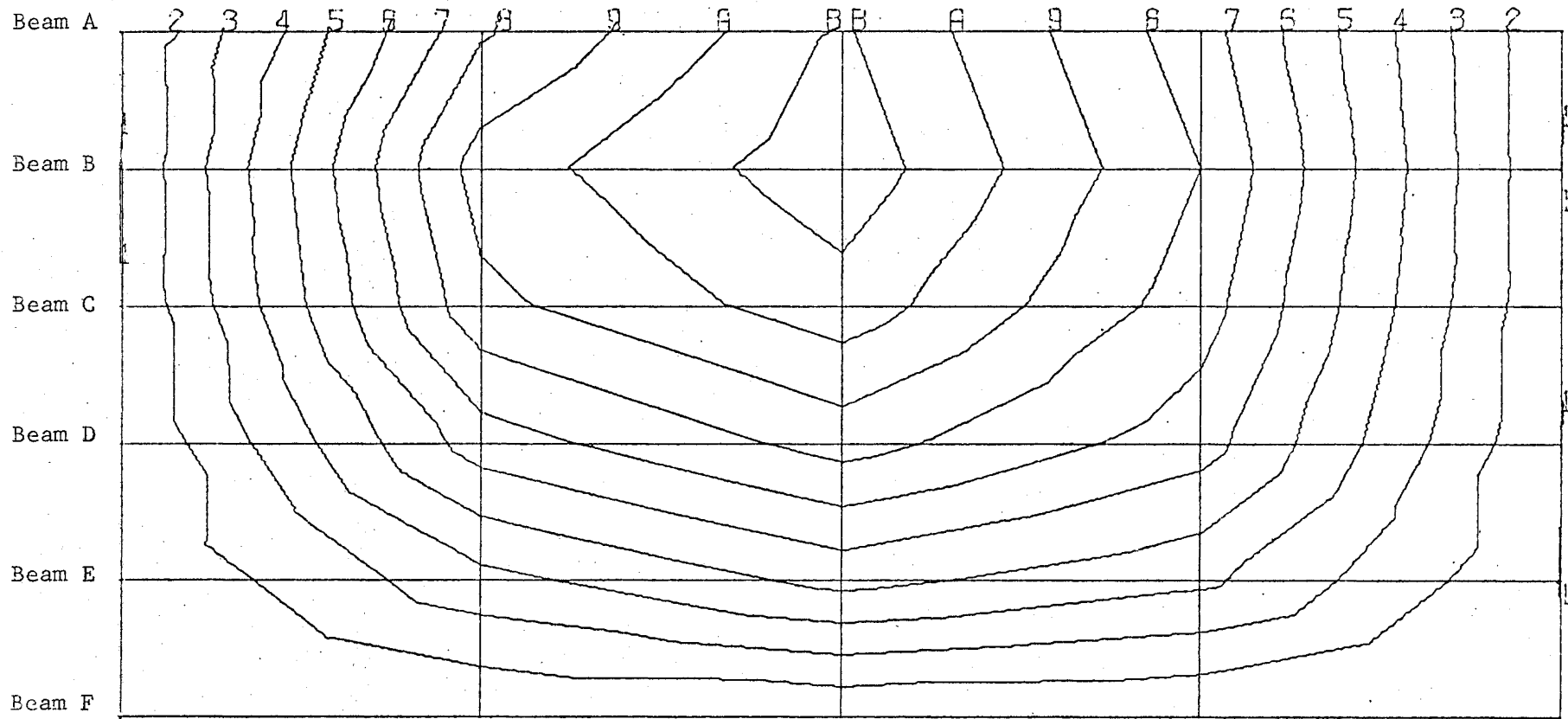
Beam A

Beam B

Beam C

Beam D

Beam E

Beam F

BENDING MOMENT(IN.-KIP) CONTOURS
CASE- 25 MPH LANE 3
FR-WHEEL DIST./BRIDGE LENGTH = 1.4769

FIGURE 91

Beam A

Beam B

Beam C

Beam D

Beam E

Beam F
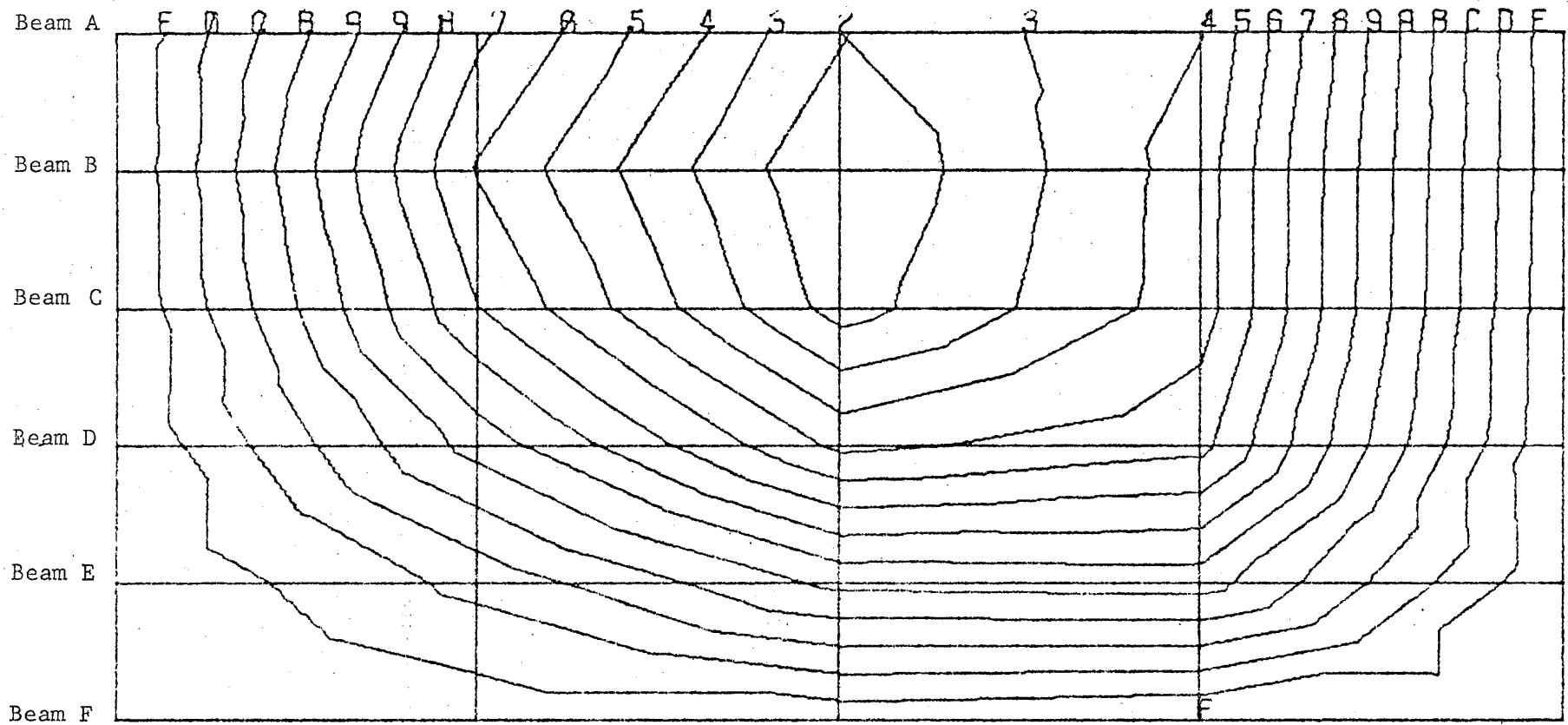
BENDING MOMENT(IN·KIP) CONTOURS
CASE- 25 MPH LANE 3
FR·WHEEL DIST./BRIDGE LENGTH _ 1·6077

FIGURE 92

DISPLACEMENT(IN.) CONTOURS
CASE- 50 MPH LANE 3
FR-WHEEL DIST./BRIDGE LENGTH = 0.70769
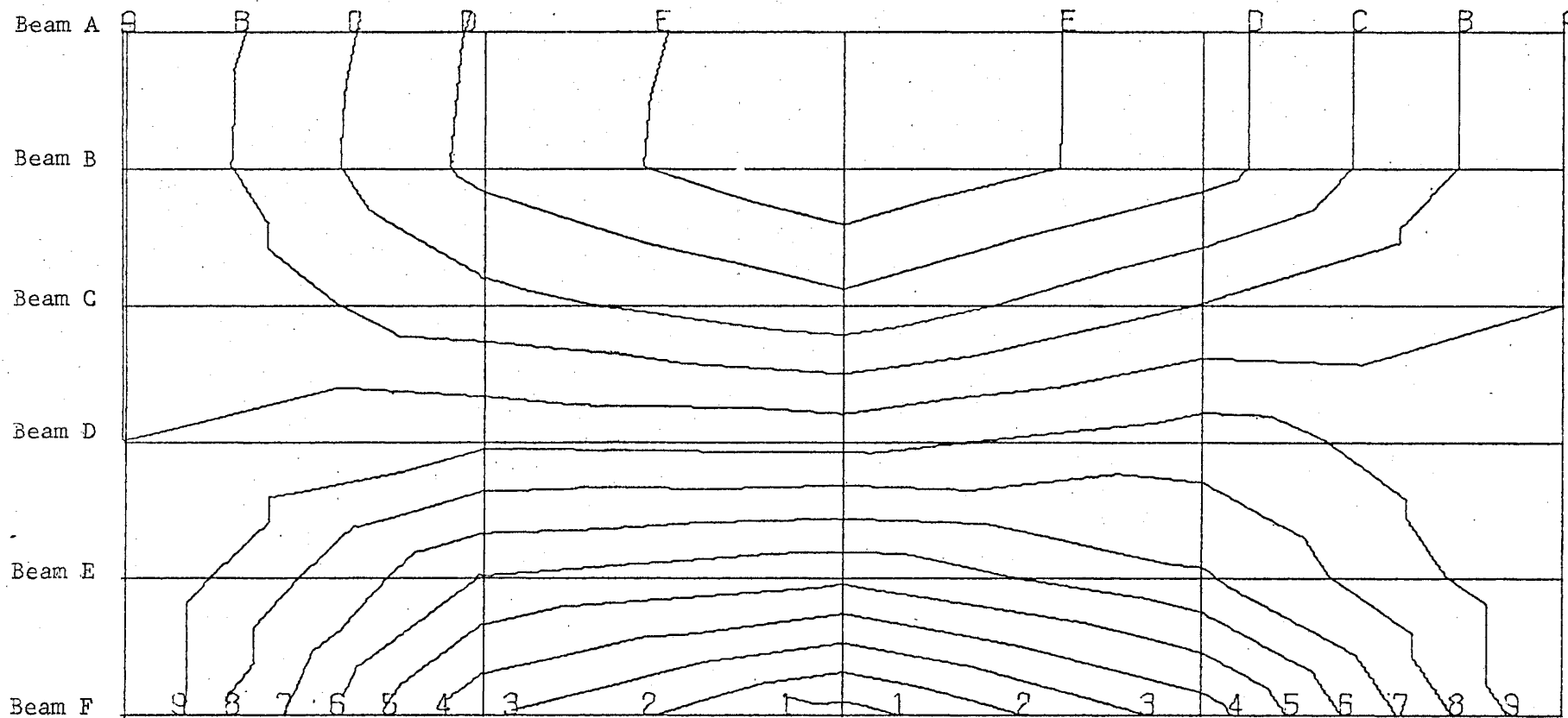
FIGURE 93

Beam A

Beam B

Beam C

Beam D

Beam E

Beam F
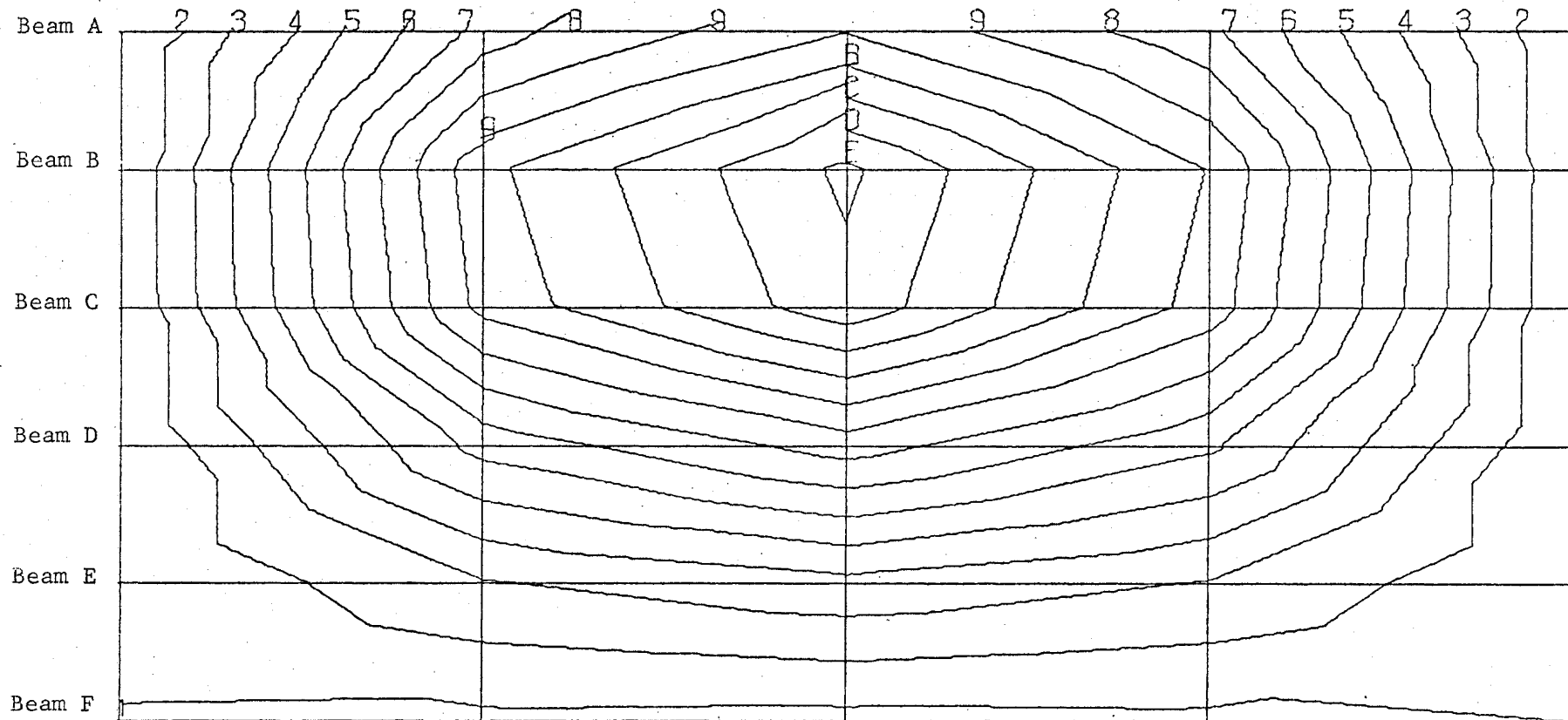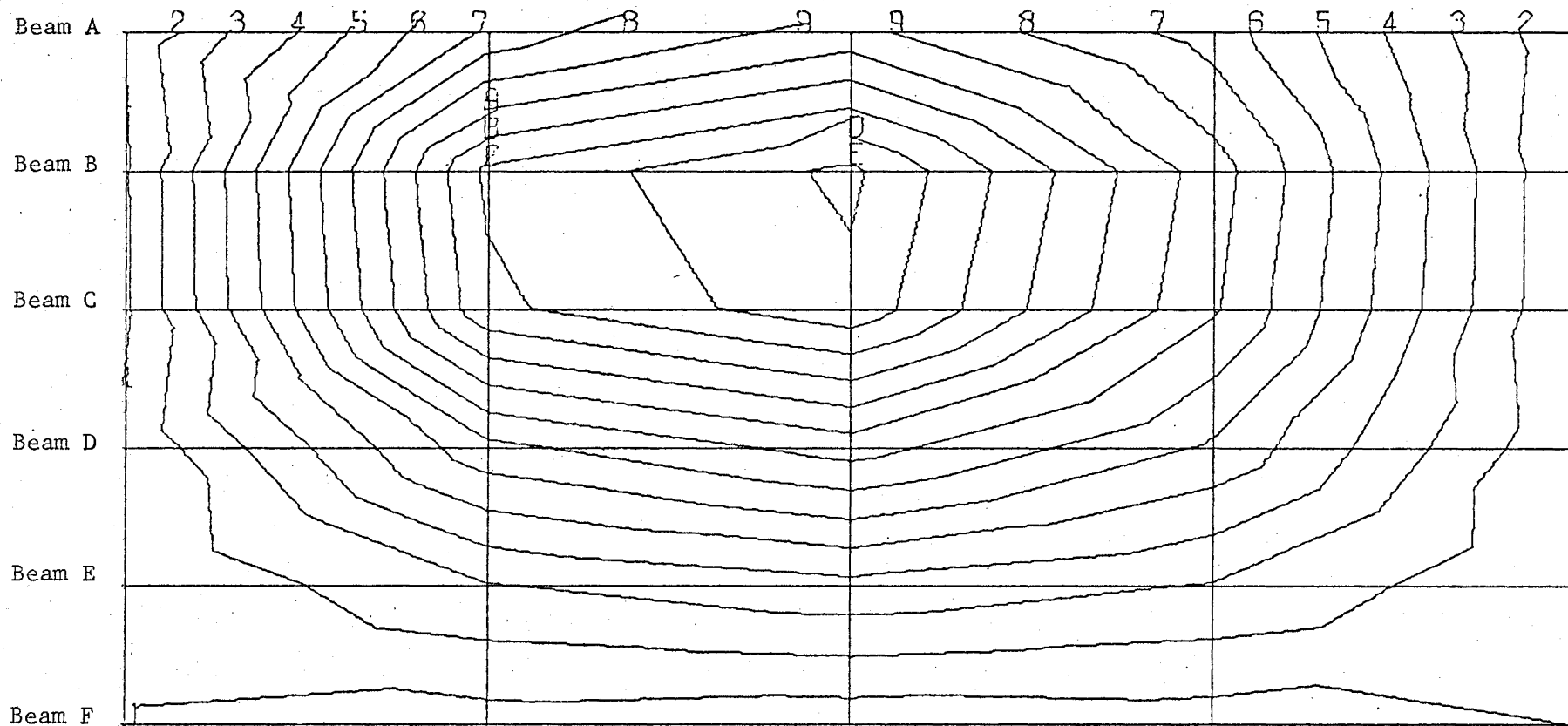
BENDING MOMENT(IN.-KIP) CONTOURS

CASE - 50 MPH LANE 3

FR-WHEEL DIST./BRIDGE LENGTH = 0.70769

FIGURE 94

DISPLACEMENT(IN.) CONTOURS
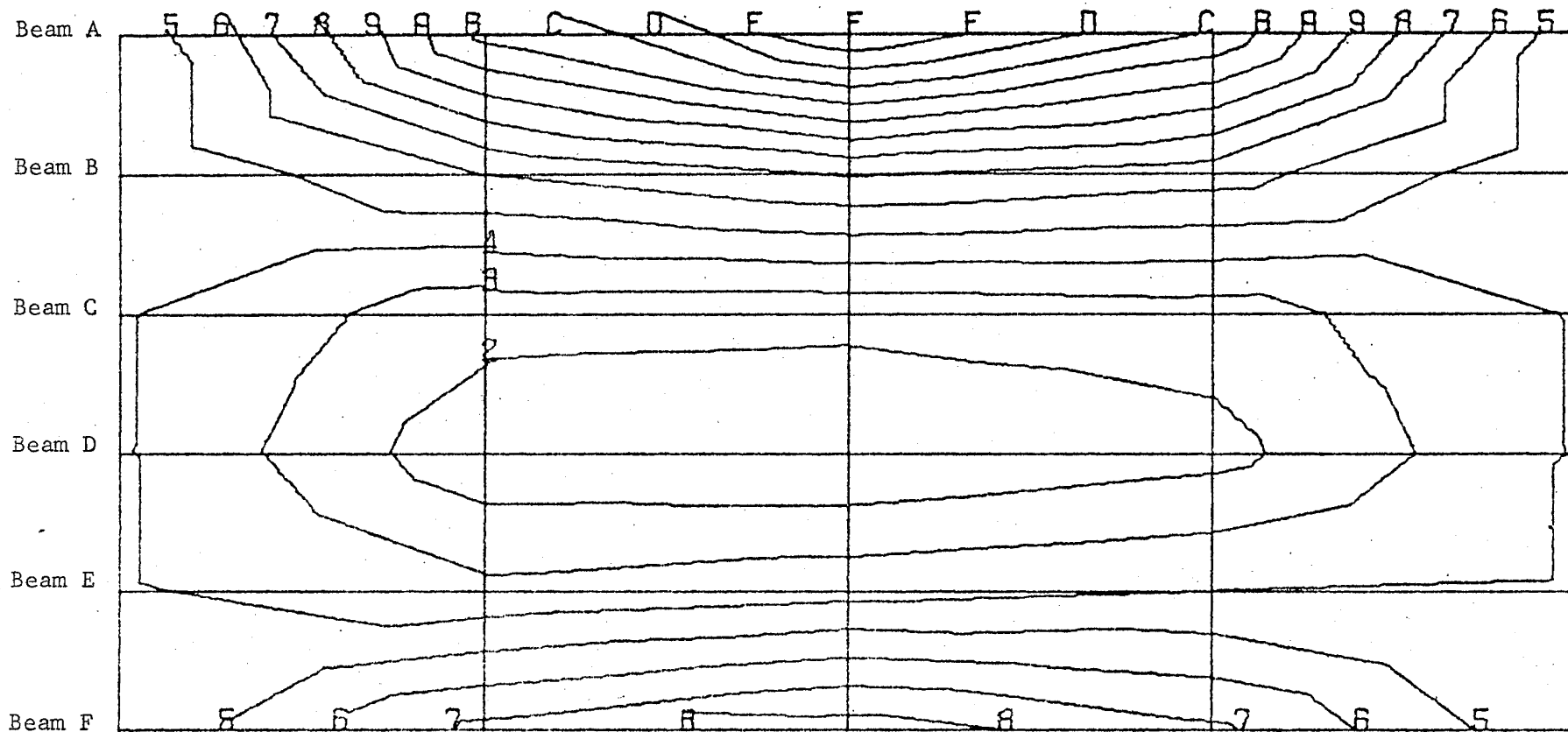CASE- 60 MPH LANE 3
FR WHEEL DIST./BRIDGE LENGTH = 1.4153
FIGURE 95

DISPLACEMENT(IN.) CONTOURS
CASE- 50 MPH LANE 3
FR-WHEEL DIST./BRIDGE LENGTH = 1.4462
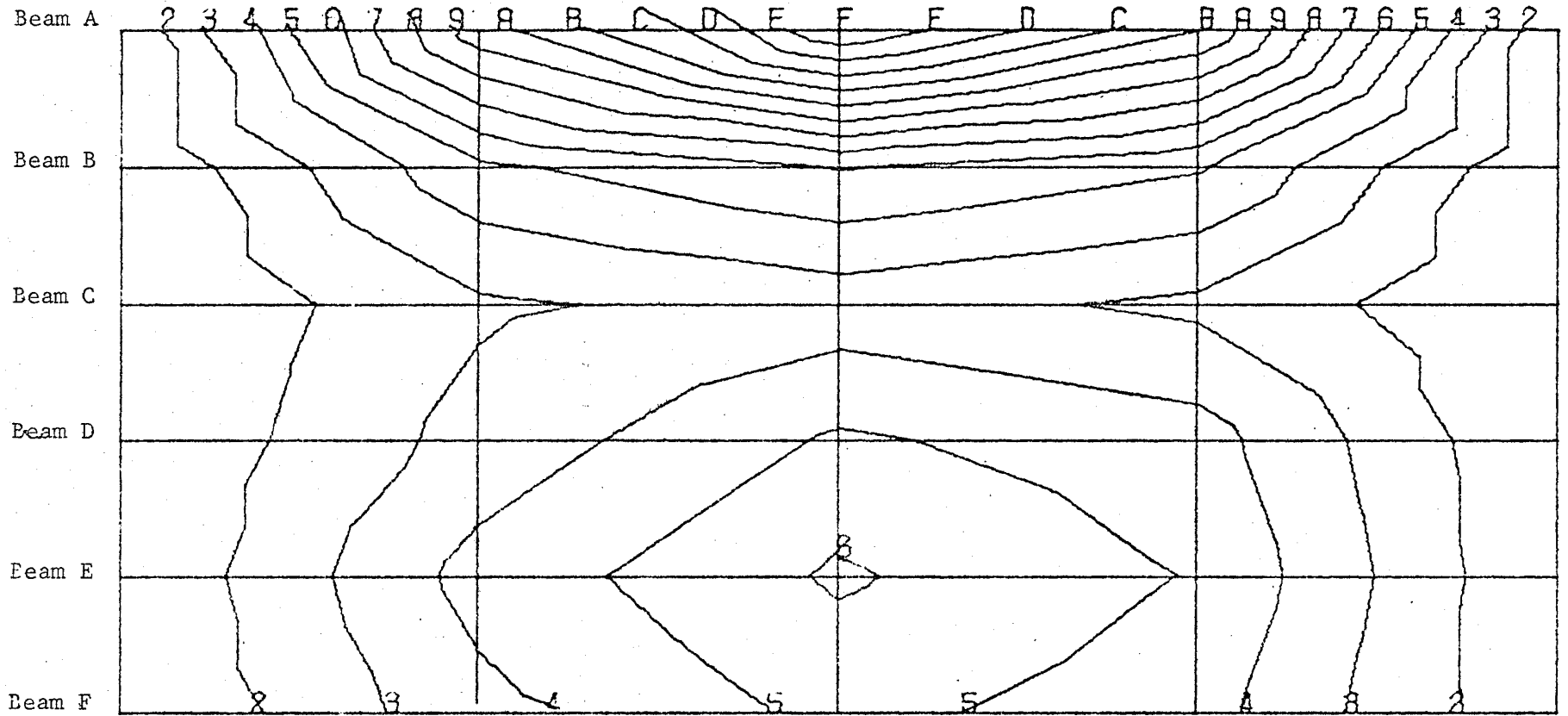
FIGURE 96

DISPLACEMENT(IN.) CONTOURS

CASE- 60 MPH LANE 3

FR-WHEEL DIST./BRIDGE LENGTH = 1.4769

FIGURE 97

BENDING MOMENT(IN.-KIP) CONTOURS
CASE- 60 MPH LANE 3
FR-WHEEL DIST./BRIDGE LENGTH = 1.4153
FIGURE 98
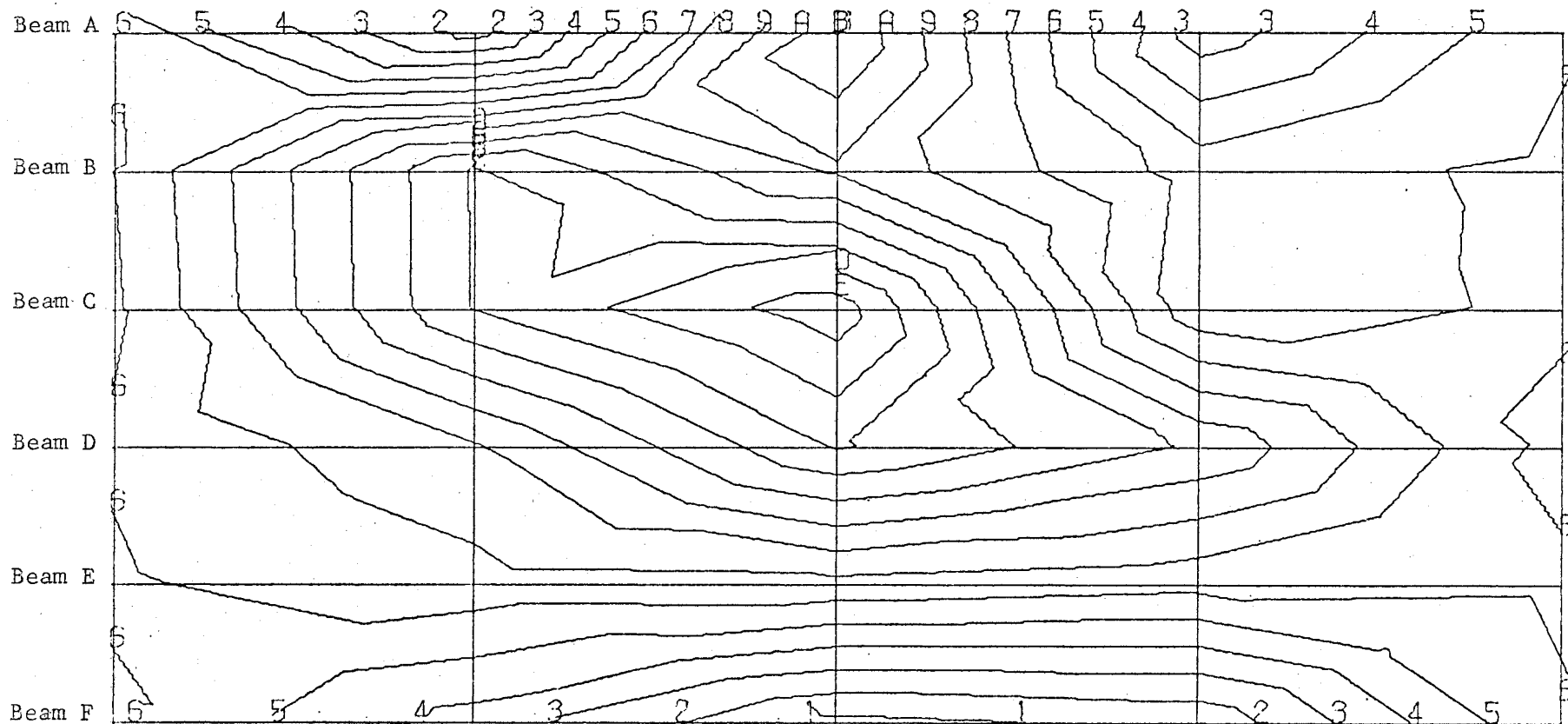
BENDING MOMENT(IN.-KIP) CONTOURS
CASE- 50 MPH LANE 3
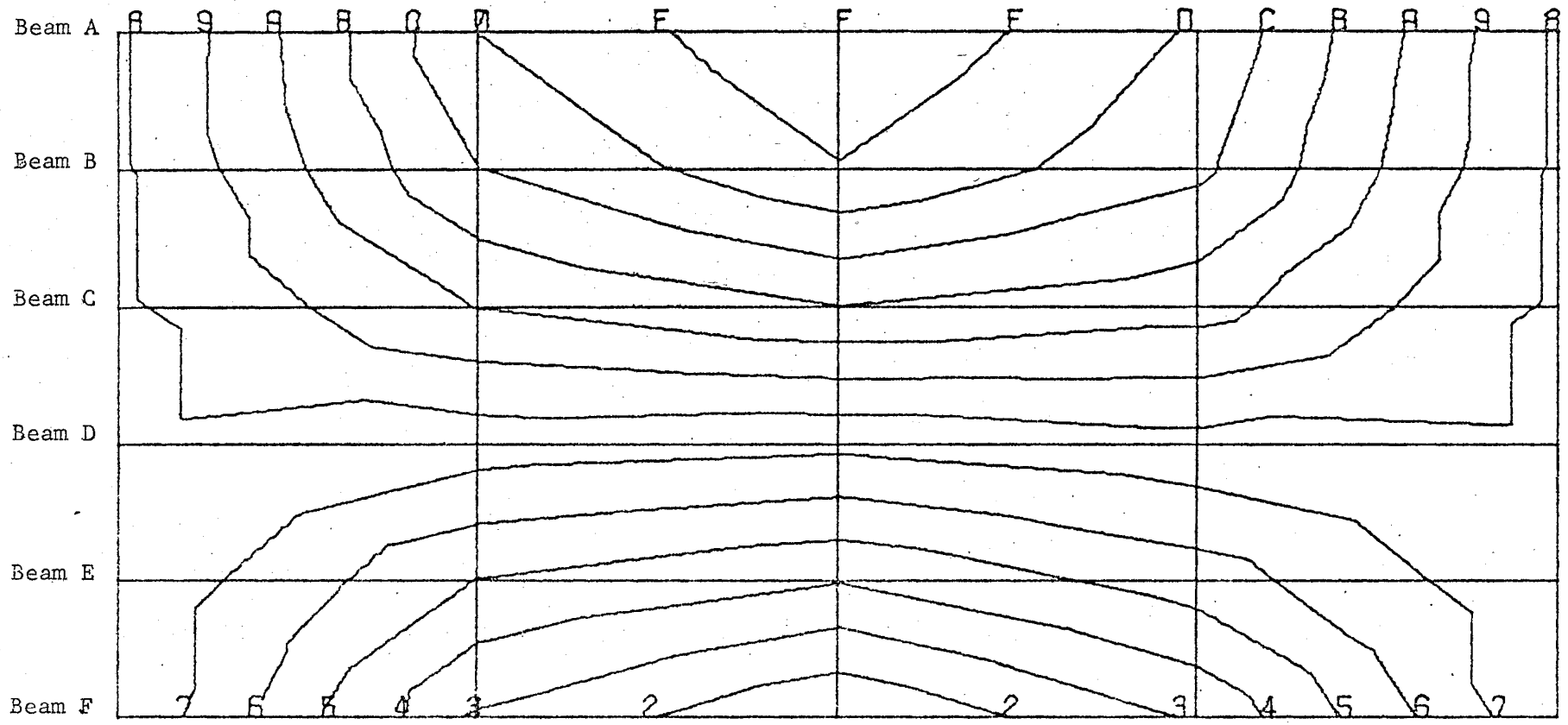FR-WHEEL DIST./BRIDGE LENGTH = 1.4462
FIGURE 99

BENDING MOMENT(IN.-KIP) CONTOURS

CASE- 50 MPH LANE 3
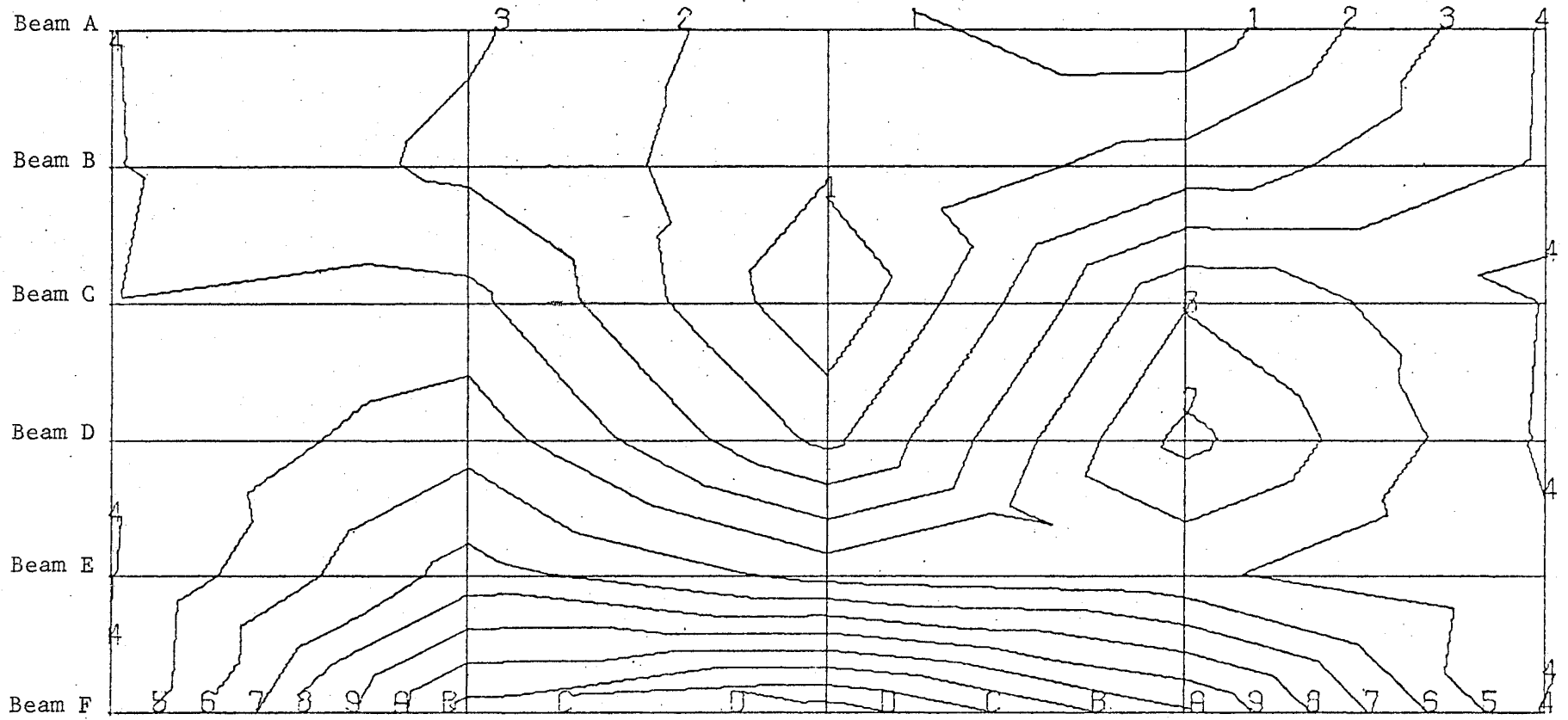
FR-WHEEL DIST./BRIDGE LENGTH = 1.4769

FIGURE 100
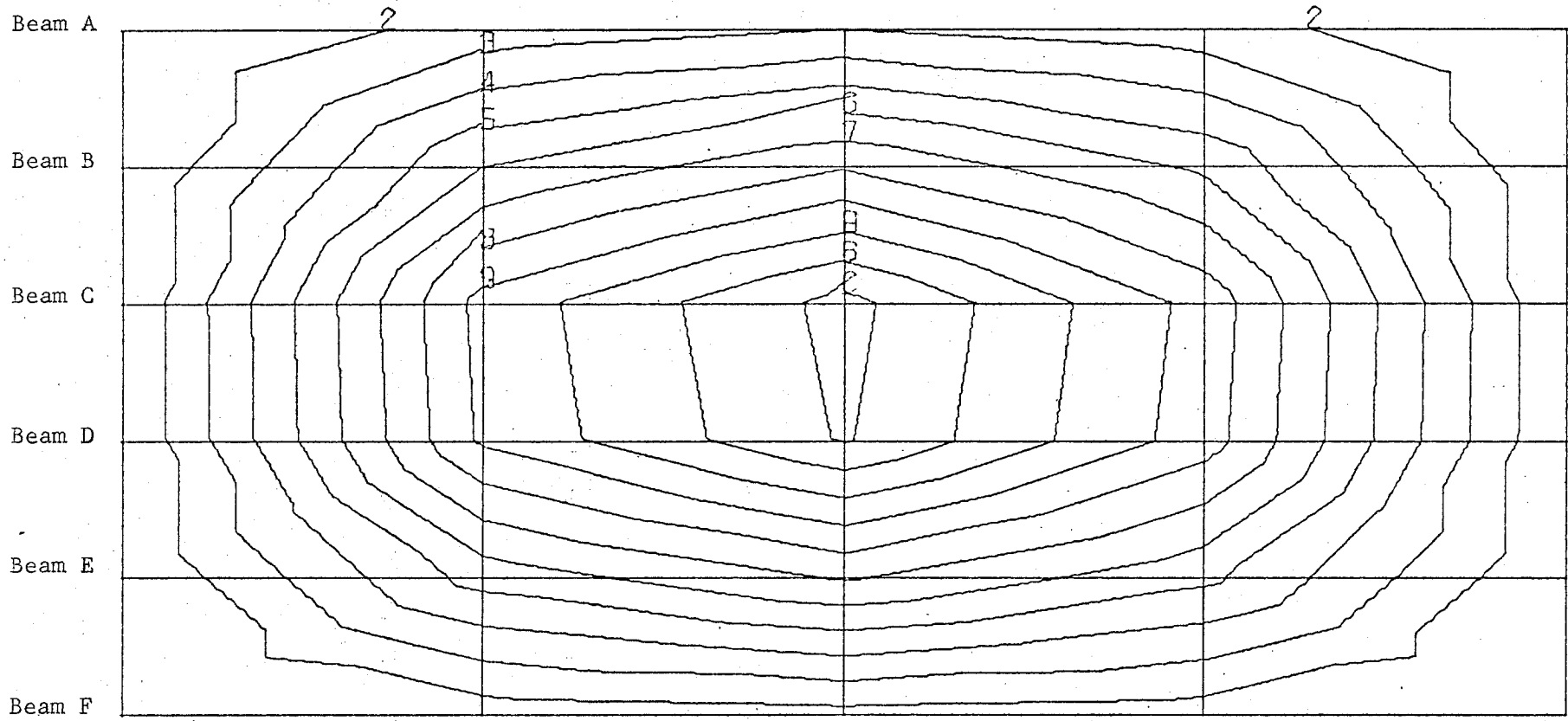
DISPLACEMENT(IN.) CONTOURS
CASE- 50 MPH LANE 5
FR-WHEEL DIST./BRIDGE LENGTH = 0.70769

FIGURE 101
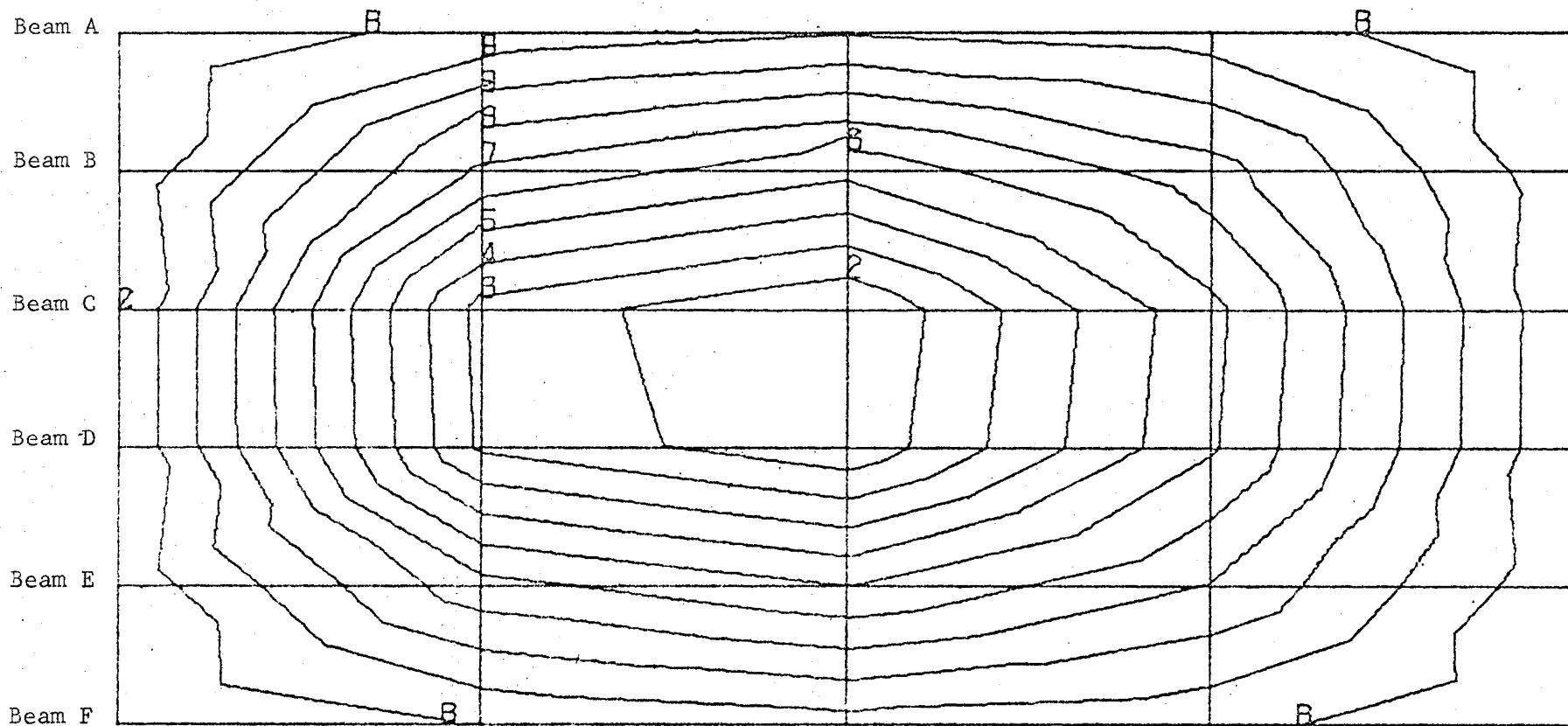
BENDING MOMENT(IN.-KIP) CONTOURS
CASE- 60 MPH LANE 6
FR-WHEEL DIST./BRIDGE LENGTH = 0.70769
FIGURE 102

Beam A

Beam B

Beam C

Beam D

Beam E

Beam F

9 8 7 6 5 4 3 2 1 1 2 3 4 5 6 7 8 9

DISPLACEMENT(IN.) CONTOURS

CASE- 50 MPH LANE 5

FR-WHEEL DIST./BRIDGE LENGTH = 1.4462

FIGURE 103

DISPLACEMENT(IN.) CONTOURS
CASE-.50 MPH LANE 5
FR-WHEEL DIST./BRIDGE LENGTH = 1.4769

FIGURE 104

Beam A

Beam B

Beam C

Beam D

Beam E

Beam F

7 6 5 4 3 2 2 3 4 5 6 7

DISPLACEMENT(IN.) CONTOURS

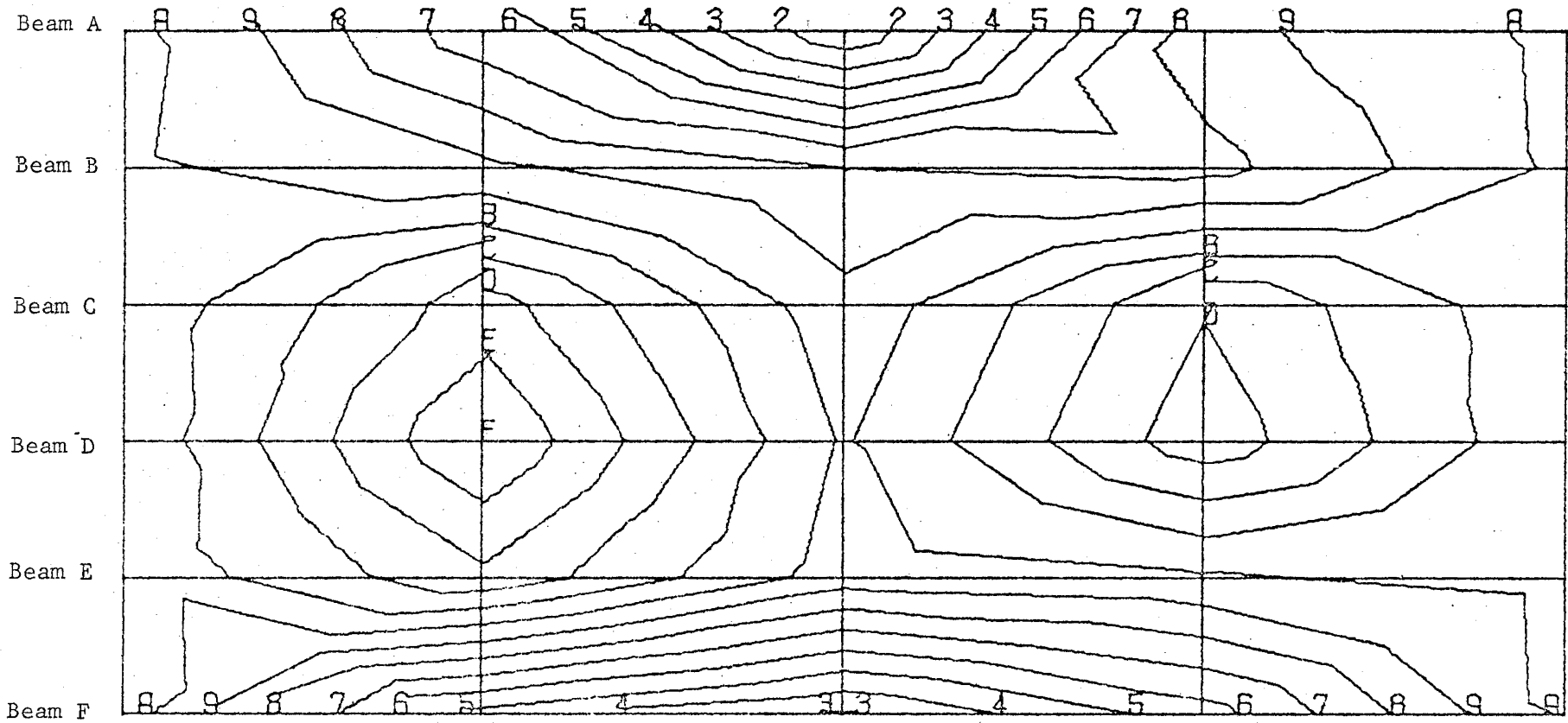CASE- 60 MPH LANE 6

FR-WHEEL DIST./BRIDGE LENGTH = 1.6077

FIGURE 105

BENDING MOMENT(IN.-KIP) CONTOURS
CASE- 50 MPH LANE 5
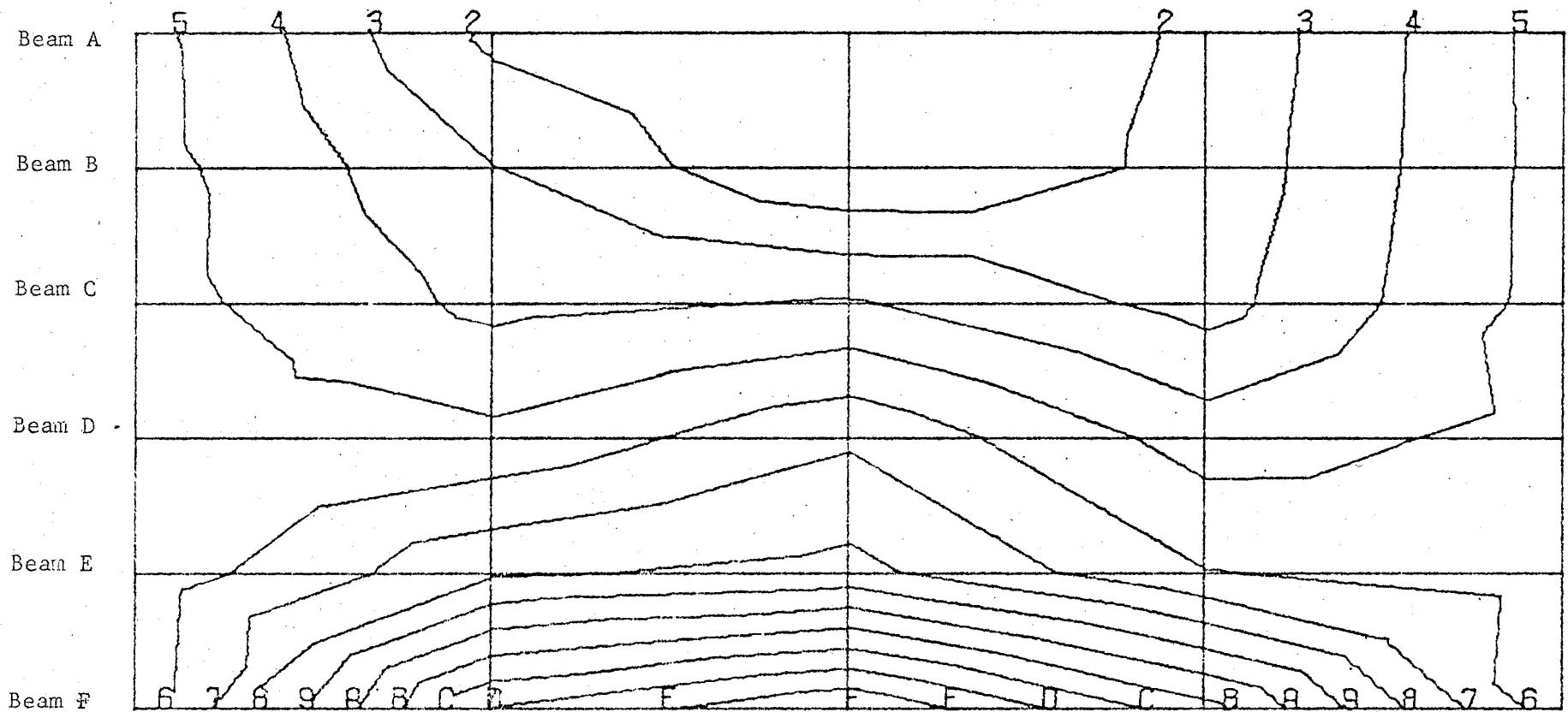FR-WHEEL DIST./BRIDGE LENGTH = 1.4462

FIGURE 106

BENDING MOMENT(IN.-KIP) CONTOURS

CASE- 60 MPH LANE 6

FR-WHEEL DIST./BRIDGE LENGTH = 1.4769

FIGURE 107

BENDING MOMENT(IN.-KIP) CONTOURS
CASE- 60 MPH LANE 6
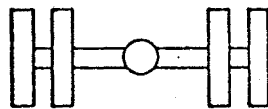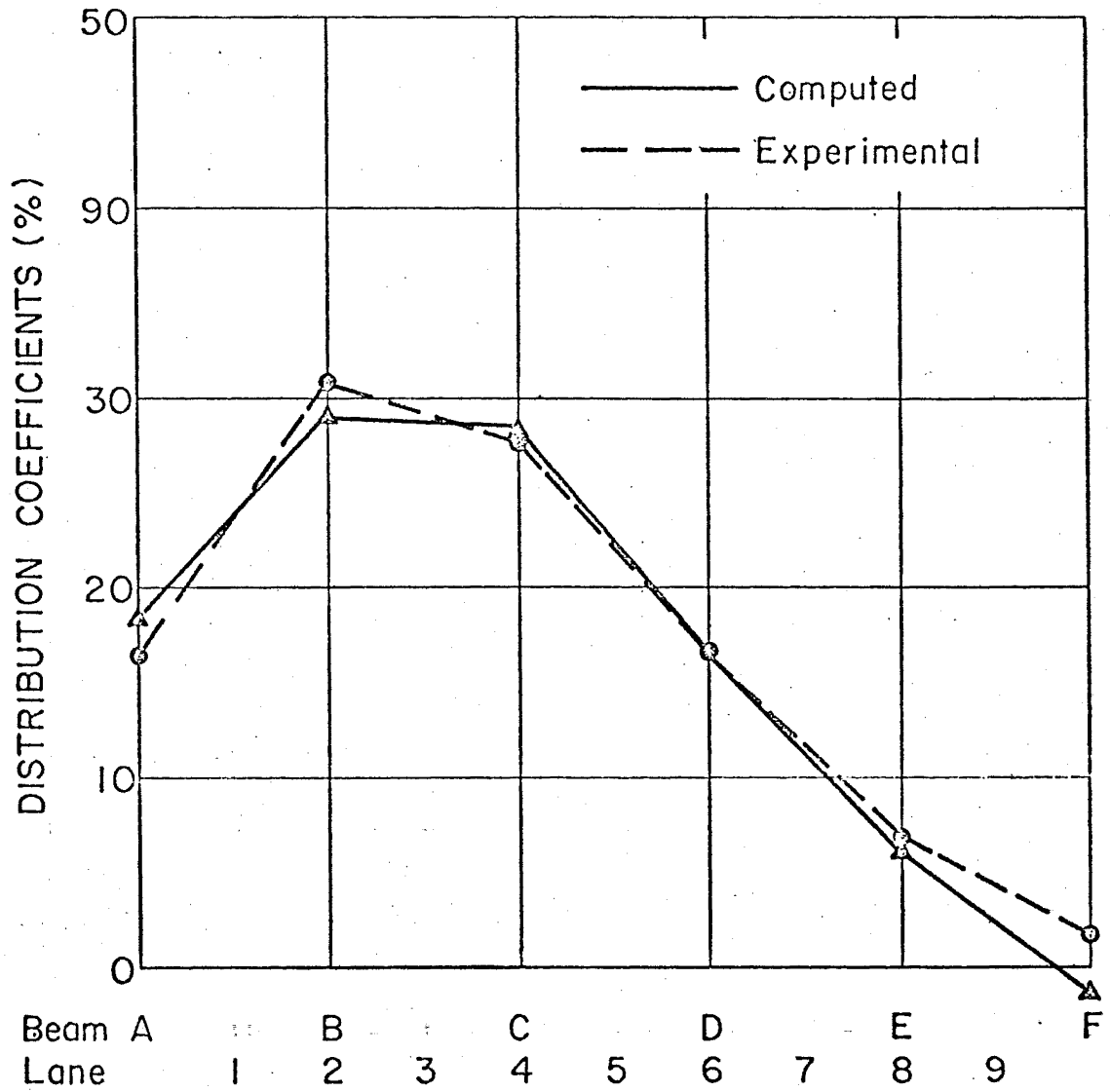FR-WHEEL DIST./BRIDGE LENGTH = 1.6077

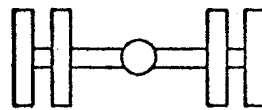FIGURE 108

Fig. 109   Distribution Coefficients – Static Lane 3
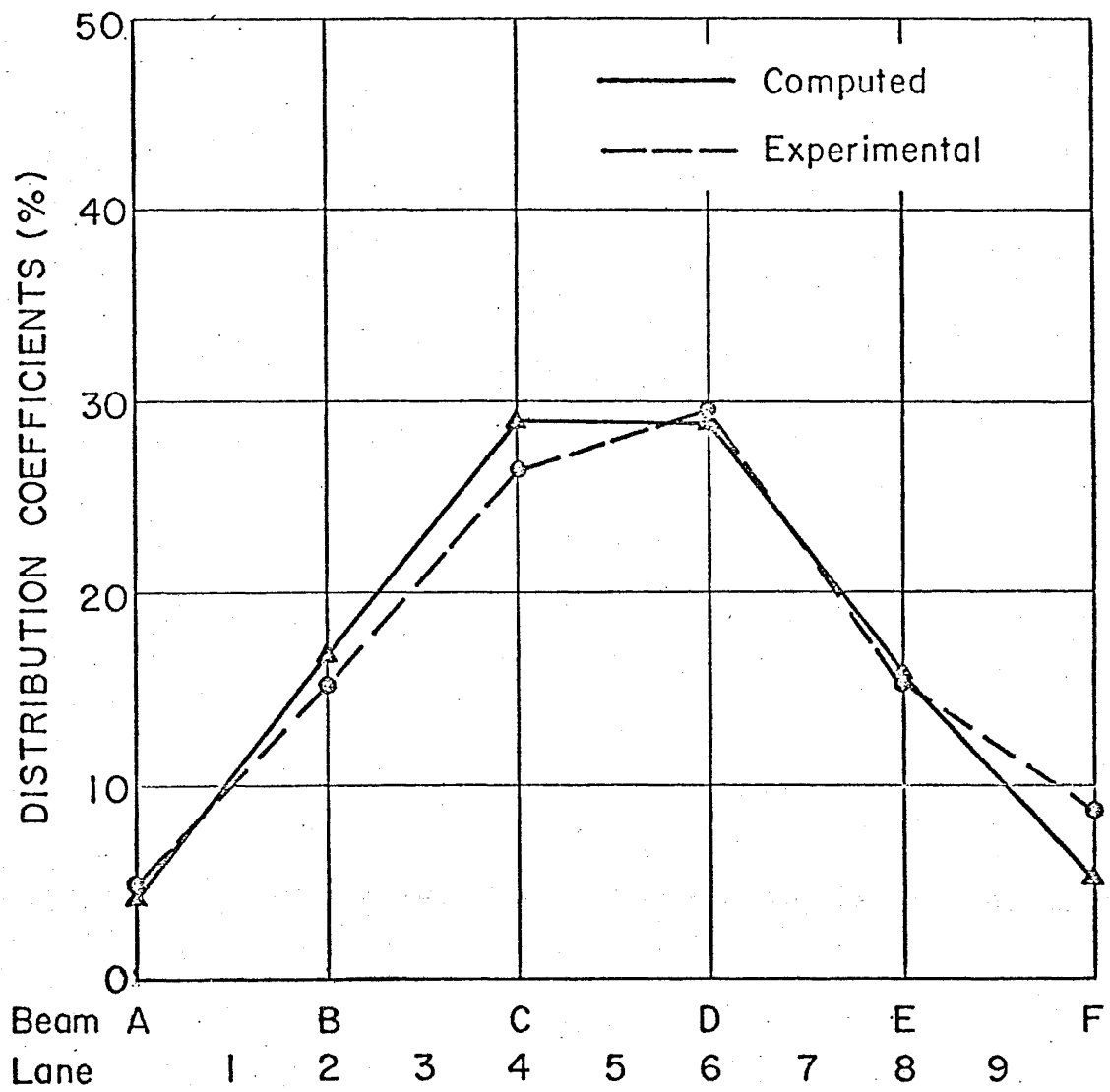
Fig. 110   Distribution Coefficients - Static Lane 5

FIGURE 111   24.4MPH-LANE 2
EXPERIMENTAL
DISPLACEMENT TIME HISTORY
BEAM B-NODE POINT 23

FR-WHEEL DIST./BRIDGE LENGTH
X (10⁻¹)

FIGURE 112   52.6MPH-LANE 2
EXPERIMENTAL
DISPLACEMENT TIME HISTORY
BEAM B-NODE POINT 23

FR-WHEEL DIST./BRIDGE LENGTH
X (10⁻¹)

FIGURE 113 54.5MPH-LANE 6
EXPERIMENTAL
DISPLACEMENT TIME HISTORY
BEAM D-NODE 13

FR-WHEEL DIST./BRIDGE LENGTH
X (10⁻¹)
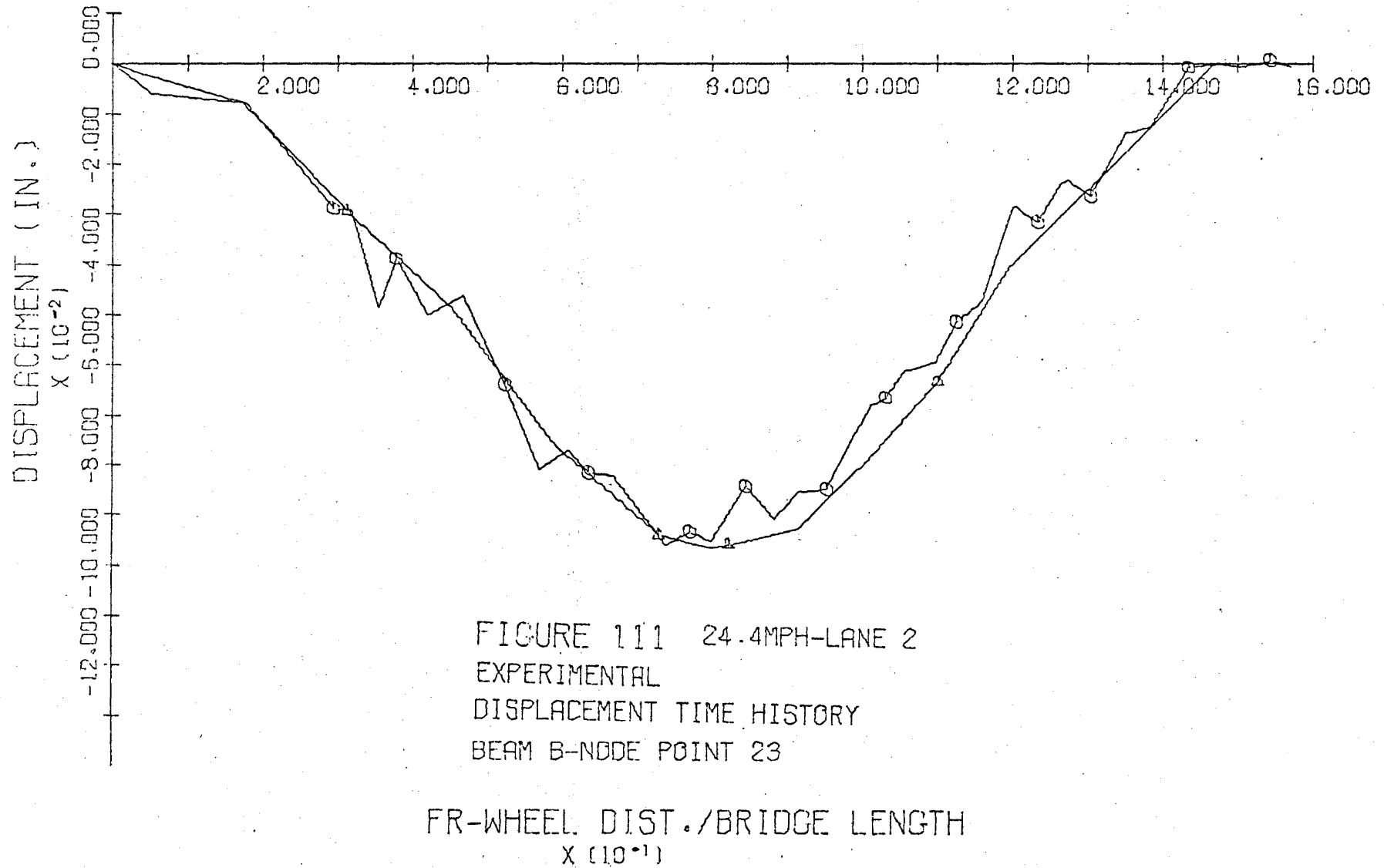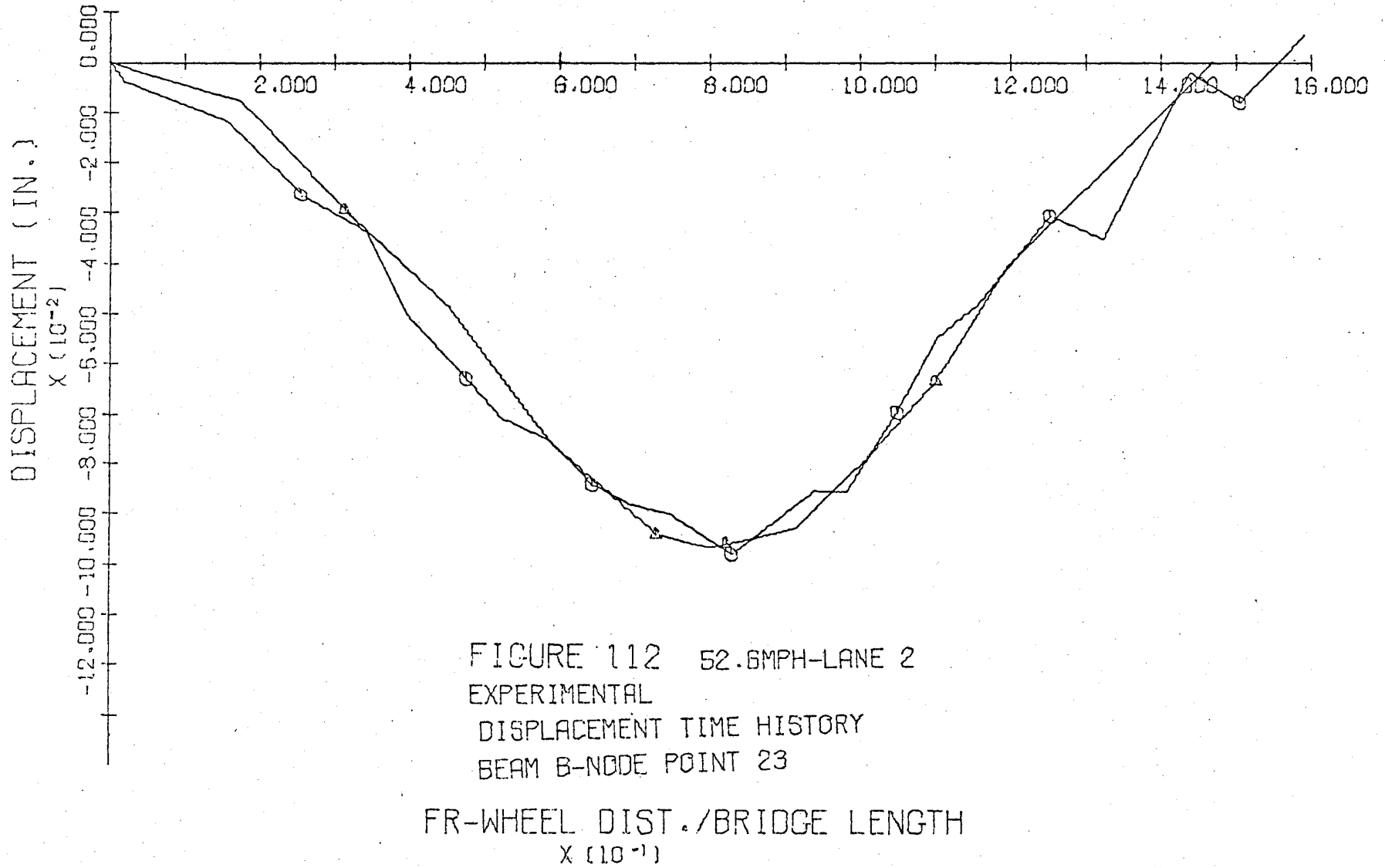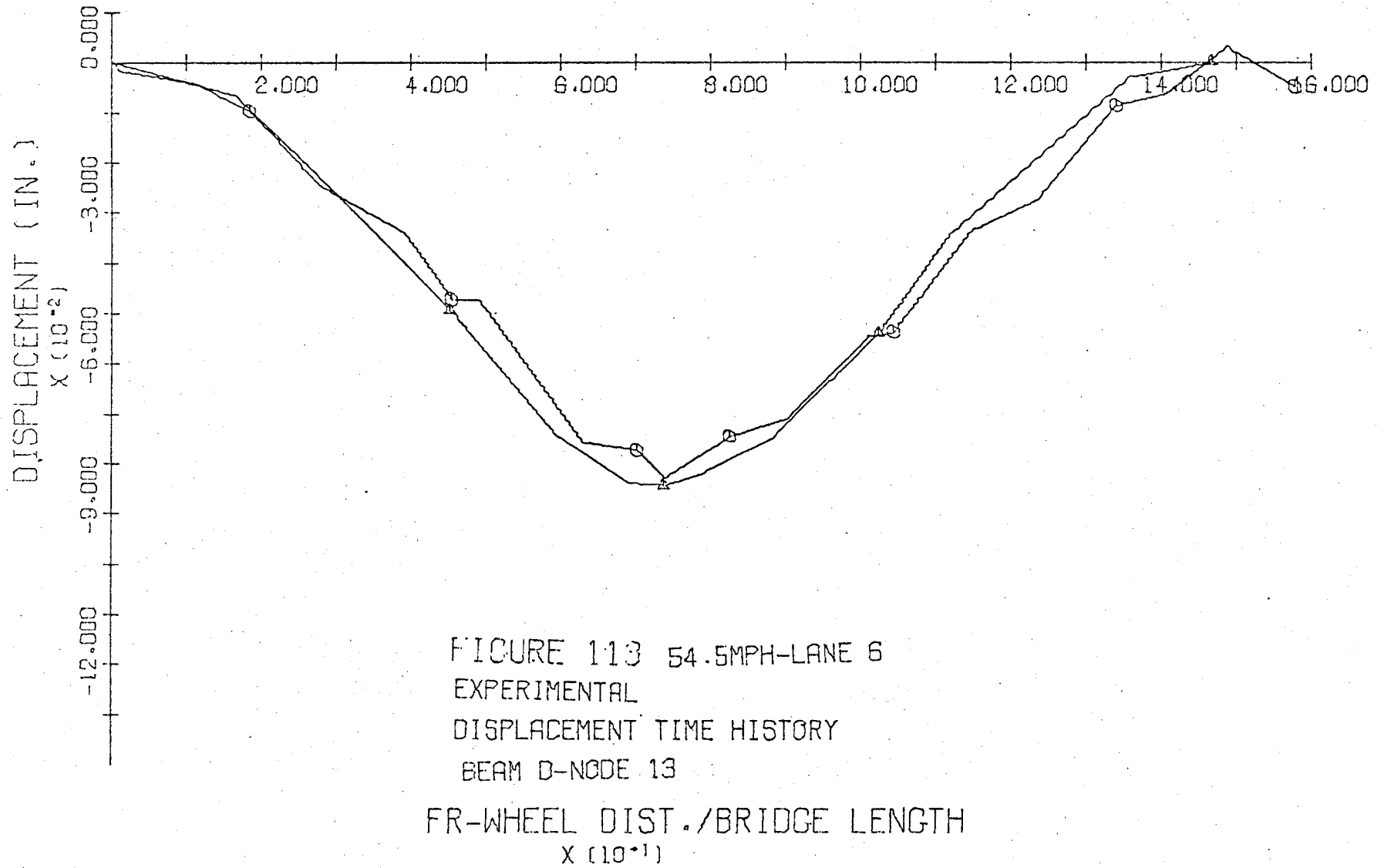
12. <u>REFERENCES</u>

1. Chen, Yan-Liang
       STRUCTURAL BEHAVIOR OF A PRESTRESSED CONCRETE BOX-BEAM
       BRIDGE, Fritz Engineering Laboratory Report No. 315.10T,
       Lehigh University, August, 1970.

2. Clough, R. W. and Felippa, C. A.
       A REFINED QUADRILATERAL ELEMENT FOR ANALYSIS OF PLATE
       BENDING, Proceedings of the Second Conference on Matrix
       Methods in Structural Mechanics, pp. 399-440, Wright-
       Patterson Air Force Base, Ohio, 1969.

3. Edgerton, R. C. and Beecroft, G. W.
       DYNAMIC STRESSES IN CONTINUOUS PLATE GIRDER BRIDGES,
       Transactions of the American Society of Civil Engineers,
       Vol. 123, Paper No. 2921, pp. 266-292, 1958.

4. Fenves, S. J., Veletsos, A. S. and Siess, C. P.
       DYNAMIC STUDIES OF BRIDGES ON THE ASSHO ROAD TEST,
       Highway Research Board Special Report 71, National
       Academy of Sciences, Washington, D.C., 1962.

5. Fleming, J. F. and Romualdi, J. P.
       DYNAMIC RESPONSE OF HIGHWAY BRIDGES, Journal of the
       Structural Division, ASCE, Vol. 87, No. ST7, Proceedings
       Paper 2955, pp. 31-61, October, 1961.

6. Hutt, J. M. and Salam, A. E.
       DYNAMIC STABILITY OF PLATES BY FINITE ELEMENTS, Journal
       of the Engineering Mechanics Division, ASCE, Vol. 97,
       No. EM3, Proceedings Paper 8211, pp. 879-899, June, 1971.

7. Ketter, R. L. and Prawel, S. P., Jr.
       MODERN METHODS OF ENGINEERING COMPUTATION, McGraw-Hill
       Book Company, 1969.

8. Linger, D. A. and Hulsbos, C. L.
       DYNAMICS OF HIGHWAY BRIDGES, Iowa Engineering Experiment
       Station, Project 370-S, Part I, Iowa State University,
       July, 1960.

9. Newmark, N. M.
   A METHOD OF COMPUTATION OF STRUCTURAL DYNAMICS, Journal
   of the Engineering Mechanics Division, ASCE, Vol. 85,
   No. EM3, Proceedings Paper 2094, pp. 67-94, July, 1959.

10. Przemieniecki, J. S.
    THEORY OF MATRIX STRUCTURAL ANALYSIS, McGraw-Hill Book
    Company, 1968.

11. American Association of State Highway Officials
    STANDARD SPECIFICATIONS FOR HIGHWAY BRIDGES, 1969.

12. Tung, T. P., Goodman, L. E., Chen, T. Y. and Newmark, N. M.
    HIGHWAY BRIDGE IMPACT PROBLEMS, Highway Research Board
    Bulletin 124, National Academy of Sciences, Washington,
    D.C., pp. 111-134, 1956.

13. Veletsos, A. S. and Huang, T.
    ANALYSIS OF DYNAMIC RESPONSE OF HIGHWAY BRIDGES, Journal
    of the Engineering Mechanics Division, ASCE, Vol. 96,
    No. EM5, Proceedings Paper 7591, pp. 593-620, October,
    1970.

14. VanHorn, D. A. and Chen, C. H.
    STRUCTURAL BEHAVIOR OF A PRESTRESSED CONCRETE I-BEAM
    BRIDGE, LEHIGHTON BRIDGE, Fritz Engineering Laboratory
    Report No. 349.4, Lehigh University, October, 1971.

15. Wen, R. K. L. and Veletsos, A. S.
    DYNAMIC BEHAVIOR OF SIMPLE-SPAN HIGHWAY BRIDGES, Highway
    Research Board Bulletin 315, National Academy of
    Sciences, Washington, D.C., pp. 1-26, 1962.